Final Report

Principal Investigator:	Steven Eugene Guffey, M.I.E., Ph.D., C.I.H.
Co-investigators:	Ismail Celik, PhD; Ibrahim Yavuz, PhD Mechanical and Aerospace Engineering, WVU
Project title:	Comparison of Concentrations at Personal Exposure Sampling Locations
Sampling Locations:	WVU
Type:	Exposure Assessment
Project dates:	7/1/01 to 6/30/05
Grant number:	1 RO1 OH07587
Funding amount:	Direct: $575,000 Indirect: $803,022
Inventions:	none

Steven E. Guffey, Ph.D., C.I.H.
West Virginia University
College of Engineering and Mineral Resources
Dept of Industrial Management and Systems Engineering
PO Box 6070
353C Mineral Resources Engineering
Morgantown, WV 26506-6070

TABLE OF CONTENTS

LIST OF ABBREVIATIONS

a_{ij}	strain rate
C	mean concentration
C_{mouth}	concentration measured at the right edge of the lips
$C_{forehead}$	concentration measured at center of the forehead
C_{nose}	concentration measured at the right side of the nose near the tip
C_{neck}	concentration measured at the pit of the neck
$C_{Lcollar}$	concentration measured at the left collar bone
$C_{Rcollar}$	concentration measured at the right collar bone
C_{Llapel}	concentration measured at the left lapel
C_{Rlapel}	concentration measured at the right lapel
C_{Cchest}	concentration measured at the center of the lower sternum
D	dimension of square cylinder
D_P	diameter of the particle
F_x	additional force in particle transport equation
f	frequency
f_1, f_{2y}	damping functions
G_{ij}	buoyancy induced production rate of turbulence
Gr	Grashof number
g_i	component of the gravitational vector in the ith direction.
h	enthalpy, mesh size
k	turbulent kinetic energy
L_{ij}	molecule diffusion
l_μ, l_ε	length scales
P	dynamic pressure
P_k	production rate of turbulent kinetic energy
Pe	Peclet number
Re	Reynolds number
Re_P	particle Reynolds number
R_{ij}	pressure redistribution
Rt	local Reynolds number
Sc_L	laminar Schmidt number
Sc_T	turbulent Schmidt number
S_{ij}	strain rate
S_T	heat generation source term
St	Strouhal number
S_ϕ	scalar generation source term
T	temperature
T_{ij}	turbulent diffusion term
T_{ref}	reference temperature
t	time
U	mean velocity
U_0	inflow velocity
U+	normalized velocity
u_i (u, v, w)	Cartesian velocity component in direction x_i

u', v', w'	velocity fluctuation components
u_τ	friction velocity
$\overline{u_i u_j}$	turbulent stress
$\mathbf{u}_P$	velocity of the particle
V	inlet velocity for the wind tunnel
x_i	Cartesian coordinate in tensor notation
y	normal distance to the wall
y+	normalized distance to the wall

ABSTRACT.

Industrial hygienist generally place air sampling probes on the mid to upper torso of workers when attempting to determine their inhaled concentrations. A review of the literature does not supply convincing evidence that concentrations measured on the chest are equal to inhaled concentrations. To determine how well surrogate locations matched concentrations at the mouth (C_{mouth}), low concentrations of ethanol in nitrogen were released between the hands of standing and seated subjects while they sat or stood in a wind tunnel. Experimental results for a manikin were compared to experimental results for human subjects and to concentrations predicted from simulations made using computational fluid dynamics.

In all cases the subjects stood or sat with their backs to the airflow because previous studies had established that exposures facing downstream produced exposures that were more than 100 times exposures when facing upstream or sideways to the flow with the source in the subjects' hands. Sampling probes were placed at the subject's mouth, nose, forehead, neck, both collars, center chest and both lapels. Airflow was drawn to 3L sampling bags using sampling pumps at 0.1L/min. Concentrations were measured using a gas chromatograph with a photo-ionization detector, which was calibrated daily over the range of sample concentrations. Test conditions included 5 levels of cross-draft velocities (11, 27, 48, 82 and 104 ft/min), two levels of body heat (unheated/heated), two levels of hair length ("2" and bald), and two levels of posture (sitting/standing).

The manikin was anthropometrically correct and could be heated to natural temperatures. In addition, body-temperature air could be "inhaled" and "exhaled" through its nose in a realistic manner. The manikin either wore a wig or was "bald." The human subjects sat or stood while doing make-work tests that involved moving their hands over the tracer gas source. Three dimensional transient computational fluid dynamics (CFD) was used to simulate exposure conditions for the manikin with and without heating.

For the manikin tests, wind tunnel velocity, heating, and posture each had a statistically significant effect for all sampling locations. Hair length had a significant effect for some locations but not others. For the unheated manikin, concentrations for all sampling locations declined monotonically with wind tunnel velocity. However, for the heated conditions, concentrations varied with an inverted-V relationship with wind tunnel velocity. For heated conditions, concentrations at the mouth were always higher for standing than sitting. Concentrations measured at the chest and shoulder levels were higher than mouth concentrations for the standing posture and were lower than mouth concentrations for sitting. Concentrations measured at the forehead location were always lower than concentrations measured at the mouth for both sitting and standing.

For the 13 human subjects the test conditions included cross-draft velocities of 11, 27, 48, and 103 ft/min, breathing/not breathing, and sitting/standing. Effects of not breathing were simulated by having the subject breathe through a long tube.

Results for the human subjects were consistent with the results for the manikin in some ways but not others. As with manikins, concentrations varied with wind tunnel velocity

($p< 0.01$) in an inverted V-shape and posture was significantly related to concentrations at all locations ($p<0.01$). However, unlike manikins, whose concentrations were roughly twice as high for standing as sitting, the ratio was inverted for humans. Breathing through a tube appeared to reduce the concentrations at most sampling sites but was not statistically significant. This appears to contradict the finding that breathing was important for manikins. However, the lack of statistical significance for humans may be due to the higher variability in results across subjects for humans than was found for manikins. If diverse manikins had been used, they may or may not have exhibited the same variability.

Concentrations for different human subjects ranged over a 4 to 1 range for the same conditions. It is likely that differing body sizes, body shapes, and lengths of hair contributed to the differences among subjects. Concentrations at the mouth were often substantially different from concentrations elsewhere. Concentrations at the humans' foreheads averaged about 85% of the concentration at the nose. The center chest averaging 136% of the nose. However, the 10% of the ratios of center chest to mouth were below 58% and the 10% were above 259%. The lapels were only slightly better. The corresponding values for collars were 75% and 126%. For the neck it was 80% and 140% and for the Nose it was 80% and 106%. Ratios of concentrations measured below the collars were much more variable than the ratio of concentrations at the nose to the mouth. The geometric standard deviation for C_{chest}/C_{mouth} was 2.12, a disturbingly high value.

The dramatic effects of velocities and postures suggest that exposure studies should consider multiple postures and cross-draft velocities. For human subjects, the forehead, collars, and adjacent to the nose were good surrogates (i.e., concentrations mostly within +20% of the mouth). The nose and forehead could be corrected by fixed amounts to estimate concentrations at the mouth. The collars were more accurate without correction but had higher standard deviations (i.e., lower precisions).

The CFD results closely matched the manikin results for the same conditions. In addition, the following was noted: 1) The heat flux from the body significantly affects the flow field and the subsequent contaminant concentration field at low Reynolds numbers; 2) the free stream turbulence plays an important role in the variation of exposure measurements at low Reynolds numbers; 3) results calculated with the Large Eddy Simulation (LES) illustrate the turbulence structure in the wake of the manikin and indicate that the flow unsteadiness plays an important role in the variation of exposure measurements; 4) calculations with various body shapes suggests that oversimplified body shapes may lead to inaccurate predictions in worker exposure assessment; 5) the concentrations measured at the lapel were very different than the concentrations measured near the mouth.

The results of this study raise strong concerns about the accuracy of samples taken anywhere below the collars when the subject is close to the source and flow is from the rear. The results from the manikin also cast strong doubts on the use of a manikin as a surrogate for humans unless it is heated and breathes realistically. The dramatic effects of posture on concentrations suggest that exposure studies should include both sitting and standing as well as variations of each. It is troubling that the effect of posture was reversed for humans and the manikin. The effects of body size and shape and hair length should be investigated in future studies.

HIGHLIGHTS/SIGNIFICANT FINDINGS.

Significant findings are similar to conclusions. These are the important results of the project, and they should relate to the specific aims of the project. The most important findings should be listed first. Separate findings should be in different paragraphs.

The overall conclusions from both the human and manikin studies are that:

1. For the manikin, all independent variables (Velocity, Posture, Hair Length, Heating, Breathing) were important, as were most interactions of the dependent variables (especially velocity and Heating).
2. When the manikin was either not heated or did not breath, it was a poor surrogate for the human subjects. The effects of velocity on concentrations were profoundly different when the manikin was at ambient or 98F body temperatures. At 98F, velocities followed an inverted V relationship with concentrations at all sample locations. At ambient temperatures the effect of increasing velocity was to decrease concentrations monotonically, a common finding in unheated manikin studies.
3. For manikins, concentrations were twice as high at the mouth when standing than when seated. Concentrations on the torso were higher than C_{mouth} when standing and lower when sitting.
4. For manikins no location was a reliable surrogate for the mouth.
5. For human subjects, the effect of increasing velocities tended to follow the inverted V relationship, just as it did for heated manikins.
6. Likewise, the effect of posture was profound for human subjects, but opposite to the manikin. That is, the concentrations were higher when sitting than standing, possibly due to subtle differences in postures.
7. For humans, breathing through a tube had no significant effect.
8. For humans, the collars, nose, and forehead were reasonably good surrogates for the mouth.
9. The CFD results suggest that turbulent intensity is an important issue and that a manikin can be realistically simulated using CFD.
10. Based on results from the human studies, concentrations at the mouth can be estimated with reasonable precision using samples taken at the forehead, adjacent to the nose, or at the collars. Concentrations at the forehead were roughly 15% less concentrations at the mouth and concentrations at the nose were roughly 5% less than concentrations at the mouth. The forehead and nose locations provided ratios to C_{mouth} that had the lowest geometric standard deviations and were unaffected by the independent variables. Thus both can provide reasonably good estimates of Cmouth by adding a fixed percentage correction to their values.

TRANSLATION OF FINDINGS.

This section provides an interpretation of how the significant findings of the project can be used in prevention of workplace diseases and injuries. If specific recommendations are made for reducing hazards on the job, the language should be as non-technical as possible in order to communicate to employers or employees. It is very important that a PI identify how these findings have been or may be adopted in the workplace. If the findings are such that they cannot yet be applied to the workplace, this section should address how these findings can be used to guide future activities.

When taking exposure samples when the source is close to the worker, the results of this study suggest that it may be important to avoid locating the inlet probe at either lapel or at the center of the chest. Based on this study, for those sites the ratio of their concentrations to the mouth under these conditions was 50% to 200%, depending on whether the subject was sitting or standing and what the cross-draft velocity was. For the greatest accuracy, sample as near the mouth as possible if the probe is small enough not to affect the flow around the face. Given the inconvenience of attaching a probe to the face, the next best locations are at the centers of either collar bone, followed by the "pit" of the neck.

Those doing exposure assessment research should take note of the profound effects of posture, body heat, and breathing on the results when a manikin was used.

Outcomes/Relevance/Impact.

This section should be a concise statement of the outcomes, relevance, and/or impact of your project.

The outcomes of the study raise serious concerns about the accuracy of sampling on the chest, especially when the source is near the worker and airflow is from the back. It is particularly important to note that the direction of the resulting sampling errors may depend on whether the subject is sitting or standing and on the level of the airflow velocity (which generally is difficult to characterize in the field). It is likely that sampling errors in the field would be a great deal less if the subject adopts many different postures and experiences a broad range of cross-draft velocities. Such diversity is more likely for 8-hour sampling than for 15-minutes sampling.

The impact of this project is to raise concerns about use of lapel and chest locations as surrogates for inhaled concentrations. It also suggests that variability in sampling results could be strongly affected by choice of sampling location. The study also should impact the selection of apparatus and methods employed by researchers investigating human exposures using manikins.

SCIENTIFIC REPORT.

This study had two very different aspects: 1) experimental studies of manikins and human subjects, and 2) computational fluid dynamics simulation to aid and explain the experimental studies. Because the methods and goals of the two aspects are so different, the PI believed it would be easier for reviewers to understand both aspects if the scientific reports were presented separately. The experimental studies are presented first all the way to Conclusions, followed by the simulation study all the way to its Conclusions.

BACKGROUND FOR THE PROJECT

Workers on the job are often exposed to airborne chemicals in levels that may be sufficient to affect their long-term health. Industrial hygienists sample their exposures and compare them to "safe" levels. In sampling these airborne chemicals, it is important that the sample fairly represent the inhaled concentration. For many years it was assumed that a sample taken anywhere in the so called "breathing zone" (BZ) would more or less equal the inhaled concentration. "The Occupational Safety and Health Administration (OSHA) considered the breathing zone to be a hemisphere forward of the shoulder with a radius of approximately 6-9 inches" (CFR, 1985). However, over time it became more and more apparent that there could be steep concentration gradients near sources. Hence, a sample taken at different locations in the supposed BZ near the body could give very different results. By 1973, the volume accepted as representing the true BZ shrunk to be "within a foot of the head as well as the upper torso" (NIOSH, 1973). Presently the most popular sampling location is the lapels and collars (but sometimes on the sternum), perhaps due to their convenience when attaching filters and probe inlets.

The surrogate sampling locations used for the study are all either currently used in practice or could be used. Currently used positions are the left and right collar and the left and right lapels. Sometimes sampling inlets are actually well below the collars and lapels, hence the selection of the center chest location. The forehead has been proposed as a sampling location by Cohen et al. (1982). The mouth location represents true "inhaled" concentrations. The adjacent nose position would be expected to be nearly the same as the mouth but somewhat more convenient for sampling. Sampler positions in front of the ear and on top of the shoulder were studied and rejected by Guffey et al. (2001) as they found concentrations there to be both erratic and substantially (~70%) lower than samples collected at the mouth.

In determining whether samples taken at a given location will have concentrations equal to inhaled concentrations, the "acid test" is to compare concentrations taken on human subjects at that location to samples simultaneously sampled near the mouths of the subjects. However, testing human subjects can be inconvenient and costly. Manikins are more convenient subjects than humans because humans must be treated with elaborate care to avoid harmful exposures and cannot be tested for long periods of time due to fatigue. However, the convenience of manikins would be of dubious benefit if the results from manikin studies do not accurately predict results with humans. The only way to confirm that a simple manikin is behaving like humans is by comparing results from manikins to results from exposed humans under similar conditions. As will be discussed later, it is an open question whether manikins of any complexity are adequate surrogates for humans in modeling inhaled concentrations. Despite the substantial reliance on

manikins in past studies, there are few published studies that even investigate whether manikins are reliable substitutes for humans in industrial hygiene sampling. This study sought to answer that question by testing both manikins and humans under similar conditions.

Manikins used in most previous experimental investigations were far from lifelike in many characteristics. Plausibly important characteristics include lifelike facial features such as hair, breathing, body temperature, anthropometrically-correct dimensions, posture, and body movement. As will be discussed, no study was found in which the manikin had all of these characteristics. If there were differences in results between such a simple manikin and a human, one could not determine whether the differences were due to these dissimilarities or to more subtle differences, such as facial features, hair style, etc. Manikins used in some previous works were just standing in uniform velocity fields with their hands straight down. In some studies, the source was placed in unrealistic locations. In the industrial work environment, the greatest exposures are likely where workers hold a source in their hands (Flynn and Shelton, 1990). In this research, the manikin held a source within its arms whether it was sitting or standing.

Likewise, although there is little question that computation fluid dynamic simulation of airflows is well-developed and highly accurate for many conditions, it had not been established that CFD could successfully model points very close to a body whose topology is as complex as a human body. This study sought to answer that question by comparing manikin results to results from CFD simulation of the same manikin under the same conditions.

Physical as well as virtual modeling of human beings is a subject of growing interest for assessing, measuring and simulating personal exposure to contaminants in the workplace. Manikins used in CFD simulations have been spheres, rectangles, sharp edged simplified shapes, or cylinder shaped models. The influence of manikin geometry on the flow pattern and contaminant dispersion at the breathing zone is still undergoing research (Brohus, 1997; Li et al., 2003; 2005). Issues which need careful consideration are those of the choice of anthropometric measures, plus the mechanical and geometrical representation of the human being (joints and body parts). Making such choices should depend on the intended use of the model. For instance, a manikin used to study air flow patterns and contaminant dispersion requires separated legs and separated arms to simulate a human being in a standing position while holding a source with his arms. Parameters that govern modeling of a human physically are simplicity, feasibility of the model, and the need to satisfy the purpose of research.

Anthropometric parameters such as height, width, and depth of the manikin parts are important for studying the proportions of physical or virtual manikins to human beings, while integral parameters such as surface area and body volume are important for studying the effects of convective and radiated heat loss from different body parts on airflow patterns and contaminant dispersion in breathing zones of workers.

This study considered whether and how heating, posture, and air velocity affect concentrations measured at several potential sampling locations on the head and torso of a manikin. Since the results will not be compared directly to a human, this study alone can not determine if any combination of treatments makes a manikin equivalent to humans for the purpose of exposure assessments. However, this study provides evidence that should be helpful in determining if these treatments are necessary to producing a faithful surrogate for humans. The logic is simple: if a treatment (e.g., heating) makes no difference in the results for a manikin, then adding body heat to unheated manikin probably is pointless whether or not the manikin is later shown to be equivalent to a human. On the other hand, if heating does make a difference to a manikin, then it

is reasonable to assume that human data would be more similar to the heated manikin than to the unheated manikins since humans also breathe.

It is important to determine if the "improvements" intended to make manikins more lifelike are needed because making a manikin similar to a human can be costly, both in direct costs and in its effects on study size. For the latter, each improvement introduces another set of potentially important variables. For example, if heating is important, is it important to heat all body parts or is heating the upper torso and head sufficient? Are the results sensitive to small changes in body temperature? If so, then future studies would have to use a diverse array of manikins or treatments to manikins, increasing the size of the studies.

Another independent variable for this study is air velocity, a crucial environmental condition that has proven important in other studies (Baldwin and Maynard, 1998; Guffey, et al 2001; Fletcher and Johnson, 1988; Fletcher and Johnson, 1996; Kim and Flynn, 1992; Kulmala et al, 1996; George et al, 1990; Flynn and Ljungqvist, 1995; Kim and Flynn, 1991a; Kim and Flynn, 1991b; Kim and Flynn, 1991; Flynn and Shelton, 1990; Flynn et al, 1995; Welling et al, 2000; Welling et al, 2001; Heist et al, 2003; Brohus, 1997; Brohus and Nielsen, 1994a; 1995; 1996b; Rodes et al, 1995; Bjorn and Nielsen, 1996a; 1996b). Five levels of velocity were tested because these studies generally have found the effects of velocity to be non-linear and because velocity could interact with other variables. For example, it is likely that the effects of heating a manikin would be quite different at low velocity ranges than at higher ones.

In comparing gas and vapor concentrations at the breathing zone of human subjects and simple manikin, Fletcher and Johnson (1988) compared nose and lapel concentrations for a human subject and a manikin in an industrial environment. Sampling at the nose, left lapel, and right lapel, they found slight differences between samples at the lapel and the nose for a human subject seated at a table with a neutrally-buoyant source on the table. The manikin showed lower breathing zone concentration values than a human subject under the same conditions. When a denser than air source was substituted, they found that concentrations varied with sampling location with the concentration at the nose the lowest. Although Fletcher and Johnson used a anthropometric manikin, their manikin did not breathe nor was it heated. In addition, the experimental conditions were not defined clearly. While, Welling et al. (2000) studied the dispersion of acetone from a low and moderate low "impulse" source in a uniform air stream flow. Concentrations were measured at 9 sampling locations (including nose level) infront of a human subject and unheated manikin. The effects of orientation and velocity of air flow, convection due to the human body, arm movement of a human being, and the type of source on the concentration gradients were studied. They tested the effects of facing, side, and back orientations to a cross-draft of 0.3 m/s. They found that concentrations were profoundly higher for the back orientation. They also tested the effects of arm movements and body heat for the back to flow orientation at 0.1, 0.3, and 0.5 m/s. They found that concentrations at the nose were higher for the human subject than the unheated manikin and were higher for arm movement than for a stationary human. However, neither of these results was statistically significant.

According to Clark and Edholm (1985), the maximum air velocity induced by body heat at face level of a standing person is 0.3-0.5 m/s. They speculated that this convection flow would strengthen the upward reverse flow and the transportation of contaminant into the breathing zone. However, smoke tests showed that when a table was used and there was a gap between the body and the table, the vertical convection flow due to body heat transported uncontaminated air from below the table into the breathing zone, thereby diluting concentrations. Guffey et al.

(2001) used a manikin to study the effect of manikin orientation (back, side to, and facing), cross draft velocity (10, 22, 47, 80) and movement of manikin torso on three sampling locations within the breathing zone. The tracer gas used was undiluted SF_6 at 0.1 l/min. It was found that concentrations at the chest were 2.9 times the concentrations at the nose, with the ratio decreasing as wind tunnel velocity increased. They concluded that the ear was not a location to sample as there was a high variability in the ear concentrations as compared to the nose. Also, concentrations at all sample locations were 100-200 times higher for the back-to-flow orientation than for the side and facing orientations. Although the manikin used in their study was anthropometrically-scaled, it did not breathe nor was it heated. Also, the SF_6 released was not neutrally buoyant, which could have had substantial effects on the results.

Malek et al. (1999) compared styrene samples taken at the nose, left lapel, right lapel, and chest of 21 workers who were spraying or rolling during boat building. They found that the average values at the nose ranged from 10% to 24% lower than samples taken at the lapels, with individual samples showing considerable variation. In addition, the ratio of nose to lapel concentrations varied by subject and by the task performed. They concluded that the variation in concentration within the breathing zone is affected by the distance between styrene source and the worker, the turbulent air flow in the breathing zone, "re-volatilization" of styrene from worker clothing and the average ventilation rate. They also found a clear correlation between concentrations measured at the chest and at the nose. However, Malek had his subjects wear bulky backpacks filled with sampling bags, thus potentially profoundly changing the air flow patterns near his subjects.

In a field study conducted by Martinelli et al. (1983), aerosol concentrations were measured simultaneously at the nose, lapel and forehead. They found considerable variability in concentrations at different sampling locations. However, the concentration at the lapel was higher than at the nose and forehead. They speculated that the discrepancies were due to re-suspension of dust from clothing, the job performed, and individual work practice differences. Cohen et al. (1982) measured exposures to styrene in a work place. They found that the concentration measured at the nose for an individual was about 76% of the level measured at the chest. However, Chatterjee et al (1969) investigated the lead concentrations in a lead acid electric accumulator (battery) factory by attaching two filter heads to the upper chest of the worker, one 5 inches below the other. The mean concentration obtained in the upper position was 22 % less than the lower one.

The effects of source type, location, and momentum was presented by Welling et al. (2000) who studied the effect of source type (point or line source) and "momentum" 0.1 and 0.8 m/s on the dispersion of acetone in the breathing zones of a human subject and an unheated manikin in a uniform air stream flow. The tracer gas used in their study was acetone. They found a 1% higher concentration at the nose level with the line source than with the point source. In addition, Kim and Flynn (1992) examined contaminant momentum, the presence of a flat plate downstream of the worker, the distance between contaminant source and the body, and the manikin's motion on concentrations at the mouth in a paint spray booth by using SF_6 mixed with helium as a tracer gas. They found substantial reductions in mouth concentrations when the spray gun emitted contaminants with high momentum. Also, reductions of 30-50% in mouth concentrations were observed due to the effect of the distance from the source and worker's motion. They also developed mathematical relationships between concentrations at the mouth and contaminant source momentum. They used an unheated, non-breathing anthropometric manikins.

Kulmala et al. (1996) studied worker's exposure experimentally and numerically in the near-wake region of an unheated, non-breathing anthropometric manikin. The effect of contaminant source location on the worker's breathing zone concentration was examined by injecting almost neutrally buoyant SF_6 (diluted to 2.8% with air) from 420 points in the wake region. The experiments were carried out using cross draft velocities of 0.25, 0.375, and 0.5 m/s. They found that the contaminant transport into the breathing zone depends strongly on the location of the release point. The airflow field was also determined numerically assuming a steady flow and using the standard k-e turbulence model. They also found that the mean recirculation length downstream from the manikin depended on free stream velocity and was 1.5 times the manikin width. They also observed that significant contaminant transport towards the breathing zone occurred only above the hip level.

George et al. (1990) tested a manikin (unheated, non breathing, half-sized) in a wind tunnel. They found that for the three cross-draft velocities tested (0.51, 0.76, and 1.27 m/s), both the mouth and chest concentrations decreased with increasing velocity. For cases where the source was held in front of the manikin at waist height, concentrations were vastly lower than when the manikin faced upstream and sidestream than when it faced downstream. That suggests that worker exposures are dominated by the periods they face a downstream source unless the background concentration is very high. Finally, they found that the concentration at the mouth decreased exponentially with increasing horizontal distance from the manikin to the source. None of the findings gave a clue to the effects of sample location, source location, velocity, or cross-draft orientation on the ratio of mouth to lapel concentrations, but it is prudent to assume that all three variables could affect that ratio.

Flynn and George (1991) found greater exposure variability when the point source contaminant was located within the separated boundary layer than when the source was outside this region as one might expect. In another work George and Flynn (1990) studied the effect of source to manikin distance on concentration at the mouth location for a half-sized unheated manikin facing downstream. As the manikin source distance increased, a substantial reduction in SF_6 concentration in breathing zone occurred especially as the source passed out of the separated region.

Limited research studied airflow patterns, wake length and width, boundary layer separation and modeling of breathing zone concentration. For example, Welling et al (2001) characterized the reverse flow zone created in front of a human being in a uniform flow using both experimental data and numerical simulation. Experiments were carried out by moving a point source of acetone vapor in front of the human subject and measuring the contaminant concentration at nose level in front of the subject. They found that the length of the reverse flow region was (0.9-1.4 m) with freestream velocities between 0.1 and 0.5 m/s for a stationary human being. With the person moving his arms, the length of reverse flow fell to between (0.5-1.2 m) for the same velocities. In addition, numerical simulations were carried out to predict the length of reverse flow using the k-ε turbulence model. Compared to experimental data, they found that the extent of the reverse flow region was predicted fairly well using numerical modeling.

Kim and Flynn (1991a) found the boundary layer separation to be an important factor in determining a worker's exposure to airborne contaminants. They developed a conceptual model to understand this phenomenon and to predict the average concentration in the reverse flow region downstream of a worker in a uniform freestream. Subsequently, the assumptions of this model were tested experimentally in wind tunnel studies. Based on these results, a revised model

(Kim and Flynn, 1991b) was presented and validated using a tracer gas method. The revised model provided a reasonable estimate of the average concentration in the reverse flow region of the mannequin. Empirical models were presented that related both the average concentration in the reverse flow region and the mouth concentration to the body dimensions and the freestream air velocity.

Flynn and Ljungqvist (1995) studied wake effects on worker exposure and ventilation design using smoke visualization. They indicated the importance of flow visualization using smoke to detect and correct problems. Moreover, they pointed out that work practices are as important as ventilation design in controlling exposures. When sampling location and the source are in the wake zone, circulation patterns with the wake transports contaminant throughout its volume. If the source is in the hands and air is flowing from the back, then the face, lapel area, and hands were all within the wake zone. For flow from the side or front, none of these locations are in the wake. Thus, one would expect dramatically higher contaminant transport to the face and chest when the flow is from the back, as has been verified in other smoke visualization studies (Kim and Flynn, 1991a; 1991b; Guffey et al., 2001) that used a manikin holding a source in its hands.

Kim and Flynn (1991a) found that "chest" concentrations were approximately three times nose concentrations when the source was within the torso wake zone for unheated, non-breathing manikin. However, they were not measuring chest concentrations on the manikin, but rather at seven points on a plane in front of the manikin. In a smoke visualization study where vortex size was estimated, Kim and Flynn (1991b) found that the wake zone profile downstream of a manikin was not uniform. The wake zone was a much shorter distance downstream at the neck than at the hips. Furthermore, different air flow patterns prevailed in the head region than the chest region. Above the chest, a downwash over the top of the head was dominant, while for the chest to elbow region a combination of downwash and vortex shedding was important. Above the hip level the net airflow was directed upwards, while below the hip it was directed downwards. Johnson et al. (1996) studied the air movement around a human and a manikin in a low speed flow field and suggested that a manikin selected for sampling studies should be heated, rounded shape, and clothed. However, Fletcher and Johnson (1996) and Homma and Yakiyama (1988) found no effect of breathing using a breathing and heated manikin placed in a uniform free stream while studying the flow field around the head and chest using laser Doppler anemometry. They found that exhalation breath did not break through the thermal boundary layer of the heated and breathing manikin they used.

The wind speeds experienced by people in indoor environments are important when investigating personal exposures. For example, Baldwin and Maynard (1998) reported that wind speeds in homes and offices are usually between 0.05 to 0.1 m/s. However, when industrial work environments were considered, the averaged wind speeds increased to 0.3 m/s. They also reported that average values of personal wind speed distributions were approximately 0.05 m/s higher than measurements from static anemometers.

The effects of heating the manikin was presented by Heist et al (2003) who studied the effect of heating and and velocity on airflow patterns around a child-size manikin in a low-speed wind tunnel. They found that when the manikin was unheated the flow pattern on the downstream side of the manikin consisted of two slowly recirculating eddies. With the addition of body heat to the manikin (heated), the flow pattern downstream of the manikin changed to a rising vertical plume with velocities on the order of 0.1 m/s. This vertical plume was capable of transporting particulate matter into the breathing zone from near the floor. As the wind speed increased from

0.1 to 0.3 m/s, the vertical plume on the downstream side of the manikin was replaced by two recirculating eddies, a flow pattern similar to that with the unheated manikin. Although they used a child-size manikin, it was an anatomically correct physical model of human form, with movable joints and latex skin. The manikin tested was heated, breathed and was clothed.

Cermak et al (2002) studied the interactions between the free convection flow around a human body, the flow of respired air, personalized supply airflow, room airflow, and their effects on the quality of inhaled air using a two dimensional Particle Image Velocimeter (PIV). The manikin used to simulate human being was breathing, heated, clothed and wore a wig. The results showed that the personalized supply airflow was able to penetrate the free convection flow due to body heat and reach directly the face of the manikin. A large velocity gradient was observed at the manikin's face with a maximum air velocity of 0.2 m/s. Several studies have shown that natural convection due to body heat from humans can produce vertical velocities on the order of 0.1 to 0.25 m/s in areas near the breathing zone. For instance, Melikov and Zhou measured profiles of vertical velocity as a function of the distance from the neck for a seated, clothed, heated, and anthropometric manikin. They found vertical velocities of 0.13 m/s at 10 mm from the neck and 0.04 m/s at 50 mm from the neck. They also introduced an "invading" flow from behind the manikin with velocities in the range form 0.1 to 0.3 m/s. This invading flow reduced the strength of the natural convection and thus the vertical velocity by one half.

Bjørn and Nielsen (1996a) used CFD to investigate the effects of pulmonary ventilation rate, convective heat output, exhalation temperature, and cross sectional exhalation area on personal exposure. Experiments showed that exhalation from one person was able to penetrate the breathing zone of another person at a distance. In these experiments, two breathing thermal manikins were used: manikin no.1 acted as contaminant source, breathing directly towards the face of manikin no.2. Tracer gas (N_2O) was added to the exhalation, and manikin no.2 was used for measuring personal exposure. Manikin no.1 exhaled through either its nose or mouth. Different distances between the two manikins were tested. Breathing was simulated by steady-state CFD with reasonably good results. The simulations showed that personal exposure was very sensitive to variations in the convective heat output (body heat) of both the exposed person and the exhaling person, the cross sectional area of nostrils, and the pulmonary rate of the exhaling person. They found that when exhalation air was heated, a substantial influence on buoyancy was seen. Exhalation did not follow the manikin's own convective airflow, however, it formed its own independent flow which penetrated the other manikin's breathing zone.

Bjørn and Nielsen (1996b) experimentally investigated in a displacement ventilated room. They found that exhalation from one person penetrated the breathing zone of another person placed nearby, thus leading to higher exposures. When two persons are placed close to each other, convective boundary layer flow interacted in such a way that the personal exposure to an ambient concentration field was altered. They used two breathing thermal manikins. For the set of experiments conducted they found that when the manikins were facing each other, interaction can take place. Horizontal distance and inclination are important parameters. If exhalation was directed towards the back, higher exposures do not occur. In the case of two persons standing close together, the exposure to ambient concentration was not altered.

Brohus (1997) presented personal exposure measurements by means of a breathing thermal manikin (BTM) developed at the Technical University of Denmark. The manikin was 1.7 m high anatomically correct female display manikin. The BTM wore tight-fitting clothes with an insulation value of 0.8 clo. Respiration was simulated by means of an artificial lung.

Contaminant concentrations were measured at chest, front of the mouth, above the head, and in the inhaled air. For the manikin placed in a uniform flow field, he found considerable deviations from inhaled for concentrations measured in front of the head and above the head. However, concentrations measured at the chest had modest deviations from inhaled.

Divisions of the sensible heat loss from the body surface into convective and radiative heat transfer rates were developed based on experimental findings (Colin et al., 1967; Ichihara et al., 1997) using a thermal manikin. Yang et al. (2002) studied the influences of wind velocity, sensible heat loss, arranged furniture, and posture on local convective heat transfer coefficient (alpha). They concluded that the local convective heat transfer coefficient (alpha) was greatly influenced by wind velocity and slightly affectd by sensible heat loss. In addition, the value of (alpha) decreased as the manikin body approached the arranged furniture. This was clear at the feet, lower legs, thighs, hands, forearms, and upper arms of the manikin. In addition, the value of (alpha) for some parts such as the feet, lower legs, thighs and hands was affected by posture even when the sensible heat loss was constant.

Silva and Coelho (2002) studied local heat transfer coefficients for different body parts in a wind tunnel using a thermal naked manikin. Tests were performed at three flow orientations (front, side, and back), for two postures (seated and standing), and for the velocity range of 0 to 4 m/s. They concluded that peripheral parts of the body have higher heat losses than central parts. On the other hand, the head had the lowest convective heat transfer coefficient, probably due to the shielding effect of hair.

SPECIFIC AIMS FOR EXPERIMENTAL AND SIMULATION STUDIES

Samples taken at the lapel are an unproven surrogate for sampling of inhaled air. The overall aim of the study is to determine the effects of important parameters on the deviations between lapel samples and samples taken at the lips during inhalation and whether samples taken at alternative sites (forehead, neck, lapel, or adjacent to the nose) are better surrogates for inhaled exposures than are lapel samples.

Our specific aims evolved in the last two years of the study as we reviewed on-going experimental and CFD results. Based on preliminary results from experimental studies and CFD simulation, we added heating (to body temperature) and artificial breathing to the manikin for the study and two distinct postures (sitting and standing) to both the manikin and human studies. We found source location and size to be less useful and dropped them from further experimentation. We believe these changes greatly strengthened the study.

These changes were not discussed in renewal reports because they occurred in the third year and the extension year of the grant. The PI's severe, extended illness crippled much of the first year, so nearly two-thirds of the work was done after the second renewal.

The following are the original specific aims followed by what we did:

(1) Experimentally determine the relationship between concentrations at the cheek adjacent to the distal end of the nose ("AdjNose") and concentrations at the lips ("mouth") during

inhalations to determine whether the "AdjNose" site can serve as a "gold-standard" for sampling, as preliminary studies suggest.

Comment: We did this for manikins, humans, and CFD simulation. Concentrations adjacent to the nose were a reasonable, but not perfect surrogate for concentrations at the mouth.

(2) Determine whether experimental results for human subjects and a mannequin are similar to CFD predictions under conditions in which mannequins and CFD are most likely to be similar to humans. Use the results to further refine the CFD modeling (e.g., add breathing and body heat, if needed) and to determine the reliability of simple mannequins as substitute for human subjects.

Comment: The effects of study variables on concentrations were remarkably similar for the manikin and CFD simulations. We had not expected the concentrations to be similar but they were surprisingly close. CFD study found that the temperature of the body was critical, which lead us to add heating/not heating to the manikin study. We could add breathing to the CFD simulation only as a constant flow. We decided to add breathing/not breathing to the manikin studies, instead. Both heating and breathing proved to be very important to the experimental results.

(3) Use numerical simulation by computational fluid dynamics (CFD) to select the most efficient set of additional human subject and mannequin experiments to study the interactive effects of source location and source size with cross-draft velocity, uniformity, and turbulence.

Comment: We did study the effects of temperature, turbulence and other variables using CFD. However, we did not simulate the effects of modifying the source size and location because the time demands for the simulations we did were even higher than we had expected and because we came to believe that posture, heating, and breathing were far more important. Given the success we enjoyed for the specific source location and size we simulated, we are very confident that our simulations would be equally successful in predicting concentrations if the source size and location were changed.

(4) For the sets of conditions selected above, conduct mannequin experiments to study the main and interactive effects of source location and source size with cross-draft velocity, uniformity, and turbulence. For a subset of tested conditions whose size depends on the reliability of mannequin results, repeat the tests with human subjects doing simulated work tasks, including tasks that involve low movement to mimic non-moving mannequins.

Comment: As stated above, we concluded that the source size and location were much less important than the effects of posture, velocity, hairlength, etc for humans. Therefore we chose only one source size and location. We placed the source in the subjects' hands and fixed the source size at 9". We considered that the most common and important location for cases where over-exposures actually occur.

(5) Further refine the CFD modeling, then determine the congruence of CFD-modeled results with a experimentally observed results for humans and mannequins. If CFD is reliable for the tested conditions, employ the CFD model to extrapolate and interpolate to conditions we did not test with human subjects.

Comment: As discussed in the report in later section, the CFD simulation results were highly congruent with the manikin and the manikin was highly congruent with results from humans.

(6) Using the results from the studies above, find simple mathematical relationships to predict inhaled concentrations using samples taken at the lapel and other surrogate sites. If such relationships predict with acceptable precision, it may be possible to "correct" sample results from surrogate sites to predict inhaled concentrations. If not, then use of the most reliable sampling site may be the best solution.

Comment: As is discussed later, it was not feasible to "correct" concentrations at surrogate sites to predict mouth concentrations. The deviations were too sensitive to too many variables, especially posture and velocity. Posture is the most problematic. We investigated only standing and sitting slightly crouching forward. Given the profound differences between results for sitting and standing, it is quite possible that even modest differences in sitting or standing postures could strongly affect deviations between concentrations at the mouth and at other locations. Likewise, the effects of velocity were non-linear ("V"- shaped) and changed interactively with posture.

(7) Using the experimental results, determine the most reliable alternative location (e.g., neck or cheek) that should be employed for conditions in which lapel sampling proves unreliable.

Comment: This was done and is discussed at length in the report.

Goals for Numerical Simulation (CFD)

The basic goal of the CFD portions at each stage of the study is to make the CFD model as accurate as possible for exposure conditions when the source is nearby. Specifically, the CFD will be employed to determine:

(1) The most important variables affecting both the concentration levels and ratios of concentrations at the sampling sites.

Comment: CFD simulations correctly showed cross-draft velocity, body temperature, and turbulent intensity to be highly important to both concentrations and ratios of concentrations. The simulations were done only for the standing condition, so the effects of posture were not predicted.

(2) The most important and efficient sets of conditions to investigate with human subjects.

Comment: As is discussed later, the interaction of cross-draft velocity and body temperature were profoundly important and were correctly predicted by CFD, leading to marked changes to the experimental study. In addition, early CFD modeling suggested which velocities were the most important to results, leading to changes to the experimental program.

(3) The interactive effects of independent variables on the relative concentrations at the sampling sites for a broad range of conditions, including those we cannot test within the wind tunnel.

Comment: Because of CFD findings, we increased the breadth of velocities used for experimental tests.

(4) The conditions for which the CFD model does well and the conditions for which it does not.

Comment: CFD did extremely well for all of the conditions we tested.

APPARATUS, PROCEDURES, RESULTS, DISCUSSION, CONCLUSION FOR EXPERIMENTAL STUDIES

Apparatus for Experimental Studies

The apparatus evolved over the first year but was largely consistent with the proposal.

Manikin

The current manikin (see Figure 1) was a 66" high, anthropometrically scaled (including facial features and short hair) male with hollow cavities in the head, torso, legs and arms. It has a rubber skin that feels reasonably like real skin. The manikin has joints in shoulders, hips, and knees. This enables it to stand or sit in a range of postures. The manikin dimensions matched the 50th percentile for women and the 5th percentile for men.

Figure 1: Test Mannikin

Figure 2: Wire used for heating

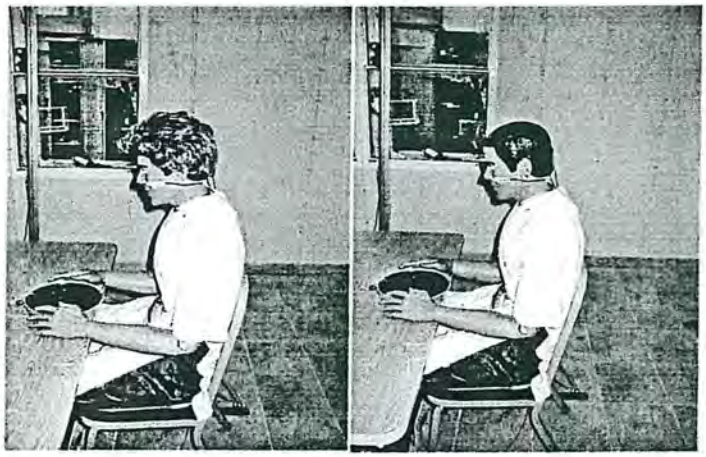

Figure 3: Clothing and Hairstyle for seated manikin

Heating the manikin head and torso skin to simulate body heat of humans was done by placing lengths of heated wires within the torso (see Figure 2) and the head and energized them with 90 watts of power to produce nearly uniform skin temperatures on the head and torso. By trial and error, we achieved the uniformity by: 1) adjusting the fraction of the wire in the head and in the torso, and 2) adding insulation at selected locations within the cavities. The average skin temperature for the manikin during experiments was ranged from 33 to 37 °C.

Clothing the manikin (see Figure 3.4) was done with loose-fitting pants and a summer weight short-sleeved shirt ("trim"). Clothing insulation was roughly 1.0 clo. The manikin was "bald" during all tests for the first manikin study and alternatively bald and wearing a wig for the second manikin study.

Figure 4: Artificial lung

Breathing by the manikin was simulated using an artificial lung as shown in Figure 2. The lung had a maximum volume of 1 liter and simulated the breathing of an average sedentary person performing light physical work. The adjusted breathing cycle consisted of inhalation (2.0s) and exhalation (2.0s). The frequency of exhaled/inhaled air for sedentary activity ranged 10 – 20 per minute which gave a pulmonary ventilation rate of 10 – 20 lpm (Christensen, 1964, cited in Kroemer and Grandjean, 1997). During experiments, pulmonary ventilation ranged from 16 to 18 lpm. While, Figure 5 illustrates a schematic diagram of the artificial lung and its breathing circuit. The lung breathing rate was adjusted by a lever. A compressed air piston assembly drew air in and expelled the same air through 1" diameter Teflon tubing. The average exhaled breath temp was 96-98 F. Metabolism, respiration, heart rate and temperature varry as a function of work load (Christensen, 1964, cited in Kroemer and Grandjean, 1997).

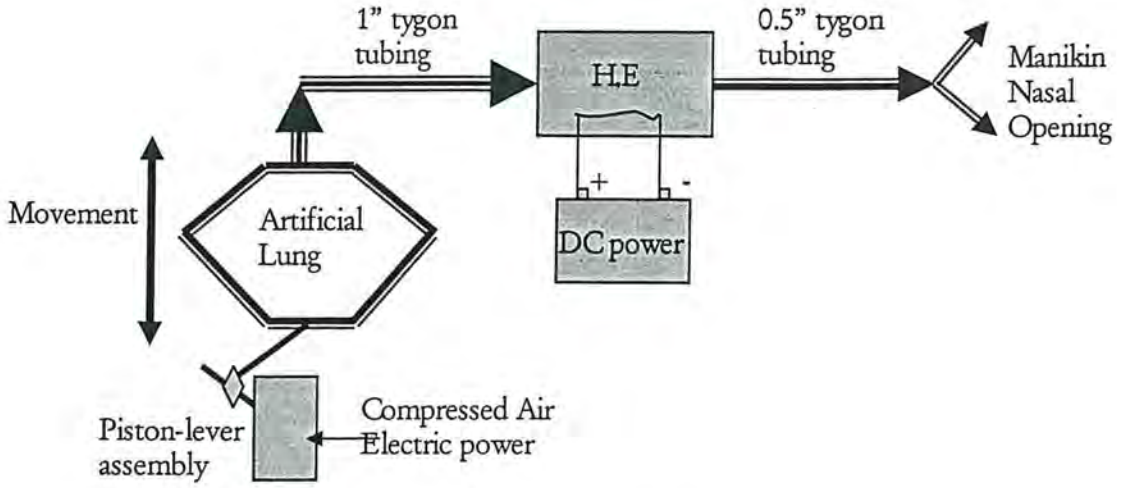

Figure 5: Schematic Flow Diagram for the Breathing Circuit

Human Subjects

The six human subjects were all WVU graduate students except one who was a visiting faculty member. They came from India, the Middle East, North Africa, USA, and Korea. They ranged from very short to tall and thin to well-rounded and included 4 females and 2 females. They wore light clothing that was roughly similar to the manikin's.

Wind tunnel

The wind tunnel had no reducing section and was relatively short compared to its length as shown in Figure 6. The wind tunnel was equipped with upstream and downstream HEPA filters and downstream activated charcoal filter panels. The working section (between the HEPA filters) was 32 ft long, 12 ft wide, and 9 ft high. The manikin was tested at the middle of the wind tunnel, thus keeping a distance of nearly 4 ft from each wall. The combined cross-section of the full sized tables with chairs and the manikin blocked less than 15% of the wind tunnel cross-section. Ethanol was removed by over 300 lbs of activated charcoal before air exits wind tunnel cross section to the fan.

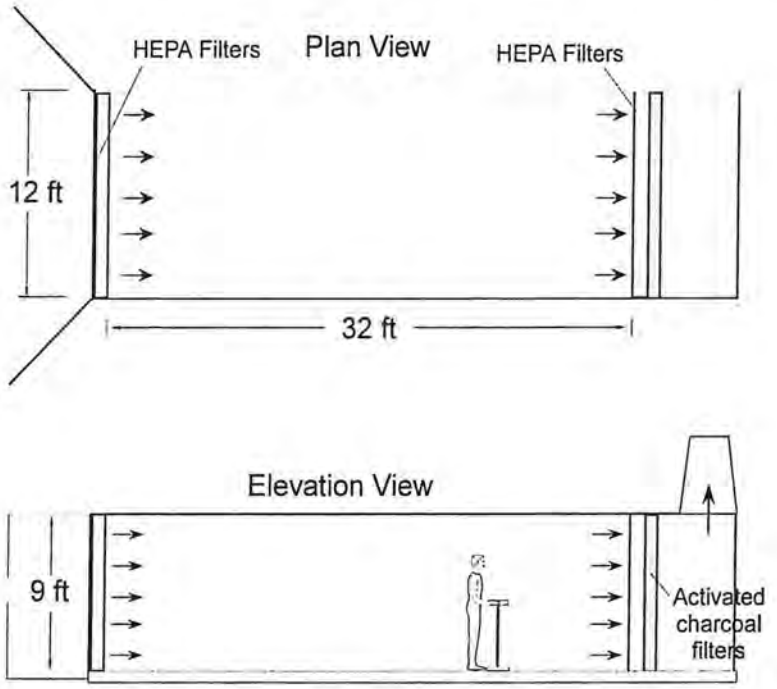

Figure 6: Wind Tunnel

To reduce thermal buoyancy effects due to different temperatures at the floor and ceiling, the floor of the building was covered by 0.75" styrene foam insulating sheet, which was overlaid by 1" plywood sheet and linoleum floor covering. Infrared thermometry had found temperatures in the air and at the walls, ceiling and floor to be within 2 °C winter and summer. Repeated rounds of constant temperature anemometry (CTA) measurements taken at 6" intervals vertically and 12" intervals horizontally found a coefficient of variation of 10% for velocity along the axis of the wind tunnel. The turbulent intensity ranged up to 15-20% near the ceiling and was 3-5% in the middle section where the manikin stands. The wind tunnel fan was controlled by a variable frequency drive allowing a range of wind tunnel velocities of 10 to 155 ft/min.

Temperature, humidity and barometric measurements

Temperatures of surfaces were measured with an infrared thermometer (Oakton, model number EW-35629 with accuracy of ±1% or ±1 deg C and repeatability of ±0.5% or ±1 deg C of full scale). Multiple points were measured on the manikin's head and torso and on the wind tunnel walls, ceiling, and floor. Air temperatures were measured with a calibrated dry bulb thermometer. Humidity was determined from a standard sling psychrometer, and barometric pressure was measured with a standard laboratory mercury barometer.

Gas and vapor sampling apparatus for wind tunnel studies

Samples were drawn from each sampling probe on the manikin in separate Teflon™ sampling lines. Each sampling line started with a 1/8" polypropylene probe pinned to the manikin's shirt or taped to the manikin face with tape. Each probe connected to roughly 4 ft of 1/8" Teflon™ tubing, which ran over the shoulder to the small of the back. There each line connected to 0.25" Teflon™ tubing, which run to the inlet port of a SKC Air-Check low-flow sampling pump and

from the pump's outlet port to a 3L Teflon™ sampling bag. The sampling pumps were calibrated with a BIOS International "Dry-Cal" (DCL-ML Rev 1.08) to a flow rate of 0.15 L/min.

Generation and dispersion of tracer gas mixtures

Ethanol was injected by a Cole-Parmer syringe pump (74900 series) into a chamber through which 1 L/min of nitrogen flowed. The ethanol dripped onto an electrical resistor energized by 10 watts of power from a regulated DC power source. The resistor was wrapped with aluminum foil to enhance evaporation, which appeared to be nearly instantaneous. The nitrogen flowrate was regulated and measured by an AALBORG mass flow meter (GFM171 flow range 0-1000 ml/min). The mixture was carried by 0.25 inch Teflon™ tubing to a 9" diameter, 1" deep aluminum pie-pan that served as a contaminant source. An acrylic cover was glued "air-tight" to the pie-pan and drilled with 99 one-eigth inch diameter holes that were uniformly dispersed across the acrylic cover. The tracer gas mixture passed from the Teflon™ tubing to a connection fitted to the sides of the pie-pan and from there through the holes in the acrylic cover. The exit velocity through the 1/8" holes was less than 1 ft/min. Extensive testing showed excellent repeatability (95% withinin source concentrations). The sampling bags used for testing the high source concentrations were not used for exposure sampling. Each bag filled about 2L during sampling. After sampling, the bag contents were analyzed, then the bags were purged and flushed with clean air and held in readiness for reuse in the next day of sampling. Analysis of ethanol/air mixtures was performed using Photovac Voyager gas chromatograph (GC) equipped with a photo-ionization detector (PID), each calibrated using headspace techniques to create a known concentration in a Teflon™ bag.

Procedures for Experimental Studies

Some aspects of procedures are described within the Apparatus section.

Sampling and Analyses

All locations were sampled simultaneously for 22 minutes for each condition. After the first 7 minutes the bags were flushed with the same concentrations as that of correct exposure. Sampling then continued for 15 minutes. Within 2 hours, the concentration of ethanol and air mixture in each bag was analyzed using Voyager gas chromatograph with a photo ionization detector (PID). Before analysis, samples collected from the source were diluted until the expected level was about 50 - 60 ppm then analyzed.

Calibration

The calibration of the PID sensor was verified every day of use by withdrawing ethanol head space air with a micro syringe and injecting it into a Teflon™ bag pre-filled with 2.4 L of clean air.

Sampling pumps were calibrated with the mass flow meter or electronic bubble meter and were verified with a 1 L bubble meter.

Leaks and other problems

Leaks and adsorption in the sampling pumps, tubing, and bags were measured by attaching bags filled with known concentrations of the tracer gases to a given sampling probe and drawing the air into sampling bags downstream of the sampling pumps. Losses of ethanol vapor to the plastic

tubing and bags were reduced to about 5% by using Teflon™ lines and bags and by pre-treating the lines and bags for 7 minutes. This was done by the simple expedient of dumping the first 7 minutes of collected sample without flushing with clean air.

Human Subjects

The PI explained the study protocol and reviewed the IRB-approved consent form with all subjects. Probes were attached to subjects' faces using hypo-allergenic medical tape and were pinned to their shirt or blouse using safety pins. Subjects were entertained with music of their choice and were given opportunities to change postures and move about between sampling tests. No problems were reported by subjects other than boredom and delays in being paid.

Methodology for Experimental Studies

The study was divided into 4 separate studies:

1. Manikin Study I: Investigate interactive effects of cross-draft velocity, posture (sitting vs standing), and body temperature (human normal vs ambient) on concentrations and ratios of concentrations at each surrogate site.
2. Manikin Study II: For a heated manikin, investigate interactive effects of breathing, hair length (bald vs short), cross-draft velocity, and posture on concentrations and ratios of concentrations at each surrogate site.
3. Human Studies: Investigate the interactive effects of posture, velocity on concentrations and ratios of concentrations at each surrogate site. Small exploratory study was included on the effects of breathing vs breathing through a tube and another on task (keeping still vs stacking).
4. Computational fluid dynamics (CFD): Preliminary studies determined the most efficient methods for CFD simulation. Later studies simulated the interactive effects of velocity, body temperature, and turbulence for the standing condition.

The two manikin studies and the human study followed nearly the same procedures. They are described next. The CFD studies will be discussed in a separate section following the manikin and human studies.

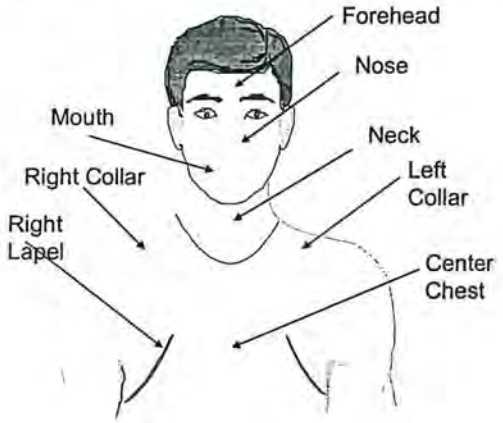

Figure 7: Sampling Locations

Variables and Fixed Conditions

The dependent variables were: 1) concentrations measured simultaneously at several locations on the torso and head of a single, anthropometrically-correct manikin or a human subject, and 2) the ratios of concentrations at other locations to the concentration measured at the mouth (see Figure 1). The independent variables are listed in Table 1. Two manikin studies were conducted with each having full factorial designs. For the second manikin study, the unheated condition was not used since heating was found to be important in Study I (see Results) and is more lifelike than non-heating.

Table 1: Levels for Independent Variables for Studies Manikin I, Manikin II, and Human

Condition	Study I	Study II	Human
Cross Draft velocity (fpm)	11, 27, 48, 82, 104	Same	11, 27, 48, 104xx
Body Heat	unheated, heated	Heated, only	Normal
Posture	Standing, seated	Same	Same
Hair length	Bald	Bald, 3" length	1" to 12"
Breathing	No	Yes, No	Normal, thru tube

There were two replications for each combination of independent variables. The significance of the independent variables and their interactions for each study were analyzed using Data desk (Odessa, NY) statistical software. The fixed conditions for the manikin study included the use of one anthropometrically-correct manikin wearing summer clothes. The manikin was stationary and none of its limbs were moved during a test. For all tests, the manikin's hands were placed on each side of the tracer gas source (a 9 inch pie-pan) in a manner intended to simulate light assembly work. The manikin was placed in the middle section of wind tunnel with its back oriented to the cross draft velocity (see Figures 2 and 6). Body posture (seated and standing) was included in this study for two main reasons: 1) postures are commonly found in work environments, and 2) the orientation of legs and arms to cross draft is perpendicular in the standing position and parallel in seated positions. Thus, it is plausible that body posture will affect air flow patterns around the manikin and hence change concentration gradients with in the breathing zone.

For the human study, the fixed conditions were the same placement in the wind tunnel as the manikin with similar postures and the same back to flow orientation to the airflow. The humans had two tasks, either: 1) keep as still as possible, or 2) move blocks from one side of the pan to another and back at a "very relaxed" pace (about 1/second). For some tests subjects breathed through a 24", 3/8" diameter tube to remove the kinetic effects of exhaled breath.

Manikin Study I Results, Discussion and conclusions

Results of Manikin Study I

For this study, the manikin was either sitting or standing and was either heated or not heated. It did not breathe or wear a wig, but it was clothed. This study was a complete factorial design with each condition tested twice in random order. Initial tests and replicates were always done at different days.

One goal of this study was to find the locations that act as the best surrogates for true inhaled concentrations. Another goal was to investigate the effects of posture, heating and velocity on concentrations measured at each location. As will be shown, all were highly significant. Although the manikin inhaled and exhaled through its nose in a realistic manner, its "lungs" did not absorb ethanol. Hence a sample taken at the mouth in the exhaled air stream should differ negligibly from a sample taken of inhaled breath alone. For that reason the concentrations at the

mouth are treated here as the "gold standard" to which all others are compared. As will be shown, the concentrations fell into three groups with similar behavior: those at the face (C_{mouth}, C_{nose}, $C_{forehead}$), those at the shoulder area (C_{neck}, $C_{l.collar}$, $C_{r.collar}$), and those at the chest ($C_{c.chest}$, $C_{l.lapel}$, $C_{r.lapel}$).

1 Repeatability of C_{mouth}

Two samples were taken simultaneously at the right edge of the mouth less than 1 mm apart. The coincident locations were intended to be redundant checks. Ideally, there should be no systematic differences between C_{mouth_1} and C_{mouth_2} regardless of the levels of other independent variables. Figure 8 plots C_{mouth1} against C_{mouth2} with all conditions included. Without accounting for velocity or any other independent variable, the two dependent variables were highly correlated (R-sq = 0.996). The linear regression slope of 1.0038 and intercept of zero confirm the two are indistinguishable. Furthermore, ANOVA found no significant effects of any independent variable. These together suggest that the samples are highly repeatable and thus that difference between other locations measured at the same time represent real deviations, not sampling or analytical error. Given the trivial differences between C_{mouth1} and C_{mouth2}, the average of both values was used for comparisons to all other locations and is henceforth referred to as C_{mouth}.

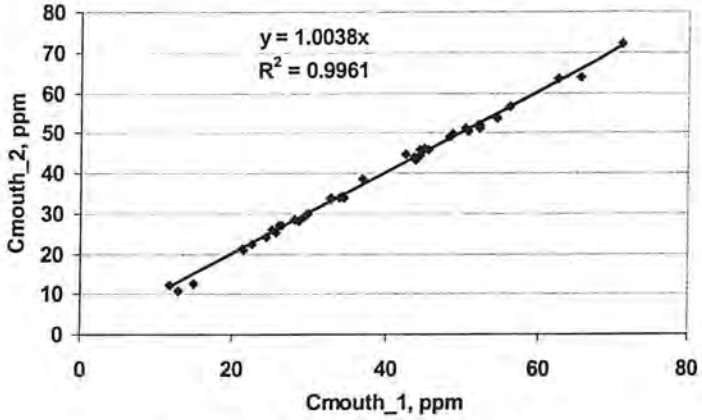

Figure 8: C_{mouth1} versus C_{mouth2}

As shown in Table 2, the average concentration values (ppm) varied with sampling location, velocity, heating, and posture where comparisons between concentrations must be matched to similar conditions. Figures 4.2 to 4.10 show the scatter and mean of concentrations and log transformed values with velocity for all sampling locations.

Table 2: Average Concentrations (Ppm) For Each Velocity Level And Manikin Treatment

Treatment	V,fpm	$C_{c.chest}$	$C_{l.lapel}$	$C_{r.lapel}$	C_{neck}	$C_{l.collar}$	$C_{r.collar}$	C_{mouth}	C_{nose}	$C_{forehead}$
Heated/ Standing	11	31.6	23.9	27.0	31.8	30.1	28.8	29.5	28.5	25.3
	27	49.3	41.1	46.9	52.5	44.1	39.4	61.3	57.8	52.0
	48	103.1	77.9	96.3	73.1	61.8	71.2	57.1	52.7	47.3
	82	51.6	43.2	46.4	46.5	37.8	44.1	44.6	41.3	39.4
	104	38.0	34.5	33.9	35.8	27.6	33.5	35.5	33.2	32.6
Heated/ Seated	11	18.6	15.6	14.4	15.0	16.3	17.4	12.8	10.1	7.8
	27	22.6	21.9	20.4	21.3	21.3	20.3	22.7	21.5	14.9
	48	32.0	31.0	29.5	43.0	37.2	38.3	48.5	50.5	37.1
	82	23.6	21.1	18.3	20.6	20.7	20.0	29.6	31.0	26.2
	104	18.4	16.2	15.3	16.1	17.0	15.3	21.9	21.8	18.9
Unheated/ Standing	11	116.5	135.3	83.9	68.5	70.2	63.9	62.9	66.8	42.2
	27	79.2	92.4	73.5	41.7	44.4	44.0	42.1	36.6	27.6
	48	67.3	76.2	54.1	40.0	43.2	40.6	33.4	29.8	30.1
	82	52.0	49.5	48.1	35.3	36.9	34.2	30.0	27.3	19.5
	104	31.8	42.5	28.5	21.8	22.3	22.9	21.2	17.8	15.6
Unheated/ Seated	11	41.8	51.7	42.6	56.4	61.2	53.2	58.8	58.2	52.7
	27	30.0	33.0	30.7	44.5	43.3	38.8	51.0	53.2	46.0
	48	22.9	26.1	23.2	39.8	39.3	35.6	47.4	51.5	44.6
	82	20.2	22.8	22.7	34.6	33.9	32.5	38.8	38.9	33.6
	104	15.7	19.6	17.7	32.8	30.8	24.7	34.3	34.4	31.3

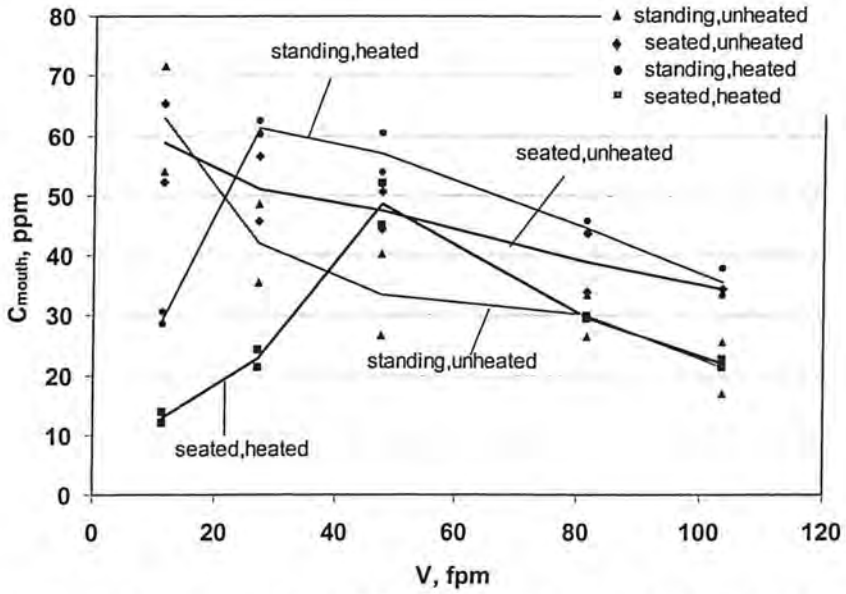

Figure 9a: Scatter and mean plot of C_{mouth} vs. velocity for all manikin treatment

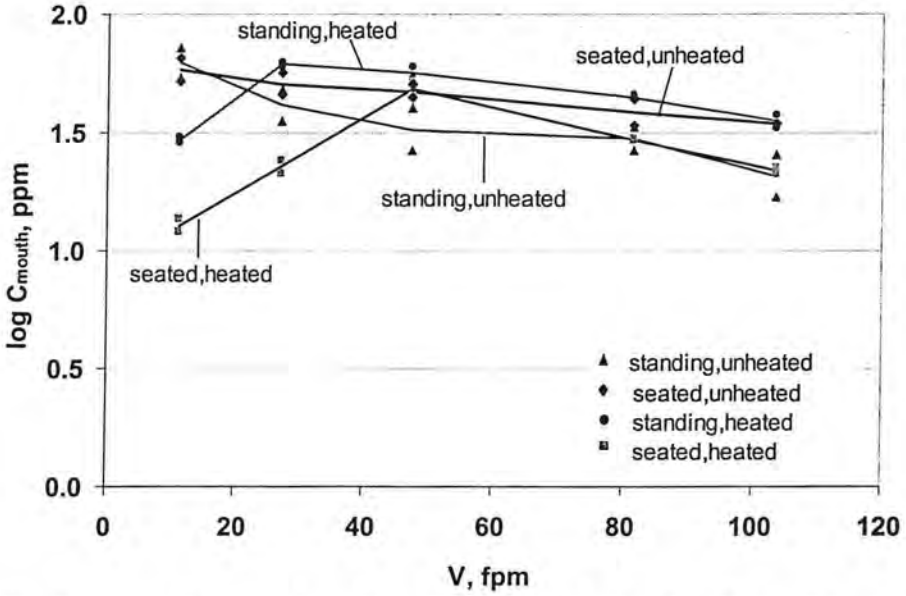

Figure 9b: Scatter and mean plot of log C_{mouth} vs. velocity for all manikin treatment

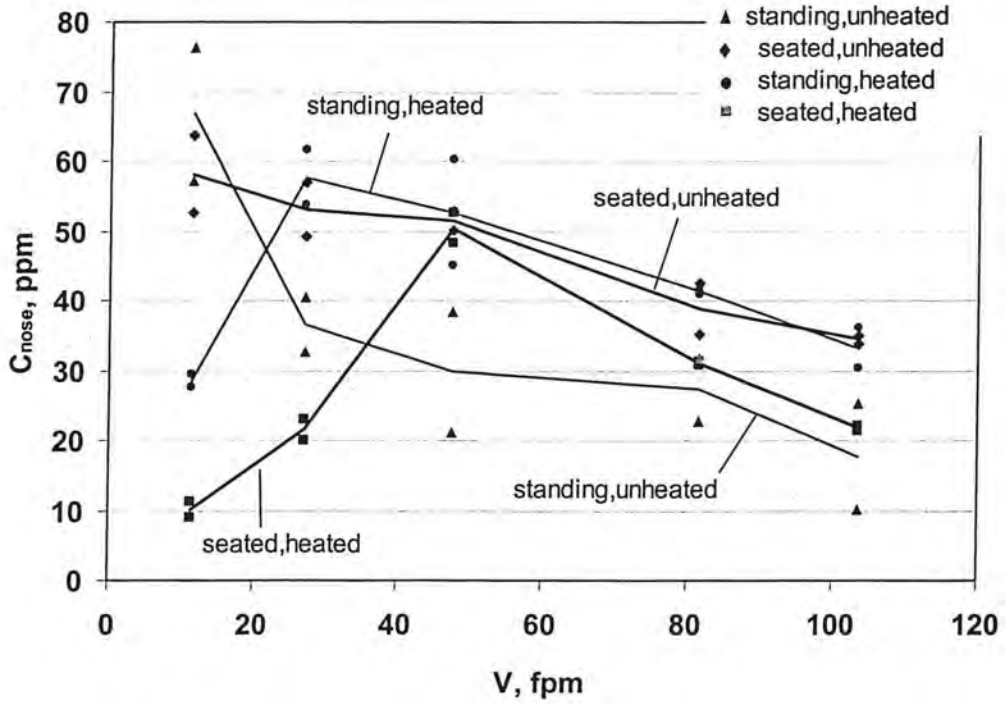

Figure 10a: Scatter and mean plot of C_{nose} vs. velocity for all manikin treatment

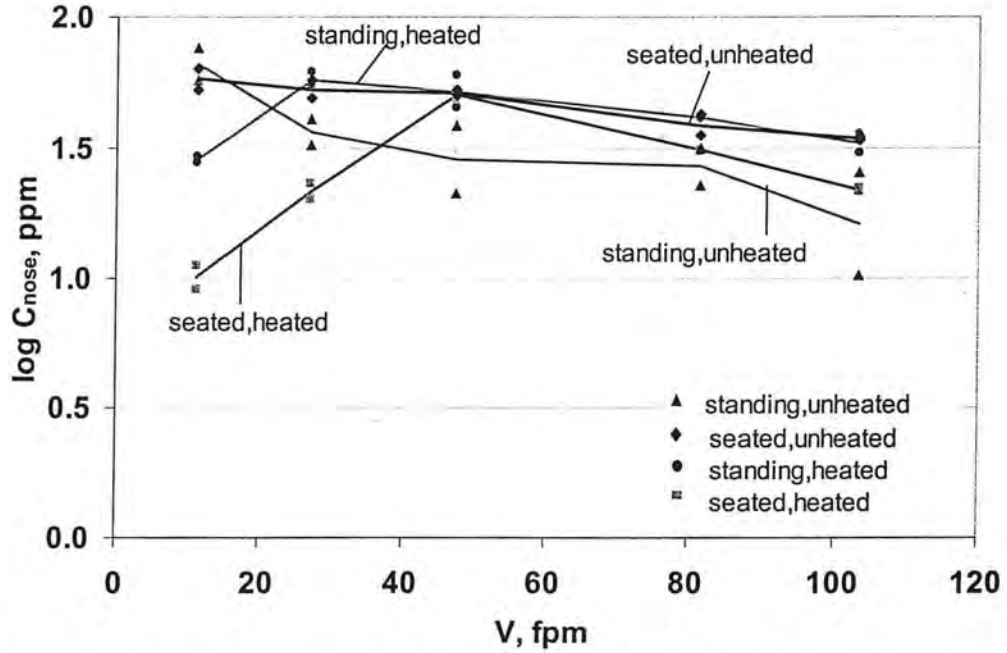

Figure 10b: Scatter and mean plot of log C_{nose} vs. velocity for all manikin treatment

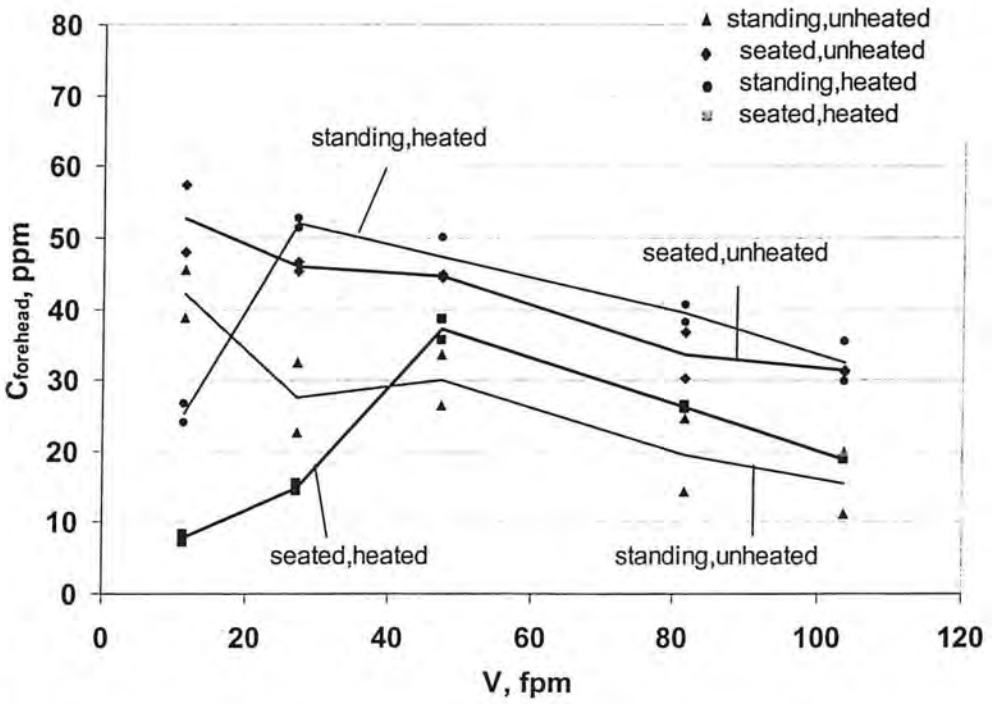

Figure 11a: Scatter and mean plot of $C_{forehead}$ vs. velocity for all manikin treatment

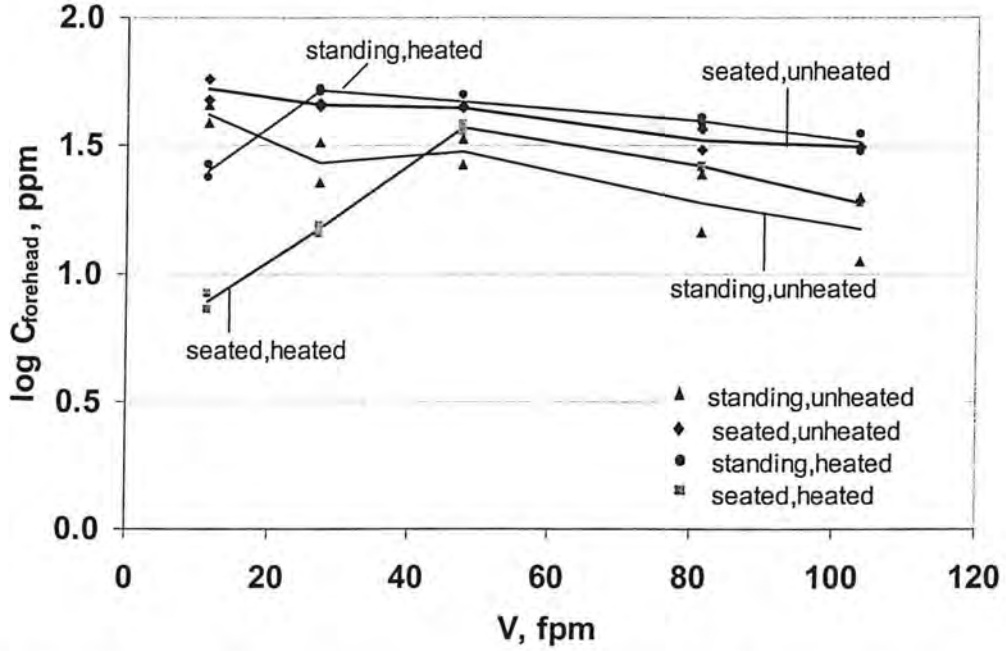

Figure 11b: Scatter and mean plot of log $C_{forehead}$ vs. velocity for all manikin treatment

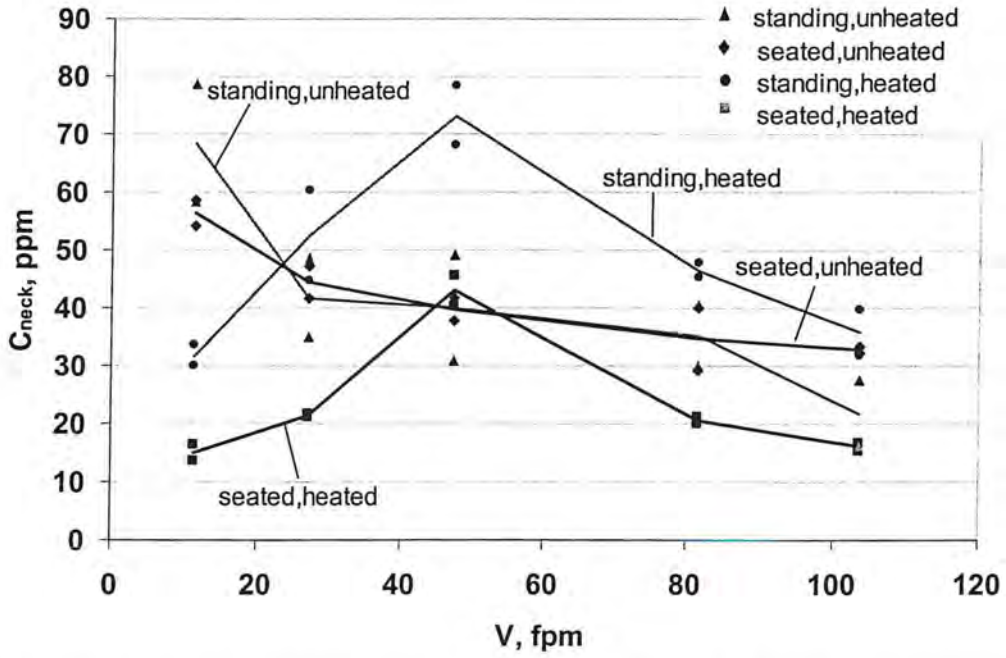

Figure 12a: Scatter and mean plot of C_{neck} vs. velocity for all manikin treatments

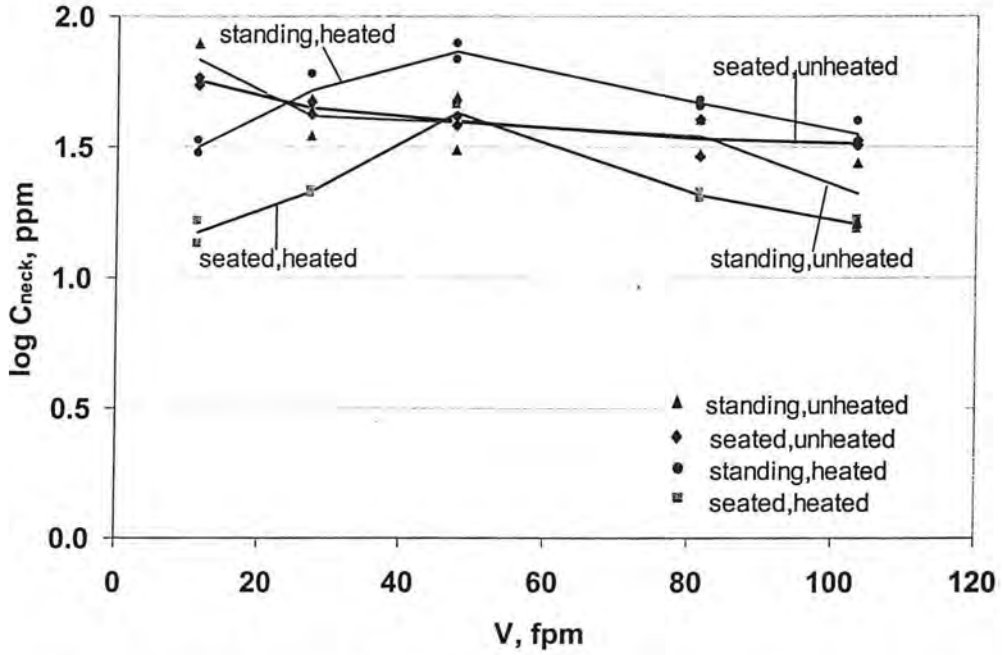

Figure 12b: Scatter and mean plot of log C_{neck} vs. velocity for all manikin treatments

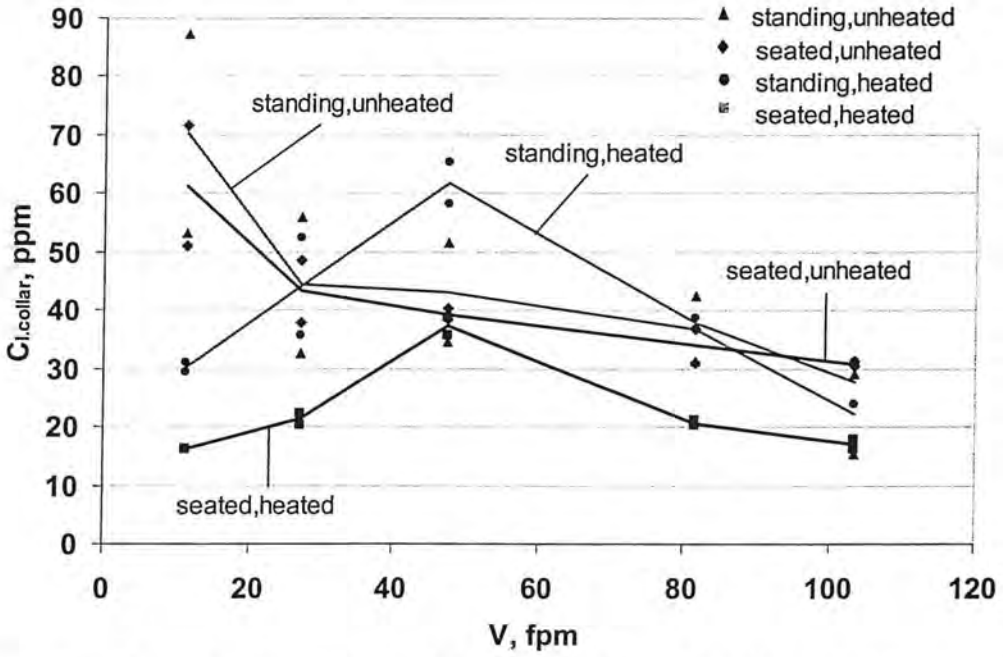

Figure 13a: Scatter and mean plot of $C_{l.collar}$ vs. velocity for all manikin treatments

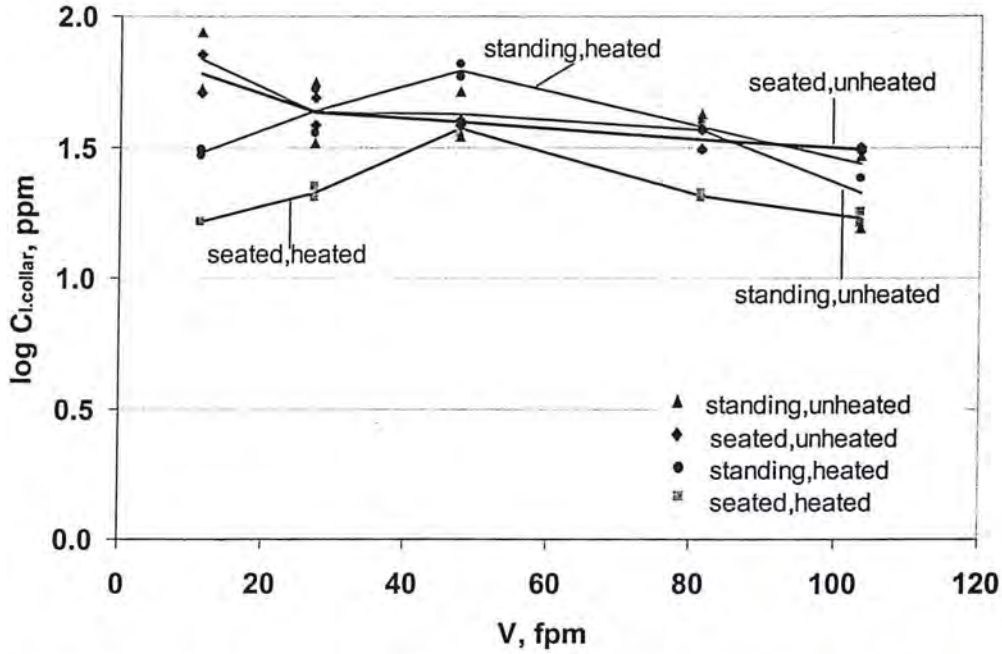

Figure 13b: Scatter and mean plot of log $C_{l.collar}$ vs. velocity for all manikin treatments

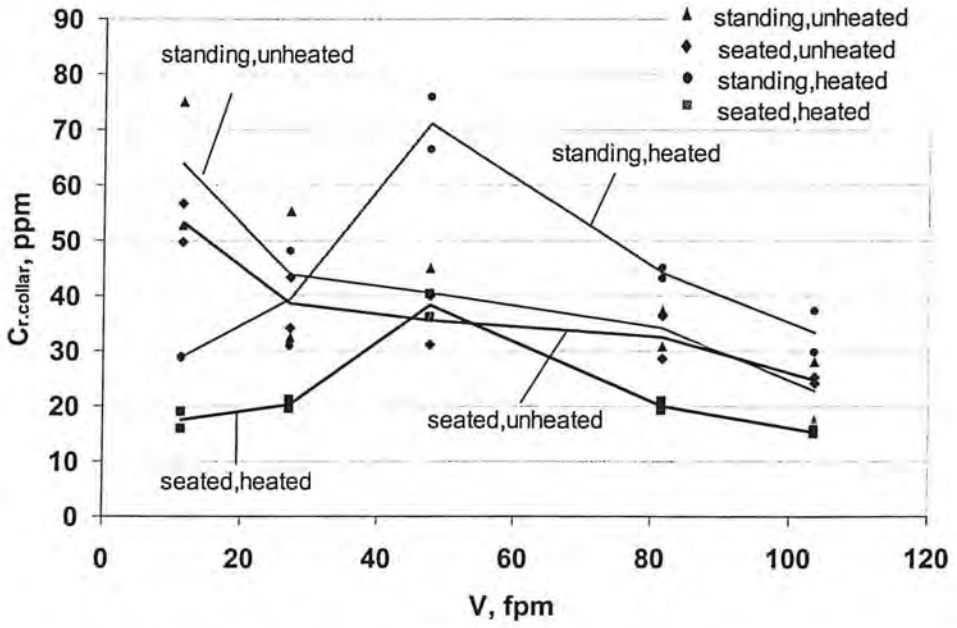

Figure 14a: Scatter and mean plot of $C_{r.collar}$ vs. velocity for all manikin treatment

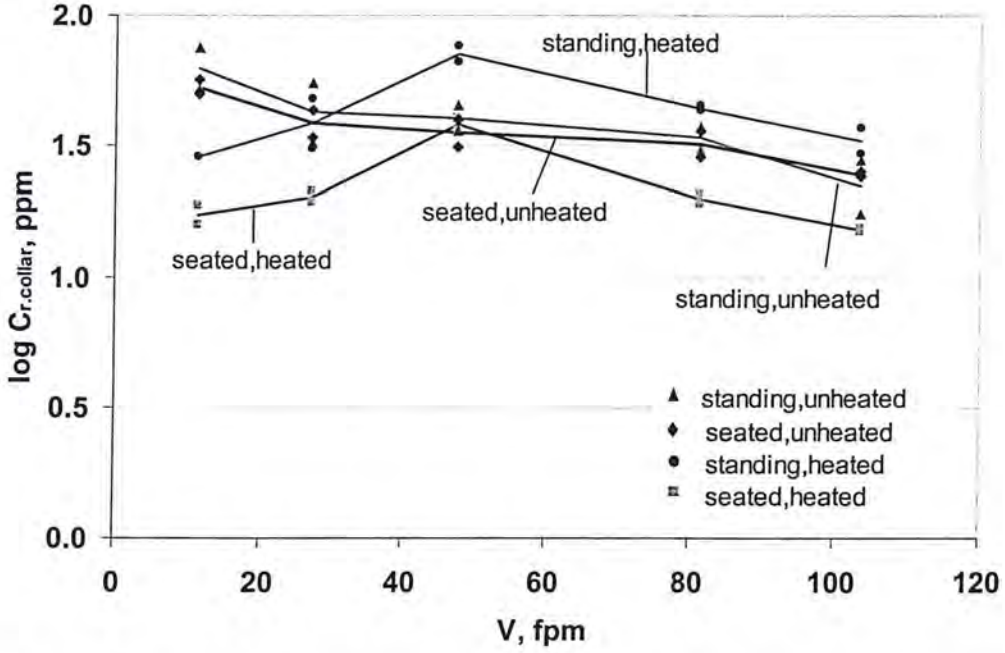

Figure 14b: Scatter and mean plot of log $C_{r.collar}$ vs. velocity for all manikin treatment

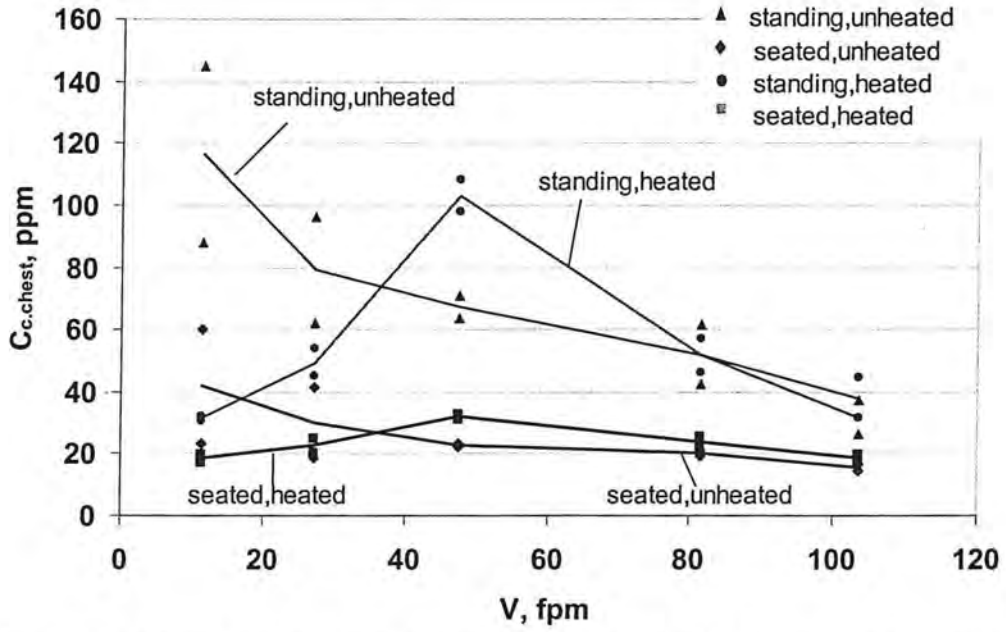

Figure 15a: Scatter and mean plot of $C_{c.chest}$ vs. velocity for all manikin treatment

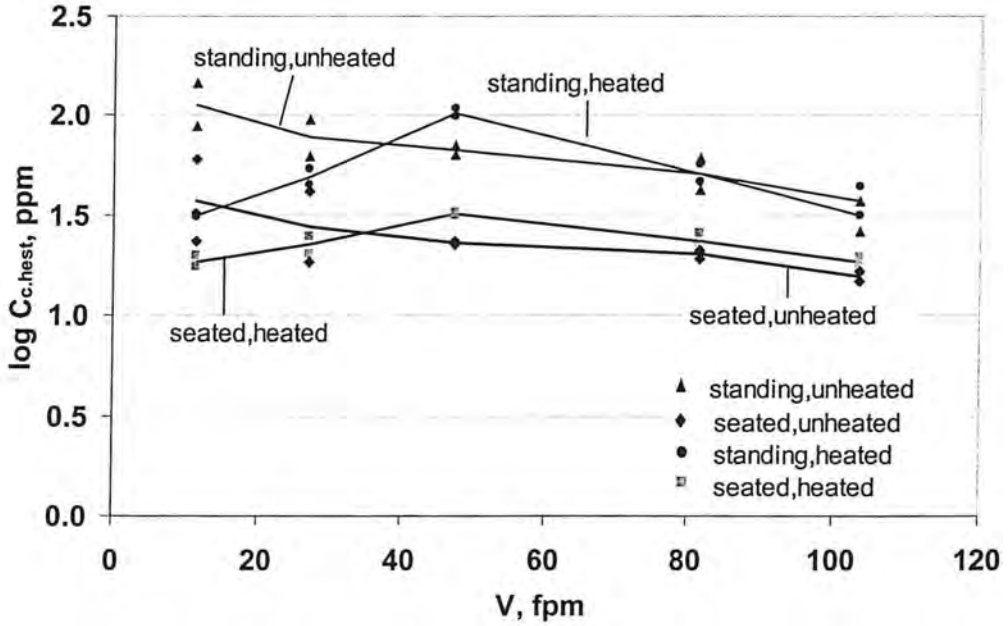

Figure 15b: Scatter and mean plot of log $C_{c.chest}$ vs. velocity for all manikin treatment

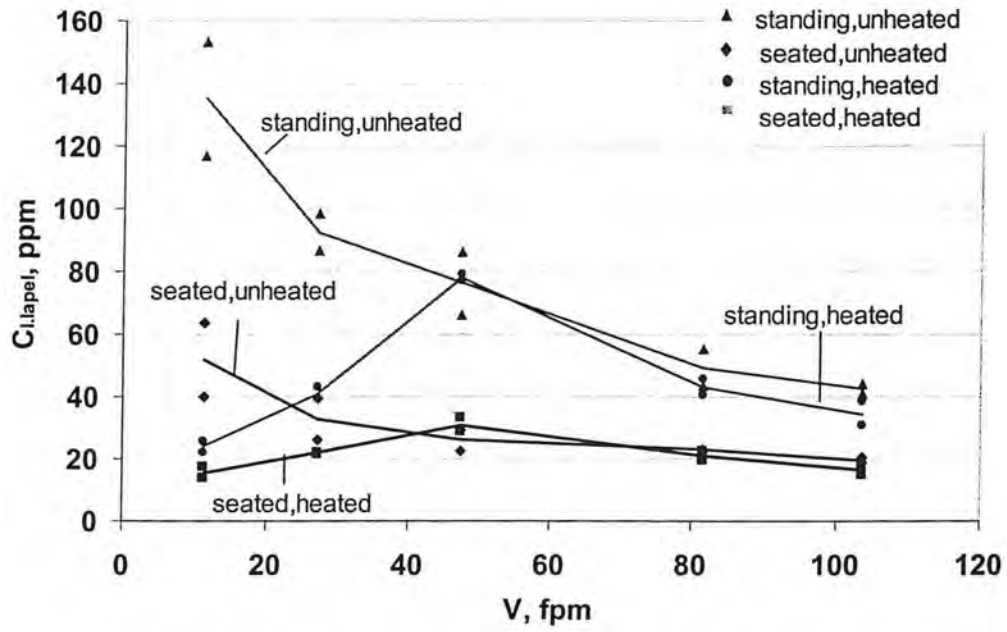

Figure 16a: Scatter and mean plot of $C_{l.lapel}$ vs. velocity for all manikin treatment

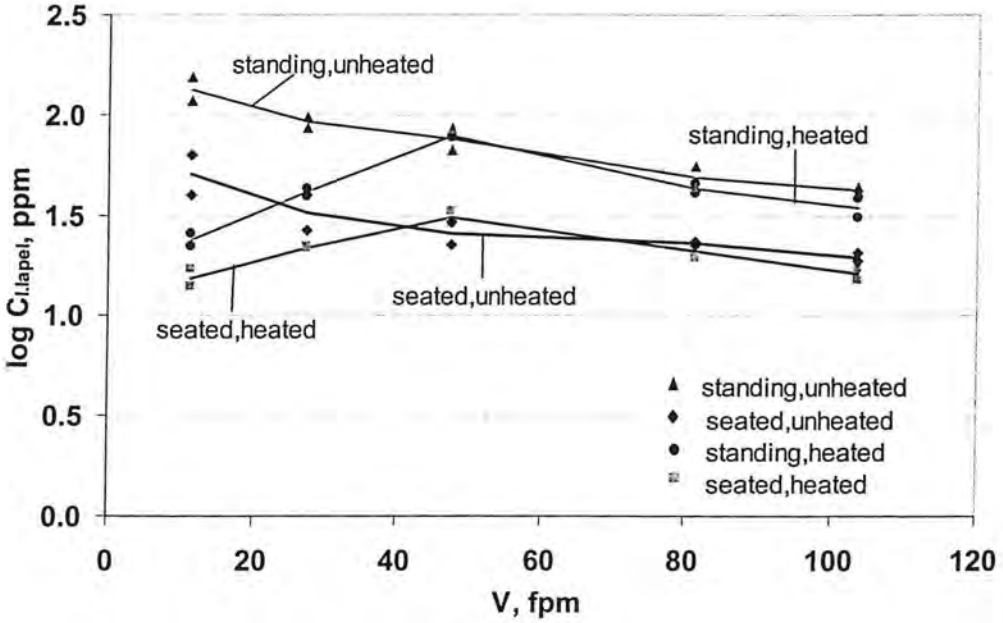

Figure 16b: Scatter and mean plot of log $C_{l.lapel}$ vs. velocity for all manikin treatment

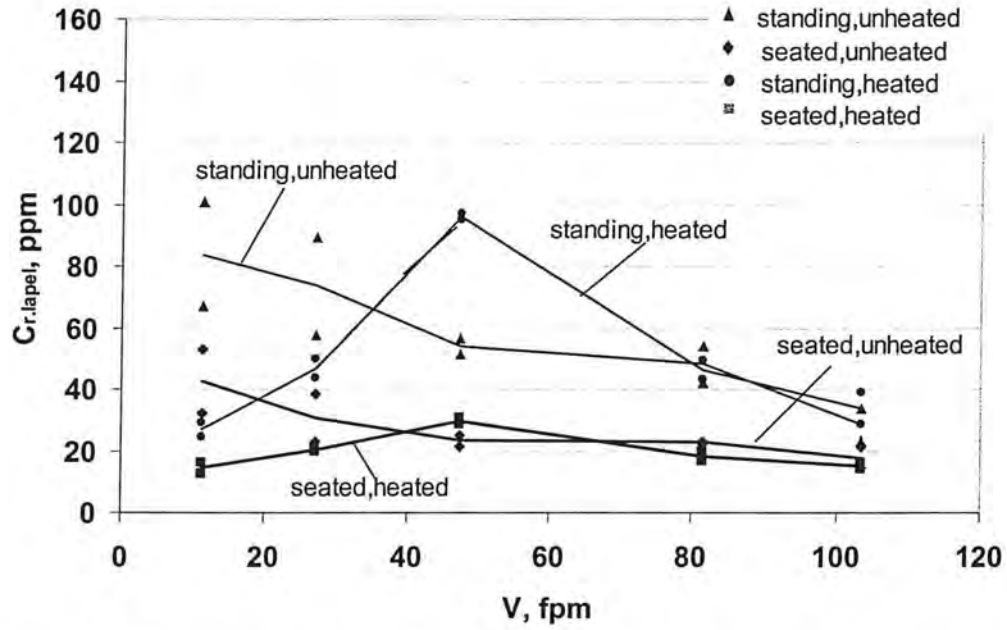

Figure 17a: Scatter and mean plot of $C_{r.lapel}$ vs. velocity for all manikin treatment

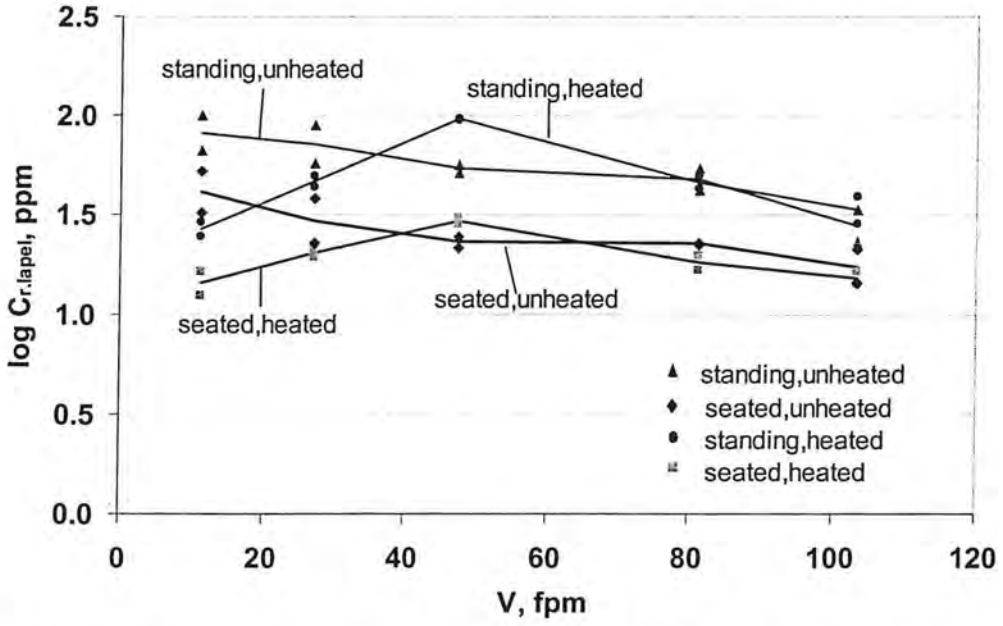

Figure 17b: Scatter and mean plot of log $C_{r.lapel}$ vs. velocity for all manikin treatment

2 Effects of Independent Variables on all Sampling Locations

As listed in Table 2, values of concentrations measured at the face (C_{mouth}, C_{nose}, $C_{forehead}$), shoulder (C_{neck}, $C_{l.collar}$, $C_{r.collar}$), and chest ($C_{c.chest}$, $C_{l.lapel}$, $C_{r.lapel}$) varied with wind tunnel velocity, heating, and posture.

4.2.1 Velocity

As shown in Figures 4.2 – 4.10, the effects of velocity on sampling locations appeared to be strikingly different for heated and unheated treatments but were similar for standing and seated postures. For unheated conditions, concentrations at all sampling locations fell more or less monotonically with increasing values of velocity. This behavior agrees with Flynn et al. (1991) and Kulmala (1996) results for their unheated manikins. These results disagree with Guffey and Flanagan (2001) whose concentrations increased monotonically with increasing velocity. However, it should be noted that the Reynolds numbers for this study (Re = 1200-12000), Guffey and Flanagan (Re = 1000-7200), Kim and Flynn (Re = 3419-17094), and Kulmala (Re = 6300, 9500, and 12700) were quite different, perhaps accounting for the differences in results between Guffey and Flanagan and the rest.

For the more lifelike conditions, a heated manikin, concentrations at all sampling locations varied in an inverted-V shape relationship with velocity for both sitting and standing postures (see Figures 9-25). C_{mouth}, C_{nose}, and $C_{forehead}$, had the peak concentartions values at 27 fpm for standing posture and at 48 fpm for sitting (see Figures 4.2 - 4.4). However, concentrations at the shoulder, C_{neck}, $C_{l.collar}$, $C_{r.collar}$, and at the chest, $C_{c.chest}$, $C_{l.lapel}$, $C_{r.lapel}$, had peak concentrations values at 48 fpm only for both sitting and standing postures (see Figures 4.5 - 4.10). Those results agree with Brohus (1997), who employed a full-sized heated, breathing manikin wearing heavy clothing and wig. The velocity range for Brohus was 0.05, 0.15, 0.3, and 0.45 m/s, while, the Reynolds numbers were (1000, 3000, 6000, and 9000).

The effect of velocity on C_{mouth}, C_{nose}, and $C_{forehead}$, is shown in Table 2. For the heated manikin in a standing posture, C_{mouth}, C_{nose}, and $C_{forehead}$, doubled as velocity increased from 11 to 27 fpm and decreased by half as velocity increased again from 27 to 104 fpm. On the other hand, for the seated posture, C_{mouth}, C_{nose}, and $C_{forehead}$, increased four times as velocity increased from 11 to 48 fpm and decreased by half as velocity increased from 48 to 104 fpm. The effect of velocity on C_{mouth}, C_{nose}, and $C_{forehead}$, is substantial and the peak concentration values occurred at 27 fpm for standing and at 48 fpm for sitting posture. For unheated manikin, C_{mouth}, C_{nose}, and $C_{forehead}$, declined monotonically with increasing velocities for both sitting and standing.

The effect of velocity on concentrations measured at the shoulder and chest levels is shown in Table 2. For the heated manikin, C_{neck}, $C_{l.collar}$, and $C_{r.collar}$, doubled as velocity increased from 11 to 48 fpm and decreased by half as velocity increased again from 48 to 104 fpm for both sitting and standing postures. However, $C_{c.chest}$, $C_{l.lapel}$, and $C_{r.lapel}$ trippled for standing and doubled for sitting as velocity increased from 11 to 48 fpm and decreased by one third its value as velocity increased again from 48 to 104 fpm for standing and by one half for sitting. It is worth mentioning that, the effect of velocity on C_{neck}, $C_{l.collar}$, $C_{r.collar}$, and $C_{c.chest}$, $C_{l.lapel}$, $C_{r.lapel}$ is substantial and the peak concentration values occurred at 48 fpm only for both sitting and standing postures. Likewise concentrations at the face, for unheated manikin, concentrations at the shoulder and chest levels declined monotonically with increasing velocities for both sitting and standing.

4.2.2 Heating

As shown in Figures 4.2 – 4.10, the effects of heating on concentrations appeared to be strikingly different for heated and unheated conditions at different velocities. For standing posture, concentrations at the face, shoulder, and chest levels were substantially higher for unheated manikin than heated one, at the lower velocity ranges (11 and 27 fpm). On the other hand, for the higher velocities (27 to 104 fpm), concentrations at the face, shoulder, and chest were substantially higher for the heated manikin. Unlike standing, concentrations at all locations for the unheated manikin were considerably higher than the heated one at all velocities for the manikin in sitting posture. It is worth mentioning that minor differences in concentrations occurred only at 48 fpm for some locations. For the unheated manikin, for both sitting and standing, concentrations at all locations had peak values at 11 fpm.

The effect of body heat on concentrations at the face, shoulder, and chest levels is shown in Table 2. At 11 fpm and for the manikin in sitting or standing posture, C_{mouth}, C_{nose}, and $C_{forehead}$, levels were 55% higher for unheated manikin than heated one. Likewise, for the same velocity, heating decreased C_{neck}, $C_{l.collar}$, $C_{r.collar}$ and $C_{c.chest}$, $C_{l.lapel}$, $C_{r.lapel}$ levels by 54% and 57% for both sitting and standing postures.

Therefore, the effect of body heat on concentrations is substantial. Heating changes the airflow patterns around the manikin's head and torso. For the heated manikin, the results show that concentrations declined monotonically above 27 fpm at the face and above 48 fpm at shoulder and chest levels. In other words, as wind tunnel velocity increased, the relative importance of body heat decreased. These results agree with Heist et al. (2003), Fletcher and Johnson (1996), Brohus (1997), and Homma and Yakiyama (1988) who studied the effect of body heat on air flow patterns around a manikin in a uniform flow field and found that heating was also significant and had substantial effects at low speed wind environments. For these studies, wind velocities were ranged 0.05, 0.15, 0.3, and 0.5 m/s.

4.2.3 Posture

The effect of posture was substantial for both the heated and unheated conditions and for all velocities. It is plausible that posture would affect concentrations because of the different orientation of arms and legs to cross draft. In the standing posture, the manikin arms and legs are perpendicular to the cross draft while in sitting posture the arms and legs are parallel to wind tunnel velocity. The arms and legs would affect air flow patterns around the manikin and hence concentration gradients in the breathing zone.

At the head, the effect of posture on C_{mouth}, C_{nose}, and $C_{forehead}$, is shown in Figures (4.2 - 4.4) and listed in Table 2. The effect of posture was neutralized with heating. Standing showed higher concentration levels than sitting for heated manikin while sitting showed higher concentration levels than standing for the unheated manikin for the entire velocity range. For example, at 48 fpm, C_{mouth}, C_{nose}, and $C_{forehead}$ were higher for standing than sitting by 15%, 4%, and 21% for the heated manikin while sitting was higher than standing for unheated. As velocity decreased to 27 fpm, concentrations were higher than sitting for the heated manikin and were lower for unheated.

The effect of posture on C_{neck}, $C_{l.collar}$, and $C_{r.collar}$ is shown in Figures (4.5 - 4.7) and listed in Table 2. Standing showed higher concentration levels for C_{neck}, $C_{l.collar}$, and $C_{r.collar}$ than sitting for the heated manikin for the entire velocity range with peak concentrations at 48 fpm. For lifelike manikin, at 48 fpm, C_{neck}, $C_{l.collar}$, and $C_{r.collar}$ were approximately higher for standing by

46% than sitting. However, for unheated manikin, minor differences were found between sitting and standing for the entire velocity range.

Unlike concentrations at the shoulder, the effect of posture on $C_{c.chest}$, $C_{l.lapel}$, and $C_{r.lapel}$ is shown in Figures 4.8 – 4.10 and listed in Table 2. For the heated and unheated manikin, $C_{c.chest}$, $C_{l.lapel}$, and $C_{r.lapel}$ were higher for standing than sitting for the entire velocity range with peak concentrations at 48 fpm for heated manikin and at 11 fpm for unheated. For example, at 48 fpm, $C_{c.chest}$, $C_{l.lapel}$, and $C_{r.lapel}$ were approximately 65% higher for standing than sitting for both heated and unheated conditions.

Therefore, the effect of posture is substantial on concentrations at the head, shoulder, and chest. However, higher differences for standing and sitting were observed at chest locations may be refferd to the presence of the table down stream the manikin which was probably affecting the wake zone and air flow pattern.

Table 3: Average Concentrations (Ppm) for Each Velocity Level and Manikin Treatments

Treatment	V,fpm	$C_{lower.torso}$	$C_{upper.torso}$	$C_{inhaled}$
Heated/ Standing	11	27.5	30.2	29.0
	27	45.8	45.3	59.5
	48	92.4	68.7	52.7
	82	47.0	42.8	43.0
	104	35.5	32.3	34.3
Heated/ Seated	11	16.2	16.2	11.5
	27	21.6	21.0	22.1
	48	30.8	39.5	49.5
	82	21.0	20.4	30.3
	104	16.6	16.1	21.8
Unheated/ Standing	11	111.9	67.5	64.9
	27	81.7	43.4	39.3
	48	65.9	41.2	31.6
	82	49.9	35.5	28.6
	104	34.3	22.3	19.5
Unheated/ Seated	11	45.3	56.9	58.5
	27	31.2	42.2	52.1
	48	24.0	38.2	49.5
	82	21.9	33.7	38.8
	104	17.7	29.4	34.3

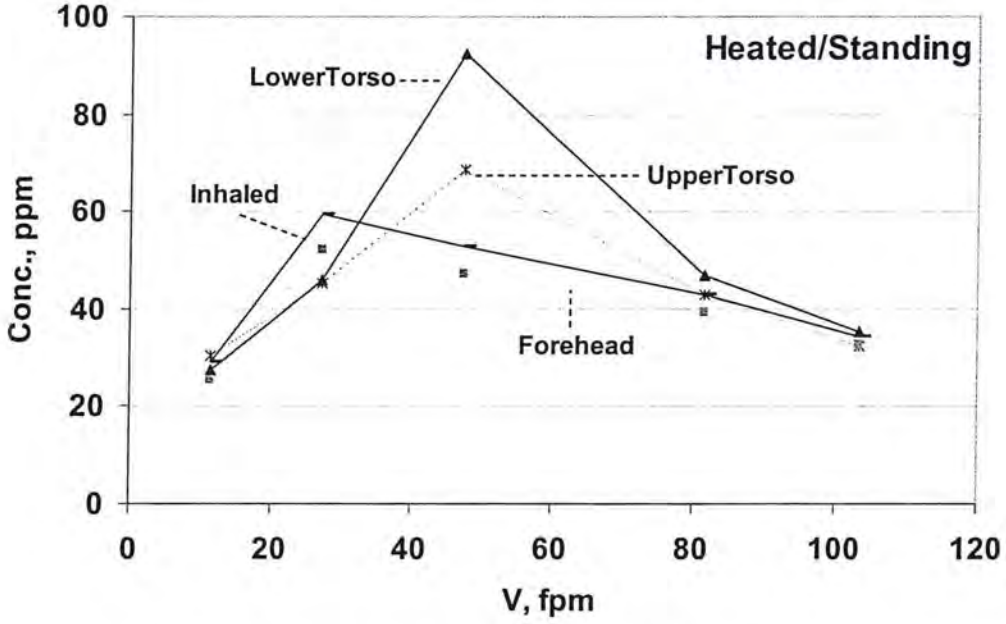

Figure 19: Mean BZ Concentration versus velocity for standing/heated manikin

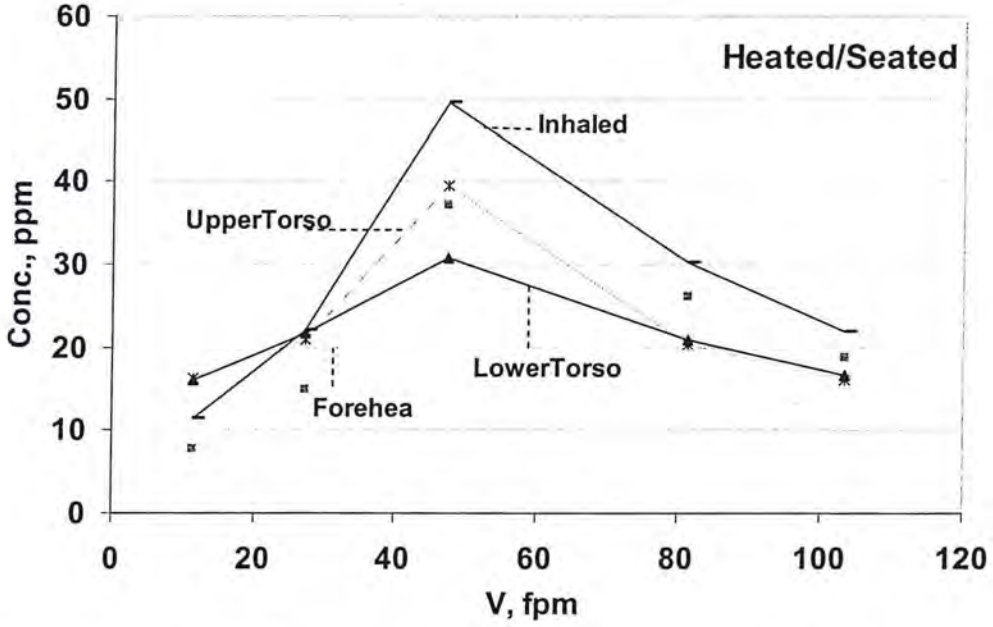

Figure 20: Mean BZ Concentration versus velocity for seated/heated manikin

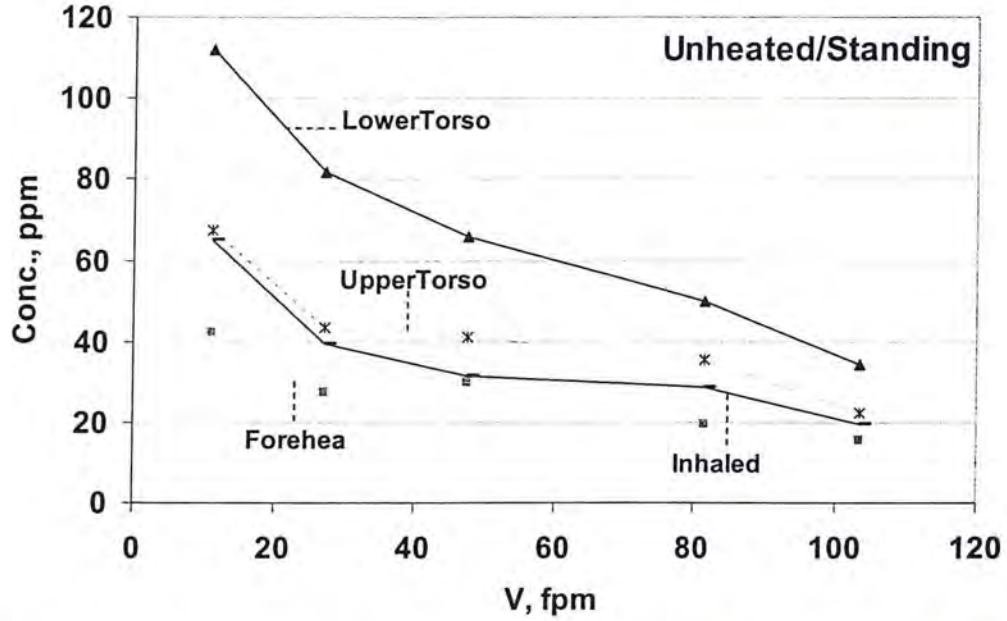

Figure 21: Mean BZ Concentration versus velocity for standing/unheated manikin

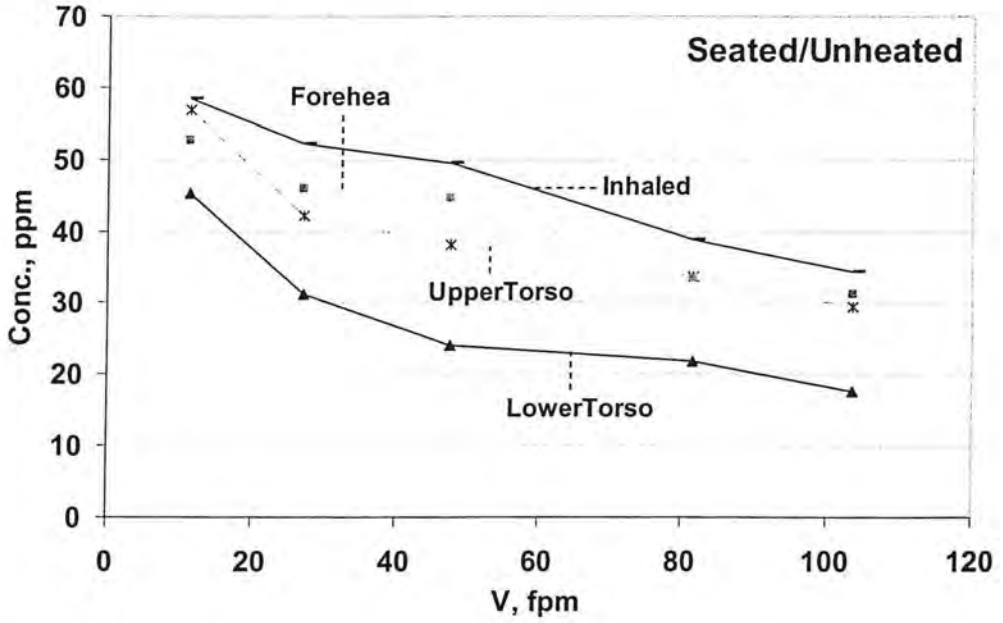

Figure 22: Mean BZ Concentration versus velocity for seated/unheated manikin

3 Effects of Independent Variables on $C_{inhaled}$, $C_{upper.torso}$, and $C_{lower.torso}$

Since concentrations near the mouth behaved similarly, the average of C_{mouth} and C_{nose} were used to compute $C_{inhaled}$. Likewise, $C_{upper.torso}$ is the average of C_{neck} and $C_{collars}$ and $C_{lower.torso}$ is the average of C_{chest} and C_{lapels}. $C_{forehead}$ was the lowest concentration level compared to (C_{mouth} and C_{nose}) so it was not used to compute $C_{inhaled}$.

Figures 19 to 22 show the effects of velocity, body heat and posture on $C_{inhaled}$, $C_{upper.torso}$, and $C_{lower.torso}$. For lifelike condition (heating), all three concentrations varied in an inverted-V shape with velocity for both sitting and standing. The location of the peak for $C_{upper.torso}$, and $C_{lower.torso}$ was the same (48 fpm) for both postures. The location of the peak for $C_{inhaled}$ was different for sitting (48 fpm) than for standing (27 fpm). The magnitudes of the peaks were about the same at a given location. However, the concentrations differed sharply by measurement locations. More importantly, the differences in concentrations were strongly affected by posture. For example, the lower torso concentrations were much higher than $C_{inhaled}$ for standing and lower for sitting (see Figures 19&20). Hence, whether a torso measurement exaggerated or underestimated the actual level depends on whether the manikin was sitting or standing.

Likewise patterns occurred for the unheated manikin. For example, the lower torso concentrations were much higher than inhaled for standing and lower for sitting for the entire velocity range (see Figures 21 & 22).

Table 4: Ratios of Concentrations to C_{mouth} for all Velocities and Manikin Treatments

Treatment	V,fpm	$C_{c.chest}/C_{mouth}$	$C_{l.lapel}/C_{mouth}$	$C_{r.lapel}/C_{mouth}$	C_{neck}/C_{mouth}	$C_{l.collar}/C_{mouth}$	$C_{r.collar}/C_{mouth}$	C_{nose}/C_{mouth}	$C_{forehead}/C_{mouth}$
Heated/ Standing	11	1.07	0.81	0.91	1.08	1.02	0.98	0.97	0.86
	27	0.80	0.67	0.76	0.86	0.72	0.64	0.94	0.85
	48	1.95	1.48	1.83	1.39	1.18	1.36	1.01	0.90
	82	1.15	0.97	1.04	1.04	0.85	0.99	0.93	0.88
	104	1.06	0.97	0.95	1.01	0.78	0.94	0.94	0.92
Heated/ Seated	11	1.45	1.21	1.12	1.18	1.28	1.36	0.80	0.61
	27	1.00	0.97	0.90	0.94	0.94	0.89	0.95	0.65
	48	0.66	0.65	0.61	0.89	0.77	0.79	1.04	0.77
	82	0.80	0.71	0.62	0.70	0.70	0.67	1.04	0.88
	104	0.84	0.74	0.70	0.73	0.78	0.70	0.99	0.86
Unheated/ Standing	11	1.82	2.15	1.32	1.09	1.10	1.01	1.06	0.69
	27	1.87	2.23	1.73	0.99	1.04	1.03	0.88	0.65
	48	2.08	2.32	1.70	1.19	1.29	1.24	0.88	0.92
	82	1.72	1.65	1.60	1.17	1.23	1.14	0.90	0.64
	104	1.51	2.10	1.35	1.01	1.03	1.07	0.80	0.72
Unheated/ Seated	11	0.76	0.91	0.75	0.98	1.03	0.91	0.99	0.90
	27	0.57	0.64	0.59	0.88	0.85	0.76	1.05	0.91
	48	0.48	0.56	0.49	0.84	0.83	0.75	1.09	0.94
	82	0.53	0.60	0.59	0.89	0.88	0.84	1.01	0.87
	104	0.46	0.57	0.52	0.96	0.90	0.72	1.00	0.91

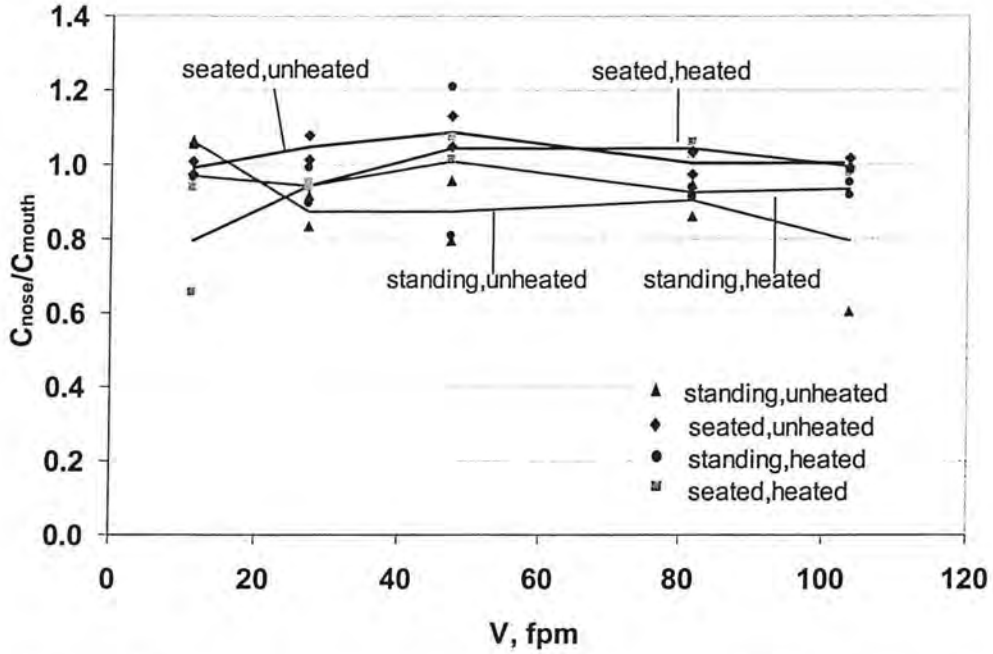

Figure 23: Scatter and mean plot of C_{nose}/C_{mouth} vs. velocity for all manikin treatments

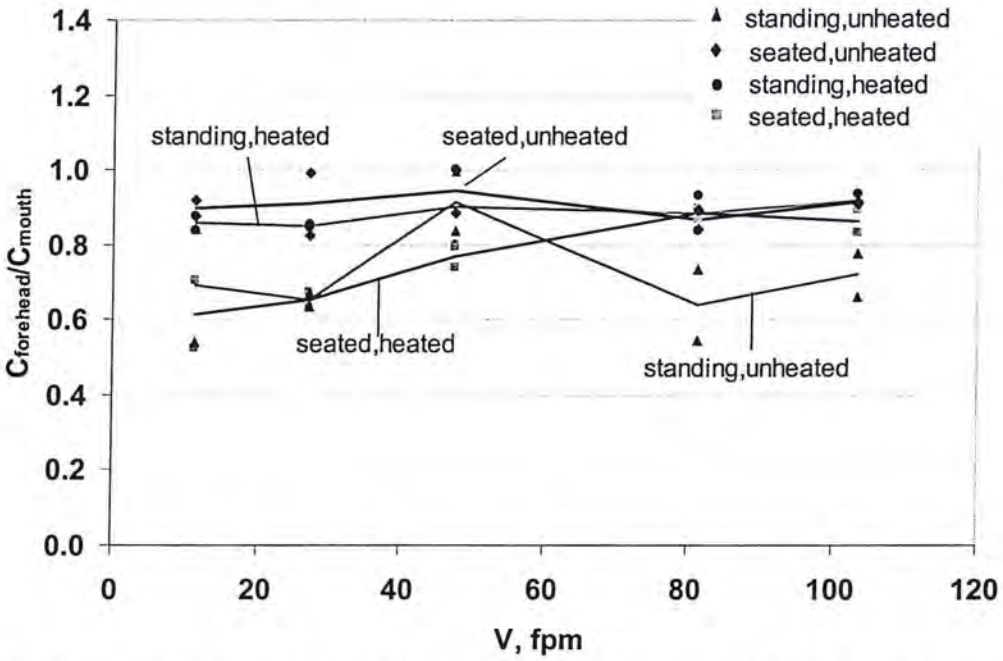

Figure 24: Scatter and mean plot of $C_{forehead}/C_{mouth}$ vs. velocity for all manikin treatments

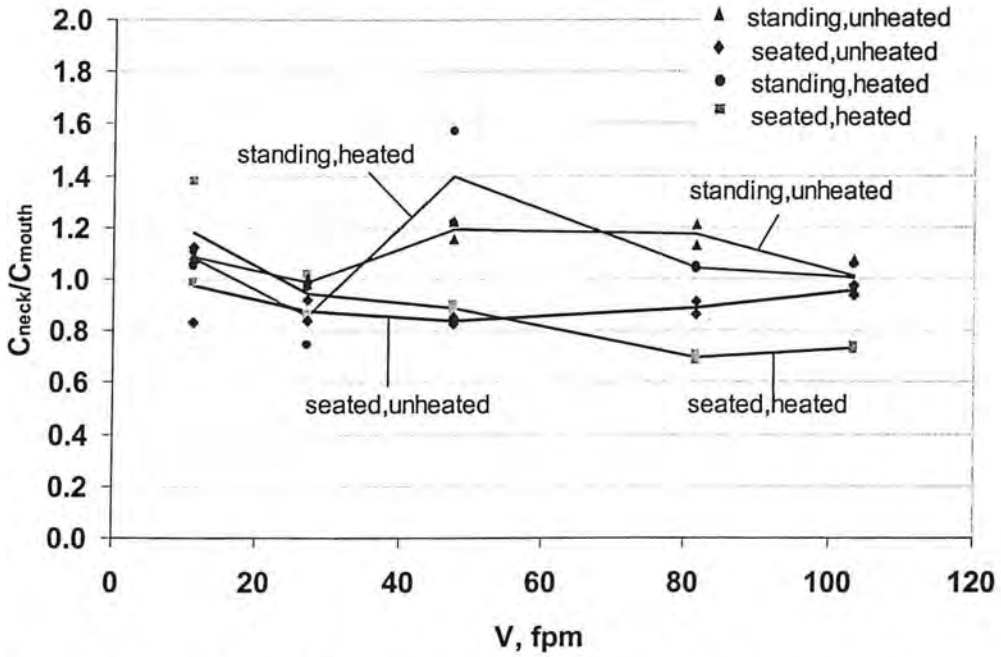

Figure 25: Scatter and mean plot of C_{neck} /C_{mouth} vs. velocity for all manikin treatments

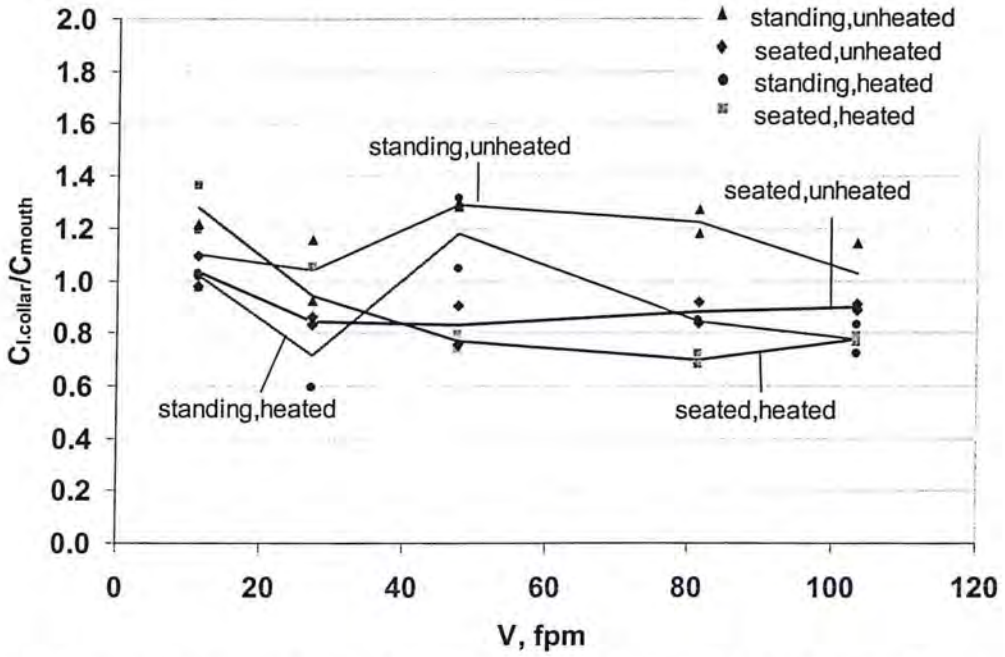

Figure 26: Scatter and mean plot of $C_{l.collar}$ /C_{mouth} vs. velocity for all manikin treatments

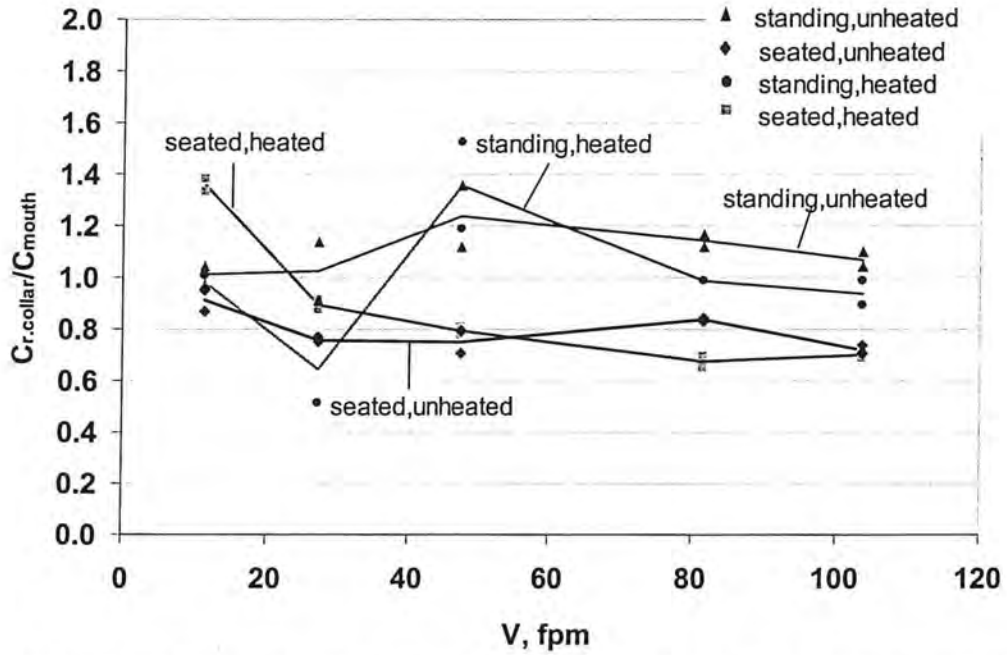

Figure 27: Scatter and mean plot of $C_{r.collar}/C_{mouth}$ vs. velocity for all manikin treatments

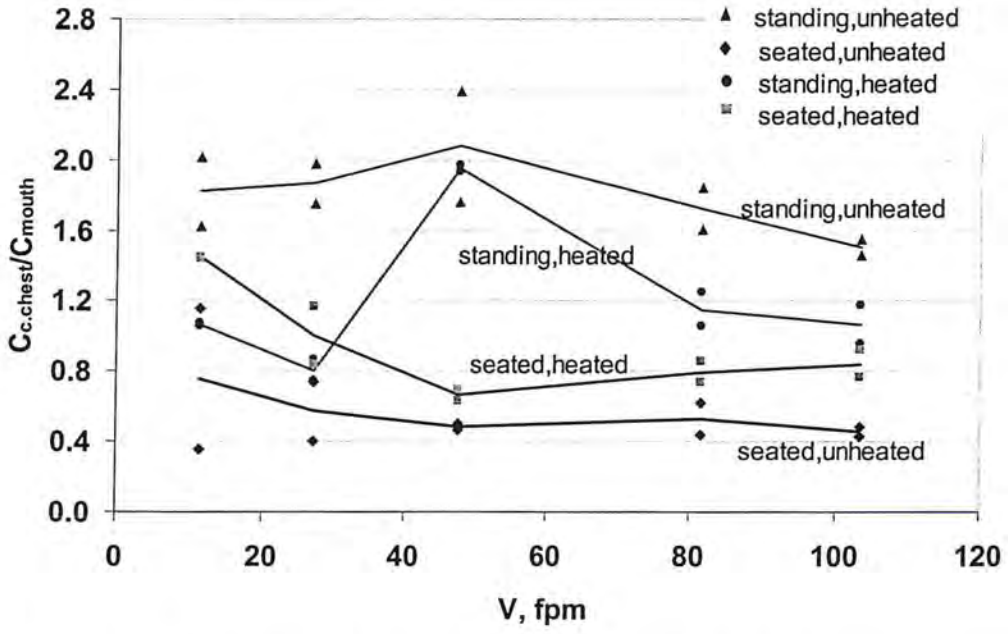

Figure 28: Scatter and mean plot of $C_{c.chest}/C_{mouth}$ vs. velocity for all manikin treatments

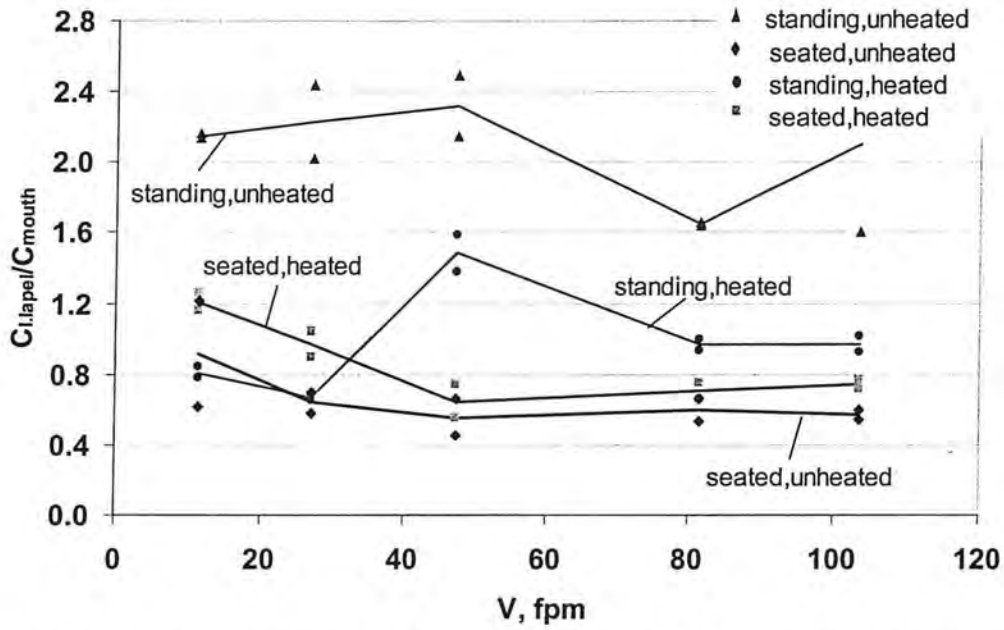

Figure 29: Scatter and mean plot of $C_{l.lapel}/C_{mouth}$ vs. velocity for all manikin treatments

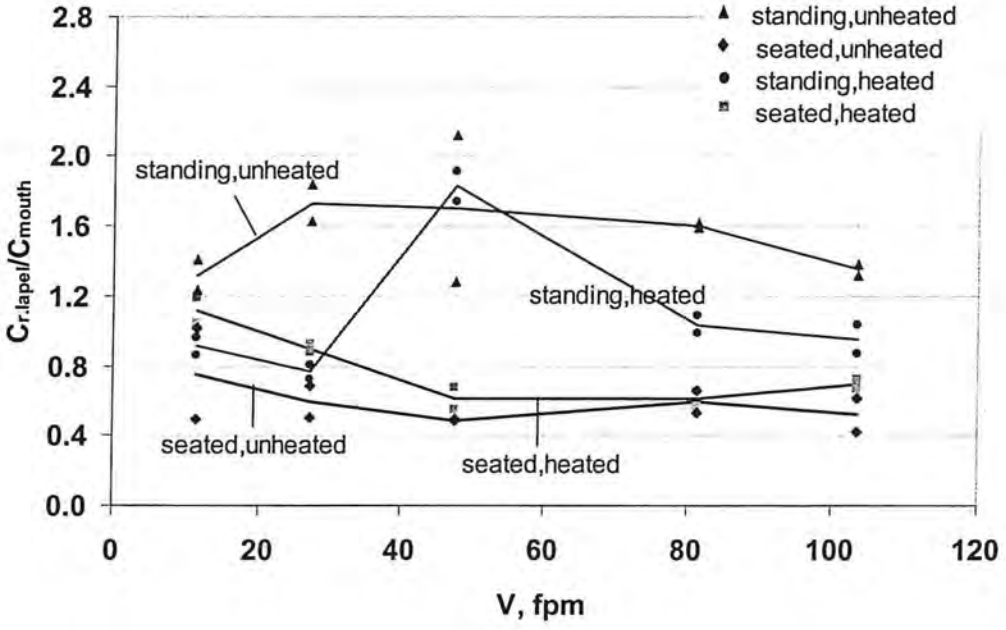

Figure 30: Scatter and mean plot of $C_{r.lapel}/C_{mouth}$ vs. velocity for all manikin treatments

4 Effects of Independent Variables on Ratio of Concentrations

The main purpose of this study was to investigate the agreement between lapels, collars, center chest, nose, neck, and forehead sampling locations to mouth location as assumed to be inhaled exposure. Concentration ratios to C_{mouth} for locations at the face ($C_{forehead}/C_{mouth}$, C_{nose}/C_{mouth}), shoulder ($C_{l.collar}/C_{mouth}$, $C_{r.collar}/C_{mouth}$, C_{neck}/C_{mouth}), and chest ($C_{r.lapel}/C_{mouth}$, $C_{c.chest}/C_{mouth}$, $C_{l.lapel}/C_{mouth}$) varied wind tunnel velocity, heating, and posture.

The effect of velocity, heating, and posture on ratios of concentrations is shown in Figures 23 to 30 and is listed in Table 4. As shown in Figures 23 – 30, for the ratios of concentrations at the shoulder and chest levels, posture had an effect on the relationship with velocity than did heating. For example, sitting had similar patterns on ratios of concentrations at the shoulder and chest whether the manikin is heated or not. However, standing showed higher peak ratios for the effect of velocity than sitting. As discussed earlier in section 4.2, for a standing heated manikin, concentrations at the mouth had peak values occurred at 27 fpm, while, concentrations at the shoulder and chest levels had peak values occurred at 48 fpm. Therefore, the ratios of concentrations at the shoulder and chest levels for a standing heated manikin had two inverted-V peaks occurred at 27 and 48 fpm. The scatter in ratios of concentration was higher at the lower velocities than at higher velocities.

As shown in Table 4, for the heated manikin, the ratio of nose to mouth C_{nose}/C_{mouth} was very close to unity for the entire velocity range and for both postures, except one value at 11 fpm for sitting posture. The ratio of forehead to mouth $C_{forehead}/C_{mouth}$ was always lower than unity for the entire velocity range, but it approached unity (0.92) at highest velocity level. It is possible that $C_{forehead}$ always underestimated mouth exposure due to the downwash patterns from the sides of the face and the top of head.

The effect of posture, velocity and heating on ratios of concentrations at the shoulder is shown in Figures 25 - 27. For lifelike conditions, C_{neck}/C_{mouth}, $C_{l.collar}/C_{mouth}$, and $C_{r.collar}/C_{mouth}$, had two inverted-V peaks with velocity at 27 and 48 fpm for standing and a declined flattened-U relationship with velocity for sitting. As listed in Table 4, C_{neck}/C_{mouth}, $C_{l.collar}/C_{mouth}$, and $C_{r.collar}/C_{mouth}$, were around (1.02) at 11 fpm for standing posture, and were around (0.94) at 27 fpm for sitting.

The effect of posture, velocity and heating on ratios of concentrations at the chest is shown in Figures 28-30. For lifelike conditions, heated manikin, ratios of concentrations at center chest, left lapel, and right lapel to mouth had two inverted-V peaks with velocity at 27 and 48 fpm for standing posture and a declined flattened-U relationship with velocity for sitting. As listed in Table 4, $C_{c.chest}/C_{mouth}$, $C_{l.lapel}/C_{mouth}$ and $C_{r.lapel}/C_{mouth}$ had values ranged (0.9-1.2) at the lower velocity levels for both sitting and standing. At 48 fpm, concentrations at the chest overestimated mouth concentrations by 1.75 for standing, and underestimated mouth concentrations by 0.65 for sitting.

Discussions of Manikin Study I

Data Desk (Data Description Inc. Ithaca, NY) software was used to do statistical analysis of results. The independent variables for this study were five levels of velocity (11, 27, 48, 82, and 104 fpm), two levels of heating (unheated,heated) and two levels of posture (standing,seated). The dependent variables were concentrations at each sampling location and ratio of concentrations. As results were quite variable, log transformation of concentration values and ratio of concentrations were used.

Dependent variables were log-transformed to produce residuals that were normally distributed. Using log ratio of concentration allowed analysis of the differences in logs of two dependent values, removing "small denominator" problems associated with actual ratios: log $\{C_{neck}/C_{mouth}\} = \{\log C_{neck} - \log C_{mouth}\}$

1 Log-Transformation of Dependent Variables

Critical value for coefficient of correlation between ordered residuals and expected values under normality when distribution of error term is normal was found to be equal (r = 0.972) for a sample of size n=40, and level of significance alpha = 0.05 (Neter et al. 1996). Table 5 listed the coefficient of correlation for externally studentized residuals versus nscores (computed using DataDesk software) for log-transformed dependent variables (concentrations and ratios of concentrations for each sampling location).

Table 5: Coefficient of Correlation for Externally Studentised Residuals Versus Normal Scores For Log-Transformed Individual Concentrations and Ratios of Concentrations

Log C_{mouth}	**0.99**	**Log$\{C_{nose}/C_{mouth}\}$**	**0.93**
Log C_{nose}	**0.95**	**Log$\{C_{forehead}/C_{mouth}\}$**	**0.97**
Log $C_{forehead}$	**0.99**	**Log$\{C_{neck}/C_{mouth}\}$**	**0.99**
Log C_{neck}	**0.98**	**Log$\{C_{l.collar}/C_{mouth}\}$**	**0.96**
Log $C_{l.collar}$	**0.99**	**Log$\{C_{r.collar}/C_{mouth}\}$**	**0.95**
Log $C_{r.collar}$	**0.99**	**Log$\{C_{c.chest}/C_{mouth}\}$**	**0.92**
Log $C_{c.chest}$	**0.96**	**Log$\{C_{l.lapel}/C_{mouth}\}$**	**0.98**
Log $C_{l.lapel}$	**0.99**	**Log$\{C_{r.lapel}/C_{mouth}\}$**	**0.97**
Log $C_{r.lapel}$	**0.99**		
Log $C_{inhaled}$	**0.98**		
Log $C_{uppertorso}$	**0.98**		
Log $C_{lowertorso}$	**0.97**		

As shown in Table 5, log transformed individual concentration and ratio of concentartions showed reasonable degree of normality for all sampling locations, except for log C_{nose} and Log

$\{C_{c.chest}/C_{mouth}\}$. Although correlation coefficients varied for each dependent variable, there was no substantial departure from linearity.

2 Analysis of Variance (ANOVA)

The independent variables for this study were five levels of velocity (11, 27, 48, 82, and 104 fpm), two levels of heating (unheated,heated) and two levels of posture (standing,seated). The dependent variables were concentrations at each sampling location and ratios of concentrations. The design is a completely randomized factorial design with two replications for each treatment combination, see Table 6. The linear statistical model used for the analysis of variance is illustrated by the following equation:

$$Y_{ijkl} = \mu + \tau_i + \beta_j + \gamma_k + (\tau\beta)_{ij} + (\tau\gamma)_{ik} + (\beta\gamma)_{jk} + (\tau\beta\gamma)_{ijk} + \varepsilon_{ijkl}$$

Where i = 1,2,3,4,5; j = 1,2; k = 1,2; l = 1,2; and τ_i, β_j, γ_k, represent the effects of wind tunnel velocity, manikin heating and posture, while $(\tau\beta)_{ij}$, $(\tau\gamma)_{ik}$, $(\beta\gamma)_{jk}$, $(\tau\beta\gamma)_{ijk}$ represent the interaction of velocity, heating and posture. ε_{ijkl} represents the random error.

Table 6: Completely Randomized Factorial Design of Experiments

		Velocity, fpm				
		11	27	48	82	104
Heated	Seated	++	++	++	++	++
	Standing	++	++	++	++	++
Unheated	Seated	++	++	++	++	++
	Standing	++	++	++	++	++

Analysis of variance was performed on log-transformed dependent variables (concentrations and ratios of concentrations for all sampling locations) for the effects of the independent variables (velocity, heating and posture) and their interaction. The outline for ANOVA table was obtained from (Montgomery, D, 1997). For the fixed effects model, test statistics for each independent variable and interaction was developed by dividing the corresponding mean square for the variable or interaction by the mean square error. All of these F tests were one tail tests. The number of degrees of freedom for any factor is the number of levels of the factor minus one, the number of degrees of freedom for an interaction is the product of the number of degrees of freedom associated with the individual components of the interaction (Montgomery, D, 1997). All tests were done at 95% confidence level (α=0.05). Data Desk software was used to compute ANOVA and the results of the F-tests were summarized as p-values.

Tables 7 and 8 list the p-values for log-transformed individual concentrations and ratios of concentrations for all sampling locations. Table 9 shows p-values for log transformed concentrations for $C_{inhaled}$, $C_{uppertorso}$, and $C_{lowertorso}$.

Table 7: p-Values from ANOVAs for Log-Transformed Individual Concentrations

Source	df	Log C_{mouth}	Log C_{nose}	Log $C_{forehead}$	Log C_{neck}	Log $C_{l.collar}$	Log $C_{r.collar}$	Log $C_{c.chest}$	Log $C_{l.lapel}$	Log $C_{r.lapel}$
Const	1	0.00	0.00	0.00	0.00	0.00	0.00	0.00	0.00	0.00
Velocity	4	0.00	0.00	0.00	0.00	0.00	0.00	0.00	0.00	0.00
Heating	1	0.00	0.01	0.00	0.00	0.00	0.00	0.09	0.00	0.00
Posture	1	0.00	0.24	0.07	0.00	0.00	0.00	0.00	0.00	0.00
VelocityxHeating	4	0.00	0.00	0.00	0.00	0.00	0.00	0.00	0.00	0.00
VelocityxPosture	4	0.00	0.00	0.01	0.44	0.47	0.99	0.54	0.34	0.26
HeatingxPosture	1	0.00	0.00	0.00	0.00	0.00	0.00	0.27	0.02	0.24

Table 8: p-Values from ANOVAs for Log-Transformed Ratios of Concentrations

Source	df	$Log(C_{nose}/C_{mouth})$	$Log(C_{forehead}/C_{mouth})$	$Log(C_{neck}/C_{mouth})$	$Log(C_{l.collar}/C_{mouth})$	$Log(C_{r.collar}/C_{mouth})$	$Log(C_{c.chest}/C_{mouth})$	$Log(C_{l.lapel}/C_{mouth})$	$Log(C_{r.lapel}/C_{mouth})$
Const	1	0.02	0.00	0.15	0.00	0.00	0.92	0.89	0.01
Velocity	4	0.75	0.07	0.01	0.00	0.00	0.25	0.15	0.36
Heating	1	0.94	0.80	0.35	0.00	0.41	0.48	0.00	0.52
Posture	1	0.06	0.33	0.00	0.00	0.00	0.00	0.00	0.00
VelocityxHeating	4	0.26	0.13	0.05	0.04	0.03	0.79	0.72	0.34
VelocityxPosture	4	0.10	0.39	0.00	0.00	0.00	0.02	0.00	0.00
HeatingxPosture	1	0.08	0.00	0.86	0.01	0.01	0.00	0.00	0.00

Table 9: p-Values from ANOVA's for Log $\mathbf{C_{inhaled}}$, log $\mathbf{C_{uppertorso}}$, and log $\mathbf{C_{lowertorso}}$

Source	df	Log $C_{inhaled}$	Log $C_{uppertorso}$	Log $C_{lowertorso}$
Const	**1**	**0.00**	**0.00**	**0.00**
Velocity	**4**	**0.00**	**0.00**	**0.00**
Heating	**1**	**0.00**	**0.00**	**0.00**
Posture	**1**	**0.04**	**0.00**	**0.00**
Velocity/Heating	**4**	**0.00**	**0.00**	**0.00**
Velocity/Posture	**4**	**0.00**	**0.72**	**0.33**
Heating/Posture	**1**	**0.00**	**0.00**	**0.41**

3 Regression Analysis

Regression analysis was performed on log transformed concentrations for each sampling location with wind tunnel velocity for each manikin treatment. Manikin treatments were divided into four groups: heated/standing, heated/seated, unheated/standing, and unheated/seated. For unheated conditions, linear regression was applied to fit the data with velocity for both standing and seated manikin. For heated conditions, a second velocity term was added to the regression model to correct for the inverted V-shape peak for both seated and standing conditions.

For unheated conditions, the regression model for concentration at the mouth, C_{mouth}, is:

$$\text{Log } C_{mouth} = \beta_0 + \beta_1 V_1$$

For heated conditions, the regression model for C_{mouth} is:

$$\text{Log } C_{mouth} = \beta_0 + \beta_1 V_1 + \beta_2 V_2$$

In case the peak concentration occurred at 48 fpm, then, $\{V_2 = (V_1 - 48)x\}$

Where: $x = 0$ if $V_1 \leq 48$ and $x = 1$ if $V_1 > 48$

In case the peak concentration occurred at 27 fpm, then $\{V_2 = (V_1 - 27)x\}$

Where: $x = 0$ if $V_1 \leq 27$ and $x = 1$ if $V_1 > 27$. Concentrations at each sampling location were fitted using the same model applied on log C_{mouth}.

Tables 10 to 13 summarize adjusted R-square, regression coefficients, and p-Values obtained from regression analysis for each sampling location and manikin treatment.

Table 10a: Regression Coefficients for heated/standing manikin

	Adj_R^2 (%)	C_0	C_1	C_2	C_3
Log C_{mouth}	95.3	1.24	0.02	-0.02	
Log C_{nose}	87.5	1.23	0.02	-0.02	
Log $C_{forehead}$	94	1.17	0.02	-0.02	
Log C_{neck}	85	1.41	0.01		-0.02
Log $C_{l.collar}$	83.2	1.39	0.01		-0.01
Log $C_{r.collar}$	82.3	1.32	0.01		-0.02
Log $C_{c.chest}$	91.3	1.33	0.01		-0.02
Log $C_{l.lapel}$	95.1	1.23	0.01		-0.02
Log $C_{r.lapel}$	93.8	1.26	0.02		-0.02

Table 10b: Regression p-Values for heated/standing manikin

	C_0	C_1	C_2	C_3
Log C_{mouth}	0.000	0.000	0.000	
Log C_{nose}	0.000	0.000	0.000	
Log $C_{forehead}$	0.000	0.000	0.000	
Log C_{neck}	0.000	0.000		0.000
Log $C_{l.collar}$	0.000	0.001		0.000
Log $C_{r.collar}$	0.000	0.000		0.000
Log $C_{c.chest}$	0.000	0.000		0.000
Log $C_{l.lapel}$	0.000	0.000		0.000
Log $C_{r.lapel}$	0.000	0.000		0.000

Table 11a: Regression Coefficients for heated/seated manikin

	Adj_R^2 (%)	C_0	C_1	C_3
Log C_{mouth}	97.9	0.93	0.02	-0.02
Log C_{nose}	98	0.79	0.02	-0.03
Log $C_{forehead}$	98.8	0.67	0.02	-0.02
Log C_{neck}	93.8	1.02	0.01	-0.02
Log $C_{l.collar}$	94.5	1.09	0.01	-0.02
Log $C_{r.collar}$	89.5	1.10	0.01	-0.02
Log $C_{c.chest}$	84.8	1.18	0.01	-0.01
Log $C_{l.lapel}$	89	1.10	0.01	-0.01
Log $C_{r.lapel}$	86.7	1.07	0.01	-0.01

Table 11b: Regression p-Values for heated/seated manikin

	C_0	C_1	C_3
Log C_{mouth}	0.000	0.000	0.000
Log C_{nose}	0.000	0.000	0.000
Log $C_{forehead}$	0.000	0.000	0.000
Log C_{neck}	0.000	0.000	0.000
Log $C_{l.collar}$	0.000	0.000	0.000
Log $C_{r.collar}$	0.000	0.000	0.000
Log $C_{c.chest}$	0.000	0.000	0.000
Log $C_{l.lapel}$	0.000	0.000	0.000
Log $C_{r.lapel}$	0.000	0.000	0.000

Table 12a: Regression Coefficients for unheated/standing manikin

	Adj_R^2 (%)	C_0	C_1
Log C_{mouth}	71.3	1.78	-0.004
Log C_{nose}	59.9	1.79	-0.005
Log $C_{forehead}$	65.6	1.64	-0.004
Log C_{neck}	62	1.82	-0.004
Log $C_{l.collar}$	54.7	1.84	-0.004
Log $C_{r.collar}$	64.5	1.80	-0.004
Log $C_{c.chest}$	77.3	2.08	-0.005
Log $C_{l.lapel}$	90.1	2.14	-0.005
Log $C_{r.lapel}$	74.5	1.98	-0.005

Table 12b: Regression p-Values for unheated/standing manikin

	C_0	C_1
Log C_{mouth}	0.000	0.001
Log C_{nose}	0.000	0.005
Log $C_{forehead}$	0.000	0.003
Log C_{neck}	0.000	0.004
Log $C_{l.collar}$	0.000	0.009
Log $C_{r.collar}$	0.000	0.003
Log $C_{c.chest}$	0.000	0.001
Log $C_{l.lapel}$	0.000	0.000
Log $C_{r.lapel}$	0.000	0.001

Table 13a: Regression Coefficients for unheated/seated manikin

	Adj_R^2 (%)	C_0	C_1
Log C_{mouth}	77.2	1.79	-0.002
Log C_{nose}	84.4	1.80	-0.003
Log $C_{forehead}$	87.5	1.74	-0.002
Log C_{neck}	74.2	1.74	-0.002
Log $C_{l.collar}$	69.7	1.76	-0.003
Log $C_{r.collar}$	74.3	1.71	-0.003
Log $C_{c.chest}$	42.5	1.57	-0.004
Log $C_{l.lapel}$	67.2	1.67	-0.004
Log $C_{r.lapel}$	56.8	1.60	-0.003

Table 13b: Regression p-Values for unheated/seated manikin

	C_0	C_1
Log C_{mouth}	0.000	0.001
Log C_{nose}	0.000	0.000
Log $C_{forehead}$	0.000	0.000
Log C_{neck}	0.000	0.001
Log $C_{l.collar}$	0.000	0.002
Log $C_{r.collar}$	0.000	0.001
Log $C_{c.chest}$	0.000	0.024
Log $C_{l.lapel}$	0.000	0.002
Log $C_{r.lapel}$	0.000	0.007

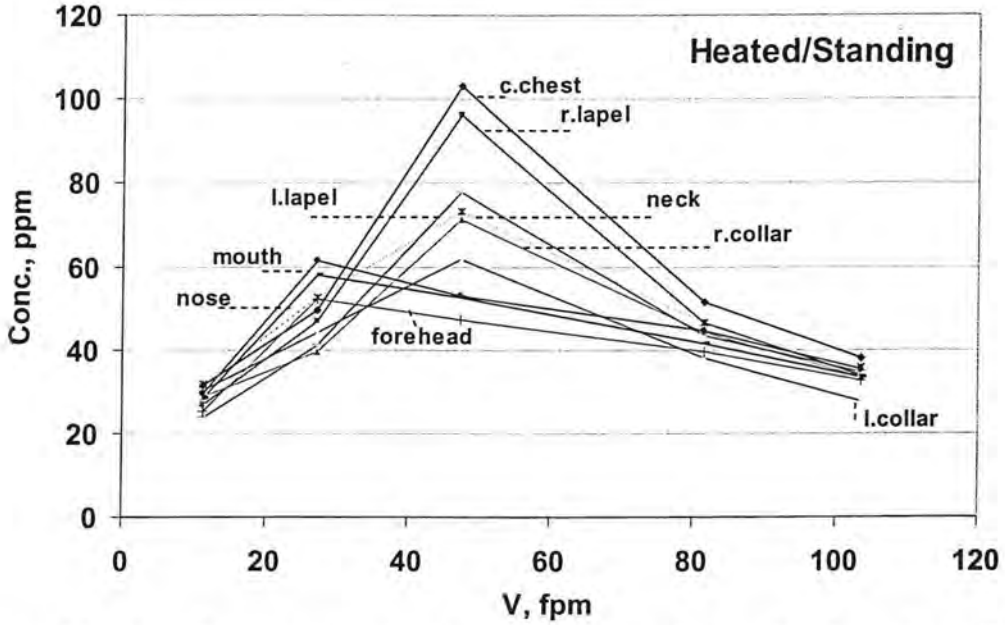

Figure 31: Mean Concentration (ppm) versus velocity for standing/heated manikin

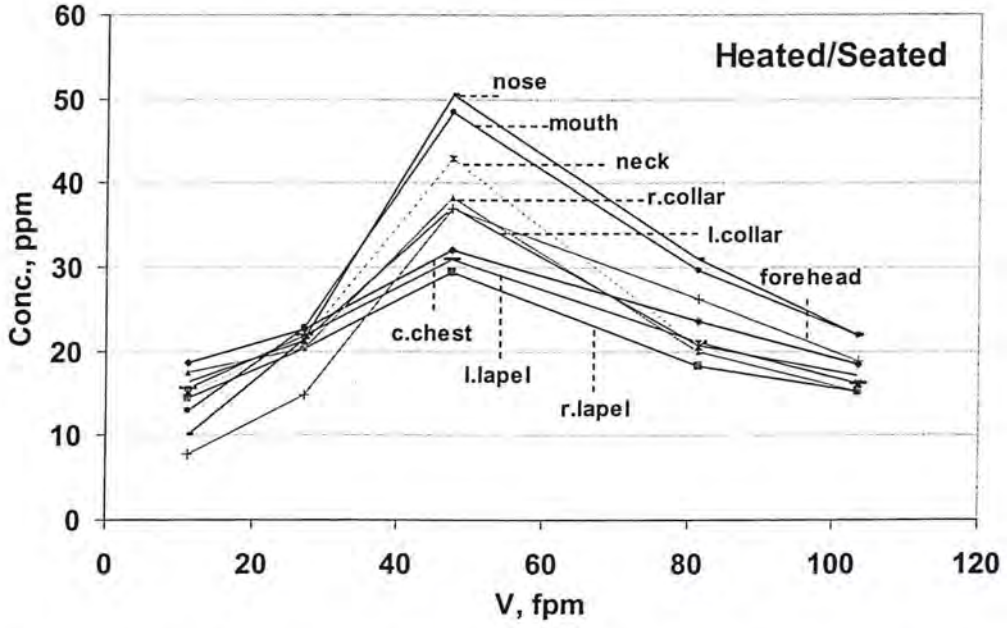

Figure 32: Mean Concentration (ppm) versus velocity for seated/heated manikin

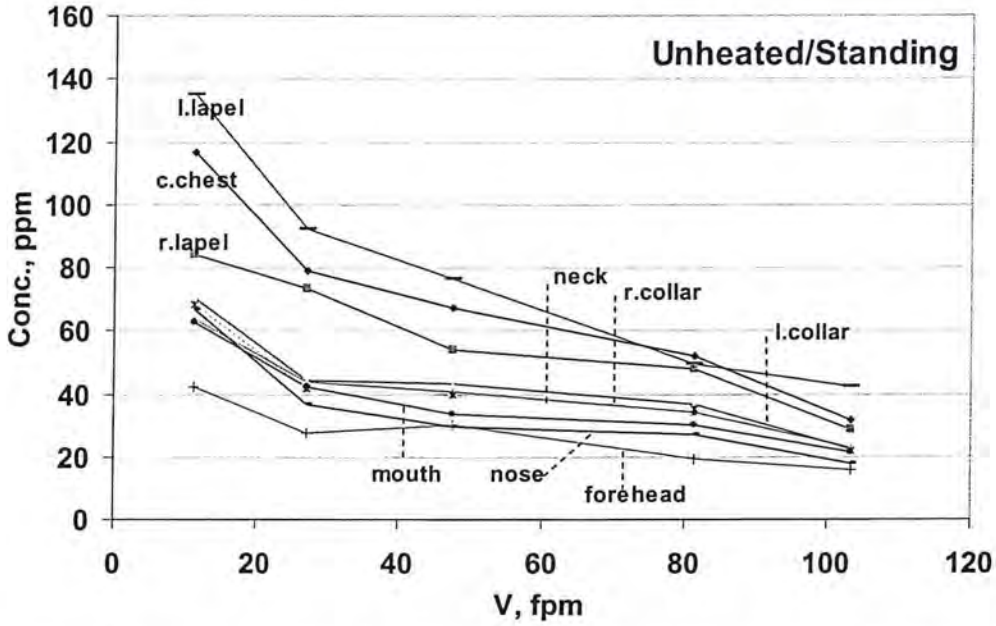

Figure 33: Mean concentration (ppm) versus velocity for standing/unheated manikin

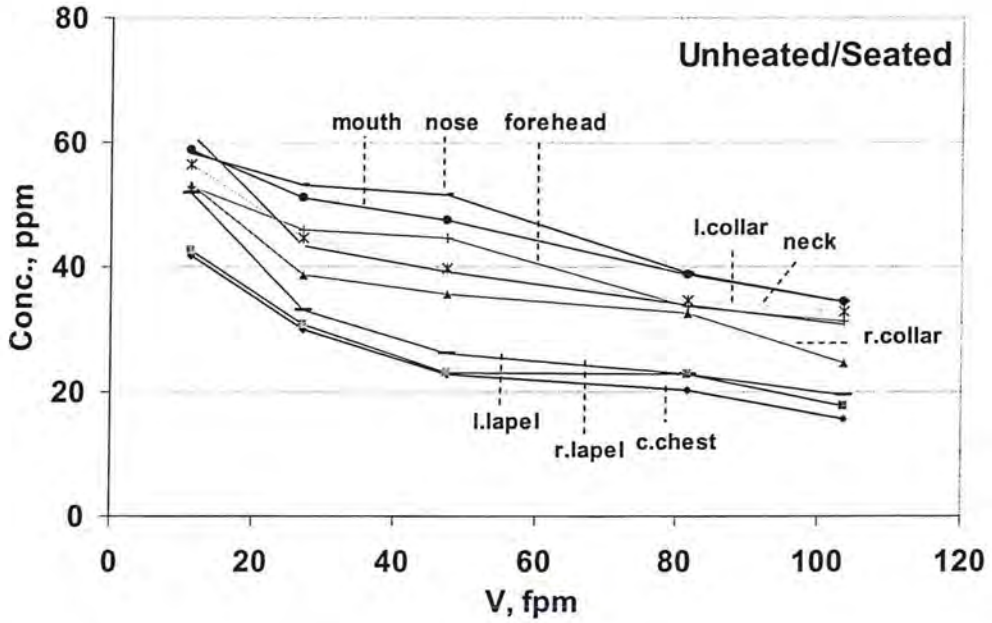

Figure 34: Mean concentration (ppm) versus velocity for seated/unheated manikin

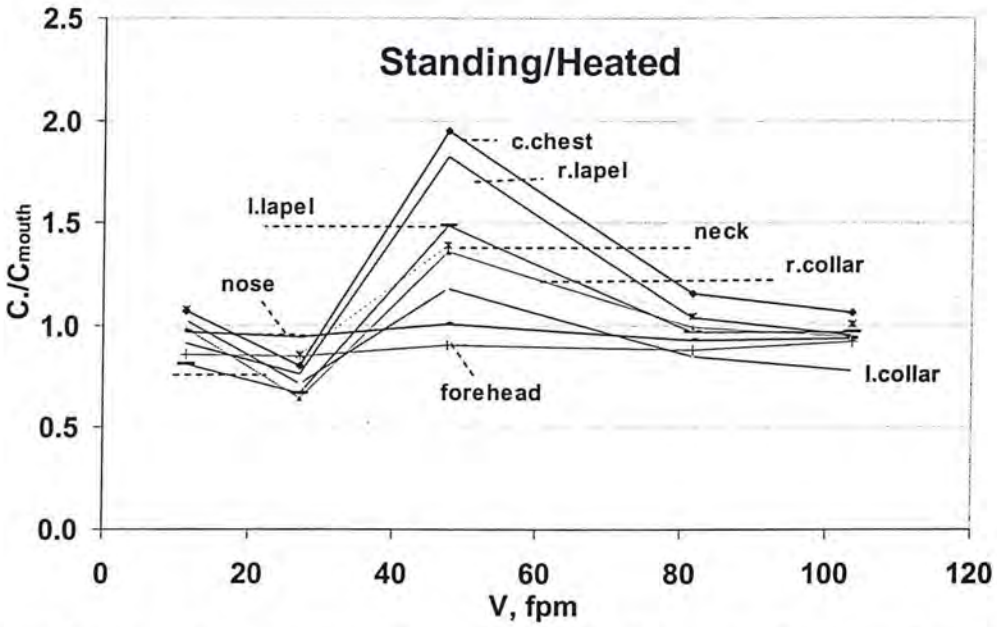

Figure 35: Concentration ratio to C_{mouth} versus velocity for standing/heated manikin

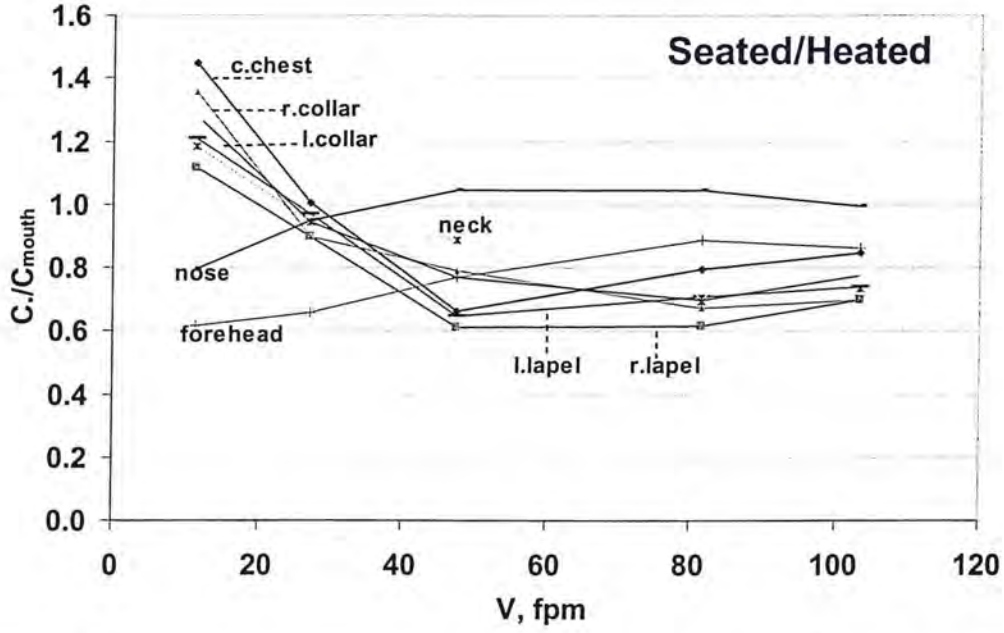

Figure 36: Concentration ratio to C_{mouth} versus velocity for seated/heated manikin

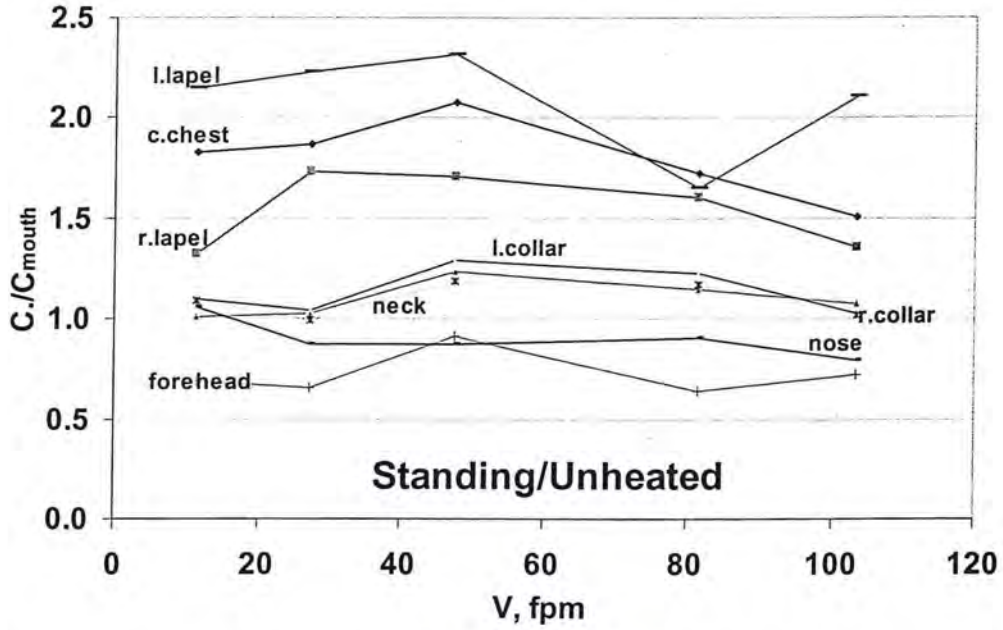

Figure 37: Concentration ratio to C_{mouth} versus velocity for standing/unheated manikin

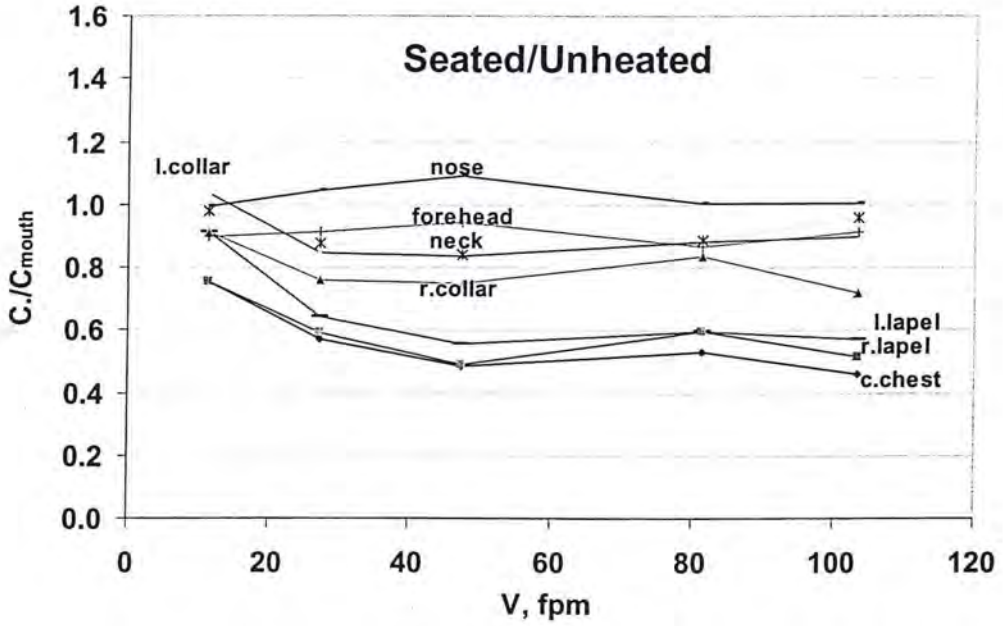

Figure 38: Concentration ratio to C_{mouth} versus velocity for seated/unheated manikin

Comparisons of individual Concentration Values and Ratios of Concentrations for all Sampling Locations

As shown in Figures 31-34, the effects of wind tunnel velocity on all locations appeared to be strikingly different for heated and unheated treatments but were similar for standing and sitting postures. For unheated conditions, concentrations at all sampling locations fell more or less monotonically with increasing values of velocity. This behavior agrees with Flynn et al. (1991) and Kulmala (1996), who tested only unheated manikins. Concentrations did not increase monotonically with increasing velocity as found by Guffey and Flanagan (2001). However, it should be noted that the Reynolds numbers for this study (Re = 1200-12000), Guffey and Flanagan (Re = 1000-7200), Kim and Flynn (Re = 3419-17094), and Kulmala (Re = 6300, 9500, 12700) were quite different, perhaps accounting for the differences in results between Guffey and Flanagan and the rest.

For lifelike conditions, heated manikin, concentrations varied in an inverted-V shape relationship with velocity for both sitting and standing. C_{mouth}, C_{nose}, and $C_{forehead}$ had peak values at 27 fpm for standing and 48 fpm for sitting. However, concentrations at the shoulder, C_{neck}, $C_{l.collar}$, and $C_{r.collar}$, and chest, $C_{c.chest}$, $C_{l.lapel}$, and $C_{r.lapel}$ had peak values at 48 fpm only for both postures. As listed in Table 2, for standing manikin, heating increased concentration levels at the mouth and nose locations for the entire velocity range, except at 11 fpm. For the same locations, the heated manikin had substantially lower concentrations for sitting at all velocities. These results were strongly supported by the analysis of variance (ANOVA) as shown in Table 33. The effect of velocity and heating were significant for log- transformed concentrations at all locations ($p<0.001$). In addition, the interaction of velocity and heating was also significant ($p<0.001$). These results agree with Heist et al. (2003), Fletcher and Johnson (1996), Brohus (1997), and Homma and Yakiyama (1988) who studied the effect of body heat on air flow patterns around a manikin in a uniform flow field and found that heating was also significant and had substantial effects at low speed wind environments. For these studies, wind velocities were ranged 0.05, 0.15, 0.3, and 0.5 m/s.

For the heated manikin, the effect of posture (sitting/standing) was quite significant on sampling locations. Sitting reduced concentration levels at chest and shoulder locations (see Figures 31-34 and Table 2). The reductions were statistically significant ($p<0.001$) for log transformed concentrations. The effect of posture on log C_{mouth} was statistically significant ($p<0.001$) but not significant for log C_{nose} and log $C_{forehead}$. The interaction of velocity and posture was not significant ($p> 0.26$) for concentrations at the shoulder and chest, but, was significant for C_{nose}, C_{mouth}, and $C_{forehead}$. Also, the interaction of velocity and posture was significant at face ($p<0.01$). This is because concentrations at the face had peak values at 27 fpm for standing and 48 fpm for sitting.

The interaction of posture and heating was very significant for locations at the face and shoulder ($p<0.001$), but not significant for chest locations. This is illustrated in Figures 31-34. For the heated and unheated conditions, $C_{c.chest}$, $C_{l.lapel}$, and $C_{r.lapel}$, had the highest values for standing, but, the lowest values for sitting, for all velocities.

Compared to individual locations, $C_{inhaled}$, $C_{upper.torso}$, and $C_{lower.torso}$ showed similar patterns with velocity, heating and posture, but, concentration levels were slightly different (see Tables 4.1 and 4.2). Analysis of Variance (ANOVA) for log transformed concentrations is shown in Table 9. Velocity, heating, and posture had a statistically significant effect ($p<0.001$) on $C_{inhaled}$, $C_{upper.torso}$, and $C_{lower.torso}$. Likewise, the interaction of velocity and heating had same significance.

The interactions of velocity and posture and heating and posture on the three levels had similar significance when compared to concentrations at individual locations.

As shown in Figures 35-38, unlike individual concentrations, the effect of velocity on ratios of concentration appeared to be different for heated and unheated conditions and for standing and seated postures. The ratio of nose to mouth C_{nose}/C_{mouth} varied very closely to unity for all treatment combinations and did not show any specific patterns. This was strongly supported by the analysis of variance (ANOVA), shown in Table 8. The effects of velocity, heating, and posture and their interactions velocity x heating, velocity x posture, and heating x posture, on log $\{C_{nose}/C_{mouth}\}$ were statistically insignificant ($p>0.06$). C_{nose} was located adjacent to the distal end of the nose on the left side, very closely to C_{mouth}. This strongly suggests that C_{nose} could be a good surrogate location for C_{mouth}.

The effect of independent variables and their interactions on log $\{C_{forehead}/C_{mouth}\}$ was also statistically insignificant, except for the interaction of heating x posture ($p<0.001$). $C_{forehead}$ consistently underestimated mouth exposure for the effect of independent variables. This is because of the downwash airflows coming from the sides of the face and the top of head. Since, the bias of $C_{forehead}/C_{mouth}$ was consistent, a mathematical relationship could be developed to estimate mouth concentrations using the forehead. However, sampling at the face of the worker is not a recommended practice for industrial hygiene practitioners.

As listed in Table 8, the effect of posture on log-transformed ratios of concentrations at the chest was statistically significant ($p<0.001$). $C_{c.chest}/C_{mouth}$, $C_{l.lapel}/C_{mouth}$, and $C_{r.lapel}/C_{mouth}$ varied with posture. Concentartions at chest locations overestimated mouth for standing and underestimated mouth concentrations for sitting (see Figures 35-38). The ratio $C_{c.chest}/C_{mouth}$ was approximately 2.1 for the unheated standing manikin and 1.95 for heated manikin. This agrees with (Malek et al, 1999) and (Welling et al, 2000) who tested human subjects and agrees also with (Guffey, et al., 2001), (Kim and Flynn, 1992) and (Kulmala et al., 1996) who tested unheated manikins and found that concentrations at the chest were higher than concentrations at vicinity of mouth (e.g. nose). For the unheated standing manikin, the ratio $C_{c.chest}/C_{mouth}$ was 2.1 for this study and 2.9 for (Guffey, et al., 2001). The differences agree qualitatively and disagre quantitively, because the manikin used in this study was anthropometrically correct, while, the one used in (Guffey et al., 2001) was 60% smaller. It is worth mentioning that the bias in chest concentrations is consistent for the effects of heating and velocity, but varies with posture. In industrial environment, workers are either sitting or standing. If a task is performed while standing, workers sit during breaks only, far from the source. As sampling at the chest overestimate mouth concentrations, it will provide over protection to worker. Therefore, developing a mathematical relationship to estimate mouth concentrations using concentrations measured at chest might be important. This would suggest that sampling at center chest location is a good surrogate for estimating mouth concentrations.

As listed in Table 8, ANOVA, the effect of velocity, posture, and the interaction of velocity and posture was statistically significant ($p<0.01$) on log transformed ratios of concentrations at shoulder level. Although heating was not significant for ratios of concentrations at the neck and the right collar, the interaction of velocity and heating was slightly significant ($p<=0.05$) for both ratios. It is worth mentioning that there are differences in statistical significance for the ratios of three sampling locations. This could be related to the fact that samplers at the shoulder level were in contact with clothing for both collars while neck sampler was in contact with manikin

skin. Also, both collars had downwashed air flows coming from above the shoulder level and washing both of them. This is not the case for the neck location.

Tables 5.6 to 5.9 listed regression coefficients, p-values and adjusted R-squared for log transformed concentrations for each sampling location. Log transformed concentartions were regressed versus wind tunnel velocity for each manikin treatment.

For unheated conditions (seated and standing), wind tunnel velocity was highly significant ($p<=0.009$) for all sampling locations, except for Log Cc.chest that had significane at ($p=0.024$) for unheated/seated. The concentrations at all sampling locations decreases as wind tunnel velocity with increases (see Tables 5.8 and 5.9). This was observed by the negative sign for velocity coefficient (C_1). Velocity coefficient (C_1) ranged from (-0.002 to -0.005) for both seated and standing. The regression constant (C_0) varied substantially from sampling location to another and from seated to standing. For example, (C_0) ranged from 1.64 – 2.14 for standing and from 1.60 – 1.80 for seated. Regression coefficient (C_0) values at chest level were higher than mouth level for standing and lower for seated. Adjusted R-squared (R^2) ranged 60% – 80% for both seated and standing for most sampling locations. This indicated that about 60% of the data can be represented by these regression models.

For heated manikin conditions, wind tunnel velocity was highly significant ($p<0.0001$) for all sampling locations for both seated and standing. Velocity coefficients (C_1) and (C_2) ranged from (0.01 to 0.02) and from (-0.01 to -0.02) respectively for both seated and standing. Velocity coefficient (C_1) was lower than (C_2) for all sampling locations (see Tables 5.6 and 5.7). The regression constant (C_0) varied substantially from sampling location to another and from seated to standing. For example, (C_0) ranged from 1.17 – 1.39 for standing and from 0.67 – 1.18 for seated. Regression coefficient (C_0) values at chest level were higher than mouth level for seated and were almost same for standing, except for Log $C_{c.chest}$ (1.33). Adjusted R-squared (R^2) ranged in the 80% – 90% for both seated and standing for most sampling locations. This indicated that about 90% of the data can be represented by these regression models. In conclusion, adjusted R-squared (R^2) for heated conditions were higher than unheated. Regression coefficient (C_0) values varied from seated to standing and from heated to unheated for all sampling locations.

Manikin Study II Results, Discussion and conclusions

Results of Manikin Study II

For this study, the manikin was either sitting or standing, breathing or not breathing and wearing a wig or bald. The manikin was heated and clothed throughout the whole study. This study was a complete factorial design with each condition including replicates (2) tested in random order. Initial tests and replicates were always done on different days.

As in Study I, one primary goal was to find the locations that act as the best surrogates for true inhaled concentrations. Concentrations measured at the mouth were assumed to equal "inhaled" volume. The secondary goal was to determine whether breathing, hair style, posture, and velocity affected concentrations measured on the manikin. Although the manikin inhaled and exhaled through its nose in a realistic manner, its "lungs" did not absorb ethanol. Hence a sample taken at the mouth in the exhaled air stream should differ negligibly from a sample taken of inhaled breath alone. As will be shown, the concentrations fell into three groups with similar

behavior: those at the face (C_{mouth}, C_{nose}, $C_{forehead}$), the shoulder (C_{neck}, $C_{l.collar}$, $C_{r.collar}$), and the chest ($C_{c.chest}$, $C_{l.lapel}$, $C_{r.lapel}$,).

Repeatability of C_{mouth}

Two samples were taken simultaneously at the right edge of the mouth less than 1 mm apart. The coincident locations were intended to be redundant checks. Ideally, there should be no systematic differences between C_{mouth_1} and C_{mouth_2} regardless of the levels of other independent variables. As shown in Figure 6.1, C_{mouth1} and C_{mouth2} are highly correlated (R-sq = 0.99) even when no independent variables are included in the regression model. The linear regression slope of 0.996 and intercept of zero confirm the two are indistinguishable.

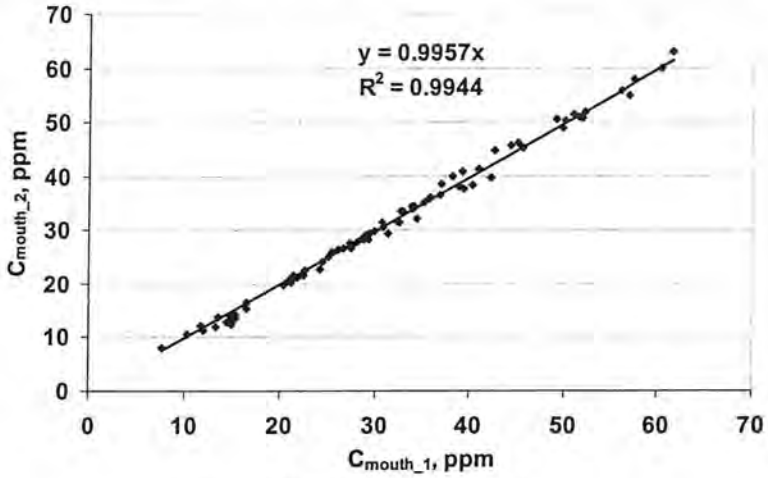

Figure 40: C_{mouth_1} versus C_{mouth_2}

Furthermore, ANOVA found no significant effects of any independent variable. These together suggest that the sampling procedures are highly repeatable and that differences between other locations measured at the same time represent real deviations at those times, not sampling errors. Given the trivial differences between C_{mouth1} and C_{mouth2}, the average of both values was used for comparisons to all other locations and is henceforth referred to as C_{mouth}.

As shown in Tables 6.1a and 6.1b and Figures 41 to 49, the average concentration values varied with sampling location, velocity, breathing, wig, and posture. Hence, comparisons between concentrations must be matched to similar conditions. Appendix C shows scatter and mean plots for log transformed concentrations with velocity for all sampling locations.

Table 15a: Average Concentration Values (Ppm) For Each Velocity Level and Manikin Treatment (Seated)

Treatment	V,fpm	$C_{c.chest}$	$C_{l.lapel}$	$C_{r.lapel}$	C_{neck}	$C_{l.collar}$	$C_{r.collar}$	C_{mouth}	C_{nose}	$C_{forehead}$
Seated/NoBreathing/NoWig	11	18.6	15.6	14.4	15.0	16.3	17.4	12.8	10.1	7.8
	27	22.6	21.9	20.4	21.3	21.3	20.3	22.7	21.5	14.9
	48	32.0	31.0	29.5	43.0	37.2	38.3	48.5	50.5	37.1
	82	23.6	21.1	18.3	20.6	20.7	20.0	29.6	31.0	26.2
	104	18.4	16.2	15.3	16.1	17.0	15.3	21.9	21.8	18.9
Seated/ Breathing/NoWig	11	12.8	9.2	10.8	15.7	15.6	12.1	15.9	13.3	9.3
	27	18.3	17.9	15.2	33.7	26.7	24.5	34.9	35.0	25.9
	48	21.2	23.0	21.9	36.7	34.7	36.8	48.3	46.8	44.3
	82	17.4	14.1	18.0	28.9	29.5	25.9	31.5	34.1	28.1
	104	16.3	12.7	12.9	25.0	28.0	21.9	26.6	28.4	21.9
Seated/ NoBreathing/Wig	11	9.8	7.3	7.2	28.3	23.5	31.9	18.6	15.9	12.8
	27	14.1	13.1	13.5	44.1	26.6	41.3	53.5	48.9	45.9
	48	19.7	18.6	20.4	37.4	25.8	33.4	44.3	43.0	42.1
	82	13.2	11.2	11.5	29.0	22.9	29.2	33.7	32.2	32.8
	104	10.0	10.7	9.3	25.0	21.4	24.3	31.3	28.9	27.6
Seated/ Breathing/ Wig	11	8.6	6.4	6.6	12.4	7.0	13.6	10.7	6.1	6.6
	27	15.5	13.4	12.5	19.9	18.0	17.1	24.6	26.0	26.8
	48	18.8	16.9	16.2	27.9	25.9	22.1	32.0	35.6	38.7
	82	14.8	12.6	10.1	24.6	24.0	23.4	27.7	30.0	28.6
	104	7.6	9.5	7.8	23.0	22.2	21.3	26.5	27.7	24.2

Table 15b: Average Concentration Values (Ppm) For Each Velocity Level and Manikin Treatment (Standing)

Treatment	V,fpm	$C_{c.chest}$	$C_{l.lapel}$	$C_{r.lapel}$	C_{neck}	$C_{l.collar}$	$C_{r.collar}$	C_{mouth}	C_{nose}	$C_{forehead}$
Standing/NoBreathing/NoWig	11	31.6	23.9	27.0	31.8	30.1	28.8	29.5	28.5	25.3
	27	49.3	41.1	46.9	52.5	44.1	39.4	61.3	57.8	52.0
	48	103.1	77.9	96.3	73.1	61.8	71.2	57.1	52.7	47.3
	82	51.6	43.2	46.4	46.5	37.8	44.1	44.6	41.3	39.4
	104	38.0	34.5	33.9	35.8	27.6	33.5	35.5	33.2	32.6
Standing/ Breathing/No Wig	11	25.9	12.9	17.3	25.0	25.9	18.8	20.3	21.4	18.6
	27	29.6	17.1	19.9	41.1	34.8	25.6	40.1	42.4	36.8
	48	62.3	38.5	53.5	49.5	44.1	42.0	38.5	39.1	31.9
	82	37.5	25.2	29.9	32.4	32.9	28.1	30.1	31.6	29.0
	104	30.1	23.5	22.3	26.2	28.4	21.6	25.1	28.4	25.4
Standing/ NoBreathing/ Wig	11	53.5	35.1	38.3	41.3	44.4	36.7	30.3	29.2	27.1
	27	59.6	44.9	52.0	54.1	50.7	57.7	41.2	38.2	32.1
	48	65.3	54.2	68.0	61.6	55.0	59.0	54.3	51.5	44.7
	82	37.5	28.6	33.3	39.0	31.0	38.6	39.6	36.2	36.8
	104	36.4	25.9	34.5	30.0	22.7	34.1	34.1	29.7	30.3
Standing/ Breathing/ Wig	11	28.4	9.3	10.6	27.5	19.9	12.3	16.9	20.1	16.8
	27	27.4	12.5	18.7	36.7	29.3	21.8	38.8	37.3	30.8
	48	38.2	23.3	22.3	32.5	25.3	18.1	26.7	35.7	28.6
	82	32.9	18.5	18.7	25.5	21.3	17.0	21.3	31.0	23.0
	104	31.3	16.5	15.0	23.3	18.4	13.6	19.9	30.6	24.3

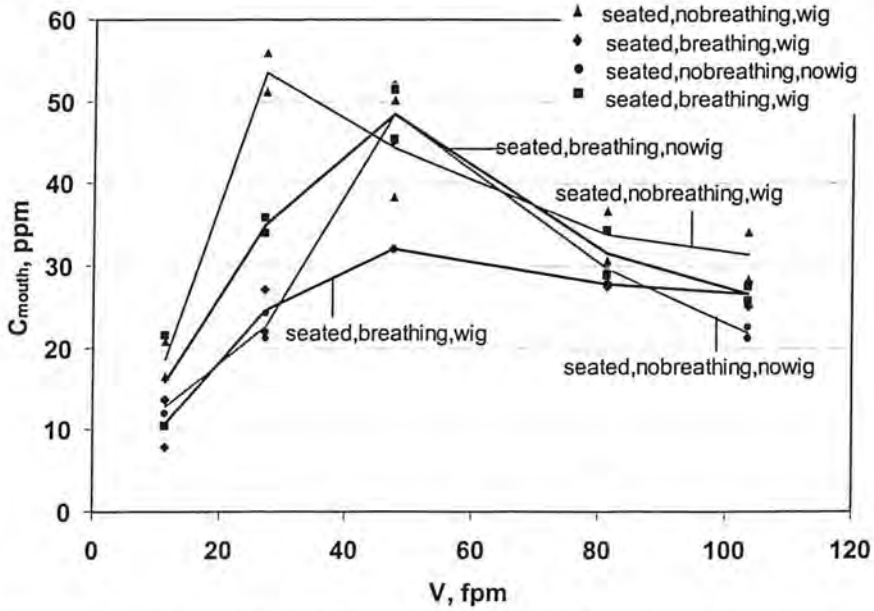

Figure 41a: Scatter and mean plot of C_{mouth} vs. velocity for all manikin treatment (seated)

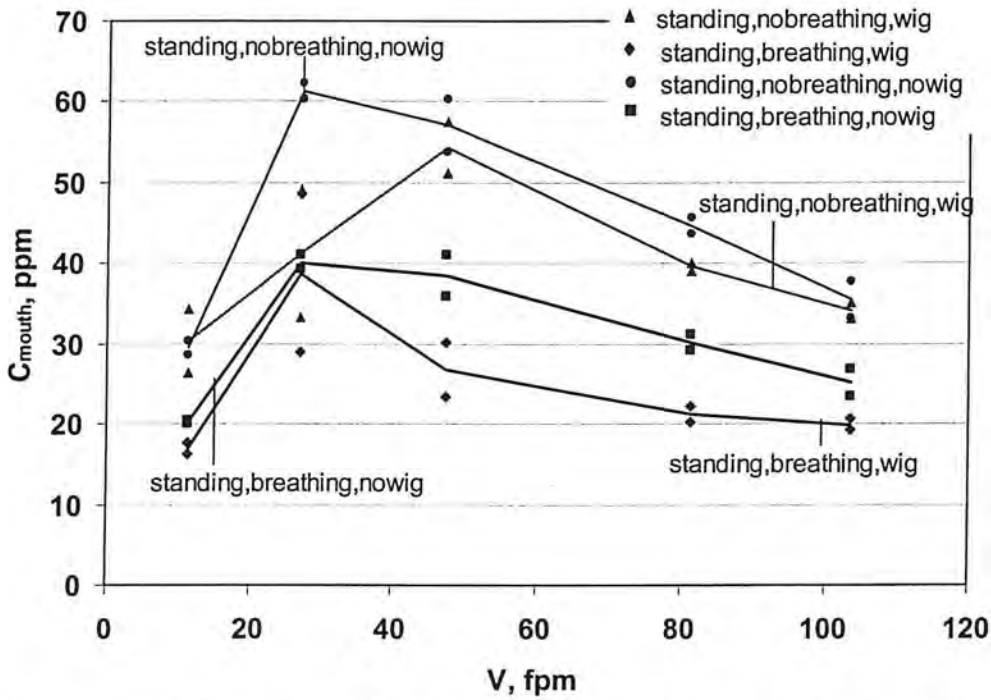

Figure 41b: Scatter and mean plot of $C_{m\,outh}$ vs. velocity for all manikin treatment (standing)

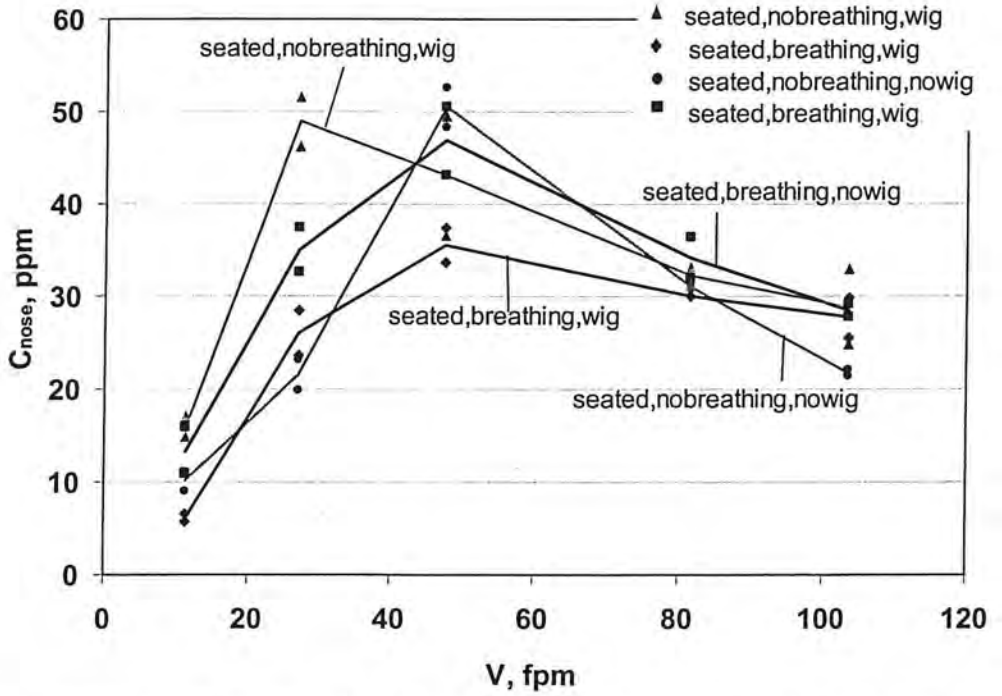

Figure 42a: Scatter and mean plot of C_{nose} vs. velocity for all manikin treatment (seated)

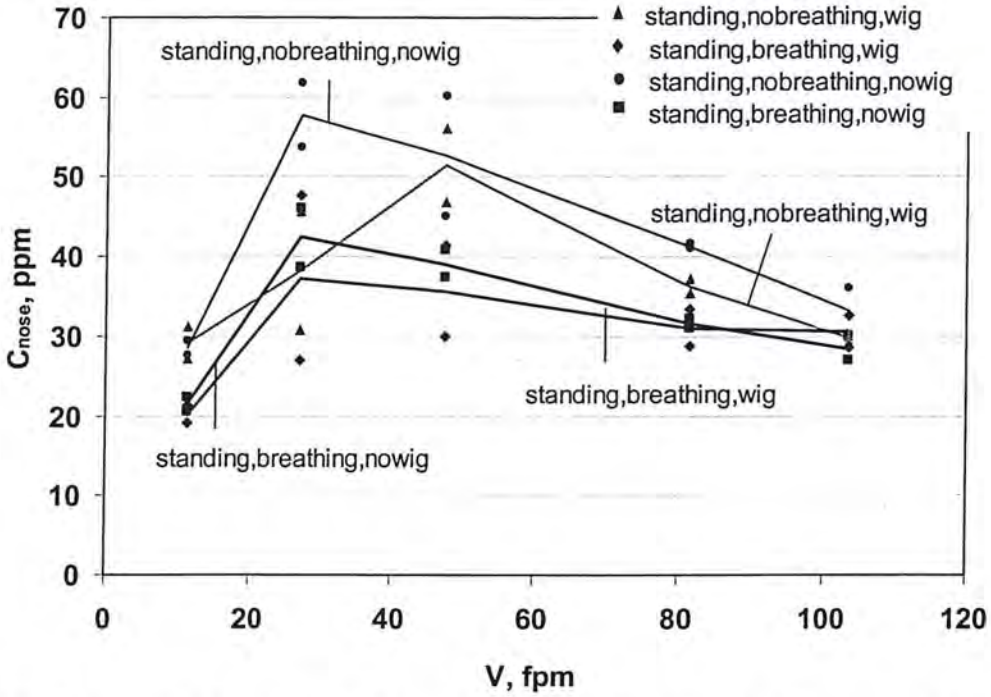

Figure 42b: Scatter and mean plot of C_{nose} vs. velocity for all manikin treatment (standing)

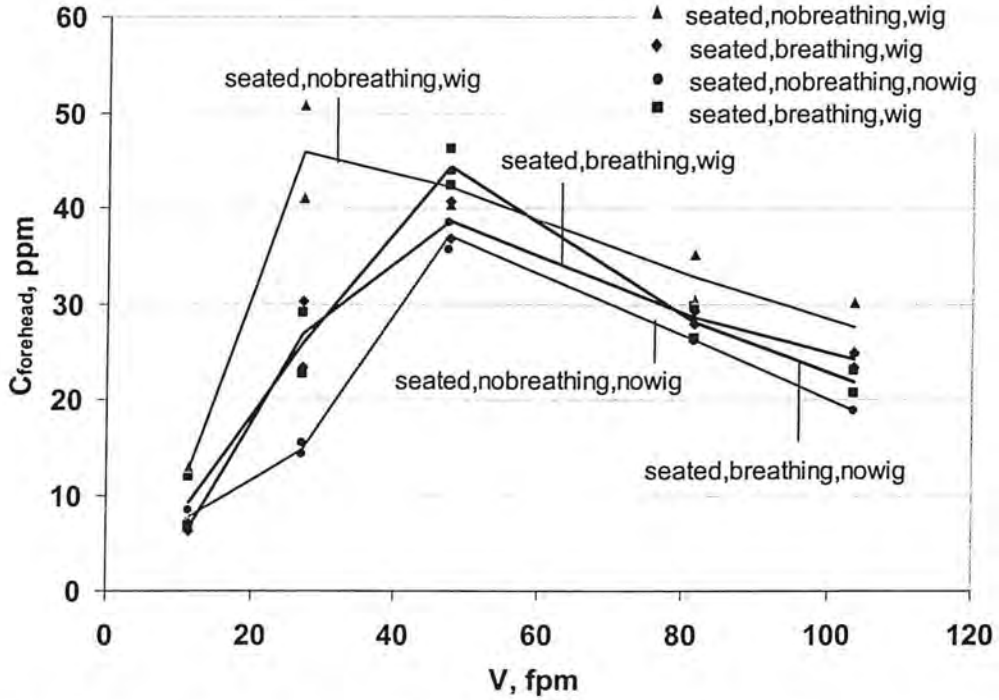

Figure 43a: Scatter and mean plot of $C_{forehead}$ vs. velocity for all manikin treatment (seated)

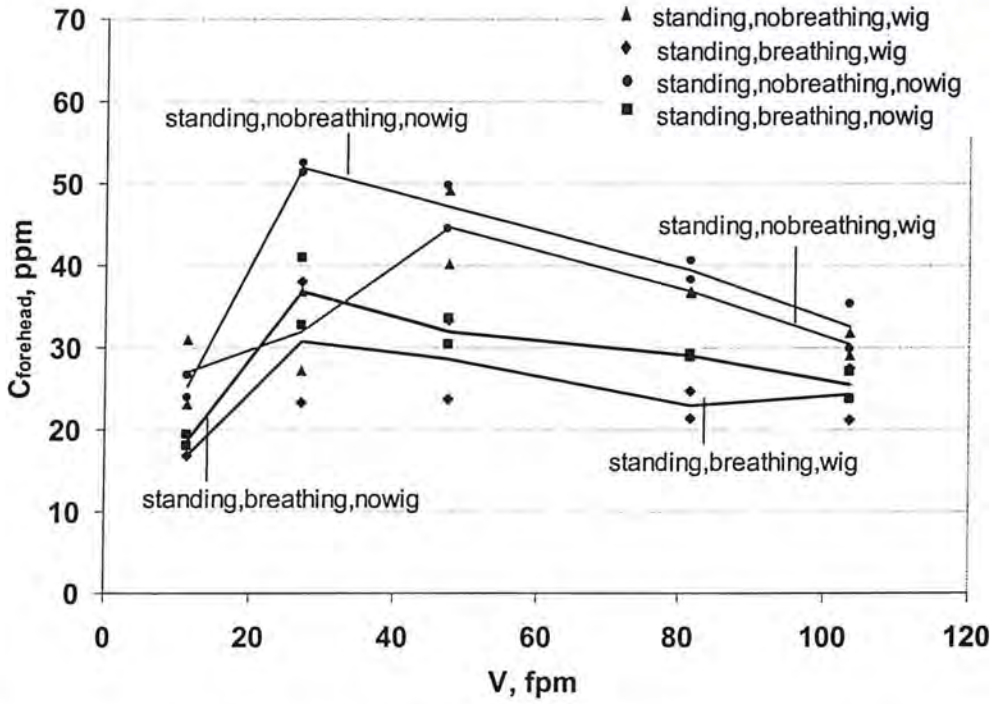

Figure 43b: Scatter and mean plot of $C_{forehead}$ vs. velocity for all manikin treatment (standing)

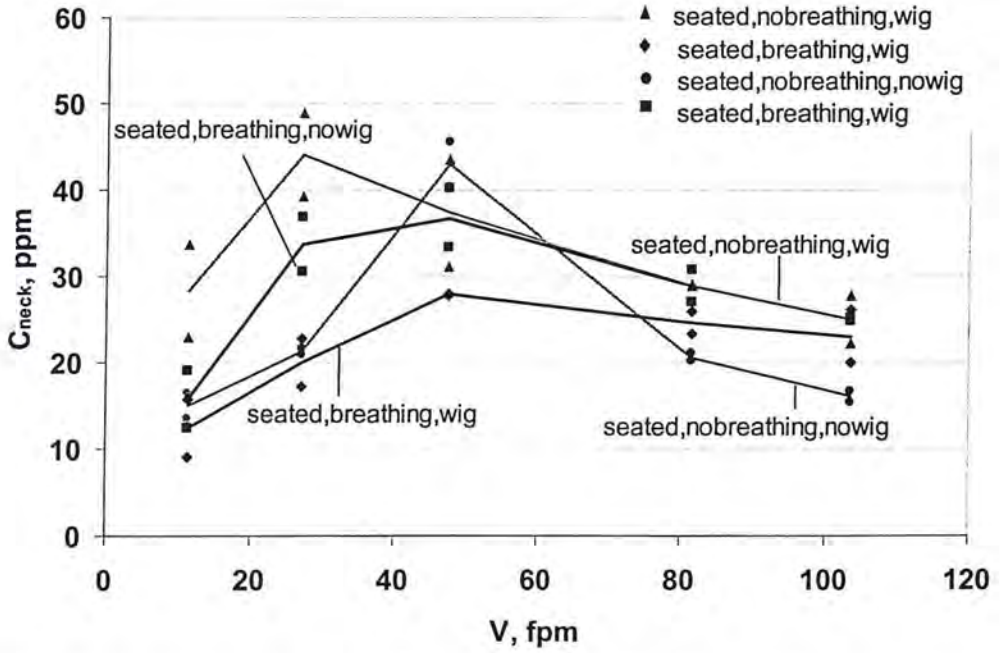

Figure 44a: Scatter and mean plot of C_{neck} vs. velocity for all manikin treatments (seated)

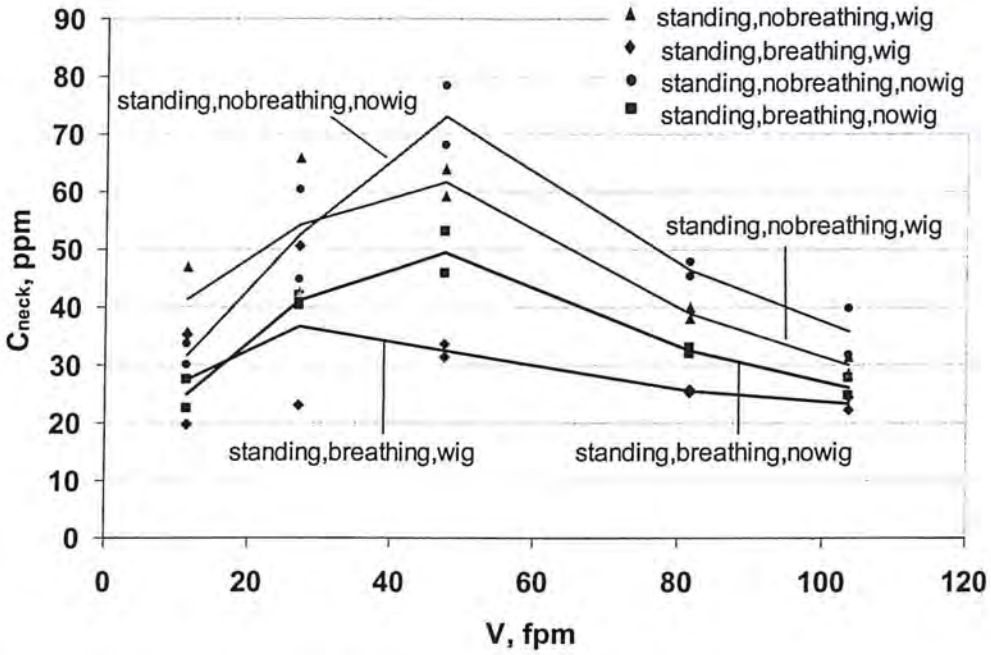

Figure 44b: Scatter and mean plot of C_{neck} vs. velocity for all manikin treatments (standing)

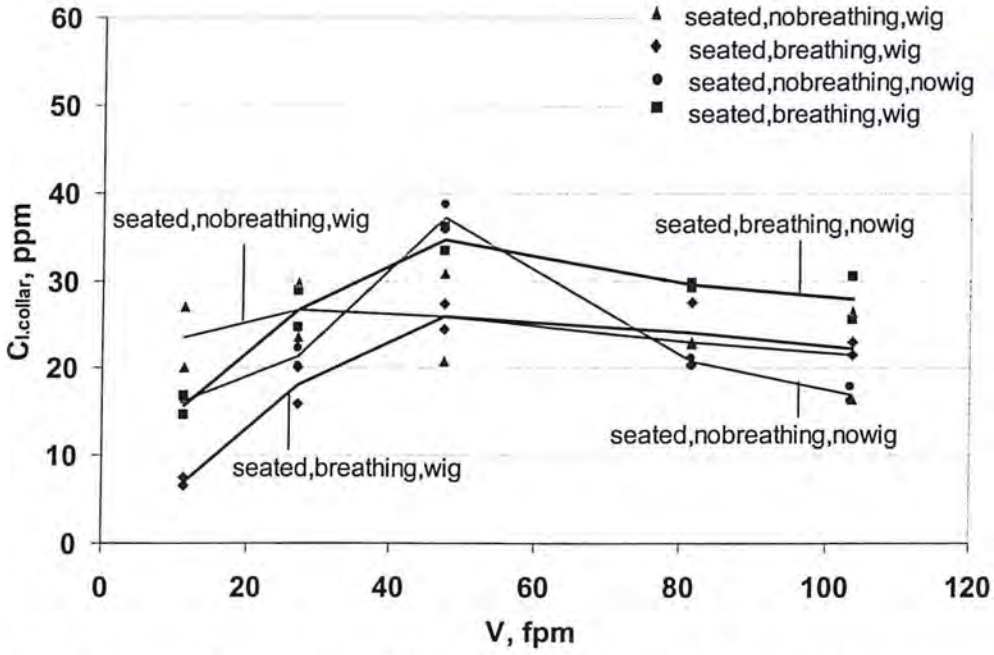

Figure 45-a: Scatter and mean plot of $C_{l.collar}$ vs. velocity for all manikin treatment (seated)

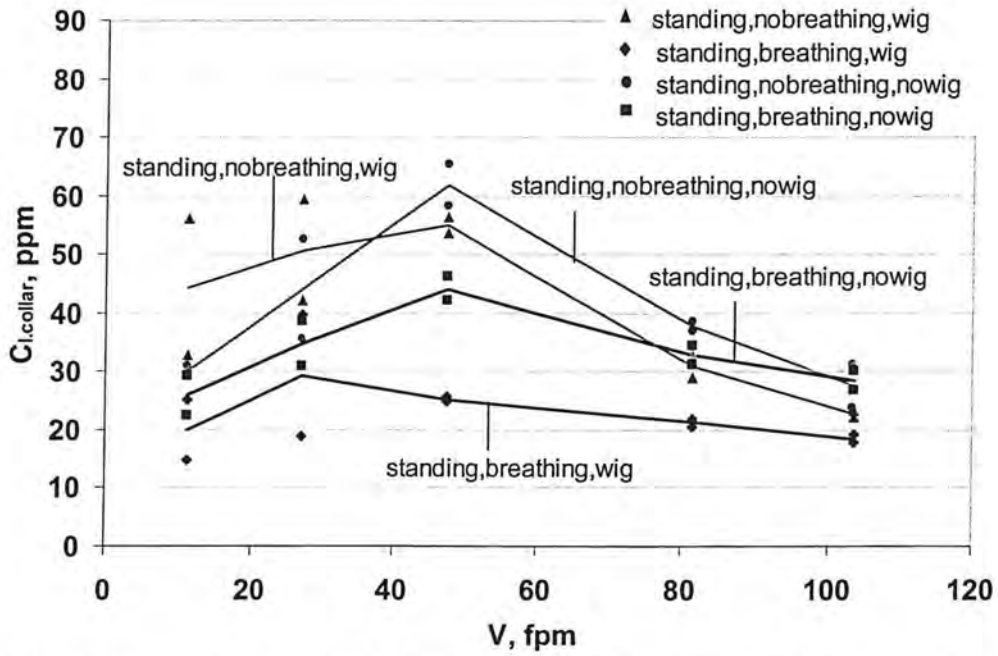

Figure 45-b: Scatter and mean plot of $C_{l.collar}$ vs. velocity for all manikin treatment (standing)

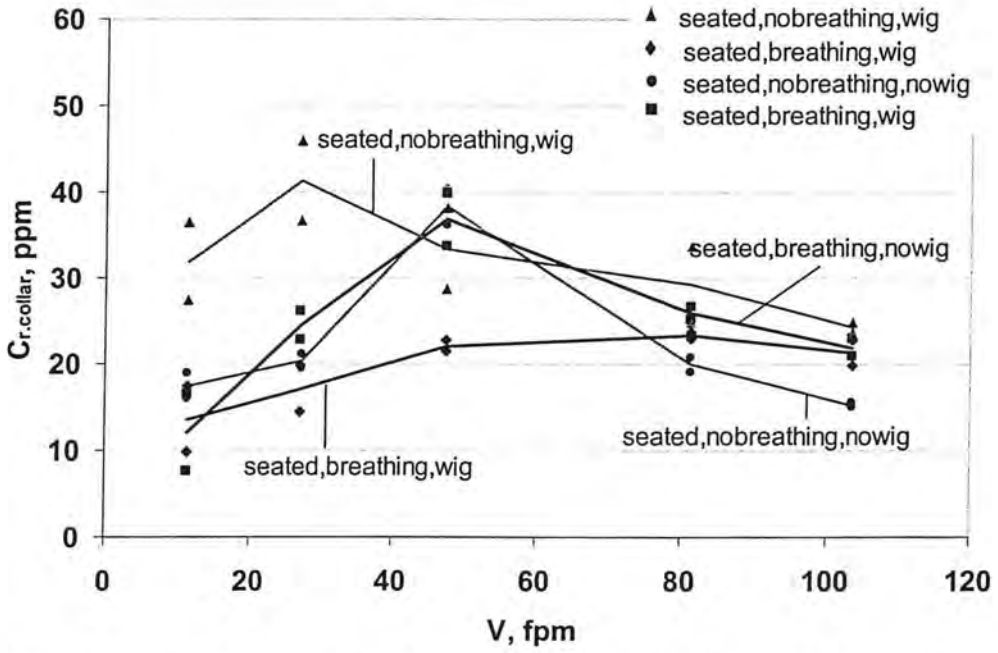

Figure 46-a: Scatter and mean plot of $C_{r.collar}$ vs. velocity for all manikin treatment (seated)

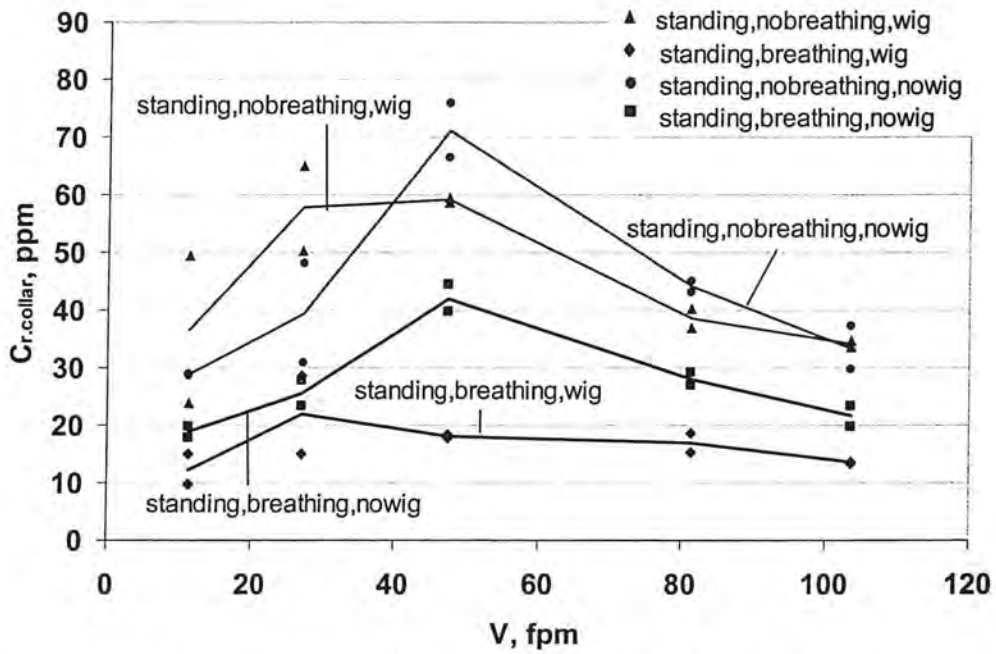

Figure 46-b: Scatter and mean plot of $C_{r.collar}$ vs. velocity for all manikin treatment (standing)

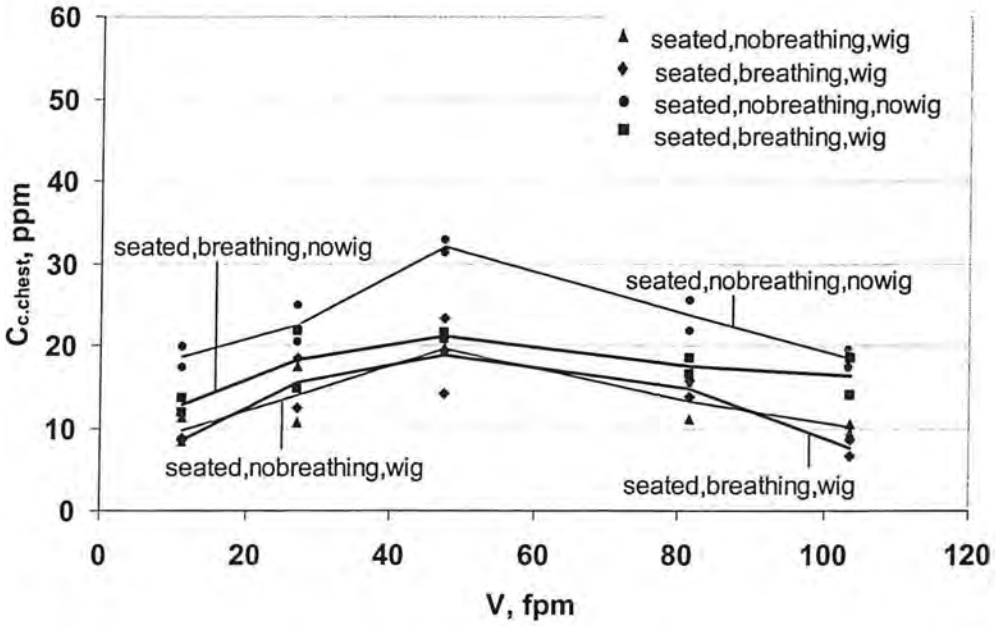

Figure 47a: Scatter and mean plot of $C_{c.chest}$ vs. velocity for all manikin treatment (seated)

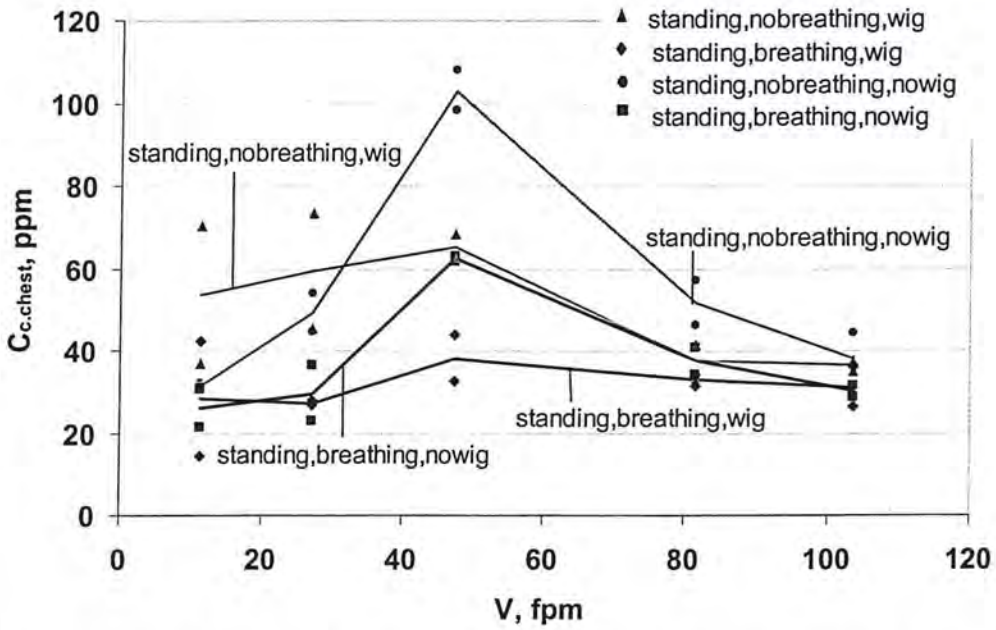

Figure 47b: Scatter and mean plot of $C_{c.chest}$ vs. velocity for all manikin treatment (Standing)

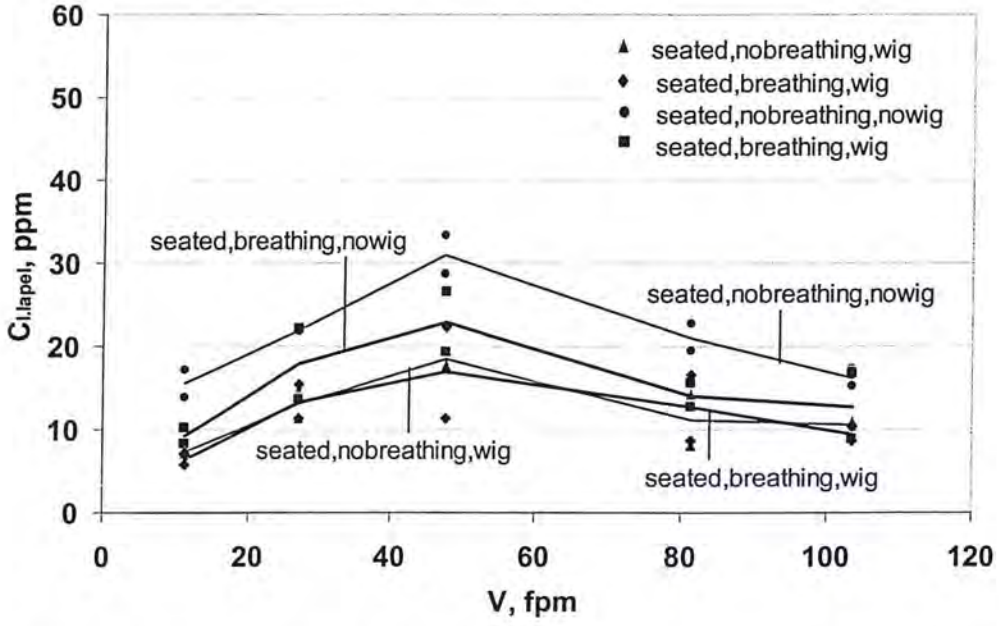

Figure 48a: Scatter and mean plot of $C_{l.lapel}$ vs. velocity for all manikin treatment (seated)

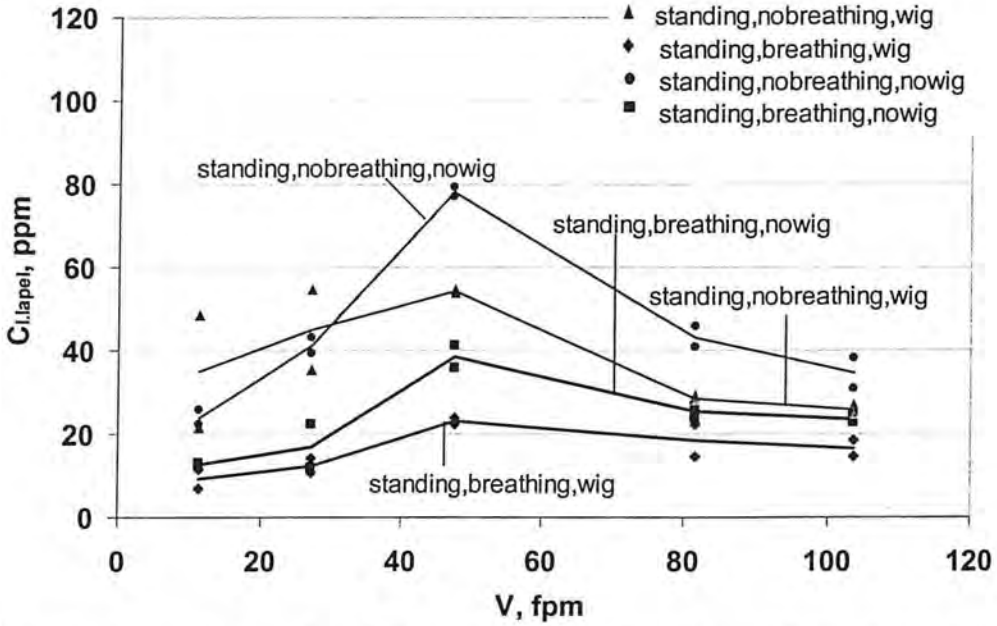

Figure 48b: Scatter and mean plot of $C_{l.lapel}$ vs. velocity for all manikin treatment (standing)

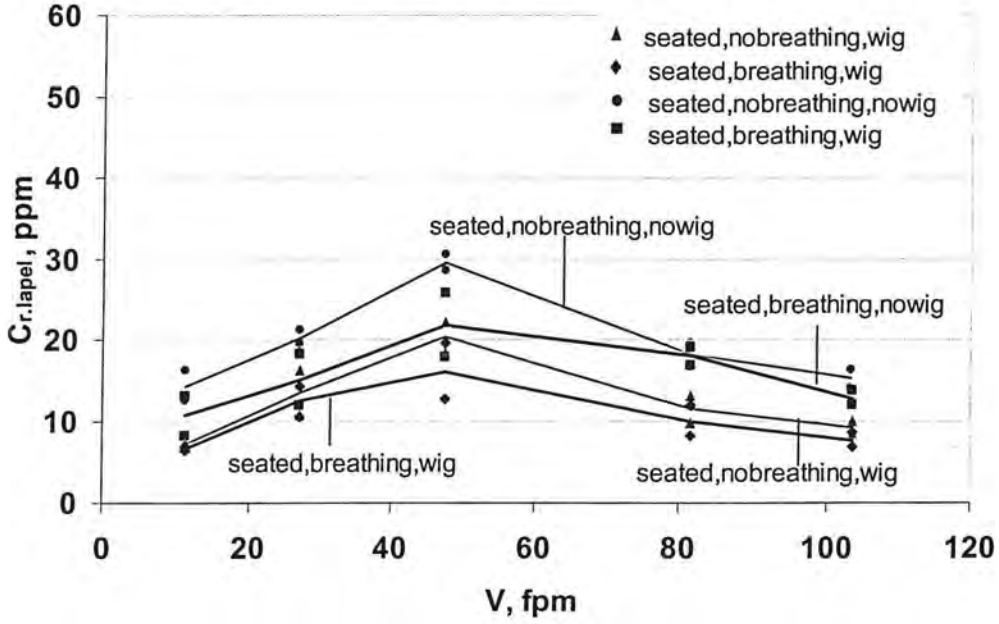

Figure 49a: Scatter and mean plot of $C_{r.lapel}$ vs. velocity for all manikin treatment (seated)

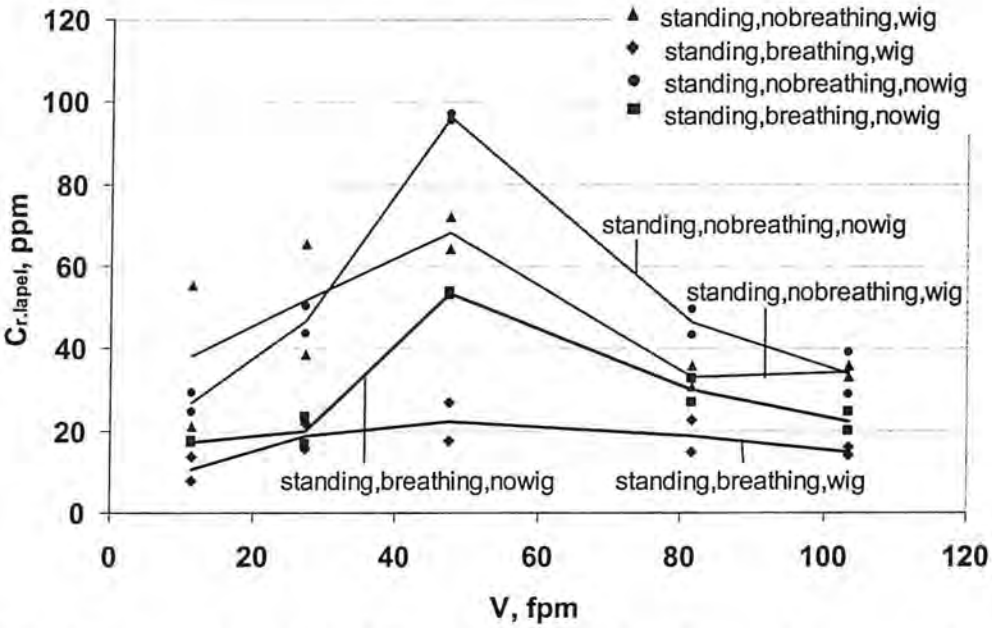

Figure 49b: Scatter and mean plot of $C_{r.lapel}$ vs. velocity for all manikin treatment (standing)

2 Effects of Independent Variables on all Sampling Locations

As listed in Tables 15a and 15b, concentration values of sampling locations at the face (C_{mouth}, $C_{forehead}$, C_{nose}), at the shoulder (C_{neck}, $C_{l.collar}$, $C_{r.collar}$), and chest ($C_{c.chest}$, $C_{l.lapel}$, $C_{r.lapel}$,) varied with different combinations of wind tunnel velocity, breathing, wig and posture. Generally, sampling locations were grouped based on two criteria: 1) similar patterns with velocity, breathing, wig and posture and 2) similar concentration levels. The following illustrates the effects of breathing, wig, posture and velocity on sampling locations.

6.2.1 Velocity

As shown in Figures 6.2 – 49, the effects of velocity appeared to be similar from one sampling location to another within each group for any given treatment combinations. As was true for a heated manikin in Study I, concentrations varied in an inverted-V shape relationship with velocity. Peak concentration levels occurred at either 27 or 48 fpm for all treatment combinations. These results agree with Study I of this work and with Brohus (1997), who studied the effect of heating on concentrations using full-sized, heated, breathing manikin wearing heavy clothing and wig at similar velocities.

The effect of velocity on concentrations at the face is shown in Figures 6.2 - 6.4. For breathing, with or without a wig, C_{mouth}, C_{nose}, and $C_{forehead}$ had peak values at 27 fpm for the standing manikin and 48 fpm for sitting. However, for the effect of wig only, C_{mouth}, C_{nose}, and $C_{forehead}$ had peak values at 48 fpm for standing and 27 fpm for sitting posture. As shown in Tables 6.1a and 6.1b, the difference in the means of various treatments was substantial at the low and middle velocities, but minor at the highest level (104 fpm).

The effect of velocity on concentrations at the shoulder is shown in Figures 44 - 46. For lifelike conditions, with or without a wig, C_{neck}, $C_{l.collar}$, and $C_{r.collar}$ had flat peaks at 27 and 48 fpm for both sitting and standing postures. However, for the effect of wig only, C_{neck}, $C_{l.collar}$, and

$C_{r.collar}$ had peak concentrations at 27 fpm for sitting and 48 fpm for standing. As shown in Tables 6.1a and 6.1b, the difference in the means of various treatments was substantial at 48 fpm for standing and moderate at 27 fpm for sitting.

The effect of velocity on concentrations at chest level is shown in Figures 47-49. $C_{c.chest}$, $C_{l.lapel}$, and $C_{r.lapel}$ had peak values at 48 fpm for both sitting and standing. The peaks were wider for sitting than standing. As shown in Tables 6.1a and 6.1b, for lifelike conditions, the difference in the means of various treatments for the three locations was modest at all velocities for sitting and was substantial at 48 fpm for standing.

6.2.2 Breathing

As shown in Figures 41 – 49, the effects of breathing on sampling locations appeared to be substantial for all sampling locations, and for both sitting and standing manikin. For a breathing manikin, with or without a wig, concentrations at all sampling locations varied in an inverted-V shape relationship with velocity. The peak concentrations varied with posture and wig. Breathing reduced concentrations for all sampling locations. The effect of breathing was greater for locations at the face and shoulder for the manikin wearing a wig for both postures.

As will be discussed later, the effect of breathing was substantial for all sampling locations. In addition, these findings agree with Heist et al. (2003), Fletcher and Johnson (1996), and Wood and Birkett (1979) who tested the effect of breathing for chid-size manikin and for adult sized manikin standing in a low speed flow field (0.1 - 0.5 m/s). Heist et al. (2003) found that breathing affected air flow patterns around the manikin in the vicinity of the mouth and nose, while, Wood and Birkett (1979) found that breathing action had little effect on a personal sampler located on manikin's lapel. In addition, Fletcher and Johnson (1996) found that breathing was confined to thermal boundry layer and did not influence the general flow field.

The effect of breathing, for the manikin wearing a wig, on concentrations at the face is shown in Figures 6.2 - 6.4. Breathing changed the peak location for C_{mouth}, C_{nose}, and $C_{forehead}$ from 27 fpm to 48 fpm for sitting and from 48 fpm to 27 fpm for standing. As shown in Tables 6.1a and 6.1b, at 48 fpm, C_{mouth}, C_{nose}, and $C_{forehead}$ concentration values for breathing and wig conditions were 51% lower for standing manikin and 54% lower for sitting than the no breathing and wig conditions.

The effect of breathing, for the manikin wearing a wig, on concentrations at the shoulder level is shown in Figures 44 - 46. Likewise, Breathing changed the peak locations for C_{neck}, $C_{l.collar}$, and $C_{r.collar}$ in similar patterns as concentrations at the face. As shown in Tables 6.1a and 6.1b, at 48 fpm, C_{neck}, $C_{l.collar}$, and $C_{r.collar}$ concentration values for breathing and wig conditions were 47% lower for standing manikin and 25% lower for sitting than the no breathing and wig conditions.

Unlike concentrations at the face and shoulder levels, the effect of breathing, for the manikin wearing a wig, on concentrations at the chest level is shown in Figures 47 - 49. Breathing had greater effect on $C_{c.chest}$, $C_{l.lapel}$, and $C_{r.lapel}$ for the low and middle velocity levels (11-48 fpm) for standing. However, the effect of breathing on concentrations at the chest was minor at all velocities and for sitting posture. As shown in Tables 6.1a and 6.1b, at 48 fpm, $C_{c.chest}$, $C_{l.lapel}$, and $C_{r.lapel}$ concentration values for breathing and wig conditions were 42% lower than the no breathing and wig for standing manikin.

6.2.3 Wig

As shown in Figures 41 – 49, the effects of wig on sampling locations appeared to be strikingly different with or without the effect of breathing and for both for the entire velocity range. For lifelike conditions, breathing, the wig had substantial and higher effects on concentrations measured at the face and the shoulder levels than concentrations measured at the chest for sitting posture at all velocities. Interestingly, the effect of the wig varied modestly with velocity at all sampling locations for standing manikin. As will be shown later, the wig reduced concentration levels, but with the peak location varied with velocity for all sampling locations.

The effect of wig on concentrations at the face is shown in Figures 41-44. C_{mouth}, C_{nose}, and $C_{forehead}$ had an inverted-V peak concentration values at 27 fpm for standing manikin and 48 fpm for sitting, for lifelike conditions. However, for the effect of wig only, the location of the peak changed to 48 fpm for standing and 27 fpm for sitting. As shown in Tables 6.1a and 6.1b, at 27 fpm and for a breathing standing manikin, C_{mouth}, C_{nose}, and $C_{forehead}$ concentration values for wearing a wig were 3% lower than bald conditions. On the other hand, at 48 fpm, for a breathing sitting manikin, C_{mouth}, C_{nose}, and $C_{forehead}$ concentration values for wearing a wig were 34% lower than bald conditions.

The effect of wig on concentrations at the shoulder is shown in Figures 44-48. C_{neck}, $C_{l.collar}$, and $C_{r.collar}$ had peaks occured at 48 fpm for sitting and 27 fpm for standing, for lifelike conditions. However, for the effect of wig only, the location of the peak changed to 48 fpm for standing and 27 fpm for sitting. As shown in Tables 6.1a and 6.1b, at 48 fpm, for a breathing standing manikin, C_{neck}, $C_{l.collar}$, and $C_{r.collar}$ concentration values for wearing a wig were 34% lower than bald conditions. On the other hand, at 48 fpm, for a breathing sitting manikin, C_{neck}, $C_{l.collar}$, and $C_{r.collar}$ concentration values for wearing a wig were 24% lower than bald conditions.

The effect of wig on concentrations at the chest is shown in Figures 47-49. $C_{c.chest}$, $C_{l.lapel}$, and $C_{r.lapel}$ had peaks occured at 48 fpm for various treatment combinations. However, peaks were flatter for chest concentrations than shoulder and face concentrations. As shown in Tables 6.1a and 6.1b, at 48 fpm, for a breathing standing manikin, $C_{c.chest}$, $C_{l.lapel}$, and $C_{r.lapel}$ concentration values for wearing a wig were 39% lower than bald conditions. On the other hand, at 48 fpm, for a breathing sitting manikin, $C_{c.chest}$, $C_{l.lapel}$, and $C_{r.lapel}$ concentration values for wearing a wig were 12% lower than bald conditions.

6.2.4 Posture

The effect of posture was substantial for the effects of velocity, breathing, and hair style. It is plausible that posture would affect concentrations because of the different orientation of arms and legs to cross draft. In the standing posture, the manikin arms and legs are perpendicular to the cross draft while in sitting posture the arms and legs are parallel to wind tunnel velocity. The arms and legs would affect air flow patterns around the manikin and hence concentration gradients in the breathing zone.

For instance, for sitting, concentrations at the face C_{mouth}, C_{nose}, and $C_{forehead}$, had peak concentrations occurred at 48 fpm for lifelike conditions and at 27 fpm for the effect of wig only. For standing, the peak for each treatment combination shifted to the other's locations (see Figures 6.2 - 6.4). Similarly, concentrations at the shoulder level, C_{neck}, $C_{l.collar}$, and $C_{r.collar}$ had peak occurred in similar pattern to concentrations at the face. Unlike sitting, concentartions at shoulder level peaked at 48 fpm and at 27 fpm for various treatments for standing as shown in Figures 44 - 46. Concentartions at chest level, $C_{c.chest}$, $C_{l.lapel}$, and $C_{r.lapel}$ peaked at 48 fpm for

both postures and for all treatments (see Figures 47 - 49). As will be discussed later on, the effect of posture was statistically significant for all sampling locations.

Table 16-a: Average Concentrations (ppm) at lower torso, upper torso, and inhaled (sitting)

Treatment	V,fpm	$C_{lower.torso}$	$C_{upper.torso}$	$C_{inhaled}$
Seated/NoBreathing/NoWig	11	16.2	16.2	11.5
	27	21.6	21.0	22.1
	48	30.8	39.5	49.5
	82	21.0	20.4	30.3
	104	16.6	16.1	21.8
Seated/ Breathing/NoWig	11	10.9	14.5	14.6
	27	17.1	28.3	34.9
	48	22.0	36.1	47.6
	82	16.5	28.1	32.8
	104	14.0	25.0	27.5
Seated/ NoBreathing/Wig	11	8.1	27.9	17.3
	27	13.5	37.3	51.2
	48	19.5	32.2	43.7
	82	11.9	27.0	33.0
	104	10.0	23.6	30.1
Seated/ Breathing/ Wig	11	7.2	11.0	8.4
	27	13.8	18.3	25.3
	48	17.3	25.3	33.8
	82	12.5	24.0	28.9
	104	8.3	22.2	27.1

Table 16-b: Average Concentrations (ppm) at lower torso, upper torso, and inhaled (standing)

Treatment	V,fpm	$C_{lower.torso}$	$C_{upper.torso}$	$C_{inhaled}$
Standing/NoBreathing/NoWig	11	27.5	30.2	29.0
	27	45.8	45.3	59.5
	48	92.4	68.7	54.9
	82	47.0	42.8	43.0
	104	35.5	32.3	34.3
Standing/ Breathing/No Wig	11	18.7	23.2	20.9
	27	22.2	33.8	41.2
	48	51.5	45.2	38.8
	82	30.9	31.1	30.8
	104	25.3	25.4	26.7
Standing/ NoBreathing/ Wig	11	42.3	40.8	29.7
	27	52.1	54.2	39.7
	48	62.5	58.6	52.9
	82	33.1	36.2	37.9
	104	32.3	29.0	31.9
Standing/ Breathing/ Wig	11	16.1	19.9	18.5
	27	19.5	29.3	38.0
	48	27.9	25.3	31.2
	82	23.4	21.3	26.1
	104	20.9	18.4	25.3

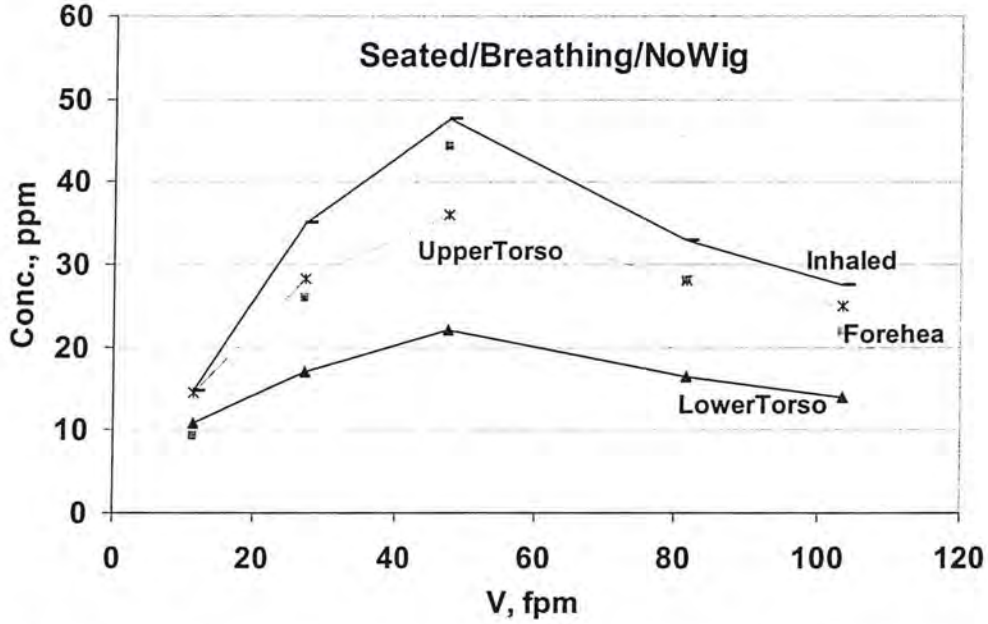

Figure 50-a: Average BZ Concentration versus velocity for all treatments

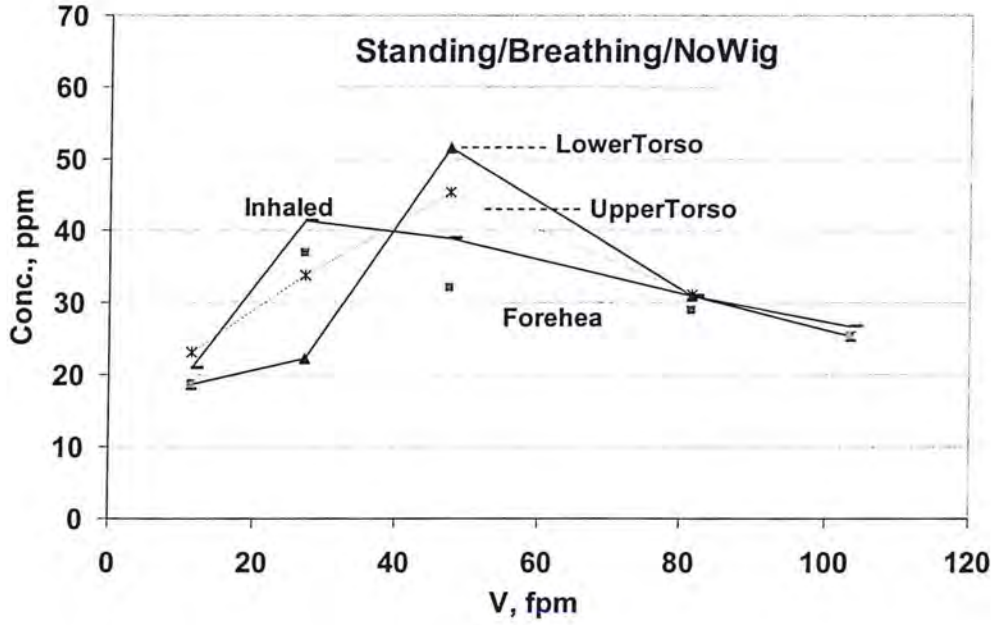

Figure 50-b: Average BZ Concentration versus velocity for all treatment

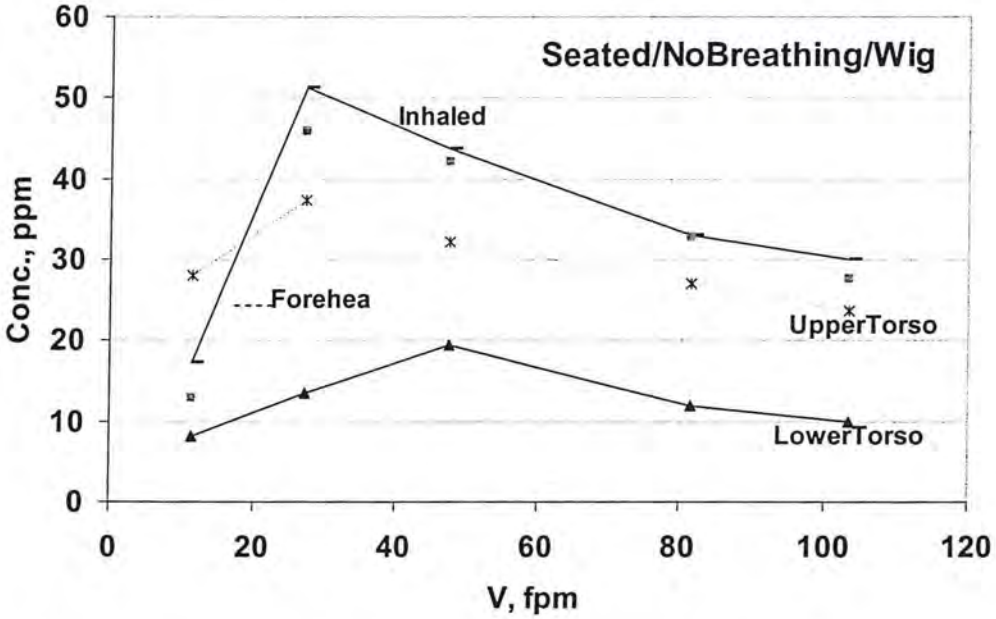

Figure 51-a: Average BZ Concentration versus velocity for all treatment

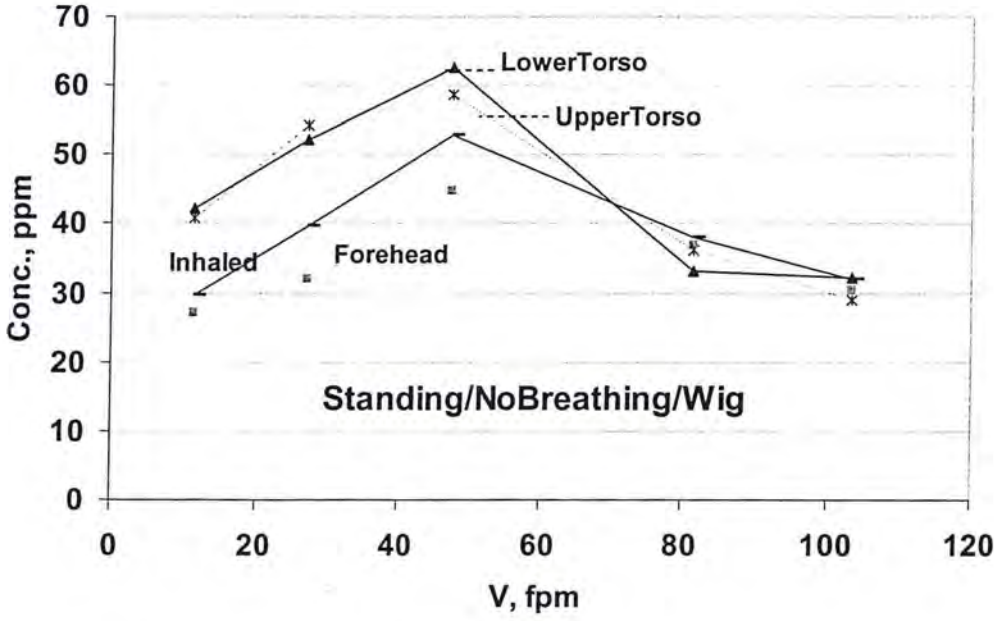

Figure 51-b: Mean BZ Concentration versus velocity for all treatment

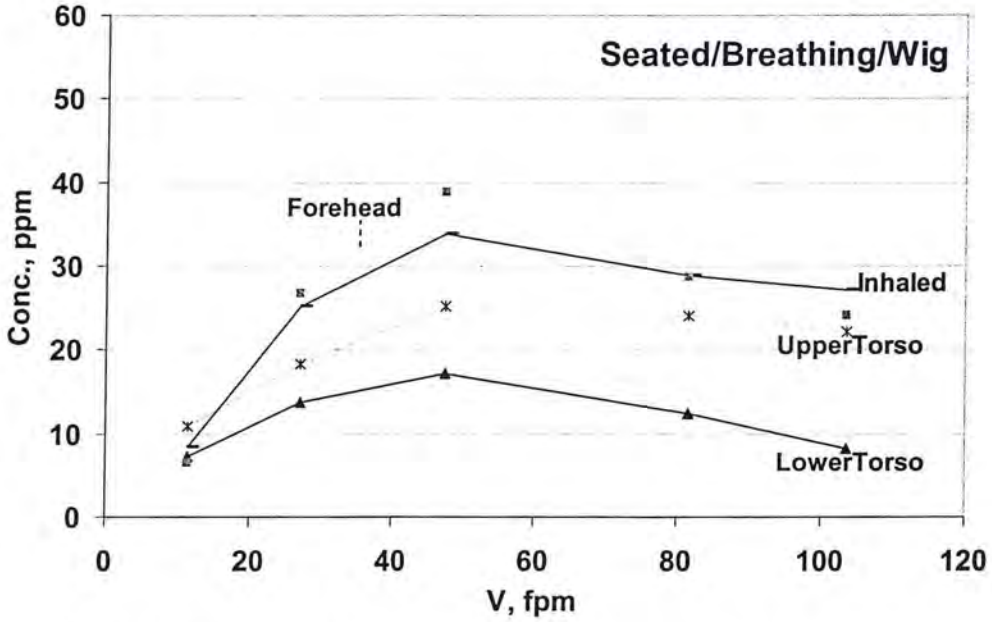

Figure 52-a: Mean BZ Concentration versus velocity for all treatment

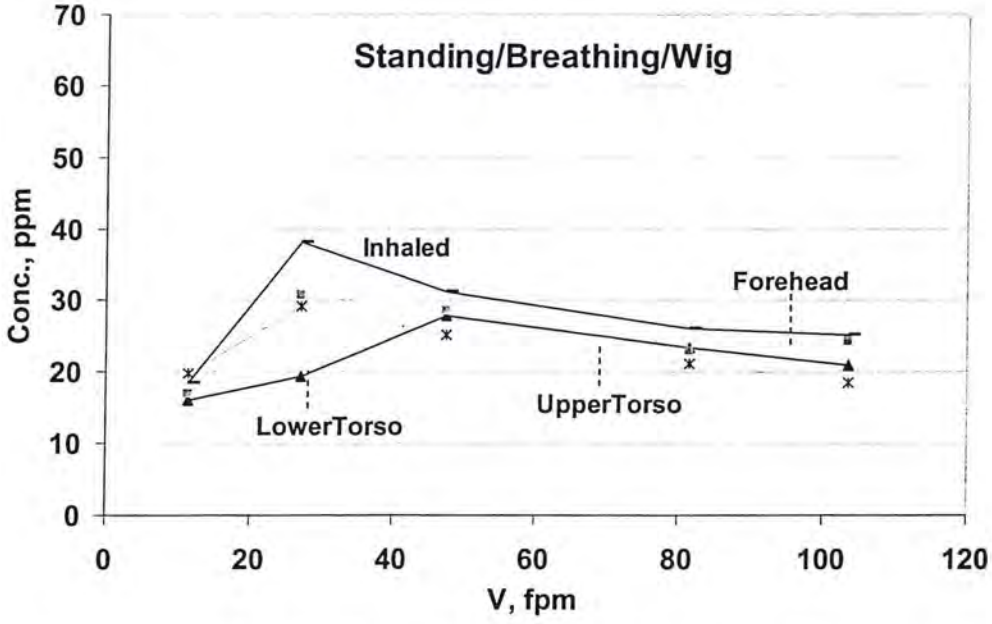

Figure 52-b: Mean BZ Concentration versus velocity for all treatment

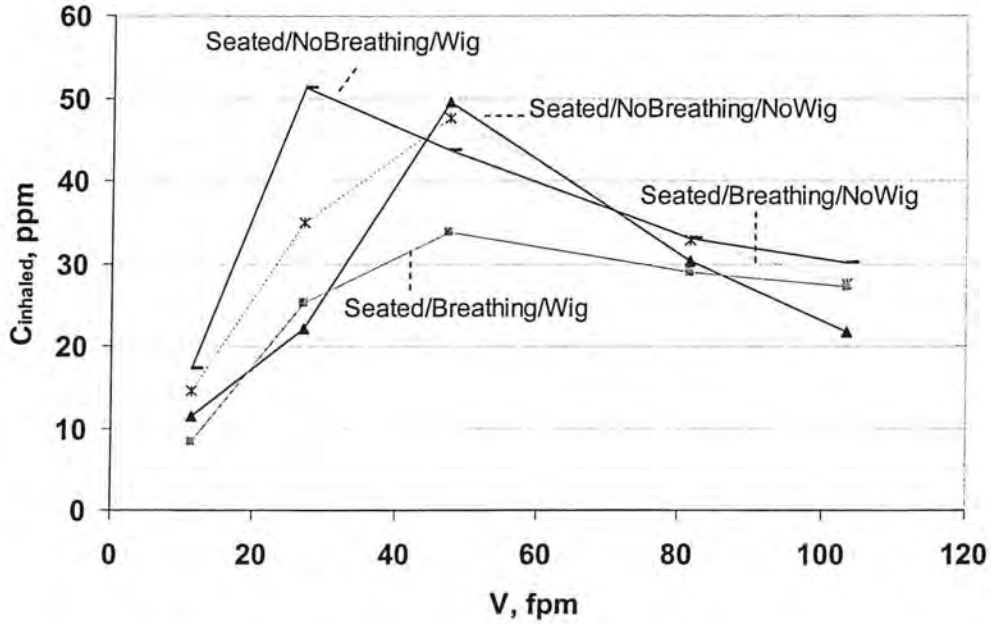

Figure 53-a: Mean plot of $C_{inhaled}$ versus velocity for all manikin treatment

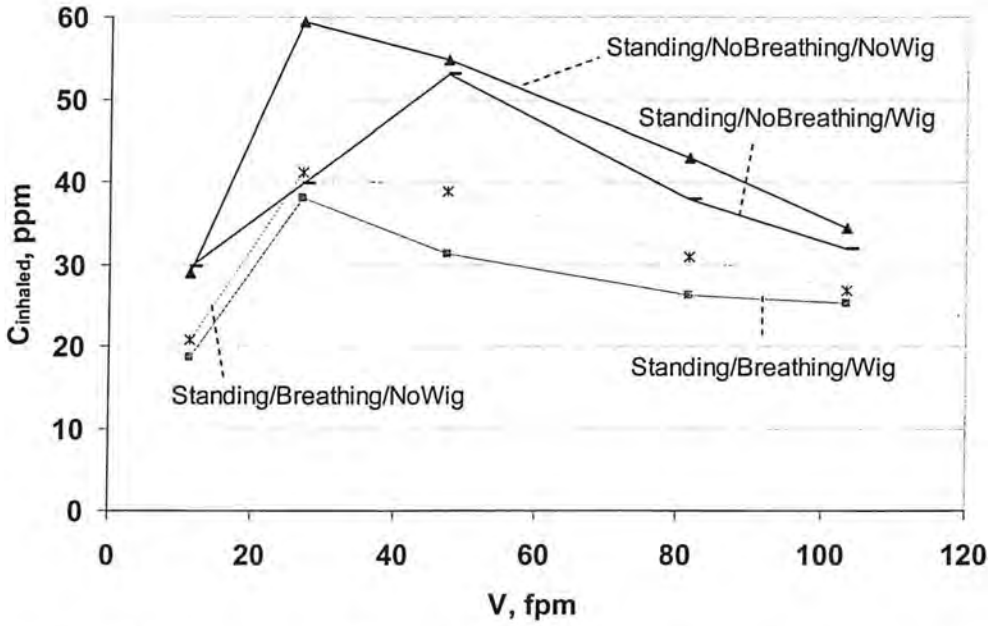

Figure 53-b: Mean plot of $C_{inhaled}$ versus velocity for all manikin treatment

3 Effects of Independent Variables on $C_{inhaled}$, $C_{upper.torso}$, and $C_{lower.torso}$

Since concentrations near the mouth behaved similarly, the average of C_{mouth} and C_{nose} were used to compute $C_{inhaled}$. Likewise, $C_{uptorso}$ is the average of C_{neck} and the two collars and $C_{lowtorso}$ is the average of C_{chest} and the two lapels. $C_{forehead}$ was the lowest concentration level compared to (C_{mouth} and C_{nose}) so it was not used to compute $C_{inhaled}$.

Figures 50 to 53 show the effects of velocity, breathing, wig, and posture on $C_{inhaled}$, $C_{uppertorso}$, and $C_{lowertorso}$. For the the most realistic conditions, breathing and wig, all three concentrations varied in an inverted-V shape with velocity for both sitting and standing. The location of the peak was different for sitting (48 fpm) and standing (27 fpm), but the magnitudes of the peaks were about the same at a given location. However, the concentrations differed sharply by measurement locations. More importantly, the differences in concentrations were strongly affected by posture. For example, the lower chest concentrations were much higher than $C_{inhaled}$ for standing and lower for sitting (see Figures 50a&b). Hence, whether a torso measurement exaggerated or underestimated the actual level depends on whether the manikin was sitting or standing.

As shown in Tables 16a and 16b, for lifelike conditions, at peak velocities, the effect of breathing and wig on $C_{inhaled}$ was substantial, 32% reduction for sitting. On the other hand, the effect of breathing only on $C_{inhaled}$ was substantial, 31% reduction in concentrations for standing. Similarlly, the effect of breathing and wig on $C_{upper.torso}$ substantially reduced concentration levels by 36% for sitting and 44% for standing.

Table 17-a: Ratios of Concentrations to C_{mouth} for all Velocities and Manikin Treatments (sitting posture)

Treatment	V,fpm	$C_{c.chest}/C_{mouth}$	$C_{l.lapel}/C_{mouth}$	$C_{r.lapel}/C_{mouth}$	C_{neck}/C_{mouth}	$C_{l.collar}/C_{mouth}$	$C_{r.collar}/C_{mouth}$	C_{nose}/C_{mouth}	$C_{forehead}/C_{mouth}$
Seated/NoBreathing/NoWig	11.3	1.45	1.21	1.12	1.18	1.28	1.36	0.80	0.61
	27.2	1.00	0.97	0.90	0.94	0.94	0.89	0.95	0.65
	47.5	0.66	0.65	0.61	0.89	0.77	0.79	1.04	0.77
	81.5	0.80	0.71	0.62	0.70	0.70	0.67	1.04	0.88
	103.5	0.84	0.74	0.70	0.73	0.78	0.70	0.99	0.86
Seated/ Breathing/NoWig	11.3	0.89	0.64	0.71	1.04	1.09	0.75	0.89	0.60
	27.2	0.53	0.52	0.44	0.97	0.76	0.70	1.00	0.74
	47.5	0.44	0.48	0.46	0.76	0.72	0.77	0.97	0.92
	81.5	0.55	0.45	0.57	0.92	0.95	0.83	1.09	0.90
	103.5	0.61	0.48	0.48	0.94	1.06	0.82	1.07	0.83
Seated/ NoBreathing/Wig	11.3	0.52	0.40	0.39	1.51	1.26	1.71	0.86	0.70
	27.2	0.26	0.24	0.25	0.82	0.50	0.77	0.91	0.86
	47.5	0.45	0.43	0.46	0.84	0.58	0.75	0.97	0.96
	81.5	0.40	0.34	0.35	0.87	0.69	0.86	0.96	0.98
	103.5	0.32	0.34	0.30	0.80	0.68	0.78	0.94	0.88
Seated/ Breathing/ Wig	11.3	0.87	0.63	0.67	1.15	0.69	1.26	0.60	0.65
	27.2	0.65	0.56	0.52	0.81	0.75	0.69	1.06	1.09
	47.5	0.59	0.53	0.51	0.87	0.81	0.69	1.11	1.21
	81.5	0.53	0.46	0.36	0.89	0.87	0.84	1.08	1.03
	103.5	0.29	0.36	0.30	0.86	0.84	0.80	1.04	0.91

Table 17-b: Ratios of Concentrations to C_{mouth} for all Velocities and Manikin Treatments (standing posture)

Treatment	V,fpm	$C_{c.chest}/C_{mouth}$	$C_{l.lapel}/C_{mouth}$	$C_{r.lapel}/C_{mouth}$	C_{neck}/C_{mouth}	$C_{l.collar}/C_{mouth}$	$C_{r.collar}/C_{mouth}$	C_{nose}/C_{mouth}	$C_{forehead}/C_{mouth}$
Standing/NoBreathing/NoWig	11.3	1.07	0.81	0.91	1.08	1.02	0.98	0.97	0.86
	27.2	0.80	0.67	0.76	0.86	0.72	0.64	0.94	0.85
	47.5	1.81	1.37	1.69	1.29	1.09	1.26	0.93	0.83
	81.5	1.15	0.97	1.04	1.04	0.85	0.99	0.93	0.88
	103.5	1.06	0.97	0.95	1.01	0.78	0.94	0.94	0.92
Standing/Breathing/NoWig	11.3	1.28	0.63	0.85	1.23	1.28	0.93	1.06	0.92
	27.2	0.74	0.43	0.50	1.03	0.87	0.64	1.06	0.92
	47.5	1.63	1.00	1.40	1.29	1.15	1.09	1.02	0.83
	81.5	1.24	0.84	0.99	1.08	1.09	0.93	1.05	0.96
	103.5	1.20	0.94	0.89	1.05	1.13	0.86	1.13	1.01
Standing/NoBreathing/Wig	11.3	1.72	1.12	1.21	1.36	1.44	1.18	0.97	0.89
	27.2	1.43	1.08	1.24	1.31	1.23	1.42	0.93	0.78
	47.5	1.21	1.00	1.26	1.14	1.01	1.09	0.95	0.82
	81.5	0.95	0.72	0.84	0.98	0.78	0.97	0.92	0.93
	103.5	1.07	0.76	1.01	0.88	0.67	1.00	0.87	0.89
Standing/Breathing/Wig	11.3	1.71	0.55	0.64	1.64	1.19	0.73	1.19	0.99
	27.2	0.75	0.36	0.49	0.92	0.73	0.55	0.96	0.80
	47.5	1.48	0.88	0.82	1.23	0.96	0.69	1.33	1.06
	81.5	1.55	0.88	0.87	1.20	1.00	0.80	1.47	1.08
	103.5	1.56	0.83	0.75	1.17	0.93	0.68	1.54	1.22

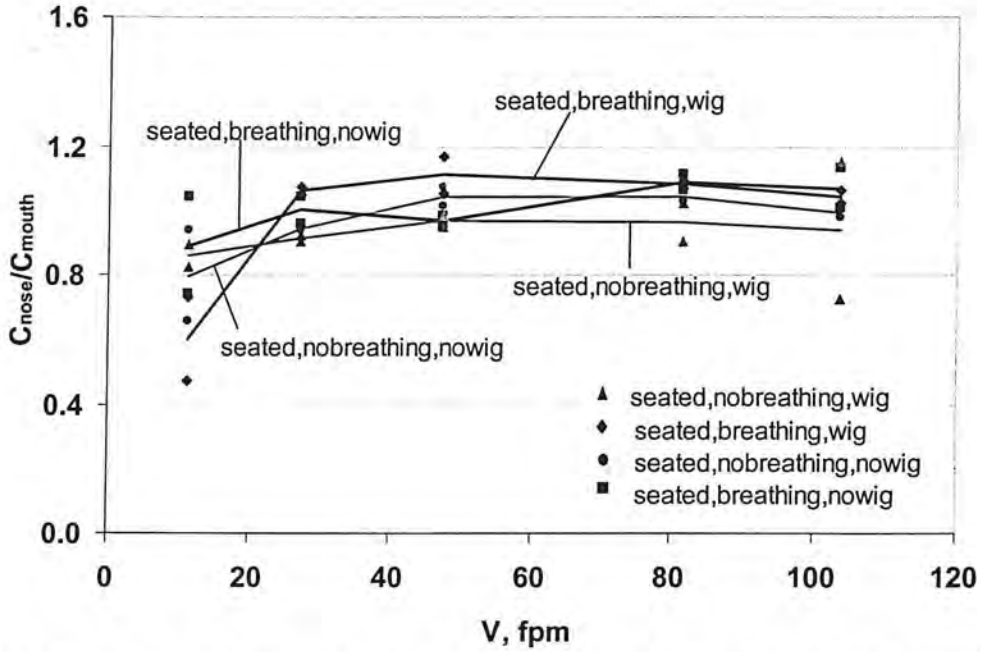

Figure 54-a: Scatter and mean plot of C_{nose}/C_{mouth} vs. velocity for all manikin treatments (seated)

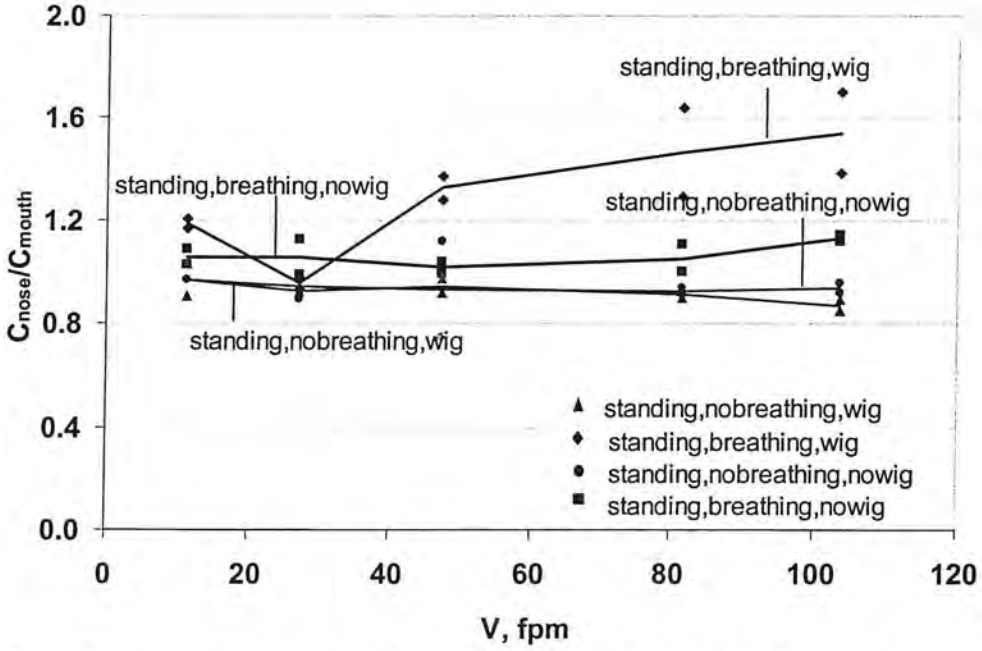

Figure 54-b: Scatter and mean plot of C_{nose}/C_{mouth} vs. velocity for all manikin treatments (standing)

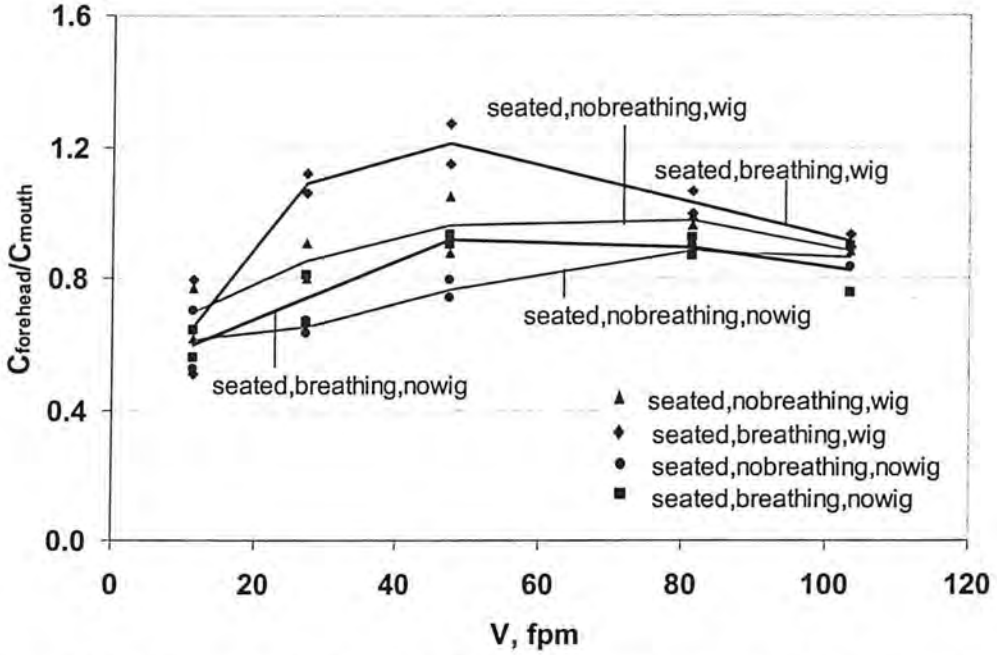

Figure 55-a: Scatter and mean plot of $C_{forehead}/C_{mouth}$ vs. velocity for all manikin treatments (seated)

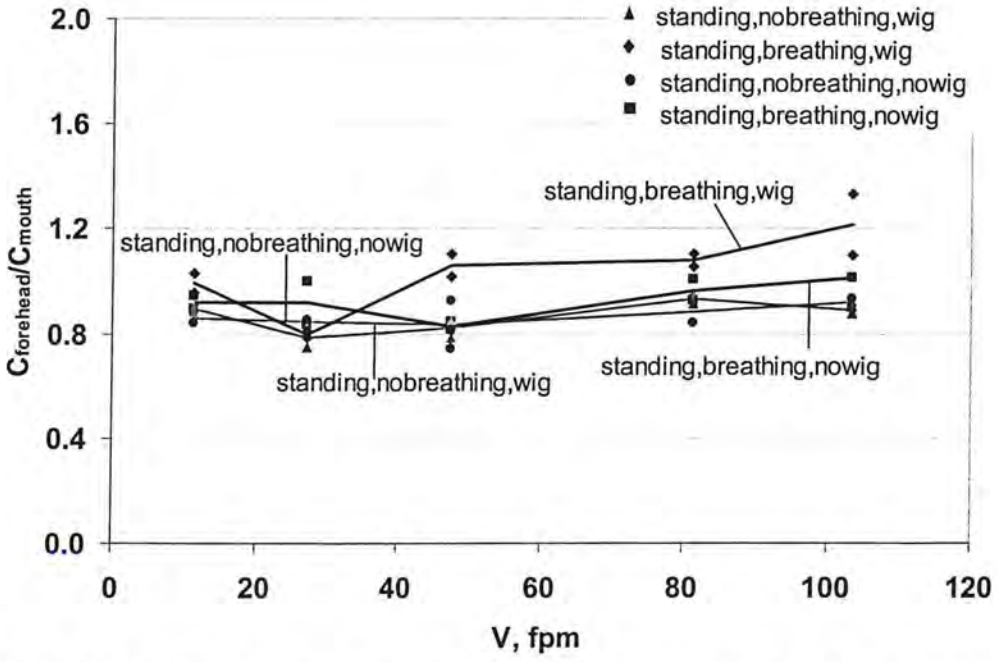

Figure 55-b: Scatter and mean plot of $C_{forehead}/C_{mouth}$ vs. velocity for all manikin treatments (standing)

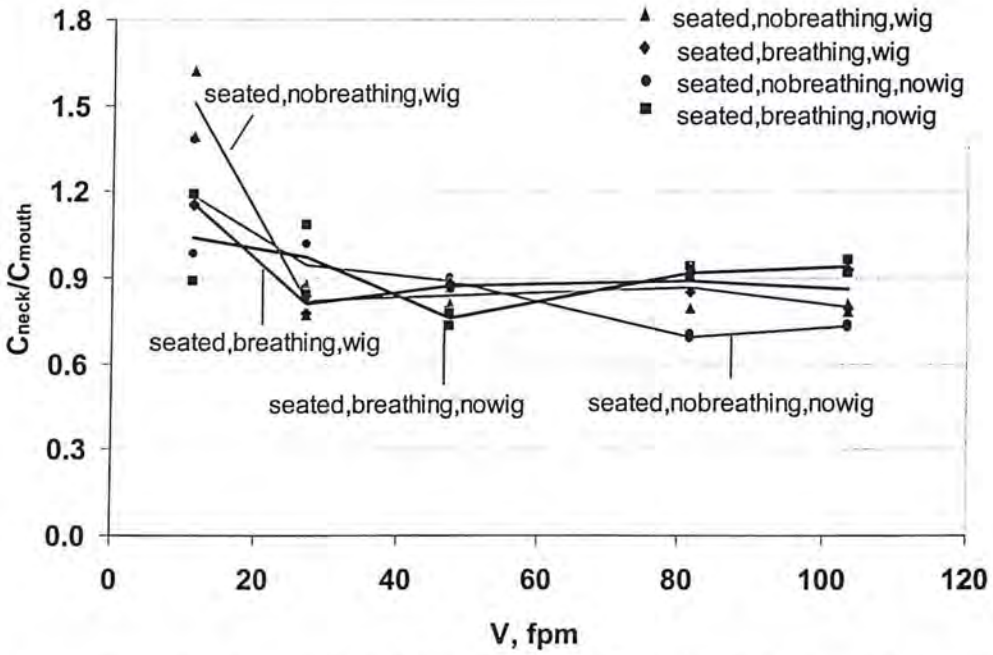

Figure 56-a: Scatter and mean plot of C_{neck}/C_{mouth} vs. velocity for all manikin treatments (seated)

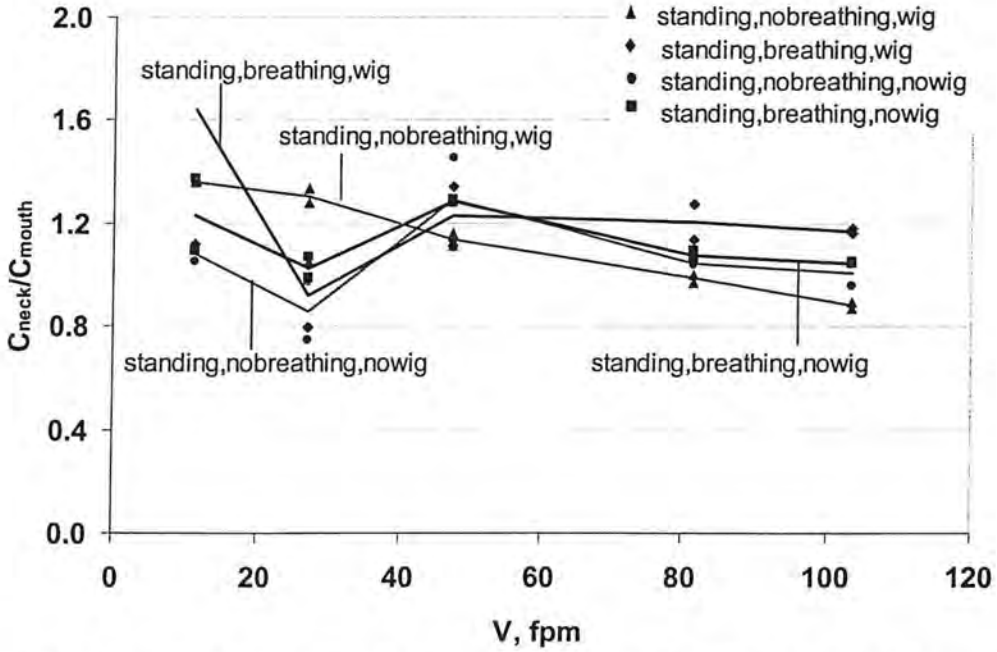

Figure 56-b: Scatter and mean plot of C_{neck}/C_{mouth} vs. velocity for all manikin treatments (standing)

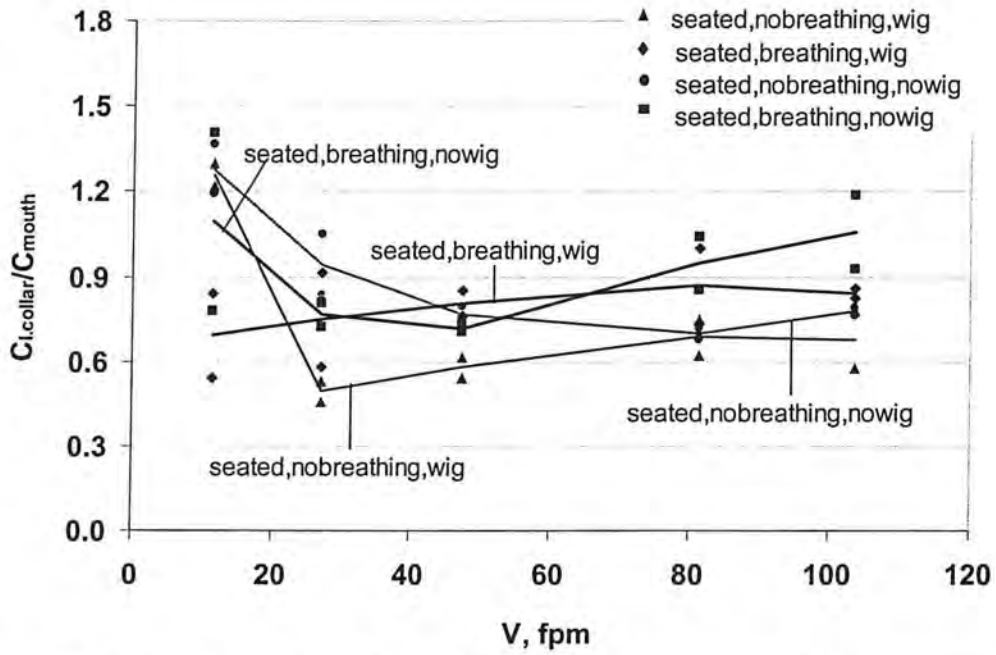

Figure 57-a: Scatter and mean plot of $C_{l.collar}/C_{mouth}$ vs. velocity for all manikin treatments (seated)

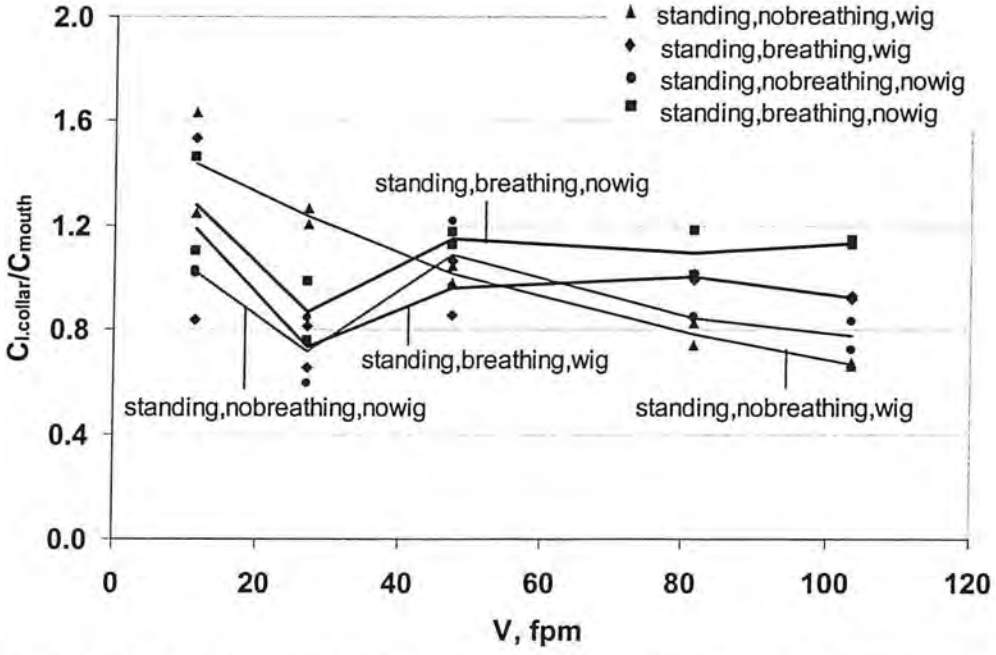

Figure 57-b: Scatter and mean plot of $C_{l.collar}/C_{mouth}$ vs. velocity for all manikin treatments (standing)

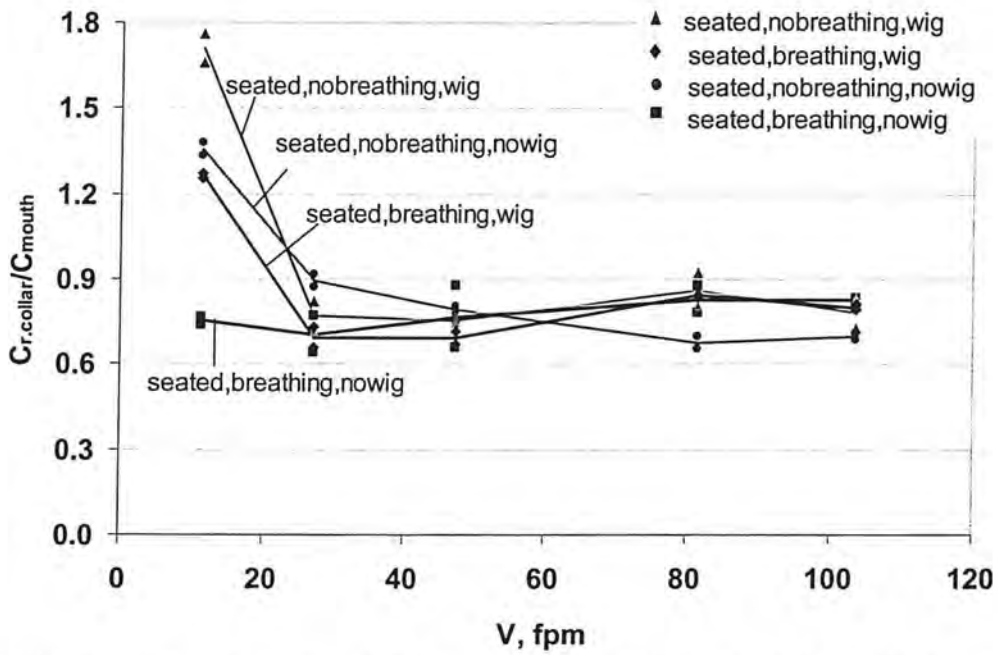

Figure 58-a: Scatter and mean plot of $C_{r.collar}/C_{mouth}$ vs. velocity for all manikin treatments (seated)

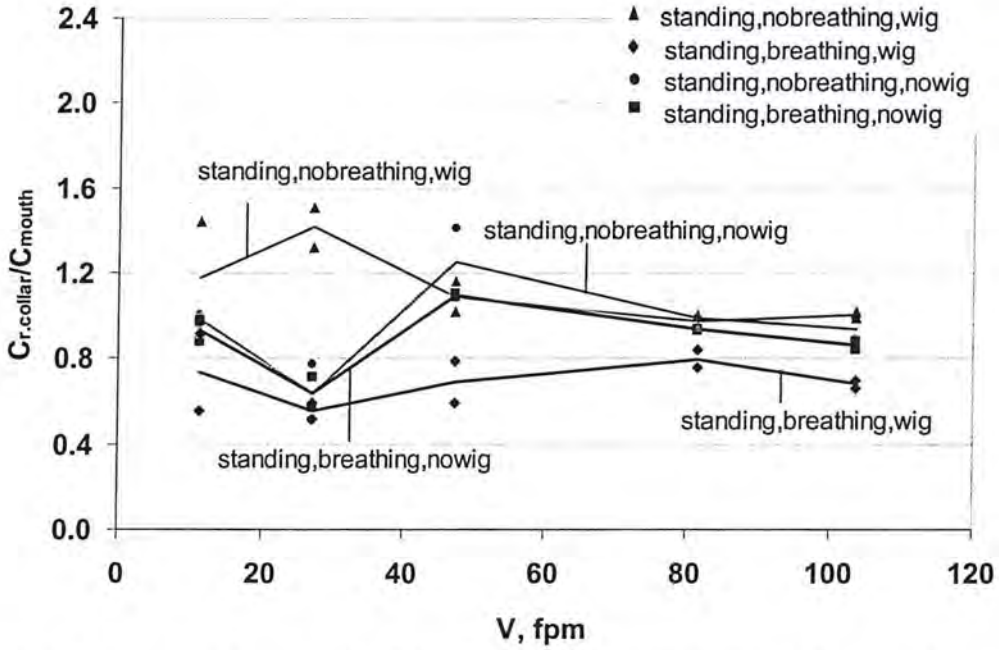

Figure 19-b: Scatter and mean plot of $C_{r.collar}/C_{mouth}$ vs. velocity for all manikin treatments (standing)

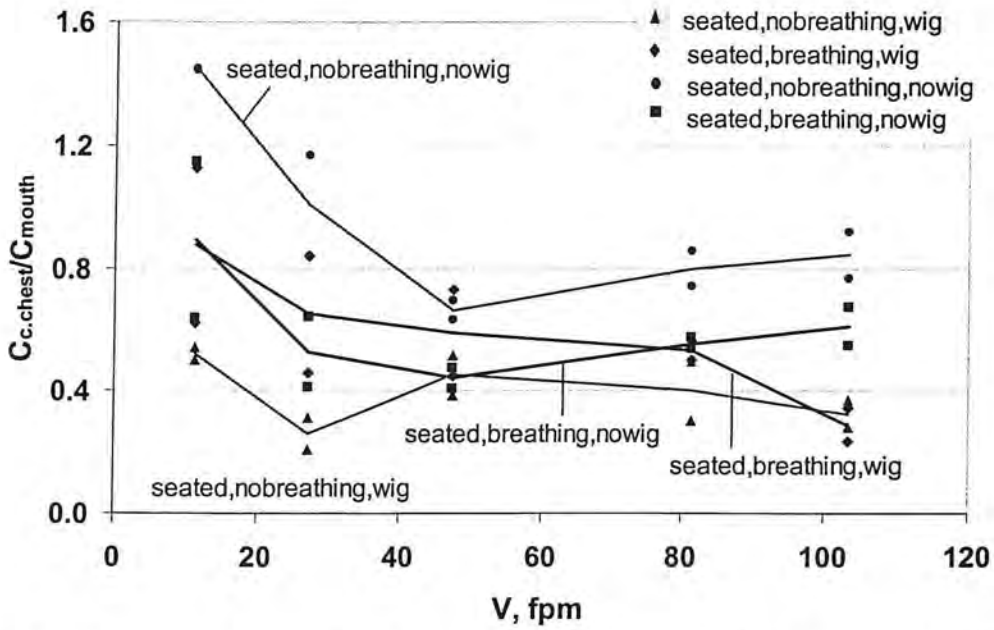

Figure 59-a: Scatter and mean plot of $C_{c.chest}/C_{mouth}$ vs. velocity for all manikin treatments (seated)

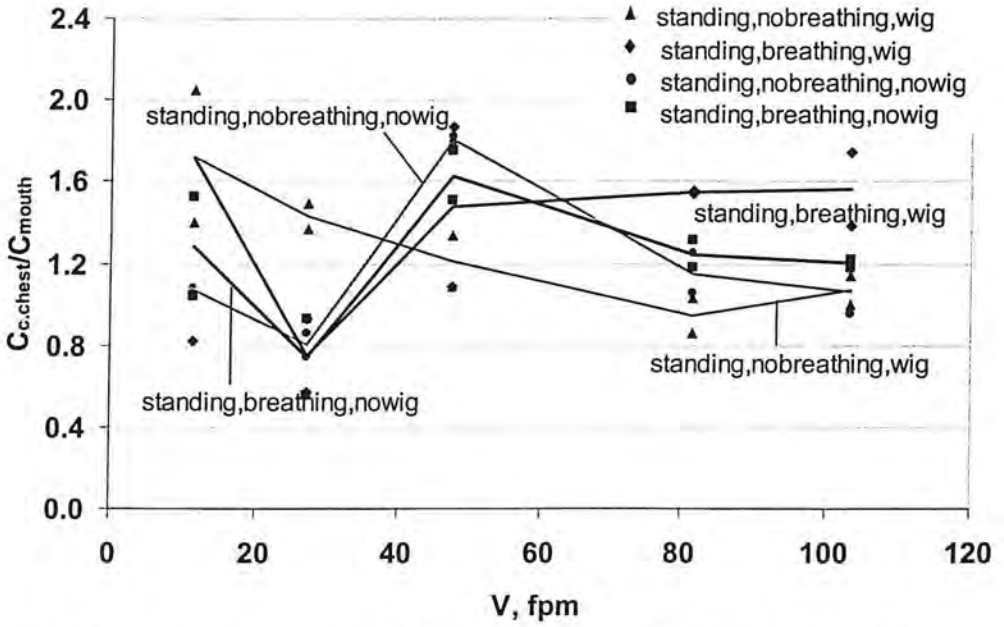

Figure 59-b: Scatter and mean plot of $C_{c.chest}/C_{mouth}$ vs. velocity for all manikin treatments (standing)

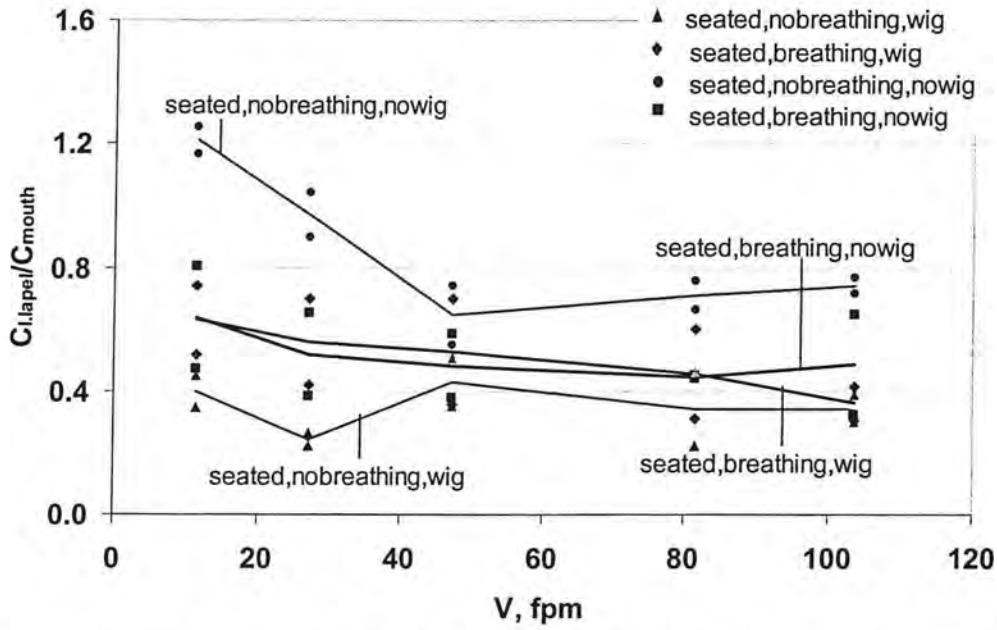

Figure 60-a: Scatter and mean plot of $C_{l.lapel}/C_{mouth}$ vs. velocity for all manikin treatments (seated)

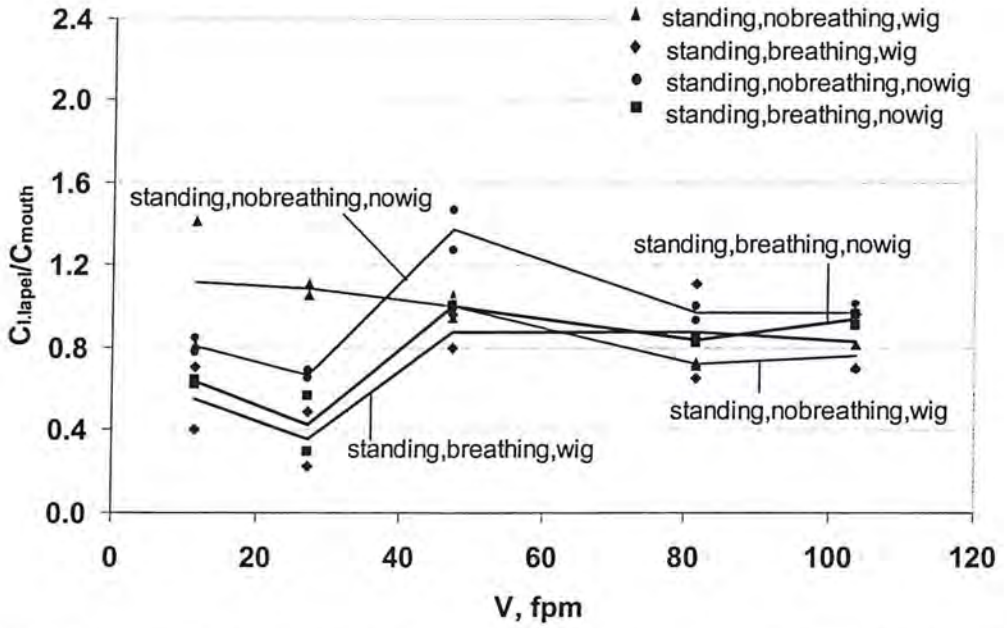

Figure 60-b: Scatter and mean plot of $C_{l.lapel}/C_{mouth}$ vs. velocity for all manikin treatments (standing)

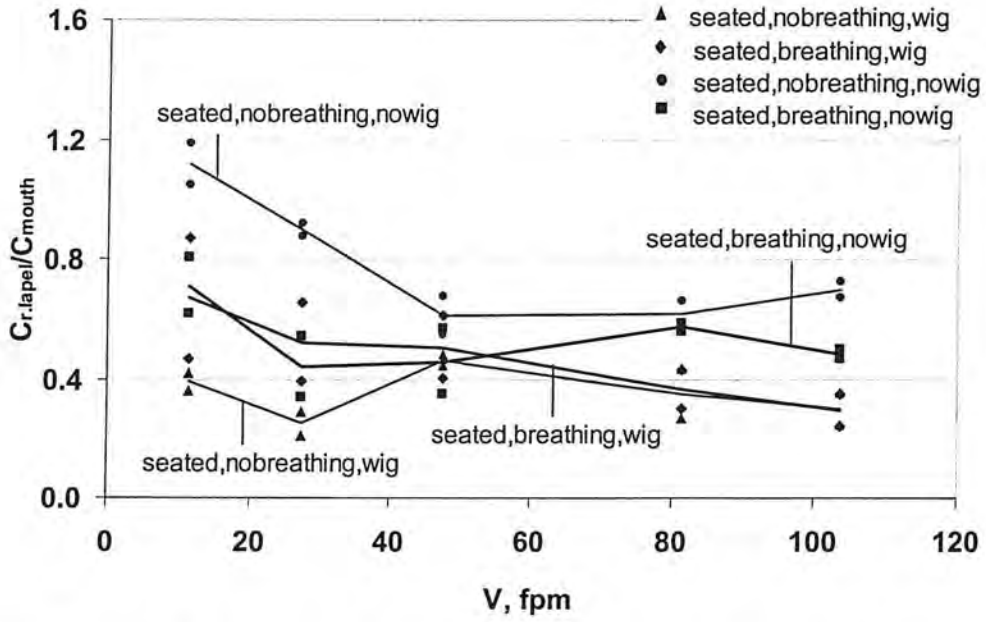

Figure 61-a: Scatter and mean plot of $C_{r.lapel}/C_{mouth}$ vs. velocity for all manikin treatments (seated)

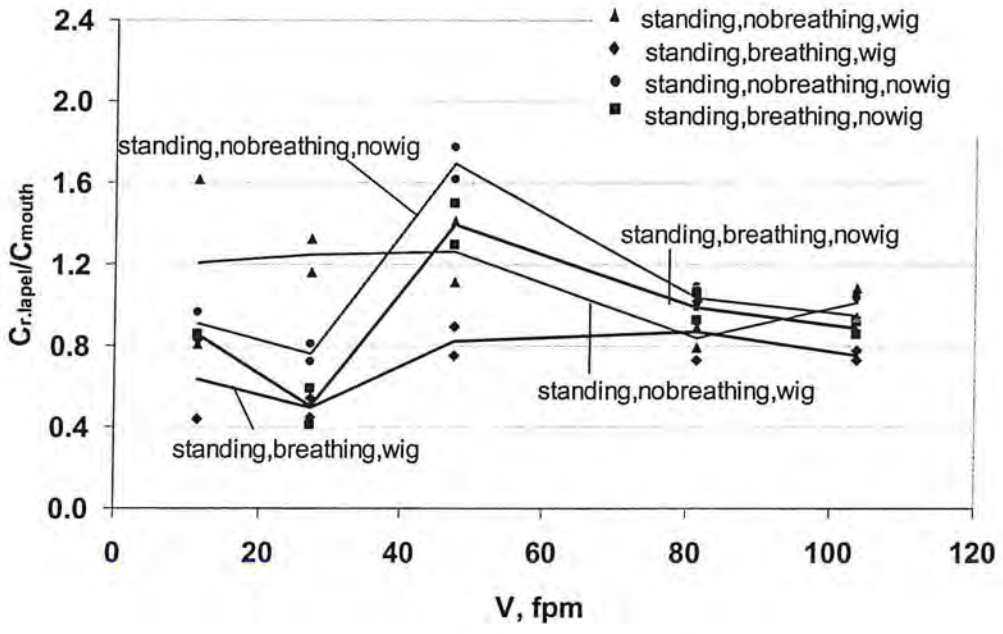

Figure 61-b: Scatter and mean plot of $C_{r.lapel}/C_{mouth}$ vs. velocity for all manikin treatments (standing)

4 Effects of Independent Variables on Ratios of Concentrations

As stated previously, we assume that concentrations measured near the mouth, C_{mouth}, are the "true" values. Thus, the differences between values measured at other locations and C_{mouth} are "errors" attributable to other sampling location. The second goal of this study was to investigate whether the measured concentrations varied with sampling location, and if they did differ, how their ratios varied with velocity, posture, breathing, and hair style.

The results are presented in terms of ratios rather than differences since the relative error is more useful to know than the absolute error, which would vary with every exposure condition. The ideal ratio between the C_{mouth} and concentrations at other locations is unity. A ratio less than unity represents underestimation and greater than unity represents over-estimation.

The results are shown in Figures 54 to 61 and Tables 17a and 17b. The effects of velocity on ratio of concentration appeared to be quite different for breathing and wig treatments and for standing and sitting postures. The scatter in ratios of concentration was higher at lower velocities. In addition, some locations had greater scatter than others.

As listed in Tables 17a and 17b, for lifelike (breathing and wig) conditions, the ratios of nose to mouth, C_{nose}/C_{mouth}, and forehead to mouth, $C_{forehead}/C_{mouth}$, had a V-peak occurred at 27 fpm for standing and a flattened inverted-V peak at 48 fpm for sitting. However, for the effect of wig only, the wig has greater effect on C_{nose}/C_{mouth} ratio at higher velocity ranges for standing. For the effect of breathing and wig, the ratio of forehead to mouth $C_{forehead}/C_{mouth}$ was closer to unity (0.91-1.22) for higher velocity ranges for both sitting and standing. As shown in Figures 55a and 55b, breathing had greater effect on $C_{forehead}/C_{mouth}$ for sitting than standing. This is because that breathing reduced mouth concentrations while the wig decreased $C_{forehead}$ concentration levels. It is worth mentioning that when neither breathing nor wig was present (Study I), $C_{forehead}$ always underestimated mouth exposure.

For lifelike (breathing) conditions, concentration ratios of neck to mouth, C_{neck}/C_{mouth}, left collar to mouth, $C_{l.collar}/C_{mouth}$, and right collar to mouth, $C_{r.collar}/C_{mouth}$, have similar patterns with velocity but different for sitting and standing (see Figures 59-61). C_{neck}/C_{mouth}, $C_{l.collar}/C_{mouth}$, and $C_{r.collar}/C_{mouth}$, had flattened V-shape with the peak concentrations occurred at 48 fpm for sitting and had two other peaks (V and inverted-V) at 27 and 48 fpm for standing. On the other hand, for breathing and wig conditions, C_{neck}/C_{mouth}, $C_{l.collar}/C_{mouth}$, and $C_{r.collar}/C_{mouth}$, had flattened V shape with velocity at 27 fpm for both sitting and standing. This relation ship was slightly different for the $C_{l.collar}/C_{mouth}$ due to the variability at 27 fpm for this location.

As listed in Tables 17a and 17b, for standing, C_{neck}/C_{mouth} over estimated mouth concentrations, while, $C_{r.collar}/C_{mouth}$ underestimated mouth concentrations. $C_{l.collar}/C_{mouth}$ was a mix of both. On the other hand, for sitting, concentrations at neck, left collar, and right collar underestimated mouth concentrations for lifelike conditions. In conclusion, ratio of concentrations at shoulder level varied from location to another and from sitting to standing with tendency to underestimate mouth concnetrations.

For lifelike (breathing and wig) conditions, ratios of concentration for center chest $C_{c.chest}/C_{mouth}$, left lapel $C_{l.lapel}/C_{mouth}$, and right lapel $C_{r.lapel}/C_{mouth}$, have similar patterns with velocity. However, the pattern is very different for sitting and standing (see Figures 59-61). $C_{c.chest}/C_{mouth}$, $C_{l.lapel}/C_{mouth}$ $C_{r.lapel}/C_{mouth}$, varied monotonically with velocity for sitting, while, two peaks occurred at 27 and 48 fpm for standing. Similar patterns occurred for the effect of breathing and bold conditions.

As listed in Tables 6.3a and 6.3b, concentrations at center chest, left lapel, and right lapel underestimated mouth concentrations for all velocities for sitting posture. However, for lifelike conditions and for standing, $C_{l.lapel}/C_{mouth}$ and $C_{r.lapel}/C_{mouth}$ under estimated mouth concentrations, while, $C_{c.chest}/C_{mouth}$ had values overestimated mouth concentrations (1.2-1.6) for all velocities. Althouhg left and right lapels underestimated mouth concentartions, the ratios were closer to one (0.85-0.99) at higher velocities than lower ones. In conclusion, ratios of concentration at chest level were more variable (wider range) for sitting than standing and tended to underestimate mouth exposures.

For lifelike conditions, concentration ratios varied from one location to another with the effect of independent variables. For example, it was found that nose and forehead concentration levels were closer to mouth levels with tendency to overestimate exposures at higher velocities. However, concentration ratios at chest levels (center chest, left and right lapel) underestimated mouth exposures while concentrations at neck, left and right collar were a mix of both of them.

Discussions of Manikin Study II

One major goal of both Study I and Study II was to determine if other sampling locations experience the same concentrations as the mouth (the "gold standard"). If not, it is of interest to know how the independent variables affect the differences. A secondary purpose was to determine what lifelike features are necessary for a manikin to be a representative surrogate for a human being for exposure sampling. Since human data were not taken for comparisons, the assumption here is that if different levels of a variable produce different results for the manikin, then the most "lifelike" conditions should be used in subsequent manikin testing. If a variable proved important in testing and if more than one level is lifelike (e.g. bald or hair), then each level should be tested in future studies.

Study I established that body heat was important. Since all humans are heated by metabolic activity, it is pointless to futher consider unheated manikins. For that reason, the manikin was heated for all test conditions in Study II. Study I also established that manikin posture was important and that cross-draft velocity was important. Since humans may sit or stand at work and the cross-draft velocities at the work station may differ, then manikins should be tested both sitting and standing and at a range of cross-draft velocities. This was done for Study II.

Study II introduced two additional variables: breathing and hair style. If breathing is important, then manikins in future tests should be tested while breathing. If results for the manikin are affected by whether it is wearing a wig or not, then since some humans have hair and some do not, manikins should be tested both with hair and without.

Data Desk (Data Description Inc. Ithaca, NY) software was used to do statistical analysis of results. The independent variables for this study were five levels of velocity

(11, 27, 48, 82, and 104 fpm), two levels of breathing (breathing, nobreathing), two levels of hair style (bald, wig), and two levels of posture (seated, standing). The dependent variables were concentrations at each sampling location and the ratios of concentrations.

As stated previously, the results (see Figures 48-49) appeared to show that breathing and hair style were important as were the interactions of breathing and hair with other independent variables. As is shown in the following sections, breathing, hair style, posture, and velocity and many of their interactions were statistically significant.

Tables 21 to 23 list the p-values from ANOVA for both log-transformed concentrations and ratios of concentrations for the effect of independent variables and their interactions. Using non-transformed dependent values had little effect on the p-values (not shown).

Table 18: Coefficient of Correlation for Externally Studentised Residuals Versus Normal Scores for Log-Transformed Individual Concentrations and Ratios of Concentrations

Log C_{mouth}	**0.972**	**Log{C_{nose}/C_{mouth}}**	**0.963**
Log C_{nose}	**0.977**	**Log{$C_{forehead}/C_{mouth}$}**	**0.973**
Log $C_{forehead}$	**0.974**	**Log{C_{neck}/C_{mouth}}**	**0.96**
Log C_{neck}	**0.983**	**Log{$C_{l.collar}/C_{mouth}$}**	**0.986**
Log $C_{l.collar}$	**0.988**	**Log{$C_{r.collar}/C_{mouth}$}**	**0.98**
Log $C_{r.collar}$	**0.97**	**Log{$C_{c.chest}/C_{mouth}$}**	**0.987**
Log $C_{c.chest}$	**0.969**	**Log{$C_{l.lapel}/C_{mouth}$}**	**0.997**
Log $C_{l.lapel}$	**0.991**	**Log{$C_{r.lapel}/C_{mouth}$}**	**0.994**
Log $C_{r.lapel}$	**0.984**		
Log $C_{inhaled}$	**0.971**		
Log $C_{uppertorso}$	**0.977**		
Log $C_{lowertorso}$	**0.966**		

1 Log-Transformation of Dependent Variables

Dependent variables were log-transformed to produce residuals that were normally distributed. Using log ratio of concentration allowed analysis of the differences in logs of two dependent values, removing the potential for "small denominator" problems associated with actual ratios:

$$\text{Log } \{C_{neck}/C_{mouth}\} = \{\log C_{neck} - \log C_{mouth}\}$$

As shown in Table 18, the R-sq values for n-scores of residuals all exceeded the "critical coefficient of correlation" of 0.985 for n = 80 (Neter et al., 1996). As shown in Table 18,

log-transformed individual concentrations and ratio of concentartions showed reasonable degree of normality for all sampling locations, except for log C_{nose} and Log $\{C_{c.chest}/C_{mouth}\}$. Although correlation coefficients varied for each dependent variable, there was no substantial departure from linearity. Normal probability plots are shown in appendix C.

2 Analysis of Variance (ANOVA)

The independent variables for this study were five levels of velocity (11, 27, 48, 82, and 104 fpm), two levels of breathing (breathing, nobreathing), two levels of hair style (bold, wig), and two levels of posture (seated, standing). The dependent variables were concentrations at each sampling location and ratio of concentrations. As shown in Table 19, the design was completely randomized factorial design with two replications for each treatment. Experiments were done on randomized order. The linear statistical model used for the analysis of variance is illustrated by the following equation:

$$Y_{ijklm} = \mu + \tau_i + \beta_j + \gamma_k + \lambda_l + (\tau\beta)_{ij} + (\tau\gamma)_{ik} + (\tau\lambda)_{il} + (\beta\gamma)_{jk} + (\beta\lambda)_{jl} + (\gamma\lambda)_{kl} + (\tau\beta\gamma)_{ijk} +$$

$$(\tau\beta\lambda)_{ijl} + (\tau\gamma\lambda)_{ikl} + (\beta\gamma\lambda)_{jkl} + (\tau\beta\gamma\lambda)_{ijkl} + \varepsilon_{ijklm}$$

Where i = 1,2,3,4,5; j = 1,2; k = 1,2; l = 1,2; m = 1,2 and τ_i, β_j, γ_k, λ_l represent the effects of wind tunnel velocity, breathing, wig and posture, while $(\tau\beta)_{ij}$, $(\tau\gamma)_{ik}$, $(\tau\lambda)_{il}$, $(\beta\gamma)_{jk}$, $(\beta\lambda)_{jl}$, $(\gamma\lambda)_{kl}$, $(\tau\beta\gamma)_{ijk}$, $(\tau\beta\lambda)_{ijl}$, $(\tau\gamma\lambda)_{ikl}$, $(\beta\gamma\lambda)_{jkl}$, $(\tau\beta\gamma\lambda)_{ijkl}$ represent the interaction terms of velocity, breathing, wig and posture. ε_{ijklm} represents the random error.

Table 19: Completely Randomized Factorial Design of Experiments

			Velocity, fpm				
			11	27	48	82	104
Breathing	Wig	Seated	++	++	++	++	++
		Standing	++	++	++	++	++
	No Wig	Seated	++	++	++	++	++
		Standing	++	++	++	++	++
No Breathing	Wig	Seated	++	++	++	++	++
		Standing	++	++	++	++	++
	No Wig	Seated	++	++	++	++	++
		Standing	++	++	++	++	++

Analysis of variance was computed for log-transformed dependent variables (concentrations and ratio of concentrations) for the effect of independent variables (velocity, breathing, hair style, and posture) and their interactions. The outline for ANOVA for fixed effects model was obtained from (Montgomery, D. 1997). For the fixed effects model, test statistics for each independent variable and interaction was developed by dividing the corresponding mean square for the variable or interaction by the mean square error. The number of degrees of freedom for any factor is the number of levels of the factor minus one, the number of degrees of freedom for an interaction is the

product of the number of degrees of freedom associated with the individual components of the interaction (Montgomery, D., 1997). All tests were done at 95% confidence level (α=0.05). Data Desk software was used to perform ANOVA and the results of performing F-tests were summarized as p-values.

Tables 20 and 21 listed the p-values from ANOVA for log transformed individual concentrations and ratio of concentrations for all sampling locations. While Table 22 shows p-values form ANOVA for log transformed individual concentrations for $C_{inhaled}$, $C_{uppertorso}$, and $C_{lowertorso}$.

Table 20: p-Values from ANOVA's for Log-Transformed Individual Concentrations

Source	df	Log C_{mouth}	Log C_{nose}	Log $C_{forehead}$	Log C_{neck}	Log $C_{l.collar}$	Log $C_{r.collar}$	Log $C_{c.chest}$	Log $C_{l.lapel}$	Log $C_{r.lapel}$
Const	1	0.00	0.00	0.00	0.00	0.00	0.00	0.00	0.00	0.00
Vly	4	0.00	0.00	0.00	0.00	0.00	0.00	0.00	0.00	0.00
Brg	1	0.00	0.00	0.00	0.00	0.00	0.00	0.00	0.00	0.00
Vly*Brg	4	0.66	0.02	0.25	0.08	0.00	0.02	0.48	0.15	0.33
Wig	1	0.07	0.16	0.29	0.56	0.00	0.24	0.00	0.00	0.00
Vly*Wig	4	0.26	0.49	0.53	0.04	0.25	0.00	0.34	0.80	0.22
Brg*Wig	1	0.00	0.00	0.00	0.00	0.00	0.00	0.50	0.74	0.10
Vly*Brg*Wig	4	0.85	0.02	0.38	0.21	0.05	0.59	0.66	0.72	0.83
Pst	1	0.00	0.00	0.00	0.00	0.00	0.00	0.00	0.00	0.00
Vly*Pst	4	0.00	0.00	0.00	0.11	0.00	0.84	0.52	0.35	0.78
Brg*Pst	1	0.00	0.05	0.00	0.00	0.00	0.00	0.02	0.00	0.00
Vly*Brg*Pst	4	0.51	0.80	0.54	0.23	0.08	0.09	0.41	0.16	0.85
Wig*Pst	1	0.01	0.22	0.00	0.04	0.53	0.00	0.00	0.09	0.07
Vly*Wig*Pst	4	0.25	0.01	0.00	0.76	0.18	0.42	0.03	0.37	0.16
Brg*Wig*Pst	1	0.01	0.00	0.00	0.00	0.53	0.90	0.09	0.01	0.02

Table 21: p-Values from ANOVA's for Log-Transformed Ratios of Concentrations

Source	df	Log{C_{nose}/C_{mouth}}	Log{$C_{forehead}/C_{mouth}$}	Log{C_{neck}/C_{mouth}}	Log{$C_{l.collar}/C_{mouth}$}	Log{$C_{r.collar}/C_{mouth}$}	Log{$C_{c.chest}/C_{mouth}$}	Log{$C_{l.lapel}/C_{mouth}$}	Log{$C_{r.lapel}/C_{mouth}$}
Const	1	0.86	0.00	0.63	0.00	0.00	0.00	0.00	0.00
Vly	4	0.00	0.00	0.00	0.00	0.00	0.00	0.03	0.00
Brg	1	0.00	0.00	0.15	0.06	0.00	0.92	0.00	0.00
Vly*Brg	4	0.07	0.23	0.08	0.00	0.00	0.75	0.41	0.37
Wig	1	0.39	0.00	0.10	0.02	0.48	0.00	0.00	0.00
Vly*Wig	4	0.46	0.42	0.08	0.86	0.01	0.72	0.97	0.70
Brg*Wig	1	0.09	0.08	0.41	0.26	0.00	0.00	0.00	0.08
Vly*Brg*Wig	4	0.07	0.64	0.22	0.27	0.50	0.93	0.98	0.67
Pst	1	0.00	0.00	0.00	0.00	0.09	0.00	0.00	0.00
Vly*Pst	4	0.00	0.00	0.02	0.12	0.00	0.01	0.00	0.00
Brg*Pst	1	0.00	0.28	0.32	0.83	0.00	0.49	0.09	0.02
Vly*Brg*Pst	4	0.34	0.05	0.19	0.12	0.07	0.15	0.05	0.23
Wig*Pst	1	0.02	0.00	0.58	0.05	0.05	0.00	0.00	0.00
Vly*Wig*Pst	4	0.44	0.01	0.17	0.10	0.00	0.02	0.29	0.01
Brg*Wig*Pst	1	0.06	0.51	0.56	0.03	0.00	0.00	0.00	0.00

Table 22: p-Values from ANOVA's for Log $C_{inhaled}$, Log $C_{uppertorso}$, and Log $C_{lowertorso}$

Source	df	Log $C_{inhaled}$	Log $C_{upper.torso}$	Log $C_{lower.torso}$
Const	**1**	**0.00**	**0.00**	**0.00**
Velocity	**4**	**0.00**	**0.00**	**0.00**
Breathing	**1**	**0.00**	**0.00**	**0.00**
Wig	**1**	**0.11**	**0.06**	**0.00**
Posture	**1**	**0.00**	**0.00**	**0.00**
Velocity/Breathing	**4**	**0.20**	**0.00**	**0.20**
Velocity/Posture	**4**	**0.00**	**0.06**	**0.49**
Velocity/Wig	**4**	**0.32**	**0.01**	**0.35**
Breathing/Wig	**1**	**0.00**	**0.00**	**0.98**
Breathing/Posture	**1**	**0.00**	**0.00**	**0.00**
Wig/Posture	**1**	**0.04**	**0.02**	**0.00**
Velocity/Breathing/Wig	**4**	**0.25**	**0.29**	**0.77**
Velocity/Breathing/Posture	**4**	**0.74**	**0.10**	**0.34**
Velocity/Wig/Posture	**4**	**0.06**	**0.62**	**0.06**
Breathing/Wig/Posture	**1**	**0.00**	**0.12**	**0.02**

3 Regression Analysis

Regression analysis was performed on log transformed concentrations for each sampling location (dependent variable) with wind tunnel velocity (independent variable) for each treatment combination. Treatments were divided into four groups which are: breathing/nowig/standing, breathing/nowig/seated, breathing/wig/standing, and breathing/wig/seated. For all treatments, linear regression was applied to fit the data with velocity for both standing and seated manikin conditions. A second velocity term was added to the regression model to model the inverted V-shape peak for both seated and standing conditions.

For example, the regression model for log C_{mouth} was:

$$\text{Log } C_{mouth} = \beta_0 + \beta_1 V_1 + \beta_2 V_2$$

In cases where the peak occurred at 48 fpm, then

$$\{V_2 = (V_1 - 48)\, x\}, \text{ where } x = 0 \text{ if } V_1 \leq 48 \text{ and } x = 1 \text{ if } V_1 > 48$$

In cases where the peak occurred at 27 fpm, then

$$\{V_2 = (V_1 - 27)\, x\}, \text{ where } x = 0 \text{ if } V_1 \leq 27 \text{ and } x = 1 \text{ if } V_1 > 27.$$

Concentrations at all sampling locations were fitted using the same steps applied on log C_{mouth}. Tables 23 to 26 summarized regression models results (adjusted Rsq, coefficients, and p-values) for all sampling locations. Detailed analysis and results are presented in appendix D.

Table 23a: Regression Coefficients for seated/breathing/wig manikin

	Adj_R^2 (%)	C_0	C_1	C_2
Log C_{mouth}	74	0.926	0.0130	-0.0154
Log C_{nose}	79.6	0.667	0.0202	-0.024
Log $C_{forehead}$	80.8	0.691	0.0203	-0.0255
Log C_{neck}	69.6	0.985	0.0099	-0.0119
Log $C_{l.collar}$	85.6	0.732	0.015	-0.0173
Log $C_{r.collar}$	56.4	1.045	0.0065	-0.0068
Log $C_{c.chest}$	61.2	0.859	0.0097	-0.0167
Log $C_{l.lapel}$	44.4	0.7363	0.0107	-0.0155
Log $C_{r.lapel}$	66.7	0.7453	0.0101	-0.0163

Table 23b: Regression p-Values for seated/breathing/wig manikin

	C_0	C_1	C_2
Log C_{mouth}	0.0001	0.0017	0.0056
Log C_{nose}	0.0008	0.0008	0.0027
Log $C_{forehead}$	0.0004	0.0005	0.0012
Log C_{neck}	0.0001	0.003	0.0088
Log $C_{l.collar}$	0.0001	0.0003	0.0013
Log $C_{r.collar}$	0.0001	0.0178	0.0656
Log $C_{c.chest}$	0.0001	0.0125	0.0058
Log $C_{l.lapel}$	0.0004	0.02	0.021
Log $C_{r.lapel}$	0.0001	0.0048	0.0029

Table 24 a: Regression Coefficients for seated/breathing/nowig manikin

	Adj_R^2 (%)	C_0	C_1	C_2
Log C_{mouth}	67.3	1.079	0.0134	-0.0189
Log C_{nose}	76.9	1.022	0.015	-0.0195
Log $C_{forehead}$	82.9	0.797	0.0187	-0.025
Log C_{neck}	57.1	1.14	0.01	-0.014
Log $C_{l.collar}$	85.2	1.12	0.01	-0.011
Log $C_{r.collar}$	70.3	0.937	0.014	-0.0184
Log $C_{c.chest}$	51.3	1.06	0.006	-0.008
Log $C_{l.lapel}$	51.5	0.891	0.0101	-0.0158
Log $C_{r.lapel}$	57	0.921	0.01	-0.013

Table 24 b: Regression p-values for seated/breathing/nowig manikin

	C_0	C_1	C_2
Log C_{mouth}	0.0001	0.003	0.003
Log C_{nose}	0.0001	0.0008	0.0014
Log $C_{forehead}$	0.0001	0.0003	0.0005
Log C_{neck}	0.0001	0.0073	0.0094
Log $C_{l.collar}$	0.0001	0.0002	0.0006
Log $C_{r.collar}$	0.0001	0.002	0.003
Log $C_{c.chest}$	0.0001	0.012	0.014
Log $C_{l.lapel}$	0.0001	0.015	0.012
Log $C_{r.lapel}$	0.0001	0.0075	0.0086

Table 25 a: Regression Coefficients for standing/breathing/wig manikin

	Adj_R^2 (%)	C_0	C_1	C_2	C_3
Log C_{mouth}	69.2	1.01	0.019	-0.023	
Log C_{nose}	53.7	1.123	0.016	-0.017	
Log $C_{forehead}$	51.4	1.05	0.0155	-0.017	
Log C_{neck}	9.2	1.33	0.0075	-0.01	
Log $C_{l.collar}$	17.5	1.168	0.010	-0.012	
Log $C_{r.collar}$	39.1	0.912	0.0149	-0.017	
Log $C_{c.chest}$	0.8	1.32	0.005		-0.007
Log $C_{l.lapel}$	71.9	0.81	0.011		-0.014
Log $C_{r.lapel}$	41.8	0.952	0.0089		-0.0123

Table 25 b: Regression p-values for standing/breathing/wig manikin

	C_0	C_1	C_2	C_3
Log C_{mouth}	0.0001	0.0033	0.0025	
Log C_{nose}	0.0001	0.012	0.014	
Log $C_{forehead}$	0.0001	0.012	0.013	
Log C_{neck}	0.0001	0.29	0.22	
Log $C_{l.collar}$	0.0001	0.14	0.11	
Log $C_{r.collar}$	0.0001	0.03	0.027	
Log $C_{c.chest}$	0.0001	0.2		0.26
Log $C_{l.lapel}$	0.0001	0.002		0.005
Log $C_{r.lapel}$	0.0001	0.023		0.03

Table 26 a: Regression Coefficients for standing/breathing/nowig manikin

	Adj_R^2 (%)	C_0	C_1	C_2	C_3
Log C_{mouth}	94.4	1.085	0.0196	-0.022	
Log C_{nose}	93.7	1.12	0.0188	-0.021	
Log $C_{forehead}$	89.7	1.067	0.0179	-0.0198	
Log C_{neck}	82.4	1.34	0.00786		-0.0133
Log $C_{l.collar}$	75.2	1.35	0.006		-0.01
Log $C_{r.collar}$	92.4	1.155	0.0098		-0.0148
Log $C_{c.chest}$	67.9	1.24	0.011		-0.016
Log $C_{l.lapel}$	76.7	0.924	0.0131		-0.0165
Log $C_{r.lapel}$	79.2	1.02	0.014		-0.02

Table 26 b: Regression p-values for standing/breathing/nowig manikin

	C_0	C_1	C_2	C_3
Log C_{mouth}	0.0001	0.0001	0.0001	
Log C_{nose}	0.0001	0.0001	0.0001	
Log $C_{forehead}$	0.0001	0.0001	0.0001	
Log C_{neck}	0.0001	0.0008		0.0003
Log $C_{l.collar}$	0.0001	0.0014		0.001
Log $C_{r.collar}$	0.0001	0.0001		0.0001
Log $C_{c.chest}$	0.0001	0.0027		0.0028
Log $C_{l.lapel}$	0.0001	0.0009		0.002
Log $C_{r.lapel}$	0.0001	0.0005		0.006

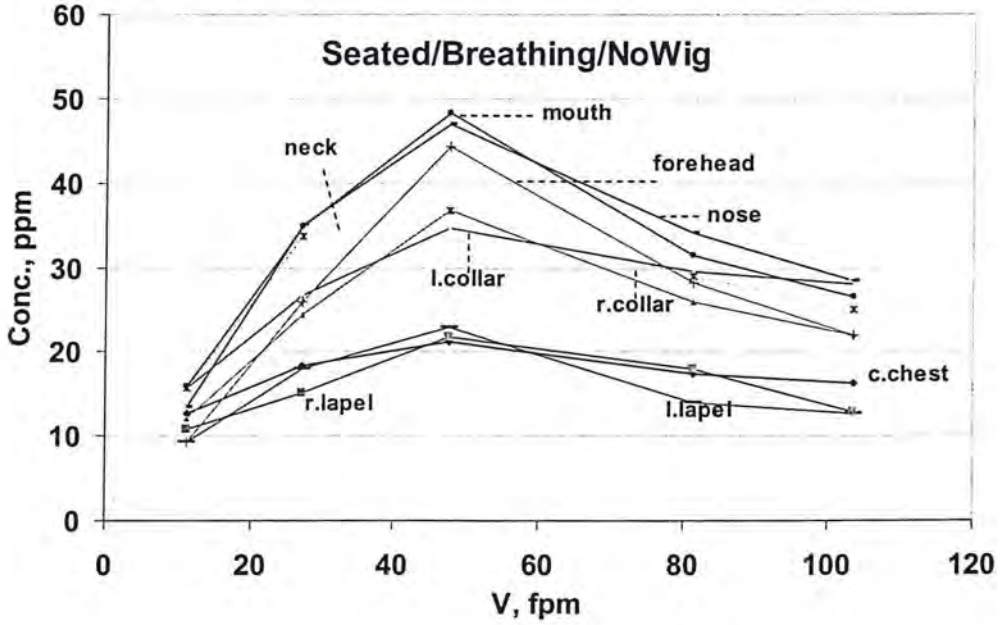

Figure 62: Mean concentration (ppm) versus velocity for seated/breathing/no wig manikin

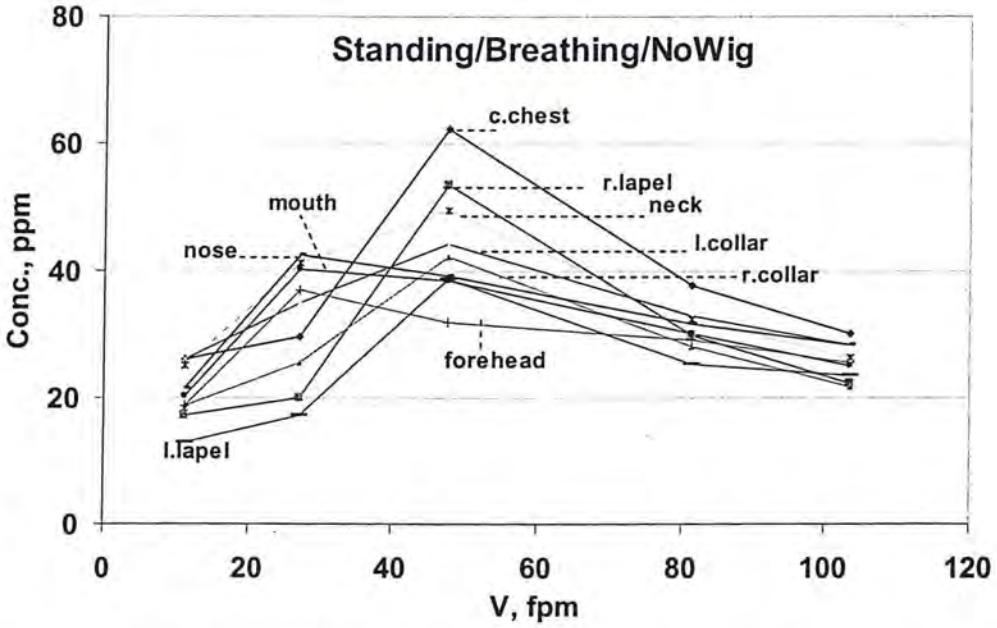

Figure 63: Mean Concentration (ppm) versus velocity for standing/breathing/nowig manikin

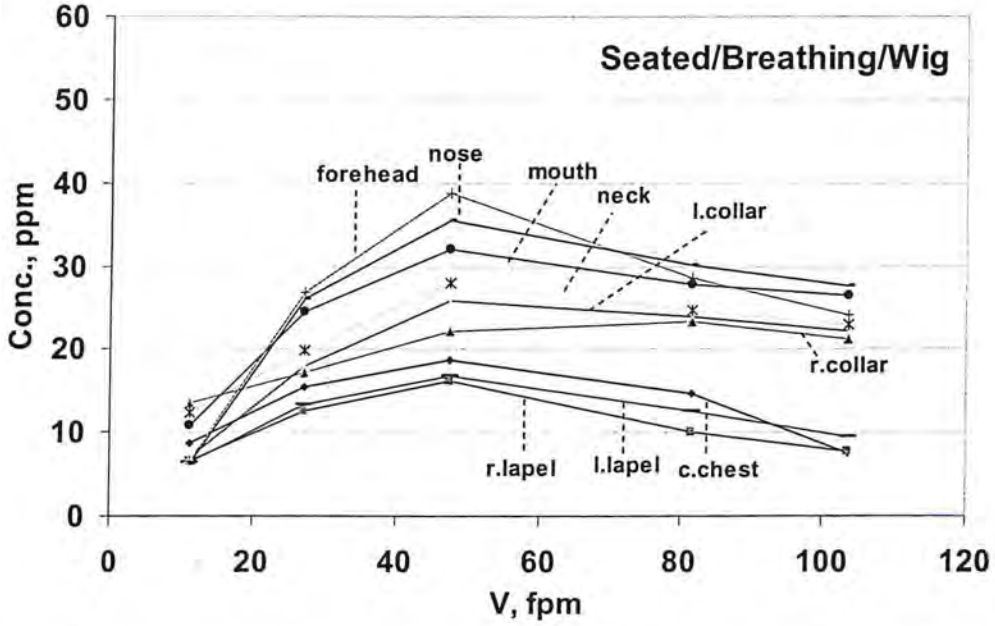

Figure 64: Mean concentration (ppm) versus velocity for seated/breathing/wig manikin

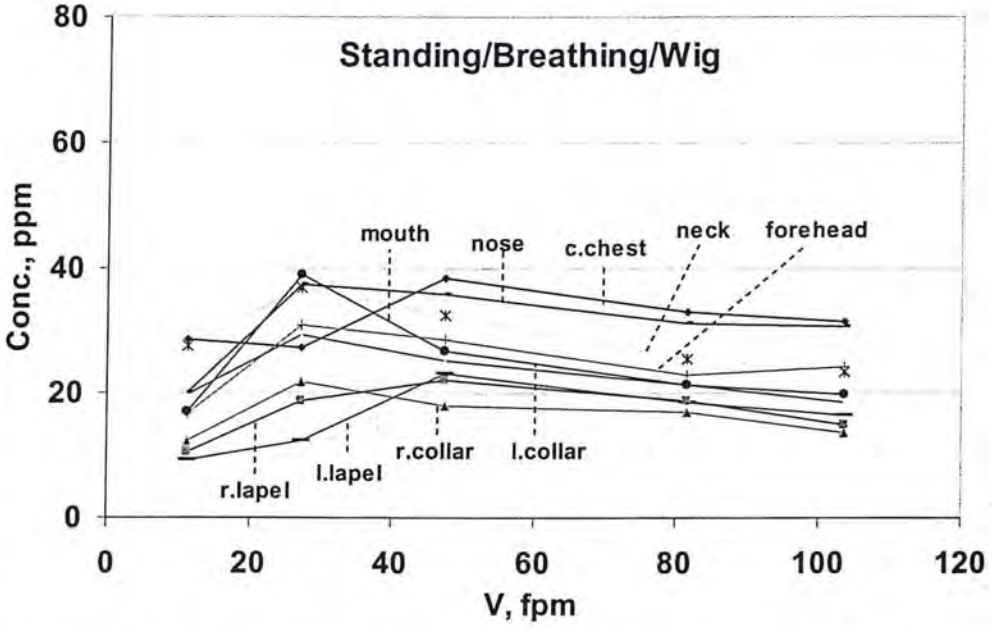

Figure 65: Mean Concentration (ppm) versus velocity for standing/breathing/wig manikin

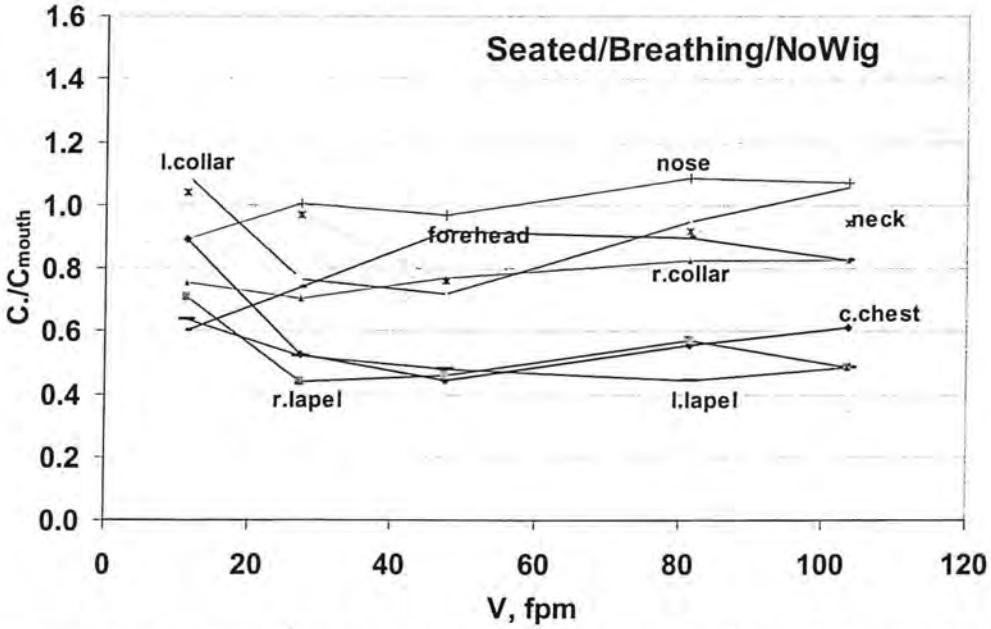

Figure 66: Concentration ratio to C_{mouth} versus velocity for seated/breathing/no wig manikin

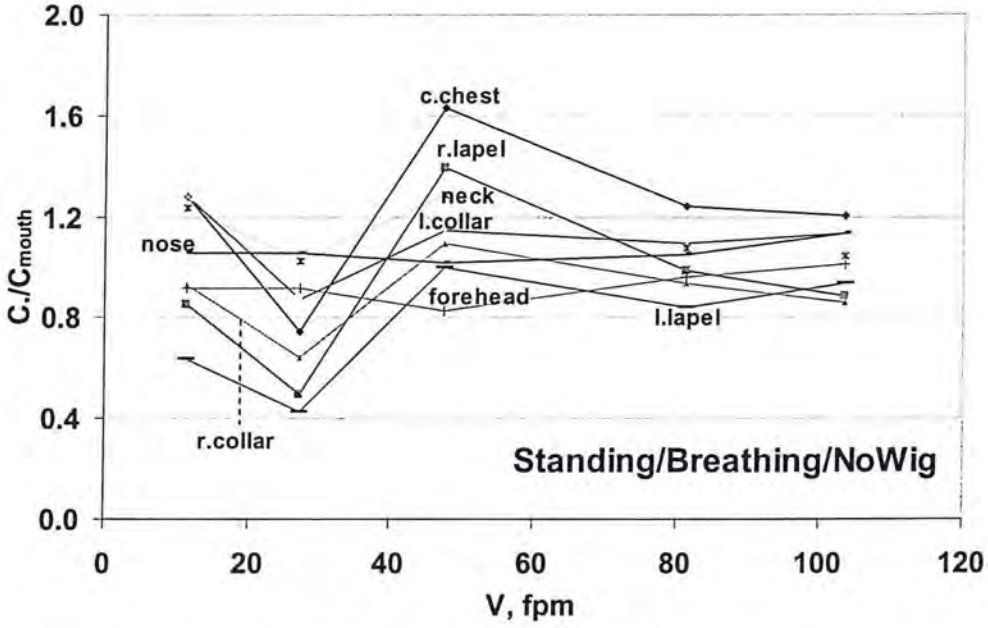

Figure 67: Concentration ratio to C_{mouth} versus velocity for standing/breathing/no wig manikin

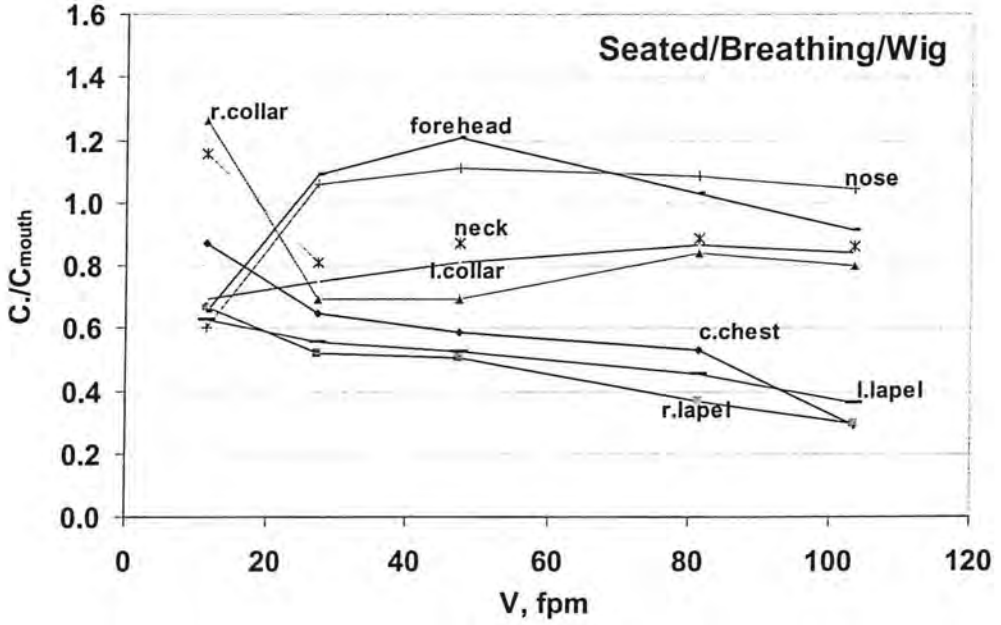

Figure 68: Concentration ratio to C_{mouth} versus velocity for seated/breathing/wig manikin

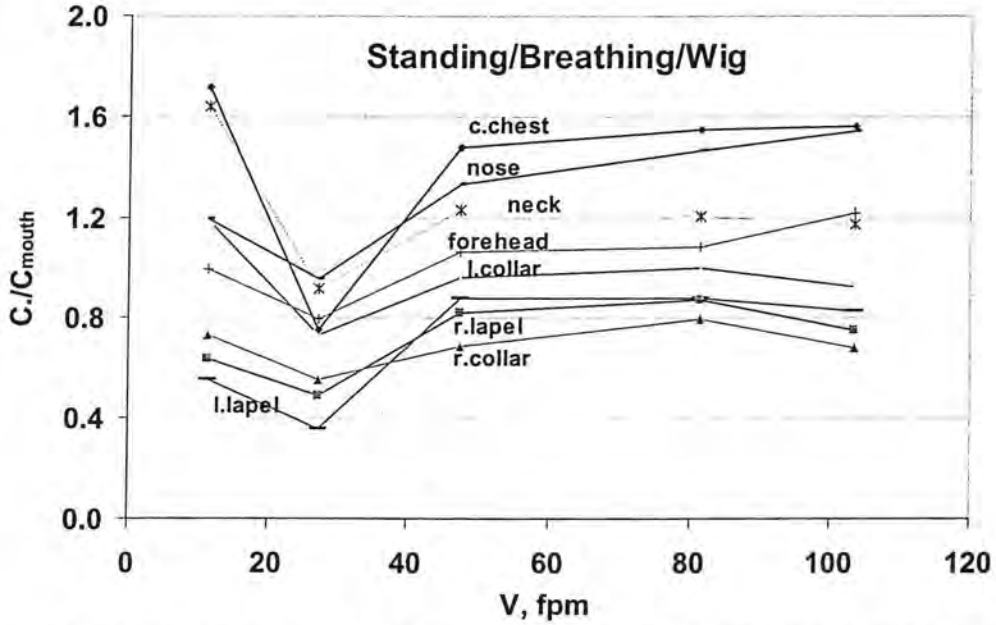

Figure 69: Concentration ratio to C_{mouth} versus velocity for standing/breathing/wig manikin

4 Comparisons of Individual Concentration Values and Ratios of Concentrations for all Sampling Locations

The effects of velocity, breathing, hair style and posture on concentrations at all sampling locations is shown in Figures 62-65. Concentrations, at all sampling locations and for all manikin treatments, varied in an inverted-V shape relationship with wind tunnel velocity. Peak concentration levels occurred at velocity range of 27 to 48 fpm. As velocity increases, concentrations at different locations increase to a peak value (2 to 3 times its original levels), then decrease as velocity continue increasing to maximum level. Likewise, for lifelike conditions, breathing substantially reduced concentration levels for sitting and significantly reduced concentration levels at all sampling locations for standing. These results were strongly supported by the analysis of variance (ANOVA) shown in Table 64. The effects of velocity and breathing were statistically significant for all sampling locations ($p<0.001$). The interaction of velocity and breathing was not significant for locations at mouth, forehead, neck and chest ($p>0.08$). This is because nose breathing diluted (reduced) concentrations at both collars more than the neck, while, one effect of breathing to be larger at low velocities than higher ones.

These results agree with Heist et al (2003), Fletcher and Johnson (1996), and Wood and Birkett (1979) who tested respectively the effect of breathing for chid size manikin, window type manikin, and for adult size manikin standing in a low speed flow field (0.1 – 0.5 m/s). Heist et al (2003) found that breathing affected air flow patterns around the manikin in the vicinity of the mouth and nose, while, Wood and Birkett (1979) found that breathing action had little effect on a personal sampler located on manikin's lapel. Fletcher and Johnson (1996) found that breathing effects were confined to thermal boundry layer and did not influence the general flow field. Apparently, all of them tested the effect of breathing on air flow patterns around manikin.

As shown in Figures 62-65 and listed in Table 20, the effect of posture (sitting/standing) was statistically significant for all sampling locations. For lifelike conditions, breathing, sitting reduced concentration levels for all sampling locations at the chest and shoulder level. Conversely, standing reduced concentration levels for sampling locations at mouth, nose and forehead. The reductions were statistically significant ($p<0.001$). However, the interaction of velocity and posture was statistically significant ($p< 0.001$) for concentrations at the face but not significant for concentrations at the shoulder and chest ($p>0.35$). This concentration levels at the face had peak values at 27 fpm for standing and 48 fpm for sitting.

It was plausible that posture would affect sampling locations because of the orientation of arms and legs to wind tunnel velocity. In standing posture, the manikin arms and legs were perpendicular to wind tunnel velocity, while, in sitting, the arms and legs were parallel to wind tunnel velocity. Another point worth mentioning, the presence of a table in front of the manikin in sitting posture would have affected air flow patterns around the manikin's face and torso.

As shown in Figures 62-65, the effects of wig on sampling locations appeared to be strikingly different for different conditions for both sitting and standing. For lifelike conditions, the wig did not affect air flow patterns around the face and torso for sitting posture, but it reduced concentration levels slightly at the face. The effect of wig in standing posture was quite different. The wig tended to decrease concentrations for sampling locations at chest level, while, slightly affected concentrations at the face level. For both sitting and standing, attaching the wig on manikin's head did not only flatten the peaks (occurred at 27 and 48 fpm) but also changed the level of the peaks for all sampling locations. This was strongly supported by the ANOVA values listed in Table 20. The effect of wig was not significant for concentrations at the mouth, nose, forhead, neck and both collars ($p>0.1$). it was statistically significant for center chest and both lapels ($p>0.001$).

It was plausible that putting the wig on manikin's head will affect the convective air flow developed above the head which should be affecting concentrations levels at the face more than the chest. It is worth mentioning that the interactions of wig and posture and wig and breathing both were statistically significant for mouth and forehead locations ($p<0.001$). The interaction of wig and velocity was not significant ($p>0.5$). Interestingly, the three way interactions of velocity wig breathing, velocity breathing posture, velocity wig posture, and breathing wig posture, were not significant for most sampling locations.

Comaped to individual concentration levels, average values for breathing zone concentrations $C_{inhaled}$, $C_{upper.torso}$, and $C_{lower.torso}$ showed similar patterns with independent variables (velocity, breathing, wig, and posture). However, concentration levels were slightly different. On the other hand, as shown in Table 22, ANOVA for log transformed $C_{inhaled}$, $C_{upper.torso}$, and $C_{lower.torso}$ showed significance for the effect of velocity, breathing and posture ($p<0.001$), similarly, the effect of wig was statistically significanrt for locations at lower torso. The interaction of breathing and wig was statistically significant for inhaled and upper torso locations ($p<0.001$) and was insignificant for lower torso ($p>098$). However, the three way interactions of velocity wig breathing, velocity breathing posture, and velocity wig posture, were statistically insignificant ($p>0.1$) for all

sampling locations, while, the three way interaction of breathing wig posture was statistically significant ($p<0.02$).

On contrary to individual concentrations, the effects of independent variables on ratios of concentrations appeared to be strikingly different for all sampling locations as shown in Figures 66-69. The effect of velocity on ratio of concentration appeared to be different for lifelike conditions and for standing and seated postures for all sampling locations. Ratios of concentrations followed similar patterns for standing where peaks occurred at 27 fpm (V-shape) and 48 fpm (inverted-V), however, patterns were different for sitting. For lifelike conditions, breathing significantly affected ratios of concentrations at the lower and higher velocity ranges for sititng.

Concentration ratios for locations at chest and both lapels were significant for sitting. This was strongly supported by the analysis of variance (ANOVA), shown in Table 21. The effects of velocity and posture on log transformed ratios of concentrations were statistically significant ($p<0.001$). However, the effect of breathing was statistically significant for ratios of concentrations for all locations ($p<0.001$), escept for neck and center chest did not show significance ($p>0.9$). The wig has no significant effect on the artio C_{nose}/C_{mouth} ($p>0.3$), however, the effect of wig on ratios of concentration at forehead, center chest and both lapels were statistically significant ($p<0.001$).

As listed in Table 21, the interactions of velocity and breathing and velocity and wig insignificantly affected log transformed ratios of concentrations at chest level ($p>0.4$). However, the interactions of velocity and posture, breathing and posture, and breathing and wig were statistically significant ($p<0.001$). This was illustrated in Figures 66-69, ratios of concentrations for $C_{c.chest}/C_{mouth}$, $C_{l.lapel}/C_{mouth}$ $C_{r.lapel}/C_{mouth}$ varied with posture (higher than unity for standing and lower than unity for seated) for lifelike conditions (with and without wig). For example, for lifelike conditions, the ratios of $C_{c.chest}/C_{mouth}$, $C_{l.lapel}/C_{mouth}$, and $C_{r.lapel}/C_{mouth}$ were approximately equal to 1.63, 1.0, and 1.40 for standing, and were equal to 0.65, 0.56, and 0.52 for sitting. This agrees with (Malek et al, 1996) and (Welling et al, 2000) who tested human subjects and agrees also with (Guffey, et al., 2001), (Kim and Flynn, 1992), and (Kulmala et al., 1996) who tested unheated standing manikins. They found that concentrations at the chest were higher than concentrations at the vicinity of mouth. However, our finding strongly disagrees (for standing) and agrees (for sitting) with (Brohus, 1997) who found that concentrations at the chest were underestimating mouth exposures for both sitting and standing. (Brohus, 1997) studied ratios of concentrations by using a breathing themal manikin, wearing heavy clothing and a wig, and was sitting and standing in low speed wind environment. For lifelike conditions, the ratio $C_{c.chest}/C_{mouth}$ was 1.63 for this study while 2.9 for (Guffey et al., 2001). The difference agrees qualitatively and disagrees quantitively because the manikin used (anthropometrically correct breathing thermal manikin wearing a wig) was different than (Guffey et al., 2001).

Tables 23 to 26 listed regression coefficients, p-values and adjusted R-squared for log transformed concentrations for each sampling location. Log transformed concentartions were regressed versus wind tunnel velocity for each manikin treatment.

For lifelike conditions (sitting), wind tunnel velocity was significant ($p<0.01$) for all sampling locations for wig conditions and was highly significant ($p<0.001$) for bald conditions. The concentrations at all sampling locations increases to a peak value as wind

tunnel velocity increases, then decreases as velocity continues incraesing (see Tables 23 and 24). This was illustrated by the positive sign for velocity coefficient (C_1) and the negative sign for velocity coefficient (C_2). The regression constant (C_0) varied substantially from sampling location to another and from wig to no wig conditions. For example, (C_0) ranged from 0.67– 1.05 for wig and from 0.8 – 1.14 for bald. Regression coefficient (C_0) values at chest level were higher than mouth level for wig and lower for bald. Adjusted R-squared (R^2) ranged in the 60% – 80% for both wig and bold for most sampling locations, except 44% for left lapel. This indicated that about 70% of the data can be represented by these regression models.

For lifelike conditions (standing), velocity was highly significant ($p<0.001$) for all sampling locations for bald conditions, and was slightly significant ($p<0.01$) for most locations, and the model was not significant for neck, left collar and center chest locations for wig conditions. Concentrations increased to a peak value as velocity increased, then decreased as velocity continued increasing (see Tables 25 and 26). This was illustrated by the positive sign for velocity coefficient (C_1) and the negative sign for velocity coefficient (C_2) or (C_3). The regression constant (C_0) varied substantially from sampling location to another and from wig to no wig conditions. For example, (C_0) ranged from 0.8– 1.33 for wig and from 0.92 – 1.35 for bold. Regression coefficient (C_0) values at chest level were higher than mouth level for wig and lower for bold. Adjusted R-squared ranged in the 70% – 90% for bald conditions and from 40% - 60% for wig. This indicated that about 80% of the data can be represented by these regression models for standing breathing bald manikin while 50% of data can be represented for standing breathing wearing wig manikin.

MANIKIN I AND II CONCLUSIONS

The main purpose of this work was to investigate the effects of velocity, heating, breathing, hair style and posture on: 1) concentrations measured at sampling locations in the vicinity of the mouth, assumed to be equal to inhaled concentrations; and 2) ratios of concentrations at different locations to mouth. In addition to, the third purpose was to test the adequacy of a manikin in sampling, as a surrogate to human subjects, by choosing the optimum combination of manikin characteristics.

Conclusions from Manikin Studies I and II

- Wind tunnel velocity had a statistically significant effect on log transformed concentrations for all sampling locations. Body heat had a statistically significant effect on concentrations for all sampling locations.
- The interaction of velocity and heating had a statistically significant effect on concentrations at each sampling location. For heated conditions, concentrations varied with an inverted-V relationship with wind tunnel velocity. For unheated conditions, concentrations varied monotonically with wind tunnel velocity.
- The effect of heating was substantial at low velocity ranges (11 to 48 fpm) and modest at higher velocities (48 to 104 fpm).

- Posture had a statistically significant effect on log transformed concentrations for all sampling locations. Posture changed the airflow patterns around the manikin due to the various orientations of legs and arms to wind tunnel velocity for sitting and standing.
- Breathing had a statistically significant effect on log transformed concentrations at all sampling locations. Breathing tended to dilute concentrations for each location, specifically at the mouth and nose.
- The wig did not have a statistically significant effect on log transformed concentrations at the face and upper torso levels. It did have a statistically significant effect on concentrations at chest level.
- The interaction of breathing and wig was statistically significant on concentrations at the face and upper torso. For lifelike conditions, the effect of wig was substantial on inhaled concentrations for both sitting and standing postures.
- The interaction of velocity and posture had a statistically significant effect on log transformed concentrations only at the face.
- The interaction of posture and heating did not have a statistically significant effect on log transformed concentrations at chest levels.
- Velocity and posture had a statistically significant effect on ratios of concentrations for all sampling locations.
- Heating did not have a statistically significant effect on ratios of concentrations for most sampling locations. Likewise, breathing and wig had statistical significance on some ratios and not for others.
- Although, the wig main factor was not statistically significant for the ratios of concentrations at forehead, the interaction of wig and posture had a statistical significance at this location.
- For lifelike conditions, concentrations at the mouth were always higher for standing than sitting.
- Concentrations measured at the chest and shoulder levels were higher than mouth concentrations for standing posture and were lower than mouth concentrations for sitting.
- Concentrations measured at the forehead location were always lower than concentrations measured at the mouth for both sitting and standing.
- The bias in measured concentrations was consistent for the effects of the independent variables such as heating, breathing, and hair style.
- Center chest, both lapels, neck, both collars, and forehead locations are not good sampling locations to estimate actual inhalation exposure.
- Nose location is the best sampling location to estimate actual inhalation exposure.

Finally, adding breathing and heating to the manikin was important and had statistically significant effect on concentrations at the mouth. Although hair style did not have statistical significance on concentrations at the mouth, the effect of hair was substantial and should be considered for more research at different levels. It was concluded that using a manikin in sampling as a surrogate to human subjects requires the addition of body heat, breathing and hair.

8.2 Recommendations for future work

This research was developed to investigate the effects of velocity, heating, breathing, hair style and posture on concentrations at the mouth and ratios of concentrations in the breathing zone of a manikin. As the results of this study are considered important for laboratory research as well as for industrial hygiene practices, further investigations to be conducted for the effects of these variables at higher levels and the addition of new variables that are plausible to be important.

It is recommended to study the effects of wider range of wind tunnel velocities, the effect of mouth breathing, and breathing rates at moderate and heavy activities that are present in industrial applications. In addition, realistic worker movements that include arms, legs and torso, hair with different length, and the interactions of these factors with breathing may have substantial effect on inhaled concentrations. Also, in any industrial environment, workers wear glasses, helmets, caps, and googles. These variables may have an effect on inhaled concentartions for workers.

Human Study Results, Discussion, and Conclusions

11.3, 27.2, 47.5, 103.5 ft/min

The apparatus and methods for the human study were the same as the manikin study with the following exceptions:

1. Only 4 cross-draft velocities were tested: 11, 27, 48, and 103 ft/min
2. Humans had two tasks: keeping very still and moving children's play blocks back and forth from one side of the pie-pan source to the other.
3. "Not breathing" was achieved by breathing through a plastic tube, which was intended to move the kinetic effects of breathing outside the wake downstream of the body.

Table 27a: Results for Human Subjects

Subj	Vel	Stand	C_{mouth1}	C_{mouth2}	C_{nose}	$C_{forehead}$	C_{neck}	$L_{Lcollar}$	$C_{Rcollar}$	C_{Llapel}	C_{Rlapel}	C_{Cchest}
4	11.3	0	19.2	19.1	20.3	19.6	19.9	18.9	18.5	21.7	20.5	22.2
4	11.3	0	13.7	13.4	14.4	13.8	16	14.5	13.9	16.4	14.5	16.4
4	11.3	0	8.7	22.3	14.9	17.1	14.7	13.1	13.9	15.2	15.6	17.4
4	11.3	1	8.5	8.4	8.3	7.8	9.2	9.1	8.6	12.2	11.8	11.9
4	11.3	1	6.1	6	5.8	5.7	6.2	6	6.4	7.6	11.4	7.4
4	27.2	0	27.1	26.9	26.9	24.9	29.1	27.8	26	32.3	34.5	37.4
4	27.2	0	28.3	28.2	25.6	24.7	29.4	27	29.4	25.9	37	35.8
4	27.2	0	22.8	22.8	22.5	21.2	23.7	22	23.5	21.3	25.5	29
4	27.2	0	15.2	13.8	16.8	16.9	15.8	15.2	14.9	14.2	13.6	14.5
4	27.2	0	18.1	8.7	18.3	19	16.7	17.5	18.8	17.6	18.5	20.9
4	27.2	1	14.4	14.3	13.5	10.8	15.1		14.7	22.8	20.3	21.9
4	27.2	1	18	18.1	15.9	15.9	18.1	16.5	18.1	19.4	20.9	19.9
4	27.2	1	10.5	10.6	10.1	9.7	11	10.7	10.8	14	11.8	13
4	27.2	1	13.3	13.1	10.3	10.1	14	12.9	14.3	18	20.7	15.1
4	27.2	1	11.5	10.9	10.4	9.8	12.7	12.4	12.4	17.9	15.7	17.1
4	47.5	0	34.9	34.2	34.2	33.8	37	34.2	33.4	32.3	34.8	36.6
4	47.5	0	27.9	27.7	27.6	26.1	29.6	27.4	27.4	23.9	32.3	33.5
4	47.5	0	18.4	11.6	18.9	19.1	19.6	18.8	18.4	19	19.6	18
4	47.5	0	30.3	23.6	31.9	30.3	23	29.8	28.9	28.6	26.3	32.1
4	47.5	1	15.8	23.7	20.1	16.2	26.2	27.5	25	27.6	32.1	32.1
4	47.5	1	18.9	19.2	17.4	16.2	20.6	20.1	20.1	25.3	24	24.4
4	47.5	1	15.5	15.7	12.4	11.7	17.3	15.8	17.2	24.6	25.2	23.6
4	47.5	1	21.4	21.4	17.5	14.4	25.1	25.5	23.6	35.8	32.5	29.2
4	104	0	31	30.1	26.3	24	33	28.8	24.5	44.2	55.1	62.5
4	104	0	24.3	24.2	23.9	22.1	25.5	25	24.7	20.3	20.5	23.7
4	104	1	8.6	8.4	7.7	7.5	9.4	9.3	9.9	15.2	15.1	15.4
4	104	1	9.4	9.4	7.5	6.3	10.3	9.6	10.4	14.4	14.8	13.7

Table 27b: Results for Human Subjects

Subj	Vel	Stand	C_{mouth1}	C_{mouth2}	C_{nose}	$C_{forehead}$	C_{neck}	$L_{Lcollar}$	$C_{Rcollar}$	C_{Llapel}	C_{Rlapel}	C_{Cchest}
6	11.3	0		10.5	10.6	10.5	12.7	11	11.1		13.2	13.9
6	11.3	0	52	50.6	49.4	43.3	58	60.5	61.2	73.2	29.3	75.6
6	11.3	0	17.3	16.4	17.8	16	22.6	21.3		18.6	13.6	41.1
6	11.3	0	39.5	39.5	39.5	39.5	39.5	39.5	39.5	39.5	39.5	39.5
6	11.3	1	10.3	10	11.2	10.1	12.6	12.7	10.5	16.1	10.3	17.7
6	27.2	0	32.8	15.9	27.7	27.5	38.3	35		35.2	24.6	61.6
6	27.2	0	39.5	39.5	39.5	39.5	39.5	39.5	39.5	39.5	39.5	39.5
6	27.2	1	17.4	18	14.5	15.1	17.7	15.4	16.7	16.1	26.8	16.6
6	27.2	1	17.5	17.6	14.6	15.5	20.4	15.7	17.6	16.4	28.5	16.7
6	27.2	1	16.3	16.4	13.9	14.1	16.3	15.7	17.4	15.8	22.8	19.7
6	47.5	0	9.9	9.8	10	9.5	13.4	10.4	10.7	13	14.1	14.3
6	47.5	0	43.2	17	43.2	36.4	46.5	43.2	45.1	66.9	49.3	94
6	47.5	0	35.3	36	39.5	37	48.4	44.7	44.6	40.8	51.6	86.6
6	47.5	1	17.8	15.8	15.9	15.2	19.1	18.2	19.5	20	29	22.2
6	47.5	1	12.5	12.4	11.7	10.5	14.8	14.2	14.6	19.7	23.4	17.5
6	104	0	37.3	26.4	27.7	27.9	41.8	35.3	37.2	47.4	63	78.8
7	11.3	0	14.5	14.7	12.6	11.9	12.5	11.5	11.5	9.7	12.3	12.9
7	11.3	0	16.2	16.4	13.6	13	13.1	12.9	12.3	12.4	8.6	12.1
7	11.3	0	9.8	9.9	8.2	8	9.4	8.7	8.8	6.2	4.9	7.5
7	27.2	0	57.2	20.4	19.7	22.3	13.8	13	14.4	10.1	7.9	9.3
7	27.2	0	22.2	22.6	21.1	19.7	17.4	15	16.5	10	8.6	11.8
7	47.5	0	30.1	30.6	24.7	24.7	30.5	25.9	26.6	13.5	32	26.9
7	47.5	0	30.1	33.3	29.6	27.2	18.6	22.4	19.1	10.9	8.9	13.1
7	47.5	0	25.8	25.3	22.8	22.5	23.3	22	22	16.7	7.1	16.9
7	47.5	0	26.3	26.4	24.3	22.5	22.5	22	8.7	11	22	16.3
7	104	0	24.7	25.1	24.3	22.9	20.9	19.6	21	13.3	10	13.2
7	104	0	19.6	19.7	20	20.5	15	16.6	16.4	11	9.2	10
7	104	0	22.4	22.2	20.7	18.4	20.3	17.6	20.1	10.2	8.7	15.3

Table 27c: Results for Human Subjects

Subj	Vel	Stand	C_{mouth1}	C_{mouth2}	C_{nose}	$C_{forehead}$	C_{neck}	$L_{Lcollar}$	$C_{Rcollar}$	C_{Llapel}	C_{Rlapel}	C_{Cchest}
9	11.3	0	13.2	13	14.2	14	12.3	11.9	12.1	10.3	10.4	10.1
9	11.3	0	29.9	28.5	22	15	36.3	-2	36.1	0.1	19.2	79.3
9	11.3	0	68.4	71.3	63.9	55.6	73.1	54.9	65.6	57.9	87.7	106.2
9	11.3	0	20.2	20.8	20.9	16.9	34	29.6	27.6	37.4	19.4	77
9	11.3	0	33.9	33	23.7	18.7	38	31	41.3	31.4	55.1	88.1
9	11.3	0	34.1	33.6	32.7	29.1	38.2	34.8	24.7	32.6	33.8	49.5
9	11.3	1	17.1	17.2	17.4	16.6	21.1	17.5	16.7	23.7	22.8	24.3
9	11.3	1	16.1	16	16	15.8	18.7	15.9	16.1	20.9	21.6	22
9	11.3	1	11.3	11.7	9.3	5.9	21.5	13.5	13.4	24.2	27.5	28.8
9	11.3	1	20.3	21	17	13.7	22.5	18	22.1	50.2	44.9	52.4
9	27.2	0	24.3	25.2	25.8	24.9	17	15.2	14.9	6.7	25.9	5.8
9	27.2	0	39.4	39.3	40.3	28.7	41.8	37.8	35.2	5.2	6.5	3.7
9	27.2	0	71.4	70.8	71	60.2	81.8	59.4	66.1	67.6	43.9	112.9
9	27.2	0	41.1	43.2	41.5	31.4	58.1	56.5	51	110.3	48.1	119.3
9	27.2	0	53.4	52	45.1	39.4	56	48.7	55.8	56.4	62.2	80.1
9	27.2	0	32.3	31.6	29.4	26.5	35.2	32.3	13.1	65.1	37.3	64.6
9	27.2	0	51.7	50.4	50.5	45.1	57.1	45.6	19.5	59.7	40.2	89.2
9	27.2	1	14.3	14.3	14.3	15	16.1	25.5	15.5	21	25.5	24.4
9	27.2	1	25.5	25.8	22.8	20.8	31.4	21.1	26.3	33.4	35.2	35.4
9	27.2	1	27.7	27.7	26.6	29.1	19.2	17.9	23.5	25.2	27.7	29.3
9	27.2	1	21.2	21.8	21.4	17	26.8	28.1	20.4	65.2	29.3	54.8
9	47.5	0	41.8	42	41.8	37.4	29.3	24	26.7	6.4	5.8	5.8
9	47.5	0	62	63.7	63.2	58.3	37.4	31.1	48.9		2.9	2.6
9	47.5	0	56.9	55.8	68	63	44	45.1	44	6.9	4.8	7.5
9	47.5	0	91.5	91.5	73.5	62.2	99.5	51.4		137.8	206.5	190.7
9	47.5	0	71.2	76.1	69.5	48.4	117.5	111.8	97.1	219.3	88	249.2
9	47.5	0	98.7	95.6	90.4	73.3	116	82	100.4	152.6	190.3	250.7
9	47.5	0	21.2	20.6	19.3	18.1	23.8	17.2	20.4	24.6	23.2	36.9
9	47.5	1	17.5	17.5	17.1	15.4	20.2	19.5	19.5	28.4	31.3	33
9	47.5	1	16.9	16.9	16.1	14.7	19.7	18	18.4	28.1	30.5	32.4
9	47.5	1	28.4	31.6	17.1	13.2	66.1	37.6	34.8	95	77.7	35.9
9	47.5	1	23.3	23.6	15	10.6	47.6	23.2	23.8	60.1	63.2	52
9	47.5	1	18.4	18.6	15.7	12.8	19.7	19.1	15	52.7	50	55.7
9	104	0	36.3	35.4	36.9	36.1	24.2	25.3	20.4	9.2	6.4	6.9
9	104	0	32	31.3	32.3		33.2			58.4	49	71.3
9	104	0	46.4	47.3	38	30.6	61.8	53.7	56.6	129.7	123.2	201.1
9	104	0	38.5	38.7	34.2	28.7	45.8	45.2	28.5	86	54.8	108.8
9	104	0	38.4	37.4	36.8	32	40.3	37.5	29.7	27.2	37.2	52.7
9	104	1	11.7	12	11.9	11.3	12.4	12.8	12.8	19.9	19.1	21.6

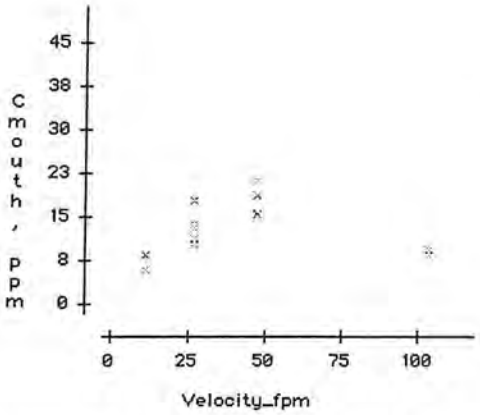

Figure 70a: Subject 1, all conditions
x = Standing, o = Sitting

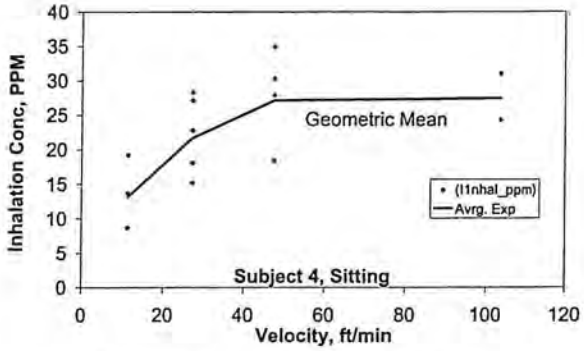

Figure 70b: Subject 4, Sitting

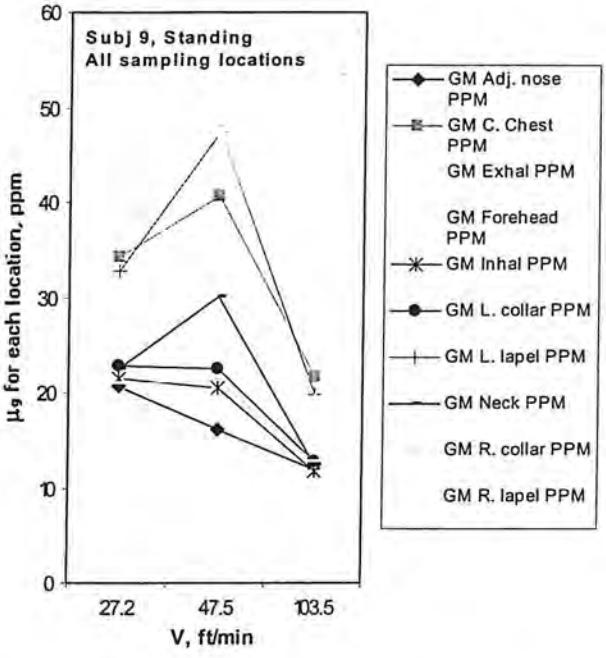

Figure 71a: Geometric Means for Standing

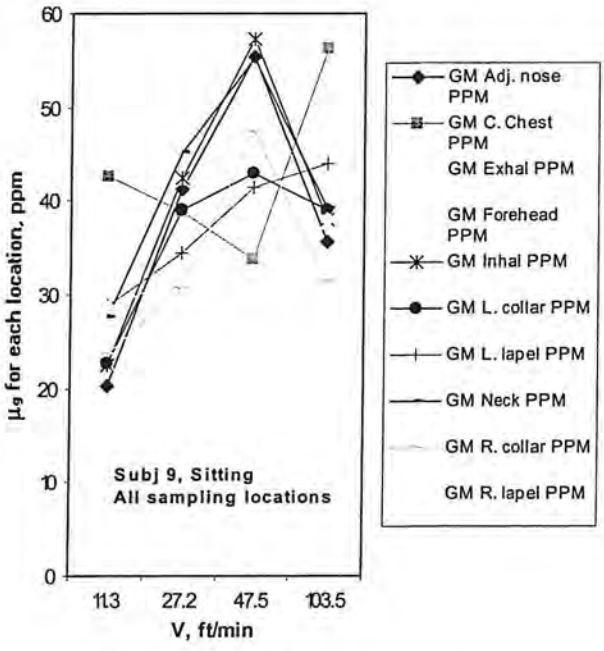

Figure 71b: Geometric Means for Sitting

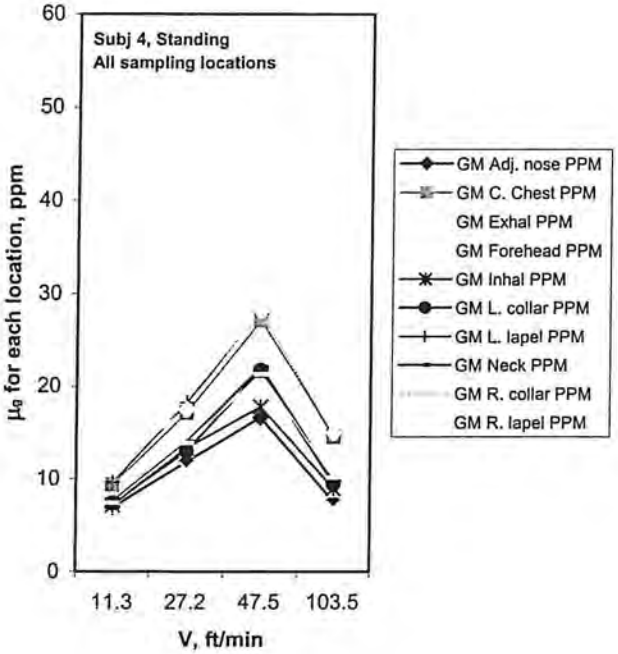

Figure 72a: Geometric Means for Standing

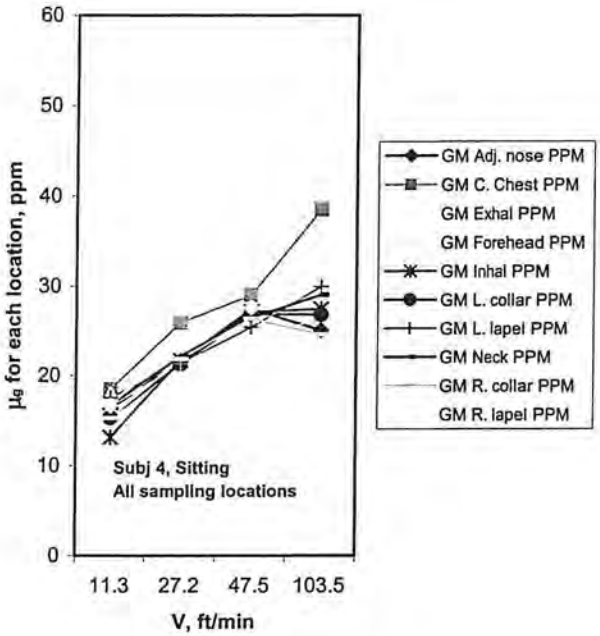

Figure 72b: Geometric Means for Sitting

Table 28: Analysis of Variance for Concentration at the Mouth

Source	df	Sums of Squares	Mean Square	F-ratio	Probabilty
Constant	1	83888.8	83888.8	539.54	0.0001
Subject	5	4802.03	960.406	6.177	0.0001
Standing	1	8129.03	8129.03	52.283	0.0001
Velocity	3	4069.33	1356.44	8.7241	0.0001
Task	1	378.085	378.085	2.4317	0.1221
Breathing	1	22.2482	22.2482	0.14309	0.7060
Error	99	15392.7	155.482		
Total	110	32661			

Results and Discussion of Human Study

Results for the human subjects (see Tables 27a, 27b, 27c) were generally, but not always, consistent with the results for the manikin.

Concentrations at the mouth: As with the manikin, concentrations varied with wind tunnel velocity ($p < 0.01$) in an inverted V-shape (see Figures 70a to 73b). However, unlike manikins, the human results showed a more consistent V-shape for Sitting than Standing. Sitting/Standing itself was significantly related ($p<0.01$) to concentrations at

the mouth (see Table 28). However, unlike the manikin, human subjects averaged roughly twice as high for sitting as standing, not the reverse.

As shown in Table 28, subject-to-subject differences also were significant. There were not enough subjects to determine if subject physiological measurements, gender, or hair length significantly affected concentrations at the mouth or at the surrogate locations.

Neither breathing through a tube or task (being still as possible or moving blocks) were significant for C_{mouth}.

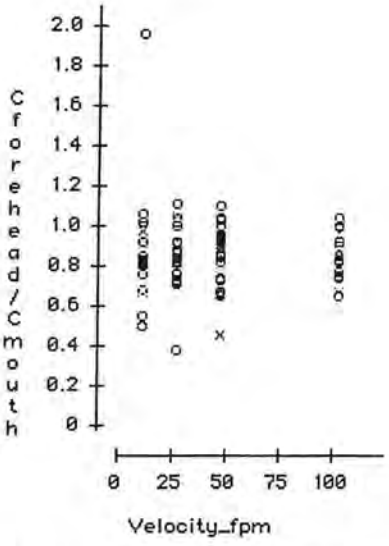

Figure 73a: Subjects, all conditions
x = Standing, o = Sitting

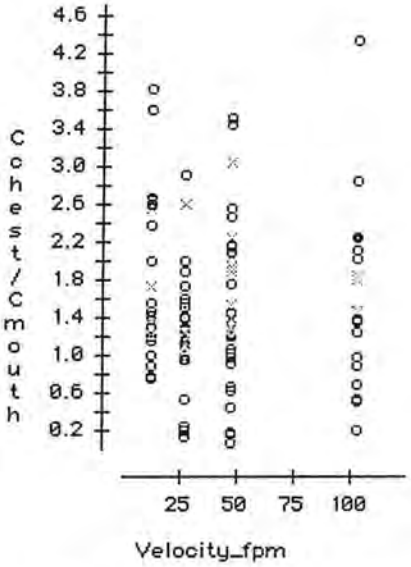

Figure 73b: All subjects, all conditions
x = Standing, o = Sitting

Table 29: Summary Statistics for Ratios to C_{mouth}

	Forehead	Nose	Neck	$Lapel_{right}$	$Lapel_{left}$	$Lapel_{avg}$	$Collar_{right}$	$Collar_{left}$	$Collar_{avg}$	C_{chest}
Median	0.86	0.95	1.07	1.13	1.16	1.22	0.99	1.01	1.00	1.36
GeoMean	0.84	0.93	1.06	1.00	1.03	1.06	0.97	0.96	0.97	1.23
GeoStd	1.23	1.18	1.32	2.33	2.04	1.87	1.29	1.32	1.27	2.12
Min	0.39	0.34	0.24	0.00	0.05	0.10	0.23	0.25	0.24	0.04
Max	1.97	1.71	2.33	3.35	2.74	3.04	1.78	1.60	1.66	4.33
10th Per	0.67	0.81	0.78	0.45	0.41	0.47	0.79	0.75	0.71	0.58
90th Per	1.03	1.06	1.39	2.10	1.91	1.91	1.26	1.22	1.25	2.59

Ratios of surrogate concentrations to C_{mouth}: As shown on Table 29 and Figures 73a and 73b, the ratios of surrogate concentrations to C_{mouth} varied widely. Concentrations at the lapels and center chest ranged from much lower to much higher than C_{mouth}. Their ratios of roughly 50% to around 200% to C_{mouth} represent extremely unreliable estimates. Note that averaging values for the two lapels did not improve their accuracy or precision. The

left and right collars and the neck were much better, having median ratios close to unity and relatively low geometric standard deviations (σ_g = 1.3). The adjacent to nose location had the lowest geometric standard deviation (σ_g = 1.18) and a median value of 0.95. It could be "corrected" by adding 5% to its values. Concentrations at the humans' foreheads averaged about 86% of the concentration at the nose but had a geometric standard deviation almost as low as at the nose. Hence, concentrations at the forehead could be "corrected" by adding about 15% to the value measured at the forehead.

Hence, if one is not willing to sample on the face, the collars are a reasonably good surrogate for the mouth. However, some samples measured at the collars were very low (e.g., 25% of C_{mouth}) and others were very high (178%).

Table 30: Linear Models Results for Ratios to C_{mouth}

Source	Forehead	Nose	Neck	$Lapel_{right}$	$Lapel_{left}$	$Lapel_{avg}$	$Collar_{right}$	$Collar_{left}$	$Collar_{avg}$	C_{chest}
Const	<0.001	<0.001	<0.01	--	--	--	--	--	--	<0.001
Subject	<0.05	--	--	<0.01	<0.05	<0.05	<0.001	<0.001	<0.001	<0.001
Posture	--	--	--	<0.01	<0.05	<0.01	--	--	--	--
Velocity	--	--	<0.05	--	--	--	<0.05	--	<0.05	--
Task	--	--	<0.001	<0.001	<0.001	<0.001	<0.01	<0.001	<0.001	<0.001
Breathing	--	--	--	--	--	--	--	--	--	--
R-sq	20%	15%	42%	43%	49%	47%	41%	37%	46%	49%

As shown on Table 30, General Linear Models regression of $Ln(C/C_{mouth})$ showed the deviation of the geometric mean ratio from unity was statistically significant for the forehead, nose, and chest. Subject-to-subject differences were significant for all but Nose and Neck, while posture affected only the lapel samples. Velocity was significant for the neck and collars, and Task was significant for all samples on the torso. Breathing did not affect the ratio for any location. In short, the ratio of surrogate concentrations to Cmouth was affected by Subject, Posture, Velocity, and Task, making it impossible to model C_{mouth} for all conditions for any location except Nose and possibly Forehead.

Discussion of Human Study

The dramatic effects of velocities and postures suggest that exposure studies should consider multiple postures and cross-draft velocities. The lapels and chest samples were poor surrogates for the nose, but concentrations measured adjacent to the nose, the forehead, and the collars generally fell within +20% of C_{mouth}.

Conclusions from Human and Manikin Experimental Studies.

The overall conclusions from both the human and manikin studies are that:

9. For the manikin, all independent variables (Velocity, Posture, Hair Length, Heating, Breathing) were important, as were most interactions of the dependent variables (especially velocity and Heating).
10. When the manikin was either not heated or did not breath, it was a poor surrogate for the human subjects. The effects of velocity on concentrations were profoundly

different when the manikin was at ambient or 98F body temperatures. At 98F, velocities followed an inverted V relationship with concentrations at all sample locations. At ambient temperatures the effect of increasing velocity was to decrease concentrations monotonically, a common finding in unheated manikin studies.

11. For manikins, concentrations were twice as high at the mouth when standing than when seated. Concentrations on the torso were higher than C_{mouth} when standing and lower when sitting.
12. For manikins no location was a reliable surrogate for the mouth.
13. For human subjects, the effect of increasing velocities tended to follow the inverted V relationship, just as it did for heated manikins.
14. Likewise, the effect of posture was profound, but opposite to the manikin. That is, the concentrations were higher when sitting than standing, possibly due to subtle differences in postures.
15. For humans, breathing through a tube had no significant effect.
16. For humans, the collars, nose, and forehead were reasonably good surrogates for the mouth.

CFD SIMULATION STUDIES – ALL ASPECTS

[Note: Figures and Tables are numbered separately for this section]

Introduction (CFD Simulation)

In this study, three dimensional computational fluid dynamics (CFD) simulations are used to investigate the distribution and level of contaminant concentrations in the breathing zone when airborne contaminants are released within an arm's-length in front of the worker who has his back to the airflow. The objective was to gain a better understanding of the fluid motion and mixing phenomena controlled by the combinations of convection, diffusion and buoyancy in the wake of a human body. A concurrent experimental work was carried out in Industrial and Management Systems Engineering Department, West Virginia University (Guffey, 2004). Some results from the experiments were used to validate the simulations.

Worker exposure in a ventilation tunnel

Ventilation systems are used to create a healthy indoor air quality and a comfortable indoor thermal condition with as low as possible energy consumption. Wind tunnels are widely used to study human exposures to airborne contaminants since they allow investigators to control airflow conditions.

In the concurrent experimental study, a wind tunnel is utilized with an inlet honeycomb grid to straighten the flow and to induce turbulence. Gaseous contaminants (ethanol vapor) are released within an arm's length of the worker who has his back to the flow. The Reynolds number based on the equivalent dimension of the torso is in the range of 2000 – 30,000 (600 – 10,000 if based on the equivalent dimension of the head). With a heated manikin, the Grashof number is about $8x10^8$. The exposure level is measured by the concentration at the breathing zone, which is represented by a single point one centimeter from the mouth center in the current numerical study.

Generally, the ventilation flow in the wind tunnel is of an incompressible, non-isothermal type with heat and mass transfer. The flow over a human body involves a very complicated flow due to the irregular body configuration. There is not much information about this kind of wake flow in the literature. However, the basic characteristics can be revealed by studying the wake flow of a cylinder and a sphere, since the head and the torso could be approximated by a sphere and an elliptic cylinder, respectively. Fortunately, these flows have been of great interest for researchers. The following is a brief review about the flow character of these two classical flows.

The experimental work by Tritton (1959) shows that at a Reynolds number of 150, the vortex street becomes turbulent in the wake downstream of a circular cylinder and at a Reynolds number of 400, the vortices become turbulent after the separation point somewhere in the wake formation region. The experiments by Achenbach (1968), on the other hand, indicate that the transition from laminar flow to turbulent flow in the boundary layer can take place even at low Reynolds number. The laminar boundary layer

will become turbulent when the Reynolds number reaches a critical value around $2x10^5$. Thereafter, the boundary layer will separate farther rearward than if it were laminar.

The variation of the sphere wake structure with Reynolds number is as follows. When the Reynolds number is lower than about 20, the flow is laminar everywhere and separation does not occur (Taneda 1956). At Reynolds numbers between about 20 and 400, a stationary, symmetric pair of vortex ring is formed at the rear of the sphere (Taneda 1956; Achenbach 1974). When a Reynolds number of about 400 is reached, the vortex ring begins to oscillate, and the wake forms horseshoe-shaped vortex loops at Reynolds numbers between about 400 and 1000 (Achenbach 1974). At Reynolds numbers above about 1000 the vortex loops diffuse very rapidly, which indicates a turbulent flow field in the wake formation region (Taneda, 1978). Similarly, at a critical Reynolds number around 10^5 the laminar boundary layer becomes turbulent before separation.

The above information indicates that most probably a turbulent wake flow is formed in the downstream of a human body after a laminar boundary separation. An unsteady vortex shedding may appear in the wake. However, the vortex may diffuse rapidly because of the flow between the arm and the torso.

Factors related to exposure levels

The worker exposure in a wind tunnel could be affected by a great number of complicating factors, many of which are not yet fully understood. These factors which could affect the worker exposure significantly in a wind tunnel are investigated. These factors include: the contaminant position, the orientation of the worker, the ventilation intensity, the level of free stream turbulence, the heat flux from the body, the body shape and the flow unsteadiness. Understanding the effects of these factors on the flow field and the worker exposure will be important for exposure control.

Turbulence models for worker exposure

To date, there are three main classes of approaches for dealing with turbulent flows: Reynolds Averaged Navier-Stokes (RANS), Large Eddy Simulation (LES) with a sub-grid scale (SGS) model, and Direct Numerical Simulation (DNS) with any turbulence model. DNS and LES are still too computationally expensive to be employed on a regular basis, and, from an engineering point of view, they provide far more information than an engineer needs.

Recently, various RANS models are used to deal with the complex turbulent flows in work places. The most widely used RANS models are those linear eddy-viscosity models with wall functions because of their robustness, economy, and reasonable accuracy for a wide range of turbulent flows. However, as it is well known, the linear eddy-viscosity models (EVM) have certain deficiencies. Most importantly, the Boussinesq hypothesis which these models are based on fails when non-trivial flows are considered (e.g., flows over curved surfaces, flows in ducts with secondary motions, flows in rotating fluids, and flows with separation). Various modifications and new modeling concepts have been proposed over the past decades, ranging from ad hoc remedies, and complex non-linear eddy-viscosity approaches to Reynolds stress models/second-moment closures. Guidance and recommendations on the application of

these models for exposure prediction would greatly ease the usage of CFD in the industrial hygiene community.

Motivation and objectives

In this study, three dimensional computational fluid dynamics (CFD) simulations are used to calculate the concentration of gaseous contaminants in the breathing zone of a worker when airborne contaminants are released within an arm's-length in front of a manikin who has his back to the airflow. The main objectives were to numerically evaluate the effect of different factors on the manikin exposure and to recommend a turbulence model preferable for this type of simulations. These factors investigated include the body shape, the heat flux from the body, the ventilation intensity, the level of free stream turbulence, and the flow unsteadiness.

Literature review (CFD Simulation)

To accurately predict the exposure levels in the working environment, one has to understand which factors are significant for work exposure and what kind of models one could use to account for these significant factors. In this literature study, two issues are of major concern. One is the factors which can impact the exposure levels in the working environment, such as the ventilation intensity. The other is modeling-related issues. Simulating work exposure is a complicated problem which comprehends turbulent flow with complex geometry, heat transfer, and mass transfer. That is why it is important to understand the pros and cons of different models for turbulence, heat transfer and mass transport. The choice for predicted worker exposure should be made based on which model can best solve this problem.

Factors affecting exposure levels

The worker exposure in a wind tunnel could be affected by a great number of complicating factors, many of which are not yet fully understood. A list of factors which are important include the following:

- Orientation of the worker
- Body shape
- Ventilation intensity
- Heat flux from the body
- Contaminant source position
- Flow unsteadiness
- Position and configuration of facilities
- Contaminant material and momentum
- Free stream turbulence
- Worker motion

This is a formidable list, and most of these continue to be the topics of research in this field. Nevertheless, all these factors which prove significant should be considered to accurately predict the exposure levels.

It is not possible to give a thorough discussion and literature review for each of these topics individually. However, a brief introduction and review with respect to six of the general and controllable of these factors will be given next. The topics and factors that are believed to be the more general and the more controllable in both the experiments and simulations include the orientation of the worker, the contaminant source position, the body shape, the ventilation intensity, the heat flux of the body, the level of free stream turbulence, and the flow unsteadiness.

The position and the configuration of the facilities, the contaminant material, size, location and momentum, and the worker motion vary significantly in different applications. In this study, these factors are fixed so that the focus is on the flow field in the wake of the human body and its relation with the exposure levels. A still fixed manikin was used in an otherwise empty wind tunnel. Gaseous contaminant was used to represent the contaminant source since it follows the flow closely.

ORIENTATION OF THE WORKER

Although the situation -- flow from the back of a worker is the main concern of this study -- some attention should be also given to the influence of the orientation of the worker because of its extreme significance. Experimental studies by George et al. (1990), Kim and Flynn (1991), Carlton and Flynn (1997), Welling et al. (2000), and Guffey et al. (2001) have shown that much higher contaminant concentrations occur at the back-to-flow orientation than when air flows from the side or from the front of the subject. Flynn and Ljungqvist (1995) reported that the reason for higher exposure levels at the back to flow orientation is that a reverse flow wake region is created downstream of the worker and this recirculation will bring the contaminant to the breathing zone.

In this numerical study, the flow from the back is considered for all cases since it is considered the worst case when the worker has a hand-held contaminant source.

BODY SHAPE

The effects of different body shapes on fluid flow and concentration patterns around the body in a wind tunnel have been evaluated to clarify if a sharp body or a block could be a surrogate for the human form in consideration of occupational and environmental health studies. Simple body shapes such as rectangular body, cylinder body and the composition of simple geometries have been widely used, despite lack of positive proof that they are capable of representing the real human body well. Brohus and Nielsen (1996) investigated the effects of body shapes using three different models, all of which were made of rectangular geometries and are insufficient to simulate a real human body accurately. In this study, a rounded body was generated to represent a human-like manikin used in the experiments as closely as possible in order to obtain accurate information about the flow field behind the manikin, especially the separation and the

reattachment of the flow around the head which may be significant in evaluating the worker exposure (Li et al. 2003, 2005).

VENTILATION INTENSITY

Usually, the wind speed in a ventilation tunnel is 0.1-1.0 m/s (Baldwin and Maynard, 1998), which is comparable with the face velocities of local ventilation hoods. A lot of experiments have been done in this wind speed range.

The experiments by George et al. (1990) reported that the contaminant concentration will decrease as the free stream velocity increases if the worker stands with his back towards the flow and there is no obstruction in the wake zone downstream of the body. However, this trend may not be followed if some object obstructs the flow field downstream of the body.

The experimental work of Saamanen, et al. (2002) showed that the breathing-zone concentration increases in the freestream velocity range of 0.1-0.3 m/s when the free stream air velocity increases. However, they used a simplified manikin which was composed of boxes. Their numerical simulations gave results which agree poorly with the experimental results.

The numerical analysis on the effect of inlet velocities on the exposure level may help to optimize the running conditions of the wind tunnel and alleviate the economic limitations to some extent. On the other hand, the current study is also used to validate the turbulence models by comparing the numerical results with the experiments.

FREE STREAM TURBULENCE

The turbulence intensity in the work places varies significantly. Experiments (Hancock and Bradshaw, 1983 and 1989; Kondjoyan, 2002) have shown that the free stream turbulence could significantly affect the transition from laminar to turbulence and thereafter the heat flux from the wall to the fluid because of its interaction with the boundary layer. Péneau et al. (2000) have recovered the same results using large eddy simulation. It could be an interesting topic to investigate the effect of the free stream turbulence intensity on the worker exposure. However, to the best of author's knowledge, there is little information in the literatures on this topic.

Welling, et al. (2000) measured the free stream air velocities, turbulence intensities and temperatures at the beginning of each experiment at 280 symmetrically distributed points, and they found that the free stream velocities and turbulent intensities changed significantly at low wind speed 0.1 m/s. They also observed that the variation of the nose concentration at that wind speed is about 90%. The reason is obvious due to the variation of the mean free stream velocity and the turbulent intensity. However, it's hard to differentiate the effect of the mean velocity and the turbulent intensity because these two factors were not controlled separately.

A thorough numerical analysis can be used to isolate the effect on the exposure levels from these two factors since it is easy to control these factors in numerical simulations.

HEAT FLUX FROM THE BODY

The heat convection from the body may affect the worker exposure in three possible ways: (1) it can transport the contaminants from the waist to the breathing zone by the action of buoyancy; (2) it may intensify the turbulence in the flow field and result in more diffusion; (3) it may cause contaminants that are "trapped" in the recirculation region near the breathing zone to rise out of that region into the free stream. Some experimental and numerical work in the literature, such as Saamanen, et al. (2002), Li, et al. (2003), Hyun and Kleinstreuer (2001) have shown that the buoyancy is important at low free stream velocities. The current study will concentrate on how the nature convection affects the flow field and thereafter the concentration field near the mouth at different Reynolds numbers.

FLOW UNSTEADINESS

Large scale unsteady motion is expected to be formed in the downstream of the body as mentioned in Section 1.1, which may result in the large variation of the exposure level at the breathing zone. Although the variation of the instantaneous exposure levels has been observed by other researchers (Welling, et al. 2000), its relation to the flow dynamics in the body wake has not been documented well. The current flow unsteadiness study utilizing LES is aimed to understand the flow dynamics in the formation and the developing of the wake flow in the downstream of human body as well as the relation to the contaminant transport. Hopefully, it will also provide some guidance on the sampling period for the experimental study.

Modeling related issues

There are three main classes of numerical techniques for dealing with turbulent flow: Reynolds Averaged Navier-Stokes (RANS), Large Eddy Simulation (LES) and Direct Numerical Simulation (DNS). DNS resolves the Navier-Stokes equations without averaging and approximation. It is viewed as an indispensable research tool to help the understanding the physics of the flow and the developing of turbulence models. However, it is simply too expensive to be employed on a regular basis, and, from an engineering point of view, it provides far more information than an engineer needs.

LES has gained overwhelming consideration in both industry and academy. The physical basis for LES is that the large-scale motions in the turbulent regime are more energetic than the small scale ones and are responsible for most of the transport. The small-scale turbulence is more universal and nearly isotropic, which makes it more suitable to be modeled. Mathematically, LES is applied by filtering the Navier-Stokes equations. The filtered quantities are modeled by a so-called subgrid scale model which relates the effects of small eddies to the resolved large eddies. Still, LES is constrained by the near-wall resolution requirements. For instance, to resolve the near-wall streaky structures, LES requires a grid density close to that for DNS with spacing of the order $\Delta y+=O(1)$, $\Delta x+=O(50)$ and $\Delta z+=O(20)$, where x+, y+, and z+ denote the streamwise, wall-normal and spanwise direction in wall unit respectively. As a result, one has to wait a long while (until 2045 according to Spalart, 2000) to use LES in large scale industrial and environmental applications (e.g., flow over a car).

Turbulence modeling with RANS equations has started nearly a century ago, when Boussinesq introduced the concept of an eddy viscosity (i.e. the Boussinesq eddy viscosity approximation, which relates the Reynolds stresses to the shear rates). Nowadays the field of classical RANS turbulence modeling is still active despite its disputable intuitive and empirical rationale. They are simple to use, computationally affordable and economical, thus appealing to industry for various applications, such as design, optimization, and prediction of off-design performances. They do not simulate the details of the turbulent motion, but only the effect of turbulence on the mean flow behavior.

NUMERICAL CONSIDERATION FOR REYNOLDS STRESS MODELS

Launder (1989) noted that if one adopts the staggered velocity/pressure node cluster, numerical stability is increased and the amount of interpolation required is decreased if the stresses are also staggered, (i.e. the normal stresses are located at the scalar node while the off-diagonal components are positioned so that they lie on the boundaries of the control volumes of the velocity components).

In a three-dimensional flow, each stress component appears in the budget equations for many of the other components. This strong intercoupling suggests that one should adopt for a simultaneous solution of the six components at a point. However, such a direct approach is spectacularly unstable, partly, because the stresses are scattered. The strategy is first to solve for the three coincident normal stresses, interpolating as necessary the 'old' values of the shear stresses. When updated values of the normal stresses have been obtained at all nodes, the off-diagonal components are obtained by a pointwise substitution.

The turbulent shear stress is often several orders larger than the molecular shear stress in turbulent flows. Treating it as a large source term creates stiffness and hence causes numerical instability in the numerical iterations.

In simple shear flow calculations the turbulent shear stress $-\overline{uv}$ in the momentum equation is usually divided and multiplied by the velocity gradient

$$\partial(-\overline{uv})/\partial y = \partial\left\{[(-\overline{uv})/(\partial U/\partial y)]\times(\partial U/\partial y)\right\}/\partial y \qquad (2.1)$$

and $(-\overline{uv})/(\partial U/\partial y)$ is treated as the eddy viscosity. In doing this, the turbulent shear stress is effectively cast into the diffusion term.

However, Hwang and Peng (1995) pointed out that in elliptic-type flows the velocity gradients will not always have the same sign as the turbulent shear stress as they do in simple shear flows. When the velocity gradient and the turbulent shear stress are of opposite sign, negative nodal coefficients will be introduced, which can lead to numerical instability.

A technique that could be used to overcome the numerical instability of the momentum equations is a modification of the numerical procedure for the eddy viscosity model. The Reynolds stresses can be expressed as

$$-\overline{u_i u_j} = -\overline{u_i u_j} + C_\mu \frac{k^2}{\varepsilon}\left(\frac{\partial U_i}{\partial x_j} + \frac{\partial U_j}{\partial x_i}\right) - C_\mu \frac{k^2}{\varepsilon}\left(\frac{\partial U_i}{\partial x_j} + \frac{\partial U_j}{\partial x_i}\right) \tag{2.2}$$

where C_μ=0.09. The second term is cast into turbulent diffusion forms in the numerical solution, and the rest into source term, which is trivial and have no serious effect on the numerical stability of the momentum equation.

Computations with a SMC model will probably require 50-200% more computer time than a linear two-equation eddy viscosity model.

Near-wall approaches

The overall success of all turbulence models in wall bounded internal as well as external flows is determined in large measure by the treatment of solid walls. Three different ways are commonly employed to compute the near-wall behavior of complex turbulent flow. They are wall functions, low-Reynolds number model (LRN), and two layer models.

Wall functions

In application of turbulence models, the most popular near-wall treatment is the wall function method because it requires much less grids ($30< y_1^+ <60$) in the near wall region. Wall functions are derived on the assumption that a Couette flow prevails, i.e. that the variation of the dependent parameters with respect to the streamwise direction can be neglected. For impermeable walls the flow equations can be solved analytically to yield the well known, law-of-the-walls:

$$U^+ = \frac{1}{k}\ln(y^+) + B \tag{2.3}$$

$$T^+ = \frac{\mathrm{Pr}_t}{\kappa}\ln(y^+) + B_T \tag{2.4}$$

Employing these equations permits one to simplify the near-wall treatment to a one-dimensional analysis for which the solution of the dependent variables is only a function of the normalized wall-distance. Naturally such a simplification reduces the computational storage and time through a reduction of the number of nodes. In addition, the convergence rate is increased as a result of the simplified equations.

Unfortunately, the universality of these wall functions is limited since they are derived from simplified governing equations. For instance, calculations of backward facing step flows with wall functions lead to more than 20% error, in the reattachment length (Rodi et al 1993). Although the basic assumptions made in the wall function approach, (i.e., flow parallel to the wall and equilibrium turbulence relations), are correct for simple wall

shear flows, a certain error will be created when the method is applied to complex wall shear flows with separated regions.

Two-layer model

In two-layer models the near-wall viscosity-affected regions are resolved, such that the dissipation rate of the turbulent kinetic energy is determined by a prescribed length scale distribution instead of by the transport differential equation.

The turbulent eddy viscosity in the near wall region is given by

$$\nu_t = C_\mu k^{1/2} l_\mu \tag{2.5}$$

and ε is determined from

$$\varepsilon = k^{3/2} / l_\varepsilon \tag{2.6}$$

The length scales l_μ and l_ε are adopted from the model

$$l_\mu = C_l y[1 - \exp(-R_y / A_\mu)] \tag{2.7}$$

$$l_\varepsilon = C_l y[1 - \exp(-R_y / A_\varepsilon)] \tag{2.8}$$

where both length scales express damping effects in the near-wall region in terms of the turbulence Reynolds number $R_y = k^{1/2} y/\nu$. Here y is the normal distance from the wall. The turbulence model moduli are given as $C_l = \kappa C_\mu^{3/4}$, $A_\varepsilon = 2C_l$ and $A_k = 70$, where κ is the Karman constant and $C_\mu = 0.09$.

In conducting the computation, the two models have to be matched at some location in a region where viscous effects have become negligible. In general, preselected grid lines are set for matching the two models within the criterion $R_y \geq 250$ recommended by Chen and Patel (1988).

Low Reynolds number model

Over the past few decades, many suggestions have been made for the extension of turbulence models to enable their use at low turbulence Reynolds numbers and to describe the flow close to a solid wall. The simplest example is the van Driest damping function (van Driest, 1956) for the mixing length. More advanced models incorporate either a wall damping effect or a direct effect of molecular viscosity, or both, on the

empirical constants and functions in the turbulence-transport equations devised originally for high Reynolds number, fully turbulent flows remote from the walls.

In the literature, a lot of work has been done on the low-Reynolds number two equation models. Patel et al. (1985) reviewed these works and suggested that the better performance of the low Reynolds number model could be achieved by: 1) selecting a damping function, f_μ, for the shear stress that is in agreement with experimental evidence and whose influence is restricted to the sublayer and the buffer layer; 2) choosing the low Reynolds number functions f1 and f2 in the ε equation with a mathematically consistent near-wall behavior; 3) fine-tuning the functions to ensure the reproduction of the well–known basic feature of wall-bounded shear flows over a range of pressure gradients. This suggestion has been followed by many later researchers (Bredberg and Davidson, 2004; Raisee, et al. 2004). They implemented the non-linear turbulence model together with the low Reynolds number model at the wall and the results has been shown to be satisfactory.

It should be noted here that the first interior nodes should be very close to the wall (y+<5) for the low Reynolds number model. The numerical experiments of Bredberg and Davidson (2004) showed that the predicted Nusselt number along the lower wall of a rib-roughened channel with y_1^+=1 and y_1^+=4 meshes could be within 5% of the grid independent result. Even though the prediction with y_1^+=10 mesh deviates by more than 25% from the experimental data, they are still encouraging when compared to other turbulence models, especially when using wall function based models.

Modeling buoyancy-driven flow

It is popular to use the simple eddy diffusivity models for turbulent flux of heat $\overline{\theta u_j}$ (or species):

$$\overline{\theta u_j} = -\frac{\nu_t}{\sigma_T'}\frac{\partial T}{\partial x_i} \tag{2.9}$$

where σ_T^t is the turbulent Prandtl number (or Schmidt number for species) which is a constant or determined from an empirical formulas. It is generally recognized that the linear eddy-viscosity models and their analogues for scalar fields cannot reproduce any flows with significant non-equilibrium effects, flows subjected to body forces, or any extra-strain rates other than simple shear. The above shortcomings can be eliminated by solving the modeled transport equations for $\overline{\theta u_j}$, closed by the equations that provide thermal scales (e.g., for $\overline{\theta^2}$ and $\overline{\varepsilon_{\theta\theta}}$). Differential transport equations have been proposed in the literature and applied with success to the computations of some simple buoyancy-driven flows. However, such models contain many terms that require separate modeling, and deriving a general closure for complex flows is a formidable task. Algebraic models based on a truncation of the differential second-moment closure have been proposed as the minimum closure level for complex flows. For instance, Hanjalic (2002) proposed a

three-equation (k-$\overline{\theta^2}$-ε) model which produced satisfactory solutions in a range of enclosed buoyancy-driven turbulent flows with different geometries and boundary condition. Abe et al. (1995) instead proposed a four-equation model (k-$\overline{\theta^2}$-ε-$\varepsilon_{\theta\theta}$) which is capable of predicting the heat transfer in separating and reattaching flows downstream of a backward-facing step.

It should be emphasized here that strong variations of all flow properties, in usually very thin boundary layers along the walls where the buoyancy exhibits the strongest effects on turbulence, requires a fine numerical resolution of the near-wall region. Thus, it is indispensable to use a low-Reynolds-number turbulence model which can fully resolve the near-wall region.

Mass transport models

When predicting the concentration of contaminants, both Eulerian and Lagrangian methods have been used in the literature. For the Eulerian method, the concentration can be calculated by solving a scalar transport equation, which approximates the turbulent diffusivity in relation with the eddy viscosity with an empirical constant, i.e., the turbulent Schmidt number. Since the contaminant concentration are very sparse for the current study (10^{-3} kg/kg air), the effect of the secondary phase (gaseous contaminants) on the main phase (air) is ignored. The Lagrangian method, however, tracks individual parcels in a Lagrangian frame. Each of the parcels represents a certain amount of gaseous contaminant and closely follows the air flow.

Flynn and Sills (2000, 2001) used the Lagrangian particle tracking method to predict human exposure to aerosols generated during compressed air spray painting in cross flow ventilated booths. They found that the predicted dimensionless breathing-zone concentrations were in agreement with the measured values.

Longest et al. (2000) applied RANS simulation in conjunction with the Eulerian scalar transport equation to investigate the distribution of CO in a Rochester-style human exposure chamber. In the current study, the predictions from the Lagrangian and Eulerian methods are compared in order to provide some guidance as to which one is better for predicting human exposure to aerosols.

The influence of critical factors on worker exposure (CFD Simulation)

This chapter first presents the computational details such as equations, grids, and the numerical method used in the current work. The results of the grid convergence study are shown next since it is important to know the numerical errors prior to the massive. Then the results of the influence of critical factors are presented and discussed. These results include the isolated influence of the body shape, the ventilation intensity, the level of free stream turbulence, the heat flux of the body, and the flow unsteadiness. Finally, the results are summarized at the end of this chapter.

Computational details

In this study, a three-dimensional wind-tunnel simulation was performed with the Fluent CFD software package (Fluent, Inc., Lebanon, NH). The geometrical configuration of the flow domain is shown in Figure 3.1, consisting of the wind tunnel (4.6m width × 2.6m height × 11m length) and a non-breathing manikin body (1.8m height). The manikin body faces downstream of the flow. Constant inlet velocity inlet and constant pressure at the outlet boundary were used. The inlet velocity was taken as 0.3 m/sec with a turbulence intensity of 0.3% to study the effect of the body shapes and the transport methods, values representative of typical working environments (Baldwin and Maynard, 1998). To investigate the thermal impact of the body, an inlet velocity of 0.1 m/sec was also used. The characteristic turbulent length scale was chosen to be 0.01 m, which represents the turbulence generating grid size at the inlet of the tunnel. The dimensions of the wind-tunnel and the sharp body configuration are illustrated in Figure 3.2. The source box is 0.3m(length)*0.3m(width)*0.05m(height) in size and the box center is 1.2m from the ground and 0.5m from the body. In addition, block and rounded body models are created as shown in Figure 3.3 to investigate the effect of the shape of the human-body on concentration levels near the breathing zone. It should be noted here that the breathing zone mentioned in the paper is represented by one point, which is 1.65m from the ground and 0.01m from the body (i.e. a point directly in front of the mouth at a horizontal distance of 0.01m).

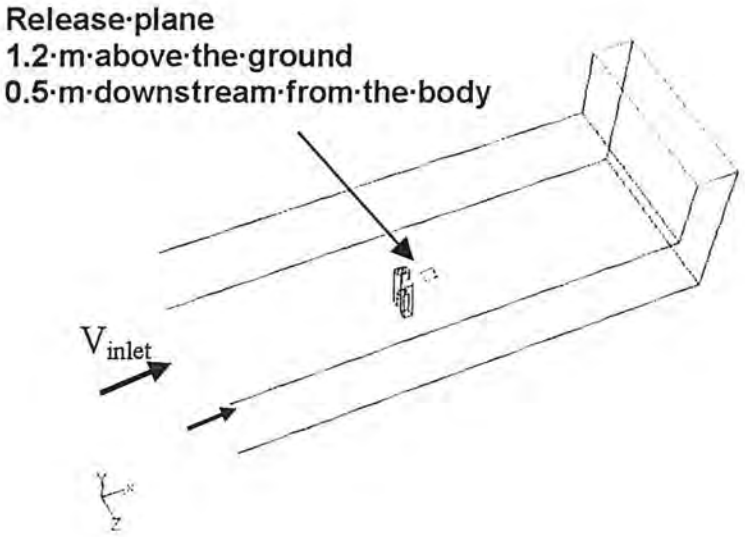

Figure 0-1 Schematic view of the wind tunnel model and location of contaminant release plane

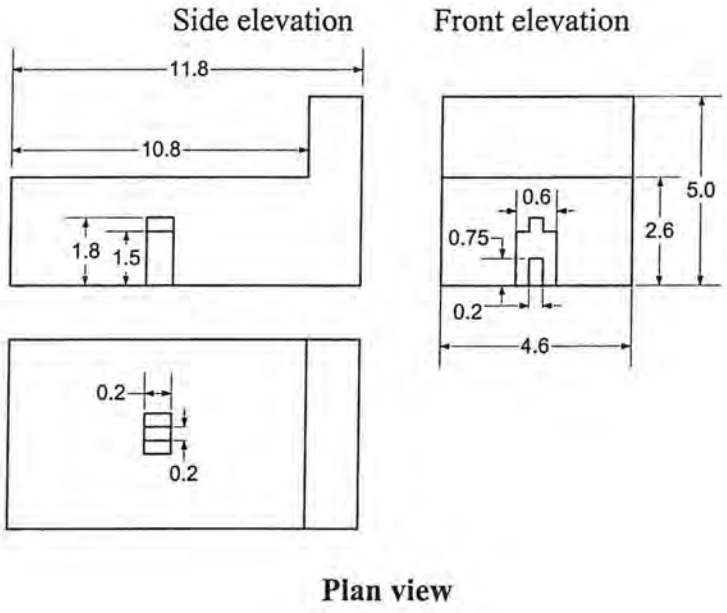

Figure 0-2 The geometry of the wind tunnel and the human body (all dimensions in m)

Different grid distributions, also known as meshes, were constructed as listed in Table 3.1 in order to quantify the discretization error using Richardson Extrapolation with Grid Convergence Index (GCI) (Roache, 1994) and Extrapolated Relative Error (ERE) (Celik

and Li, 2005). Richardson Extrapolation uses calculations on multiple sets of grids to calculate the extrapolated value of a dependent variable to zero grid size, and GCI and ERE use the extrapolated value to determine the numerical uncertainty caused by limited grid size, also known in the literature as the discretization error. For each body, the whole domain was divided to several sub-domains each with different grid sizes so that the mesh in the region around the body could be much finer than that in other regions (See Figure 3.4). It should be emphasized that the grids are refined proportionally for each sub-domain to maintain similar grids as suggested by Celik and Karatekin (1997). The only exception was mesh #3 (the sharp body), for which only the region around the body is refined based on mesh #2 in the hope to illustrate if better convergence with less cells using non-uniform grids could be achieved.

Table 0.1 Different meshes used for the grid convergence study

Mesh #	Block body	Sharp body	Rounded body
1	125,103 node 116,712 hexahedral cells	30,621 nodes 27,396 hexahedral cells	92,166 nodes 339,350 mixed cells *
2	229,874 nodes 217,212 hexahedral cells	124,326 nodes 115,824 hexahedral cells	136,302 nodes 470,234 mixed cells
3		188,583 nodes 169,430 hexahedral cells	208,600 nodes 659,110 mixed cells
4		347,595 nodes 330,598 hexahedral cells	
5		1,077,176 nodes 1,041,318 hexahedral cells	

* Mixed cells mean that some cells are hexahedral cells and the other are tetrahedral cells.

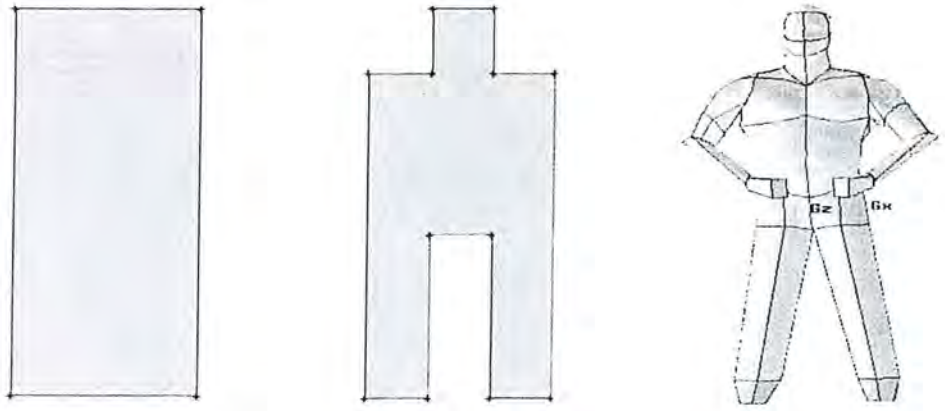

(a) block (b) sharp body (c) rounded body

Figure 0-3 Different body shapes used in the present study (not to scale)

The heat transfer boundary condition for the human body surface was taken as a convective heat flux of 25 W/m^2 (Bjørn and Nielsen, 1998), which was based on a 2000-calorie diet and corresponds to a moderate activity level of a standing person. The fluid medium was air and the contaminant was acetone vapor.

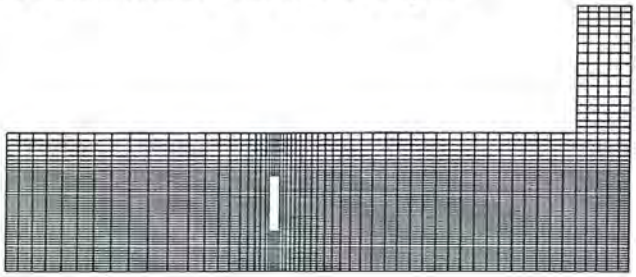

Figure 0-4 An example of a computational mesh used in the simulations (Mesh #2 for the sharp body, 115,824 hexahedral cells; the empty area represents the center of the sharp body)

The turbulence model of choice was the two-equation standard k-ε model (Launder and Spalding, 1974), which is one of the most commonly used turbulence models in practical engineering flow calculations. The k-ε model is based on the eddy-viscosity approximation which expresses the Reynolds stresses in terms of the mean velocity. The shortcomings of the eddy-viscosity approximation has been well documented in the literature (see e.g. Mathieu and Scott, 2000). Numerous more sophisticated models such as Reynolds stress model have been developed to overcome the defects of eddy-viscosity approximation. The choice of a turbulence model for a specific application should be made carefully, depending on the considerations such as the physics encompassed in the flow, the established practice for a specific type of problem, the level of accuracy required, the available computational resources, and the amount of time available for the simulation. In the present study with its complex geometry, the standard k-ε model was used because of its robustness, economy, and reasonable accuracy for a wide range of turbulent flows.

Governing equations

Standard turbulence model

The mathematical formulation of the governing equations and the turbulence models used for steady flow simulations are the time-averaged Navier-Stokes equations with the standard two-equation k-ε turbulence model.

$$\frac{\partial U_i}{\partial x_i} = 0 \qquad (3.1)$$

$$\frac{\partial U_i}{\partial t}+U_j\frac{\partial U_i}{\partial x_j}=-\frac{1}{\rho}\frac{\partial P}{\partial x_i}+\frac{\partial}{\partial x_j}\left[(\nu+\nu_t)\left(\frac{\partial U_i}{\partial x_j}+\frac{\partial U_j}{\partial x_x}\right)\right]-\beta\left(T-T_{ref}\right)g_i \qquad (3.2)$$

The Bousssinesq model (Spiegel and Veronis, 1960) is employed for the calculation of the buoyancy force. This model treats density as a constant value in all solved equations, except for the buoyancy term in the momentum equation.

The eddy viscosity, ν_t, is given by

$$\nu_t = c_\mu\frac{k^2}{\varepsilon} \qquad (3.3)$$

The turbulent kinetic energy, k, and its rate of dissipation, ε, are obtained from the following transport equations:

$$\frac{\partial k}{\partial t}+u_i\frac{\partial k}{\partial x_i}=\frac{\partial}{\partial x_i}\left[(\nu+\frac{\nu_t}{\sigma_k})\frac{\partial k}{\partial x_i}\right]+G_k+G_b-\varepsilon \qquad (3.4)$$

$$\frac{\partial \varepsilon}{\partial t}+u_i\frac{\partial \varepsilon}{\partial x_i}=\frac{\partial}{\partial x_i}\left[(\nu+\frac{\nu_t}{\sigma_\varepsilon})\frac{\partial \varepsilon}{\partial x_i}\right]+c_1\frac{\varepsilon}{k}G_k-c_2\frac{\varepsilon^2}{k} \qquad (3.5)$$

and G_k is the production rate of turbulent kinetic energy and G_b is the generation rate of k due to buoyancy,

$$G_k = \nu_t\left(\frac{\partial u_i}{\partial x_j}+\frac{\partial u_j}{\partial x_i}\right)\frac{\partial u_j}{\partial x_i} \qquad (3.6)$$

$$G_b = \beta g_i\frac{\nu_t}{\mathrm{Pr}_T}\frac{\partial T}{\partial x_i} \qquad (3.7)$$

where Pr_T is the turbulent Prandtl number for energy and is equal to 0.85. It should be noted here that the buoyancy effects on ε is neglected by default in FLUENT. The constants used in the standard k-ε model are:

$$c_1 = 1.44,\ c_2 = 1.92,\ c_\mu = 0.09,\ \sigma_k = 1.0,\ \text{and}\ \sigma_\varepsilon = 1.3$$

For the temperature distribution calculations, the energy equation can be written as:

$$\frac{\partial T}{\partial t}+u_j\frac{\partial T}{\partial x_j}=\frac{\partial}{\partial x_j}\left[(\frac{\nu}{\mathrm{Pr}_L}+\frac{\nu_t}{\mathrm{Pr}_T})\frac{\partial T}{\partial x_j}\right]+S_T \qquad (3.8)$$

where Pr_L is the laminar Prandtl number which is defined by $\mathrm{Pr}_L = C_p\mu/\kappa$ and S_T is the source term.

RNG model and low-Re RNG model

The RNG based turbulence model is derived from the instantaneous Navier-Stokes equations, using the Renormalization Group method (RNG) (Yakhot and Orszag, 1986). The mean flow is governed by the incompressible Reynolds averaged continuity and Navier-Stokes equations with an eddy viscosity assumption.

$$\frac{\partial U_i}{\partial x_i} = 0 \qquad \text{.....(3.9)}$$

$$\frac{\partial U_i}{\partial t} + U_j \frac{\partial U_i}{\partial x_j} = -\frac{1}{\rho}\frac{\partial P}{\partial x_i} + \frac{\partial}{\partial x_j}\left[(\nu + \nu_t)\left(\frac{\partial U_i}{\partial x_j} + \frac{\partial U_j}{\partial x_x}\right)\right] - \beta\left(T - T_{ref}\right)g_i \qquad (3.10)$$

The turbulent viscosity ν_t is solved by a differential equation (3.11).

$$d\left(\frac{\rho^2 k}{\sqrt{\varepsilon k}}\right) = 1.72\frac{\hat{\nu}}{\sqrt{\hat{\nu}^3 - 1 + C_\nu}}d\hat{\nu} \qquad (3.11)$$

where $\hat{\nu} = \nu_{eff}/\nu$, $C_\nu \approx 100$, and $\nu_{eff} = \nu_t + \nu$.

In the high Re limit, ν_t tends to

$$\nu_t = C_\mu \frac{k^2}{\varepsilon} \qquad (3.12)$$

where $k = \frac{1}{2}\overline{u_i' u_i'}$ and $\varepsilon = \nu\overline{\frac{\partial u_i'}{\partial x_j}\frac{\partial u_i'}{\partial x_j}}$

In this paper, the low_Re RNG turbulence model represents the model using differential equation (3.11) and the RNG turbulence model is represented by equation (3.12). The scale elimination procedure in RNG theory results in a differential equation for turbulent viscosity (Yakhot and Orszag, 1986).

$$\frac{\partial k}{\partial t} + U_j \frac{\partial k}{\partial x_j} = \tau_{ij}\frac{\partial U_i}{\partial x_j} - \varepsilon + \frac{\partial}{\partial x_j}\left[\left(\nu + \frac{\nu_t}{\sigma_k}\right)\frac{\partial k}{\partial x_j}\right] \qquad (3.13)$$

$$\frac{\partial \varepsilon}{\partial t} + U_j \frac{\partial \varepsilon}{\partial x_j} = C_{\varepsilon 1}\frac{\varepsilon}{k}\tau_{ij}\frac{\partial U_i}{\partial x_j} - C_{\varepsilon 2}\frac{\varepsilon^2}{k} + \frac{\partial}{\partial x_j}\left[\left(\nu + \frac{\nu_t}{\sigma_\varepsilon}\right)\frac{\partial \varepsilon}{\partial x_j}\right] \qquad (3.14)$$

The coefficients are $\sigma_k = \sigma_\varepsilon = 0.7179$, $C_\mu = 0.085$, $C_{\varepsilon 1} = 1.42$, and, $C_{\varepsilon 2} = 1.68 + \frac{\eta^3(1-\eta/\eta_\infty)}{1+\beta\eta^3}$, where $\eta = Sk/\varepsilon$, $\eta_\infty = 4.38$, $\beta = 0.015$, $S = \left(2\overline{S_{ij}}\,\overline{S_{ij}}\right)^{1/2}$, and $\overline{S_{ij}}$ is the mean rate of strain tensor. The RNG model has the same form as the standard k-ε turbulence model, except $C_\mu = 0.09$ is used by the latter. The model parameters in the ε equation are also different from those for the standard k-ε model. Besides the difference in the model parameters, another major difference between RNG and standard k-ε is that there is an additional term in the ε equation for the RNG turbulence model, which accounts for the effect of the rapid strain. The RNG model is known to be more responsive to the effects of rapid strain and streamline curvature than the standard k-ε model, which explains the better performance of the RNG model for certain classes of flows.

RSM model

The Reynolds stress model involves calculation of the individual Reynolds stresses, $\overline{u_i' u_j'}$, using differential transport equations. The individual Reynolds stresses are then used to obtain closure of the Reynolds-averaged momentum equation. The exact transport equations for the transport of the Reynolds stresses, $\overline{u_i' u_j'}$, may be written as follows:

$$\underbrace{\frac{\partial(\rho\overline{u_j'u_i'})}{\partial t}}_{\text{Local time derivative}} + \underbrace{\frac{\partial(\rho U_k \overline{u_i'u_j'})}{\partial x_k}}_{C_{ij}\equiv\text{Convection}} = \underbrace{-\rho(\overline{u_j'u_k'}\frac{\partial U_i}{\partial x_k} + \overline{u_i'u_k'}\frac{\partial U_j}{\partial x_k})}_{P_{ij}\equiv\text{ production}} - \underbrace{\frac{\partial(\rho\overline{u_i'u_j'u_k'})}{\partial x_k}}_{T_{ij}\equiv\text{Turbulent diffusion}}$$

$$\underbrace{-\left[\overline{u_i'\frac{\partial p'}{\partial x_j}} + \overline{u_j'\frac{\partial p'}{\partial x_i}}\right]}_{R_{ij}\equiv\text{Redistribution}} \underbrace{-2\mu\overline{\frac{\partial u_i'}{\partial x_k}\frac{\partial u_j'}{\partial x_k}}}_{\varepsilon_{ij}\equiv\text{Dissipation}} + \underbrace{\frac{\partial}{\partial x_k}\mu\left(\frac{\partial\overline{u_i'u_j'}}{\partial x_k}\right)}_{L_{ij}\equiv\text{Molecule diffusion}} \underbrace{-\rho\beta\left(g_i\overline{u_j'\theta} + g_j\overline{u_i'\theta}\right)}_{G_{ij}\equiv\text{Buoyancy production}} \quad (3.15)$$

Of the various terms in these exact equations, C_{ij}, P_{ij}, and L_{ij} do not require any modeling. However, T_{ij}, R_{ij}, ε_{ij}, and G_{ij} need to be modeled to close the equations.

The turbulent diffusion is modeled by using a scalar turbulent diffusivity as follows,

$$T_{ij} = \frac{\partial}{\partial x_k}\left(\frac{\mu_t}{\sigma_k}\frac{\partial\overline{u_i'u_j'}}{\partial x_k}\right) \quad (3.16)$$

Lien and Leschziner (1994) derived a value of σ_k=0.82 by applying the diffusion model to the case of a planar homogeneous shear flow. Note that this value of σ_k is different from that in the standard k-ε models, in which σ_k=1.0 is commonly used.

The pressure-strain term is modeled according to the proposals by Gibson and Launder (1978). The reader is referred to their paper for detailed information on the modeling of the pressure-strain term. The production terms due to buoyancy are modeled as

$$G_{ij} = \beta \frac{\mu_t}{\mathrm{Pr}_t}\left(g_i \frac{\partial T}{\partial x_j} + g_j \frac{\partial T}{\partial x_i} \right) \tag{3.17}$$

where Pr_t is the turbulent Prandtl number for energy, with a default value of 0.85.

In general, when the turbulence kinetic energy is needed for modeling a specific term, it is obtained by taking the trace of the Reynolds stress tensor:

$$k = \frac{1}{2}\overline{u_i' u_i'} \tag{3.18}$$

The dissipation tensor, ε_{ij} is modeled as

$$\varepsilon_{ij} = \frac{2}{3}\delta_{ij}\rho\varepsilon \tag{3.19}$$

The scalar dissipation rate, ε, is computed from a model transport equation similar to that used in the standard k-ε model:

$$\frac{\partial}{\partial t}(\rho\varepsilon) + \frac{\partial}{\partial x_i}(\rho\varepsilon u_i) = \frac{\partial}{\partial x_i}\left[(\mu + \mu_t)\frac{\partial \varepsilon}{\partial x_j} \right] + C_{\varepsilon 1}\frac{1}{2}\left[P_{ii} + C_{\varepsilon 3} G_{ii} \right]\frac{\varepsilon}{k} - C_{\varepsilon 2}\rho\frac{\varepsilon^2}{k} \tag{3.20}$$

where $\sigma_k = 1.0$, $C_{\varepsilon 1}$=1.44, $C_{\varepsilon 2}$=1.92, $C_{\varepsilon 3}$ is evaluated as a function of the local direction relative to the gravitational vector,

$$C_{\varepsilon 3} = \tanh\left|\frac{v}{u}\right| \tag{3.21}$$

where v is the component of the flow velocity parallel to the gravitational vector and u is the component of the flow velocity perpendicular to the gravitational vector. In this way, $C_{\varepsilon 3}$ will become zero. The turbulent viscosity, μ_t, is computed in a similar manner to the k-ε models (Eq. 3.3).

Whenever flow enters the domain, the individual Reynolds stresses, $\overline{u_i' u_j'}$ and the turbulence dissipation rate, ε, are required as inlet conditions. These quantities can be derived from the turbulence intensity and characteristic length for the current case, as follows:

$$\overline{u_i'^2} = \frac{2}{3}k \qquad (i = 1,2,3) \tag{3.22}$$

$$\overline{u_i' u_j'} = 0 \qquad (i \neq j) \tag{3.23}$$

$$\varepsilon = C_\mu^{3/4} \frac{k^{3/2}}{l} \tag{3.24}$$

where l is the turbulence length scale and is determined from the relationship with the hydraulic diameter D_H:

$$l = 0.07 D_H \tag{3.25}$$

LES simulation

Turbulent flows are characterized by eddies with a wide range of length and time scales. The largest eddies are typically comparable in size to the characteristic length of the mean flow. The smallest scales are responsible for the dissipation of turbulence kinetic energy.

In LES, large eddies are resolved directly, while small eddies are modeled. Large eddy simulation (LES) thus falls between DNS and RANS in terms of the fraction of the resolved scales. The rationale behind LES can be summarized as follows:

- Momentum, mass, energy, and other passive scalars are transported mostly by large eddies.
- Large eddies are more problem-dependent. They are dictated by the geometries and boundary conditions of the flow involved.
- Small eddies are less dependent on the geometry, tend to be more isotropic, and are consequently more universal.
- The chance of finding a universal turbulence model is much higher for small eddies.

The governing equations employed for LES are obtained by filtering the time-dependent Navier-Stokes equations in either Fourier (wave-number) space or configuration (physical) space. The filtering process effectively filters out the eddies whose scales are smaller than the filter width or grid spacing used in the computations. The resulting equations thus govern the dynamics of large eddies.

A filtered variable (denoted by an overbar) is defined by

$$\bar{\phi}(x) = \int_D \phi(x')G(x,x')dx' \tag{3.26}$$

where D is the fluid domain, and G is the filter function that determines the scale of the resolved eddies.

In FLUENT, the finite-volume discretization itself implicitly provides the filtering operation:

$$\bar{\phi}(x) = \frac{1}{V}\int_D \phi(x')dx', \quad x' \in V \tag{3.27}$$

where V is the volume of a computational cell. The filter function, G, implied here is then

$$G(x,x') = \begin{cases} 1/V & x' \in V \\ 0 & x' otherwise \end{cases} \tag{3.28}$$

Filtering the Navier-Stokes equations, one obtains

$$\frac{\partial \rho}{\partial t} + \frac{\partial}{\partial x_i}\left(\rho \overline{u_i}\right) = 0 \tag{3.29}$$

$$\frac{\partial}{\partial t}\left(\rho \overline{u_i}\right) + \frac{\partial}{\partial x_j}\left(\rho \overline{u_i u_j}\right) = \frac{\partial}{\partial x_j}\left[\mu\left(\frac{\partial \overline{u_i}}{\partial x_j} + \frac{\partial \overline{u_j}}{\partial x_i}\right)\right] - \frac{\partial \overline{p}}{\partial x_i} - \frac{\partial \tau_{ij}}{\partial x_j} \tag{3.30}$$

and τ_{ij} is the subgrid-scale stress defined by

$$\tau_{ij} = \rho\overline{u_i u_j} - \rho(\overline{u_i})(\overline{u_j}) \tag{3.31}$$

SUBGRID SCALE MODEL

The subgrid-scale stresses resulting from the filtering operation are unknown, and thus require modeling. The subgrid-scale turbulence model used in this study employs the Boussinesq hypothesis as in the RANS models, computing subgrid-scale turbulent stresses from

$$\tau_{ij} - \frac{1}{3}\tau_{kk}\delta_{ij} = -2\mu_t \overline{S_{ij}} \tag{3.32}$$

where μ_t is the subgrid-scale turbulent viscosity, and $\overline{S_{ij}}$ is the rate-of-strain tensor for the resolved scale defined by

$$\overline{S_{ij}} = \frac{1}{2}\left(\frac{\partial \overline{u_i}}{\partial x_j} + \frac{\partial \overline{u_j}}{\partial x_i}\right) \tag{3.33}$$

The subgrid model used in this study is Smagorinsky-Lilly model which was first proposed by Smagorinsky (1963). In this model, the eddy viscosity is modeled by

$$\mu_t = \rho L_s^2 \left|\overline{S}\right| \tag{3.34}$$

where Ls is the mixing length for subgrid scales and

$$\left|\overline{S}\right| \equiv \sqrt{2\overline{S_{ij}}\,\overline{S_{ij}}} \tag{3.35}$$

Ls is computed using

$$L_s \equiv \min\left(\kappa d, C_s V^{1/3}\right) \tag{3.36}$$

where κ is the von Karman constant, d is the distance to the closest wall, Cs is the Smagorinsky constant, and V is the volume of the computational cell. Lilly (1966) derived a value of 0.17 for Cs for homogeneous isotropic turbulence in the inertial subrange. However, this value was found to cause excessive damping of large-scale fluctuations in the presence of mean shear and in transitional flow as when near a solid boundary, and has to be reduced in such regions. In short, Cs is not a universal constant, which is the most serious shortcoming of this simple model. Nonetheless, a Cs value of around 0.1 has been found to yield the best results for a wide range flows, and is the default value in FLUENT.

These three dimensional equations are solved using a segregated grid approach with pressure projection. The well known QUICK scheme (Leonard, 1979) is used for all the convective terms, and a central differencing scheme is used for the diffusion terms. Two types of boundary conditions are applied to the system under study, namely the wall boundary conditions and the entry-exit conditions. All of the solid walls in this investigation are at rest. Therefore, both the mean and fluctuating velocities of the fluid at these boundaries are identically zero for the turbulent flow, as there is no slip and no mass-transport at the walls. In addition, wall functions are used to model the near wall region with an empirical logarithmic velocity profile in terms of the distance from the wall. The inlet boundary condition is set as a specified velocity inlet, whereas the exit (outlet) boundary condition is set as a specified pressure outlet.

Eulerian scalar transport

If a species (acetone vapor in the present study) is added to the system, the mean concentration can be calculated by making use of the following transport equation:

$$\frac{\partial C}{\partial t} + \frac{\partial}{\partial x_i}\left[u_i C - \left(\frac{\nu}{Sc_L} + \frac{\nu_t}{Sc_T}\right)\frac{\partial C}{\partial x_i}\right] = S_\phi \qquad (3.37)$$

Here, Sc_L is the laminar Schmidt number and Sc_T is the turbulent Schmidt number. The mass flow rate of the scalar is $\dot{m}$=1.0e-4 kg/s. The volume $\forall$ of the source region is ~0.005 m^3. The source term S_ϕ is set to $\dot{m}/\forall$ kg/(m^3·s). The source region is 1.2m above the ground and 0.5m downstream of the human body. The values of Sc_L = 1.42 (Mills, 1999) and Sc_T = 1.30 are selected for the purpose of this study.

Lagrangian trajectory tracking

Although gaseous vapor is used in this study, the Lagrangian model is investigated because it can be easily adapted in the simulation of aerosols. For the Lagrangian simulation of gaseous contaminants, each of the parcels represents a certain amount of acetone vapor and closely follows the air flow. These fictitious particles are released from the plane shown in Figure 3.1. In order to conform to the Eulerian scalar transport method, the flow rate, and the diameter of the representative particles are set equal to 0.1 g/s, and 1 μm, respectively.

Modeling gases with 1 μm aerosols presents negligible errors because they follow airflows so faithfully, as is demonstrated elsewhere mathematically (Hjelmfelt and Mockros, 1966). Indeed, one of the most important laboratory measurement devices for velocity and turbulence, Particle Image Velocimetry, uses much larger aerosols (up to 50 μm, Saga et al., 2000) to track the fluid motions.

Also, it has to be mentioned that the concentration levels for the Eulerian method are calculated at the cell center for that particular cell, and the concentration levels using the Lagrangian method are calculated by dividing the cumulative trajectory mass by the volume of that particular cell they are residing in. In both methods one would get a single value for that particular cell.

The results are presented and discussed in two parts. First, the grid convergence and iterative convergence are investigated, which is followed by the predictions of the impact of critical factors which includes the body shape, the transport model, the turbulence model, the ventilation intensity, the free stream turbulence and the heat released from the body. The second part will be the main focus of this study.

Grid convergence and iterative convergence

The five different numerical grid distributions listed in Table 3.1 were used to assess the grid dependency of the RANS results for the sharp body simulations. The streamwise

velocity component (velocity component in x direction as shown in Figure 3.1), turbulent kinetic energy (k), and concentration distributions (with Eulerian method) along four different vertical lines on the center-plane for all grid distributions are shown in Figure 3.5, where d represents the downstream distance of the vertical line measured from the body. It can be seen that mesh #1 and mesh #2 are so coarse that the turbulent kinetic energy profiles predicted with them in the downstream of the leg are much higher than the ones with other meshes. With mesh #3, #4 and #5, the results are very close in the downstream of the upper body, which is believed to be the most important region for the worker exposure. It has been mentioned earlier that mesh #3 is refined just in the region around the body based on mesh #2 and it has less cells than mesh #4. However, the turbulent kinetic energy with mesh #3 is even closer to the result with mesh #5 (the finest grid) at some regions. Since running a case with mesh #3 takes less time than with mesh #4, it has been used to study the effect of body shapes and transport methods.

The values of turbulent kinetic energy and concentration for the sharp body with mesh #2, #4 and #5 are listed in Table 3.2, where h is the averaged grid size calculated as

$$h = \sqrt[3]{\frac{volume}{number\ of\ cells}} \tag{3.38}$$

and h5 is the finest average grid size. Convective transport due to recirculation regions formed in the wake of the body and the diffusive nature of the gaseous contaminants causes a nonzero concentration field upstream of the source. Using Richardson extrapolation on the concentration data which shows monotonic convergence, the observed order of the numerical schemes can be calculated which is consistent with the initial arrangement (QUICK for convection terms and central differencing for diffusion terms). The extrapolated "exact" concentration was 0.00489 kg/m^3. The grid convergence index of concentration at the breathing zone for mesh #2 is approximately 11% (Extrapolated Relative Error is about 9%). For the turbulent kinetic energy data at the breathing zone, non-monotonic convergence was shown since k(#5) < k(#2) < k(#4) while h5 < h4 < h2. The relative error of k for mesh #2 was 8% based on mesh #5.

The concentrations at the breathing zone (mouth) using the Eulerian method are compared in Figure 3.6, where h1 is the coarsest average grid size. Figure 3.6 shows that the lowest exposure is predicted for the simulations with the rounded body. The concentrations do not asymptotically approach to some value as expected. Instead, the cells composing the source region change with the mesh itself, which affect the grid convergence in terms of concentration as a function of the source position and source size (Kulmala et al., 1996). Additional setup effort was needed to keep the source region exactly the same for each mesh. On the other hand, for the purpose of this study, it is shown clearly that the body shape has significant influence on the predicted worker exposure.

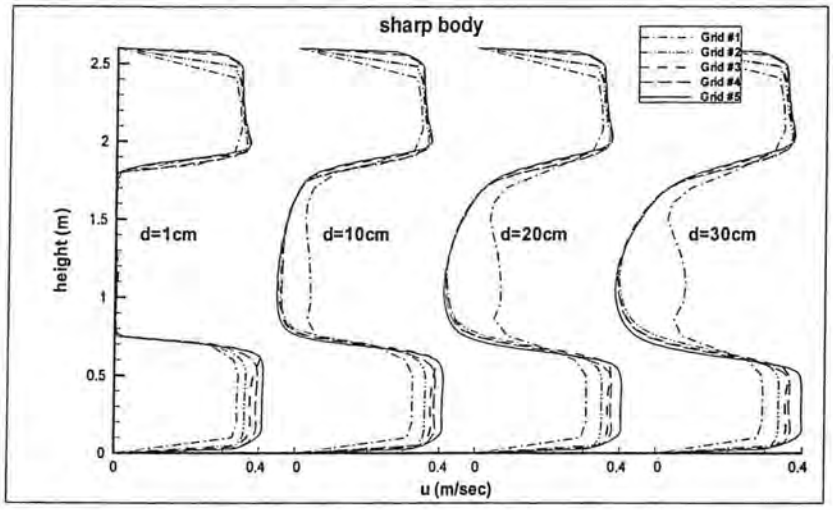
sharp body
Grid #1
Grid #2
Grid #3
Grid #4
Grid #5
height (m)
d=1cm
d=10cm
d=20cm
d=30cm
u (m/sec)

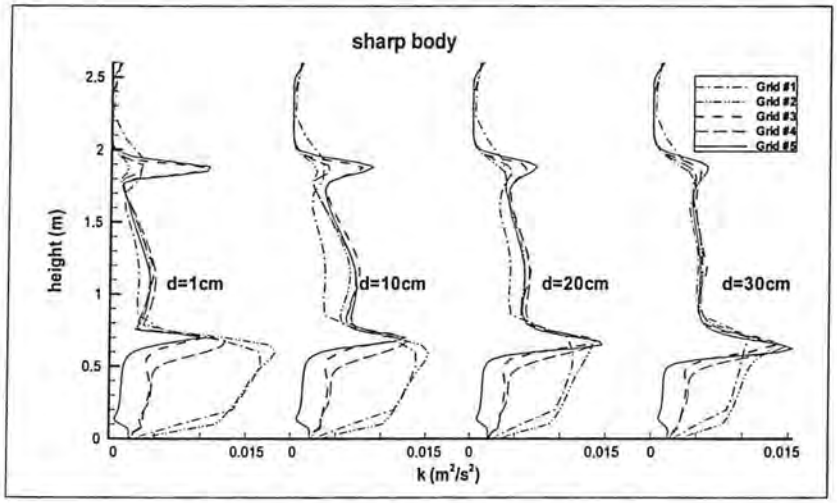
sharp body
Grid #1
Grid #2
Grid #3
Grid #4
Grid #5
height (m)
d=1cm
d=10cm
d=20cm
d=30cm
k (m²/s²)

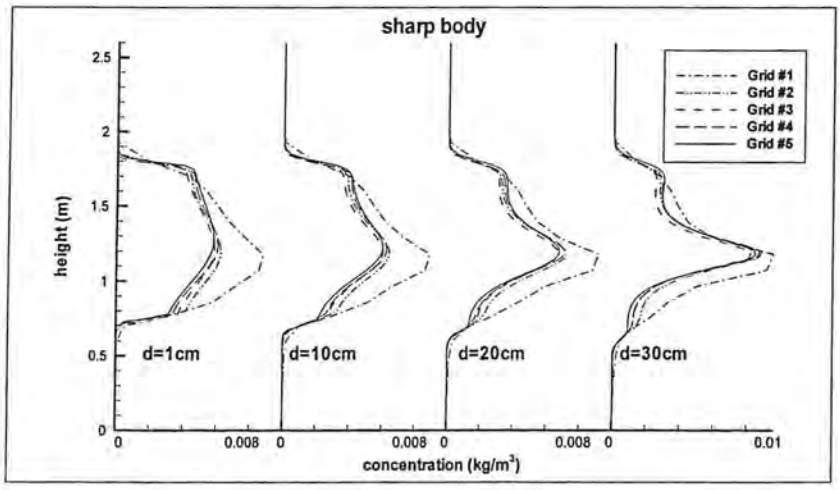
sharp body
Grid #1
Grid #2
Grid #3
Grid #4
Grid #5
height (m)
d=1cm
d=10cm
d=20cm
d=30cm
concentration (kg/m³)

Figure 0-5 Streamwise velocities, turbulent kinetic energy, and concentrations at several vertical lines downstream of the body on the central plane with different grid distributions for the sharp body

Table 0.2 Turbulent kinetic energy and concentration at the breathing zone for the sharp body

	Grid #5	Grid #4	Grid #2
h/h5	1.0	1.465	2.08
$k(m^2/s^2)$	0.001799	0.001939	0.001814
Concentration(kg/m^3)	0.00482	0.00472	0.00448

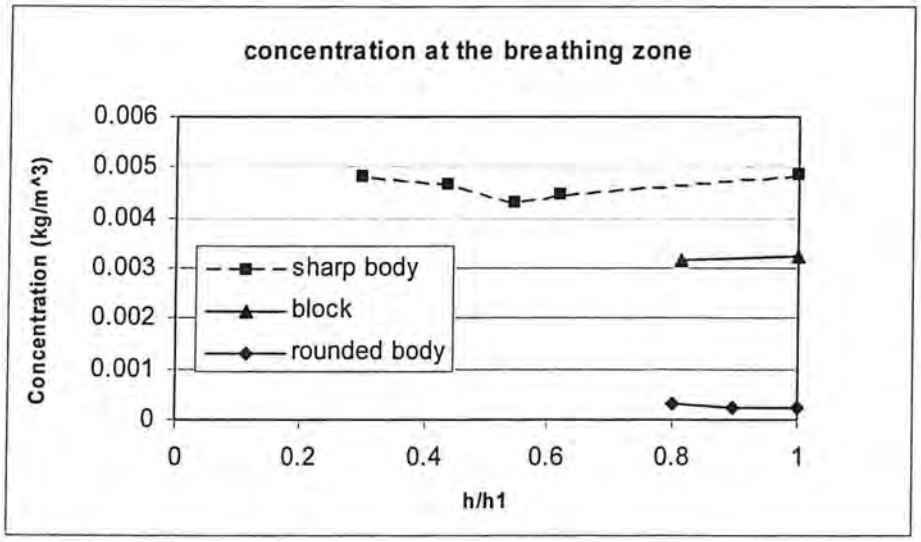

Figure 0-6 Concentrations at the breathing zone with different grid distributions and different body shapes

There was no distinguishable difference between the results at a residual criterion of 0.001 and of 0.0001, so a residual of 0.0001 used in this study should achieve a good convergence in terms of iteration convergence. The streamwise velocity component at the mouth also was monitored in the calculation to check if it approached an asymptotic value when the assigned residual was reached, in order to avoid false convergence by using a fixed value of residual.

Influence of critical factors on worker exposure

Effect of the body shape

Comparison of the flow-field predictions with the block, the sharp, and the rounded body indicated that the predicted flow-field with the block has one large recirculation region,

whereas the sharp and rounded bodies each induced two smaller recirculation regions (Figure 6). The recirculation zone around the head suggests that contaminants trapped in that region are more likely to be inhaled. Moreover, the contaminants accumulated in the waist region could be transferred to the breathing zone from the lower recirculation zone. However, the flow around the sharp and rounded bodies shows different separation profiles, which is an important issue. For the sharp body, the flow separates at the corner of the head, whereas with the rounded body, the air flows along the forehead and separates from the body near the eye level. This means that such small issues as the hairstyle, the size and shape of the hat worn, and the angle of the forehead could affect the exposure levels. Another important issue is the clothes. If the worker wears an apron, the shape will be more like a sharp body since the apron blocks the flow between legs. This indicates that the clothes the worker wear may significantly change the flow field and the subsequent exposure levels.

Using the Eulerian method for each body shape, the predicted non-dimensionalized concentration levels of the contaminant gas at various locations were compared for trend analysis (see Figure 3.8). It is clear that the block body cannot be used to represent a worker accurately. With the sharp and rounded body, the concentration level at the chest region is higher than that at the breathing zone (C_{chest}/C_{nose} is 13.6 for the rounded body). This observation qualitatively agrees with experimental results (Guffey et al., 2001) which concluded the concentrations at the chest averaged about 2.9 times the concentrations at the nose and the ratio decreased significantly with increasing velocities (C_{chest}/C_{nose}=2.4 at V_{inlet} =0.24 m/s). It should be noted that these experimental conditions were different from the current study in some aspects. For instance, SF_6 was used in the experiments and the geometric average of the concentrations at three points (left chest, middle chest and right chest) was taken to represent the concentration in the chest area. In addition, the manikin shape and the source size in the experiments are also different. These differences may contribute to the different ratios of C_{chest} to C_{nose} found in the calculations and the experiments. However, the same trend observed by both the calculations and the experiments suggests that it may not be a good practice to measure the concentrations around the chest area as surrogates for the inhaled concentrations, as is current practice. With the block figure the concentration ratio of chest to nose is reversed, which illustrates that the trend could be inaccurately predicted with crude representatives of the human body.

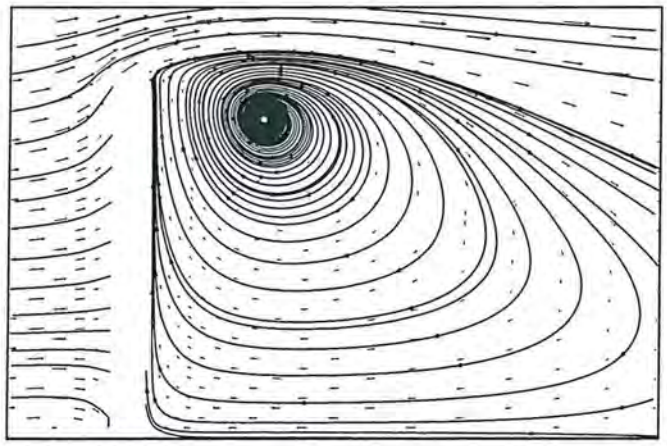

a) block

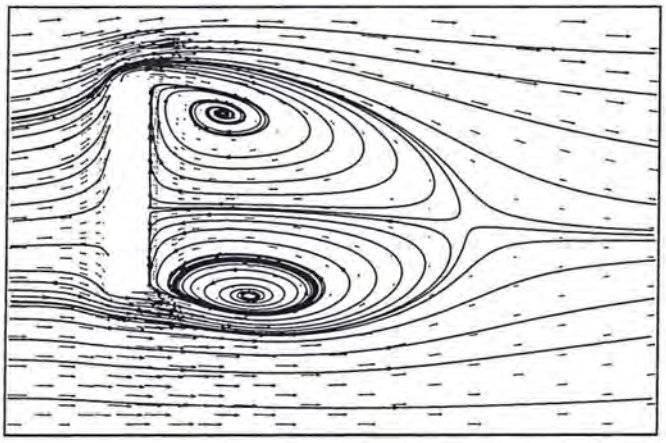

b) sharp body

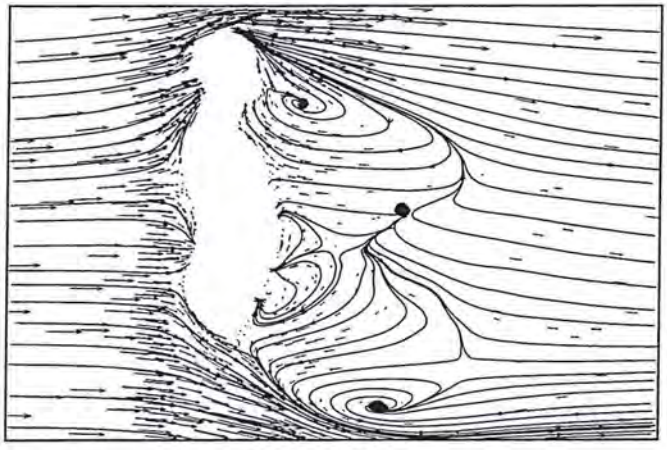

(c) rounded body

Figure 0-7 Comparison of the flow field with a block, a sharp body and a rounded body – velocity vectors and streamlines on the center plane (side elevation)

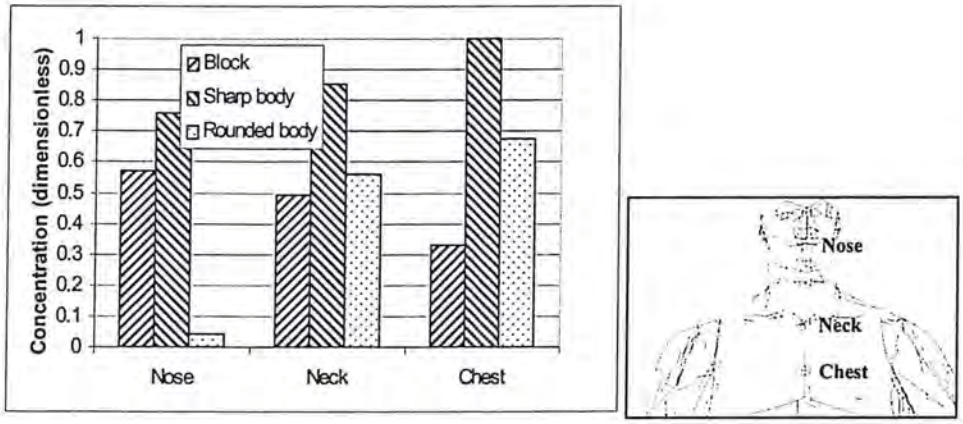

Figure 0-8 Comparison of normalized concentration at different points 1.0 cm downstream of human body for different body shapes (Normalized with the highest concentration value)

Figure 3.9 presents the predicted concentration distributions 1cm downstream of the body obtained from the simulations using the Eulerian scalar transport method. It is seen that the contaminants are accumulated at the top of the block, whereas the contaminants for the sharp and rounded body are diffused over a much wider region of the body accumulating mostly in the chest region. This again shows that using less accurate shapes for the human body may lead to inaccurate results.

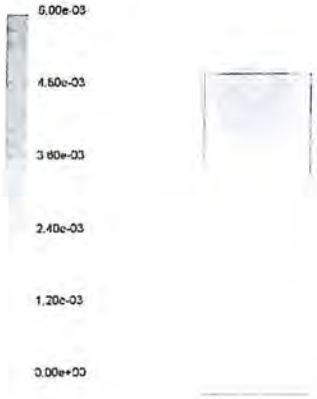

(a) block

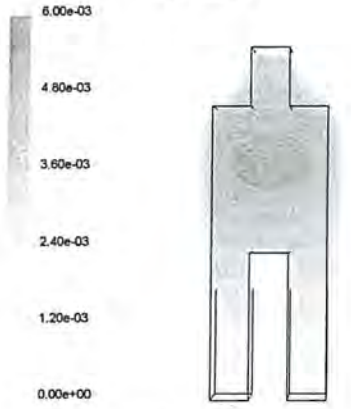

(b) sharp body

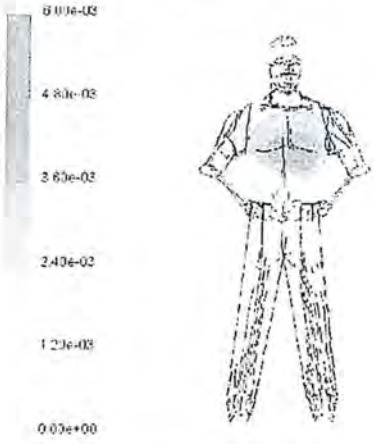

(c) rounded body

Figure 0-9 Concentration distribution; Eulerian method, on a cross-section 1.0 cm downstream of the body

Effect of the contaminants transport model

Using the Lagrangian method, the concentration at a plane 1.0 cm downstream of the body is shown in Figure 3.10d. Compared to the results of the Eulerian method in Figure 3.9b, it can be argued that both methods predict the concentration levels on the same order, although the Lagrangian method shows much more randomness, which is directly associated with the method itself since a random velocity component is added to the mean fluid velocity to simulate trajectory dispersion due to turbulence. It has been seen during the simulations that the number of trajectories tracked in the Lagrangian

simulations is also an important factor affecting the predicted concentration levels. The more trajectories tracked, the smoother the concentration contours become (see Figures 3.11c and 3.11e), since a better averaging over a volume can be applied to calculate the concentration levels.

The symmetry-plane concentration contours are shown in Figures 3.11a, 3.11b and 3.11c for both the Eulerian method and the Lagrangian method. The latter was repeated for different numbers of representative particle trajectories. Here again, the Eulerian method exhibits a more diffusive concentration field than the Lagrangian method. The latter shows a higher degree of irregularity because of the applied discrete random walk tracking model used in the FLUENT code. Nevertheless, the predictions of the two methods are in fairly good agreement with each other (see also Figure 3.11).

The local concentrations at different locations 1.0 cm downstream of the sharp body are compared for both the Eulerian and Lagrangian predictions in Figure 3.11. The values are normalized by dividing by the highest concentration value (C_{max} = 0.00484 kg/m^3) that was predicted for both simulations. This was done since the trend of the concentrations is the main concern of this study, not the absolute values of the concentrations. The Eulerian method predicts a more uniform concentration when compared to the predictions obtained via the Lagrangian method. Although it is true that tracking more trajectories creates a more uniform concentration field for the Lagrangian method, it has to be noted that it is very computationally expensive to use a large number of trajectories. It is noteworthy to mention that both methods tend to predict higher concentrations near the lapel compared to the mouth/nose level.

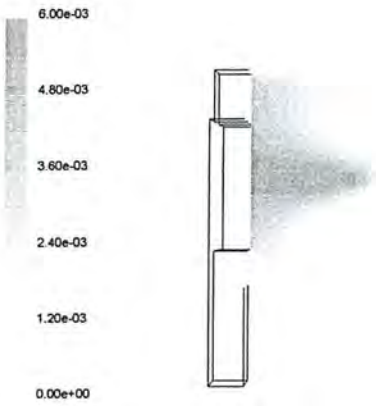

(a) Eulerian model (side view)

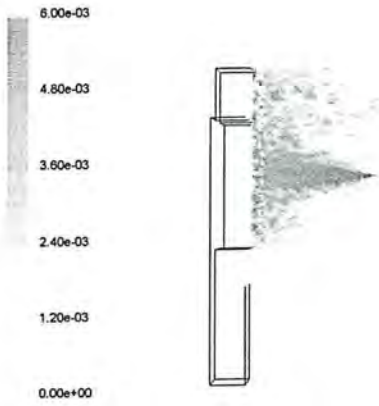

(b) Lagrangian model (3,480 trajectories) (side view)

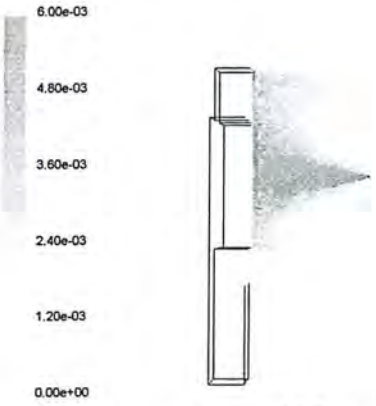

(c) Lagrangian model (35,100 trajectories) (side view)

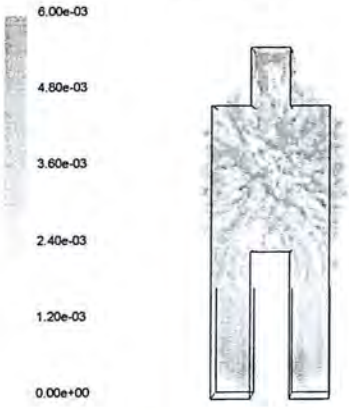

(d) Lagrangian model (3,480 trajectories)

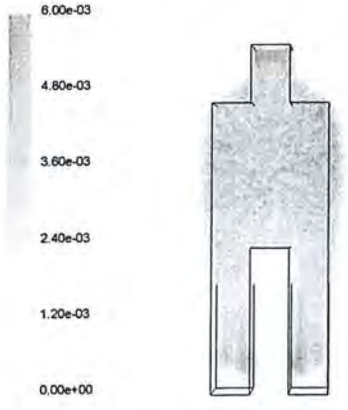

(e) Lagrangian model (35,100 trajectories)

Figure 0-10 Concentration contours a,b,c) on the center plane d,e) on a cross section 1.0 cm downstream of the body

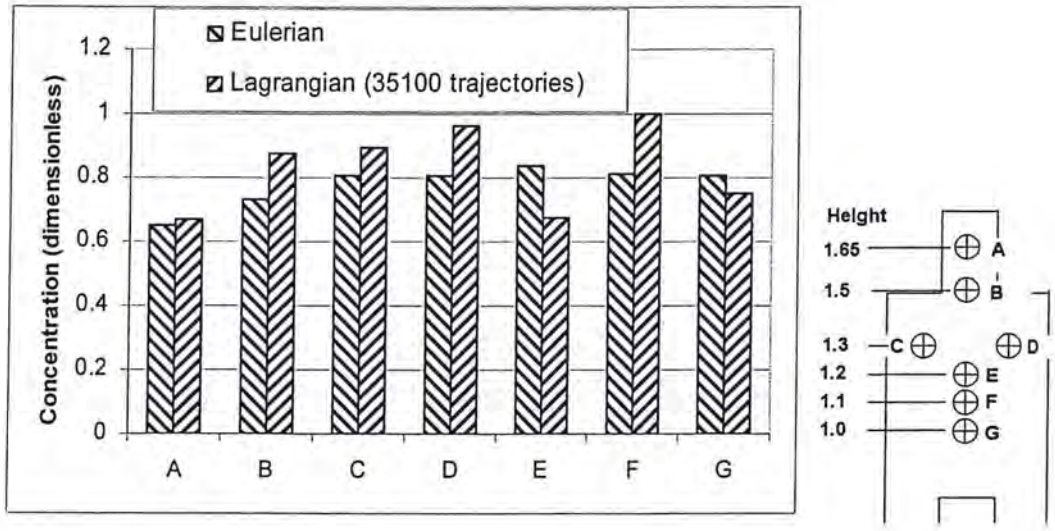

Figure 0-11 Normalized concentrations at different locations at a cross section 1 cm downstream of the sharp body

Variation of turbulence models

Turbulence levels and turbulence length scales associated with the turbulent eddies are probably one of the most important factors that can influence the dispersion of aerosol particulate. Hence, it is essential that turbulence models used are capable of accurately predicting the major characteristics of the turbulent flows in the working environment. Simulations were performed with four different models, namely, standard k-ε turbulence model, RNG k-ε turbulence model, Reynolds Stress turbulence model, and Large Eddy Simulation (LES). The results from each are compared to the predicted concentration levels at critical locations in the vicinity of the face of the simulated manikin.

The governing equations solved are the well-known Reynolds Averaged Navier-Stokes equations (RANS) and the equation of continuity. In the RANS approach the turbulent stresses resulting from the time averaging of non-linear terms need to be calculated with an appropriate turbulence model, hence the use of the turbulence models mentioned above.

The governing equations employed for LES are obtained by filtering the time-dependent Navier-Stokes equations in physical space. The filtering process effectively filters out eddies whose scales are smaller than roughly the computational cell size. The resulting equations governing the dynamics of large eddies are very similar to the RANS equations, but in this case, the turbulent stresses are replaced by subgrid stresses. The Smagorinsky-Lilly subgrid-scale model (Lilly, 1966) is employed to solve the subgrid stresses in the present application. For values of the model constants and detailed information about these models, the reader is referred to the Fluent manual.

Constant velocity inlet and pressure outlet boundary conditions were used. The inlet velocity was taken as 0.3 m/s with a turbulence intensity of 0.3%. These values were rough estimates to the experimental conditions and they are also representative of a usual working environment (Baldwin and Maynard, 1998). The characteristic length scale was chosen to be 0.01 m, which represented the turbulence generating grid size at the inlet of the tunnel. All of the solid walls in this investigation were at rest; therefore, both the mean and fluctuating velocities of the fluid at these boundaries were identically zero for the turbulent flow, as there was no slip and no mass-transport at the walls. Standard wall-function boundary condition was applied at the grid nodes nearest to the walls. Tracer gas was released from an inert surface, which was approximated by a 0.3m x 0.3m square and located 1.0m high from the floor and 0.25m downstream from the body. For the present study, the unheated body is considered.

In the present application the source term S is set to $0.0216\times\rho$. The volume of this region is 0.00463 m^3, such that the mass flow rate of the scalar is 0.0001 kg/s. The values of Sc_L = 0.32 and Sc_T = 0.70 in Eq. 3.38 (Lan and Viswanathan, 2001) are selected for the purpose of this study.

RESULTS

The streamlines colored by y-velocity magnitude on the center-plane are shown in Figure 3-12(a) for the case with standard k-ε turbulence model. As the plane slices the human-body in the center, the flow between the legs also can be seen in this figure. It created a re-circulation region around the waist. The contaminants are usually trapped within such recirculation zones if turbulent diffusion is not dominant. It should be noted that if the worker wears an apron, the exposure he/she would receive could be quite different from the one observed in this study.

It can be seen from Figure 3.12 that the convective flow will bring the contaminant upward from the waist region. This flow is partly due to buoyancy as it is seen in Figure 3.13. This suggests that the heat flux from the human body could contribute to the worker exposure. Figure 3.12 shows that air flows along the forehead and separates from the body near the eye level. This means that such small issues as the hairstyle, the size and shape of the hat worn, and the angle of the forehead could affect the exposure levels.

Figure 3.12 further shows that the overall quantitative features of the flow patterns seen in the vicinity of the body are very similar for the RANS simulations regardless of the turbulence model used. There are big differences in the predicted turbulent kinetic energy profiles (see Fig. 3.14) when different turbulence models are used. The LES results (Fig. 3.12d), which were averaged over a three minute interval, do depict significantly different flow patterns compared to RANS results. This leads to species concentration prediction as observed in Figure 3.15.

The turbulent kinetic energy and the tracer gas concentration determined with the Eulerian method are depicted in Figure 3.13 and 3.14 for different turbulence models at different horizontal distances from the mouth along a vertical line in the middle plane. The standard k-ε turbulence model exhibited much higher turbulence kinetic energy

levels than RNG turbulence model and RSM. This usually leads to a more diffusive concentration field. The turbulent kinetic energy profiles obtained from the RNG turbulence model and RSM are very similar. The subgrid turbulent kinetic energy, Ksgs, presented in Figure 3.14 indicates that most of the energetic large eddies are captured by the LES technique. Note that Ksgs represents the unresolved part of the turbulent kinetic energy by LES. This is apparent from the low levels of Ksgs compared to K obtained from RANS. As for computation time, RSM took approximately 50% more time than the RNG turbulence model which took a little bit more time than standard k-ε turbulence model. Because of its unsteady nature, the LES model required 500% more time than the RANS turbulence models. The contaminant concentration profiles shown at various locations in Figure 3.14 indicate that except very near the body all models exhibit similar results. However, as seen in Figure 3.12d near the face of the body, LES results are significantly different than the other models.

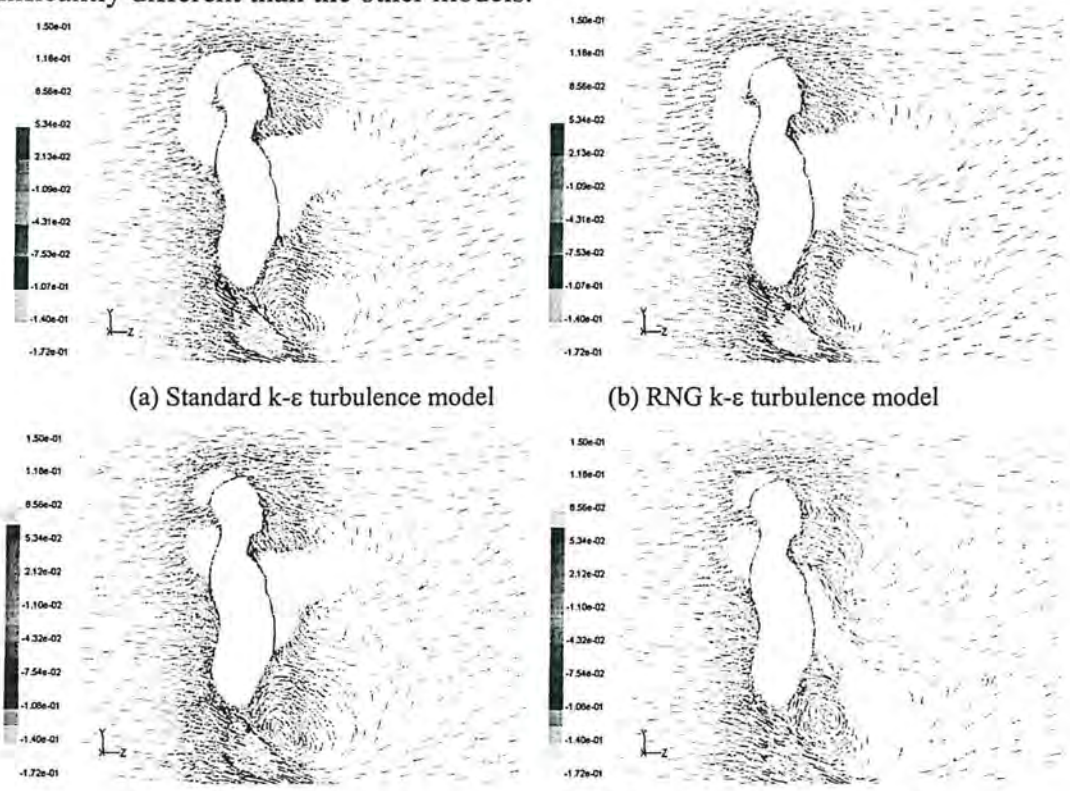

(a) Standard k-ε turbulence model (b) RNG k-ε turbulence model

(c) RSM (d) LES (Averaged flow field)

Figure 0-12 Streamlines colored by y-velocity in the middle cross section plane with different turbulence models

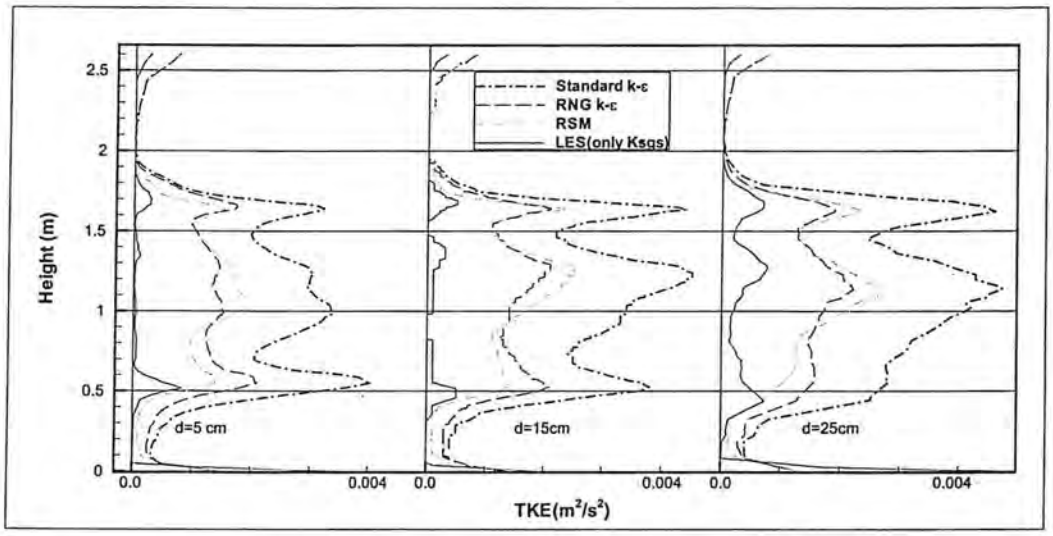

Figure 0-13 Tke/subgrid Tke at different horizontal distances from the mouth along a vertical line in the middle plane (Ksgs = Subgrid scale turbulent kinetic energy)

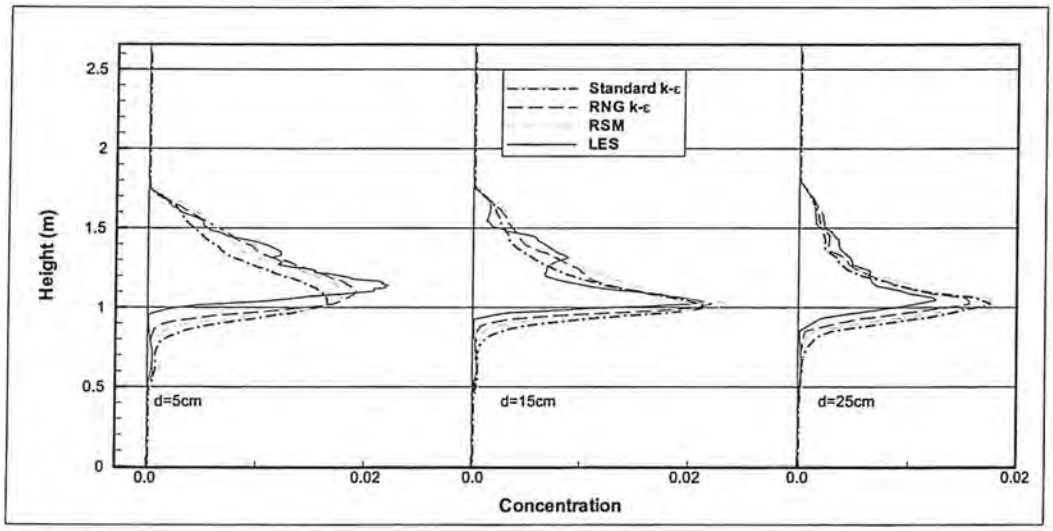

Figure 0-14 Scalar concentrations (kg/m^3) at different horizontal distances from the mouth along a vertical line in the middle plane

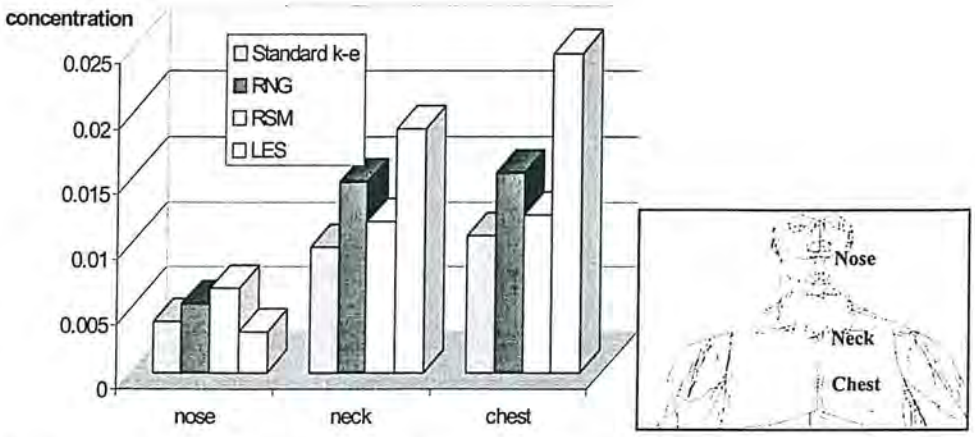

Figure 0-15 Concentration (kg/m^3) levels at different sampling locations with different turbulence models; Eulerian scalar transport

The results from this study show that significant differences in predicted concentration levels are observed when different turbulence models are utilized. The coefficient of variation for species concentrations predicted with four different turbulence models ranged between 30-40%. That is why one of the objectives of this study is to recommend a suitable turbulence model for worker exposure studies.

Effect of ventilation intensity, free stream turbulence, and heat flux from the body

The simulations have been performed using the Fluent CFD software package (Fluent, Inc., Lebanon, NH). The geometrical configuration of the flow domain is shown in Figure 3.16, consisting of the wind tunnel (4.6m width × 2.6m height × 7m length), and a manikin (1.69m height). The manikin body faces downstream of the isothermal flow. The fluid medium is air.

A source pan (ϕ=0.23 m) as shown in Figure 3.17 is used to release the mixture of nitrogen and ethanol vapor from 90 small holes (5 mm) in the experimental study. The source pan is 1.04m above the ground at the manikin's waist height and 0.25m downstream of the manikin's torso. The mass flow rates of nitrogen and ethanol vapor are 1.98e-5 kg/s and 9.34e-7 kg/s, respectively. The mass average velocity of the released mixture is 0.0026 m/s in the vertical direction. The nitrogen is treated as air in the numerical study since this approximation greatly simplifies the calculation without loss of accuracy (By numerical experimentation it has been verified that the concentration at the breathing zone is not affected by the presence of the nitrogen). Source terms including mass, momentum in the vertical direction, as well as turbulence quantities such as k and ε are added to the corresponding equations in the source pan region (the red region in Figure 3.16).

Constant velocity inlet and pressure outlet boundary conditions were used. The inlet velocity was varied in the range 0.051-0.762 m/sec (10-150 fpm) with a turbulence

intensity of 10%, values representative of typical working environments (Baldwin and Maynard, 1998). The characteristic turbulent length scale was chosen to be 0.01 m, which represents the turbulence generating honeycomb size at the inlet of the tunnel. At solid surfaces the usual non-slip and impermeability conditions are applied. The standard wall function is used for the calculation with turbulence models.

A rounded body, which is used in experiments and is thinner than the one used in the body shape study, is utilized in the simulations. Tetrahedral grids are generated. There are a total of 1,575,222 tetrahedral cells. The smallest tetrahedral grid size on the manikin surface is around 0.005 m. The mesh around the body is much thicker than in other regions. From the extensive grid study (Li, et al. 2005), it is expected that the grid convergence index (GCI) for the concentration at the breathing zone is less than 5% since the grid used in this study is much finer than grid #3 in the study for the body shape effect.

The heat generation rate of the heated body in the experiments was approximately 90W. It is released from the upper-body surface (excluding the arms) by both convection and radiation. Whereas the heat released by the radiation was unknown, it is assumed that all the generated heat is released from the body by convection through the upper-body in the first run of the simulations with the heated body. This boundary condition is also called 'B1' in the later discussion. The second run is done after the experiments which provide temperature difference as listed in Table 3.3 between the upper-body and the inlet airflow. The averaged temperature is specified on the upper-body and the head for the thermal boundary condition in the second run. This is the 'B2' boundary condition referred to in the discussion that follows.

The Reynolds number (as listed in Table 3.3), which represents the ratio of the inertial force and the viscous force, is calculated by $\mathrm{Re} = UD/\nu$, where the U is the inlet velocity and D is the equivalent dimensions of either the head or the shoulder. The Grashof number is about $8\text{x}10^8$, which measures the ratio of the buoyancy force to the viscous force and is computed from $Gr = \frac{g\beta\Delta TL^3}{\nu^2}$, where g is gravity, β is the thermal expansion coefficient, ΔT is the temperature difference, and ν is the kinematic viscosity.

The SIMPLE scheme was used to handle the pressure-velocity coupling. QUICK Scheme was applied for the convection terms in the momentum and scalar transport equations. The second order upwinding scheme was used for the convection terms in the k and ε equations. Central differencing was utilized for the diffusion terms in all equations.

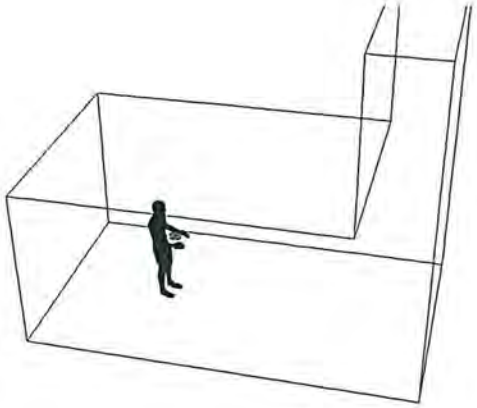

Figure 0-16 Schematic view of the computational domain (short domain)

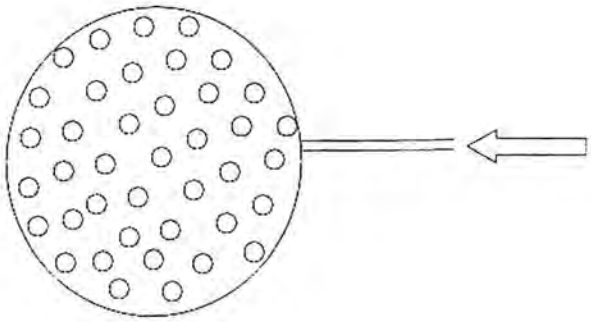

Figure 0-17 Top view of the source pan

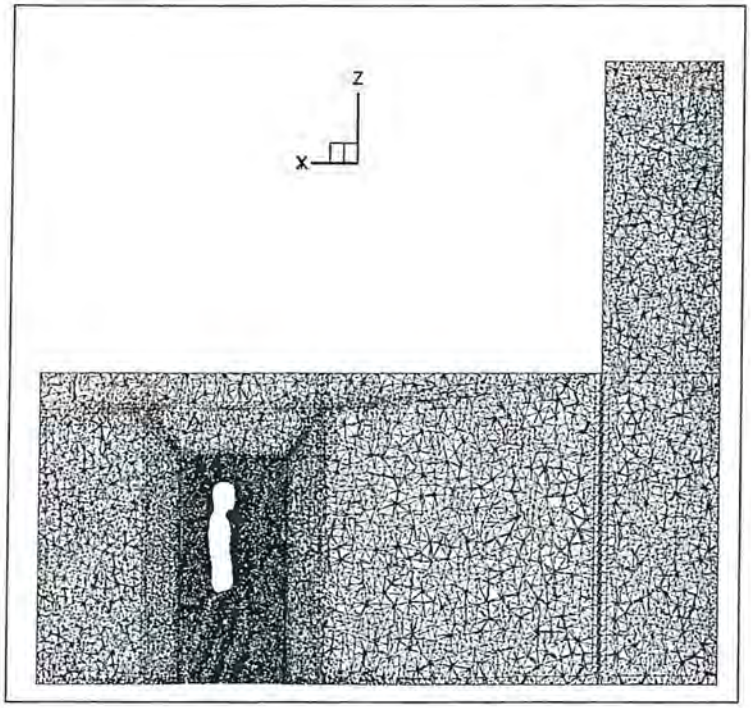

Figure 0-18 The computational mesh in the center plane

Table 0.3 Reynolds number at different ventilation intensity

U(inlet) (fpm)	10	20	40	60	80	100	120
U(inlet) (m/s)	0.05	0.10	0.20	0.30	0.41	0.51	0.61
Re (based on head size)	686	1373	2746	4119	5492	6865	8238
Re (based on shoulder size)	2073	4147	8294	12441	16588	20735	24882
Averaged temperature difference(K)	9	9	10	10	10	9	9

Sensitivity of RNG turbulence model to the low Reynolds number modification

Before the effect of Re is analyzed, some issues should be addressed on the unsteadiness of the flow. It can be seen from Figure 3.19 that the concentration at the breathing zone (represented by a point 1 cm downstream of the mouth) predicted with low_Re RNG varies significantly with iteration (pseudo time marching). Without appropriate averaging, the instantaneous concentrations calculated with low_Re RNG should not be compared with the experimental data, since the measurements in the experiments were obtained on a relatively long time (15 minutes) sampling, and hence represent ensemble averaged values. To obtain reasonable mean concentrations, at least 1000 iterations are necessary for low_Re RNG, but 500 iterations would be enough for RNG model.

Simulations with low_Re RNG demand more computational cost than that with RNG. The mean data shown in Figure 3.20 are averaged values of 1000 iterations for low_Re RNG and laminar flow, and 500 iterations for RNG. A detailed LES simulation could provide the typical frequencies of the flow, which could clarify if 15-minute sampling time is sufficient for the contaminant sampling.

Figure 3.20 presents the comparison of the numerical and experimental results of the concentration at the breathing zone with RNG, low-Re RNG and laminar flow for the unheated case. The numerical results with both low_Re RNG and RNG agree well with each other. At low Reynolds number (V(inlet)< 30 fpm (0.15 m/s)), low_Re RNG and RNG result in 20-30% difference for the exposure levels in the breathing zone. The results predicted with RNG turbulence model are closer to experimental data, although the calculations with low-Reynolds number modification also agree satisfactorily with the experimental results. The concentrations in the breathing zone simulated with the laminar flow are the largest among the three choices. Since the RNG turbulence model requires less computational effort and achieves relatively better agreement with experiment than the low-Re version, it is chosen to serve as the turbulence model for the subsequent evaluation of the effect of the free stream turbulence and the heat release from the body.

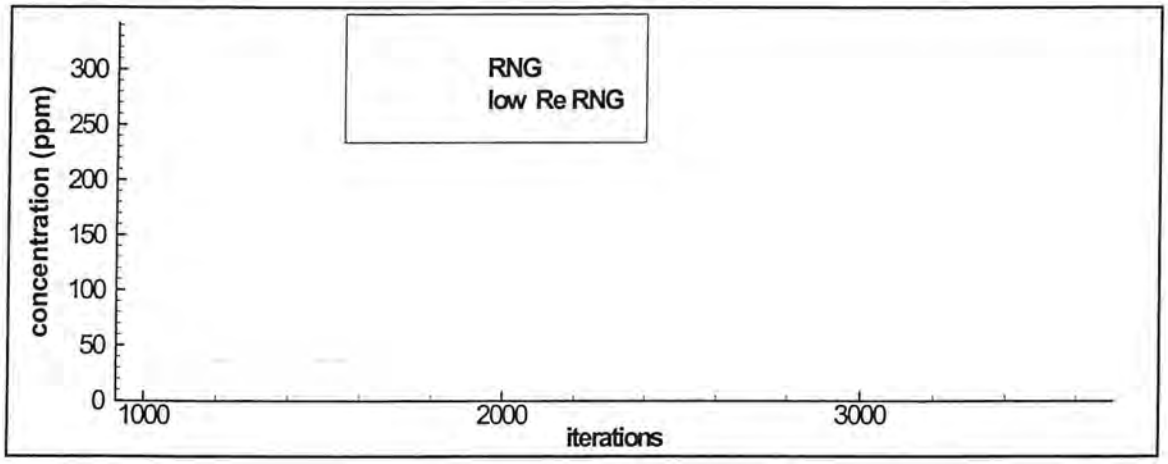

Figure 0-19 Concentration at the breathing zone vs. iterations at an inlet velocity of 30 fpm (0.15 m/s)

Both experiments and simulations (Figure 3.20) show that, with the unheated body, the concentrations at the breathing zone decrease as the ventilation intensifies, which agrees with the experimental results by George et al (1990). The exposure levels decline quickly especially when the inlet velocity is less than 50 fpm (0.25 m/s). The concentrations at the breathing zone change less in the Re range of 50 -150 fpm (0.25-0.75 m/s). Overall, the predictions with the RNG turbulence model agree very well with the experimental data. The only exception is in the low Reynolds number region, e.g., V(inlet)=10 fpm, where the simulated concentration is much higher than the measurements.

The effect of the free stream turbulence on the worker exposure is presented in Figure 3.21. It is seen that the overall trend for the concentration at the breathing zone goes down as the free stream turbulence intensifies, despite of the marginal change as turbulence intensity varies from 10% to 40%. At V(inlet)=10 fpm (0.05 m/s), the exposure level descends from 107 ppm to 55 ppm as the turbulence intensity increase from 40% to 60%. In the experiments, higher turbulence intensity has been observed at the low Reynolds number (Welling, et al. 2000; Guffey, 2004), which may be the reason for the discrepancy between the simulations and the experiments shown in Figure 3.20.

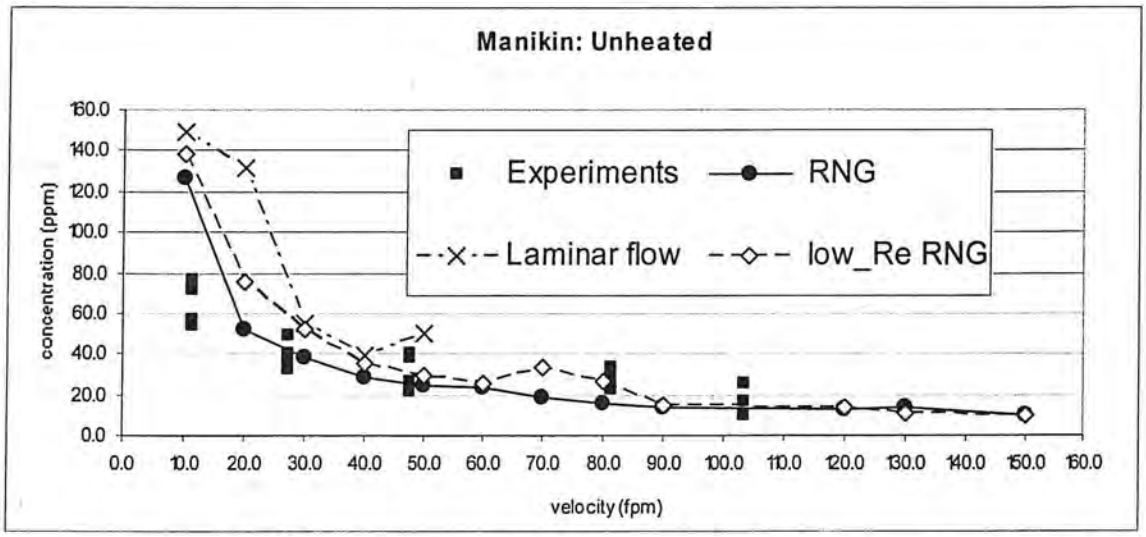

Figure 0-20 Comparison of the numerical and experimental results of the concentration at the breathing zone; free stream turbulence level is 10%.

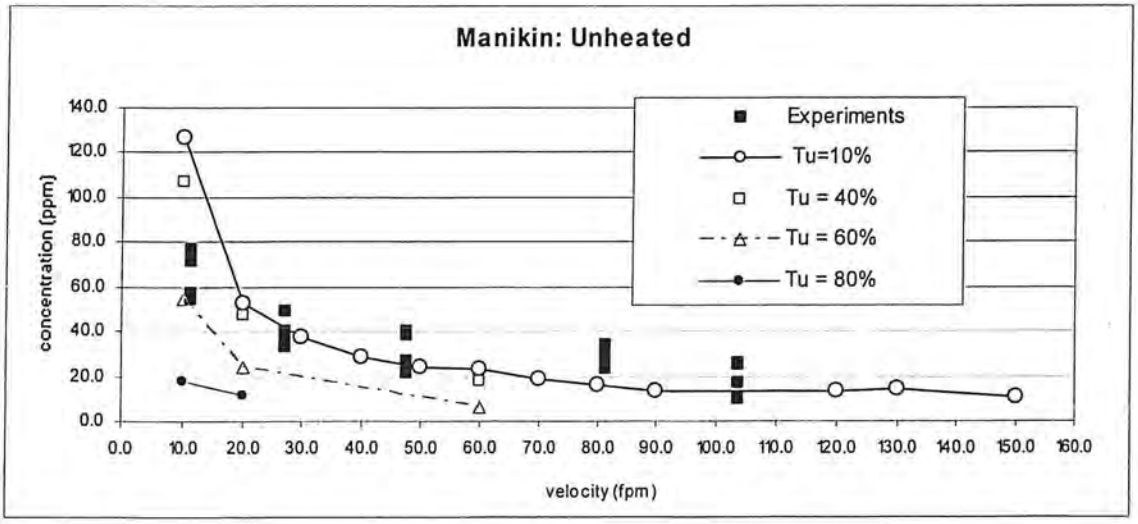

Figure 0-21 The effects of the ventilation intensity and the free stream turbulence on the concentration at the breathing zone (with RNG turbulence model)

Nevertheless, with the heated body, the trend was very different, as is shown in Figure 3.22. The concentration at the breathing zone first increases as the ventilation intensity increases. The exposure levels reach a peak at a ventilation velocity of around 40-60 fpm. Then it drops as the velocity increases further. Again, the predictions with the temperature boundary conditions agree well with the measurements. The calculations with full heat convection (B1) results in lower predicted exposure levels than the one measured in the experiments. This suggests that the worker would benefit from less radiation if the heat he generates remains constant. However, it is not convenient to control the radiation in practice. Furthermore, the heat flux by sweating/evaporative cooling is not considered in the current experiments and simulations. The evaporative cooling is not negligible when the worker is at a heavy duty. More importantly it affects the comfort level of the worker. Comprehensive consideration on both the exposure and the comfort level index would be desired for today's working environment.

It is interesting to note that the exposure levels from numerical simulations for the heated body show a zigzag (i.e. a wavy) pattern from V(inlet)=30 fpm (0.15 m/s) to V(inlet)=50 fpm (0.25 m/s) when the temperature boundary condition (B2) is specified. Although the experimental data is too coarse in this region to verify this, the relatively larger variation at V(inlet) = 47 fpm (0. 24 m/s) may indicate that the slope of the curve should be larger than the one formed by connecting the experimental data by a straight line. The reason for the zigzag pattern could be due to the alternating dominance of the buoyancy force and the inertial force. Even wider zigzag region is found in the simulations with heat flux specified (B1).

Comparing Figure 3.20 and Figure 3.22, it can be stated that the exposure levels with the heated body are higher than the ones with the unheated body in the V(inlet) range of 30-100 fpm. Nevertheless, at low Reynolds number (V(inlet)=10), the exposure levels with the heated body are lower. Keeping this in mind and more discussion will be provided later when detailed flow field information is presented.

The convection and the radiation heat release rates are plotted against the ventilation intensity in Figure 3.23. The convection heat release is computed by integrating the heat convection on the whole upper-body, and the radiation is calculated by subtracting the convection from the total heat generation rate. It is seen that, as the ventilation intensifies, the heat release via convection is also intensified. It is interesting that a rough calculation yields 59 W for the radiation heat transfer, based on an emissivity of 0.96 for the manikin (Bräuer et al. 2002). This further confirms the current simulations.

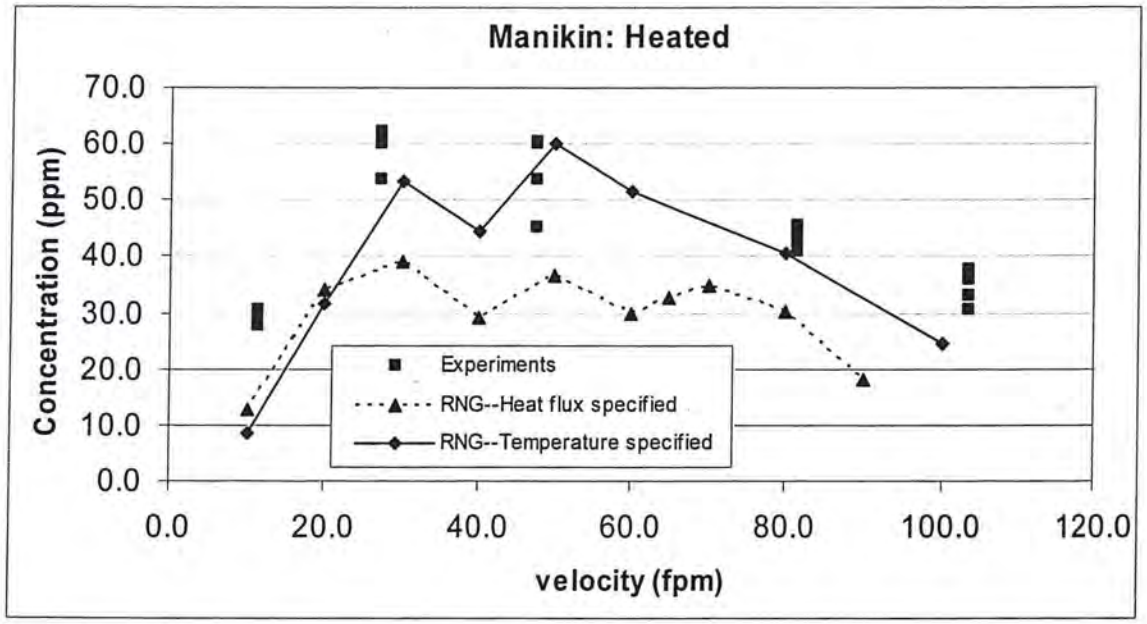

Figure 0-22 The effect of the ventilation intensity and the body heat on the concentration at the breathing zone; Tu=10%

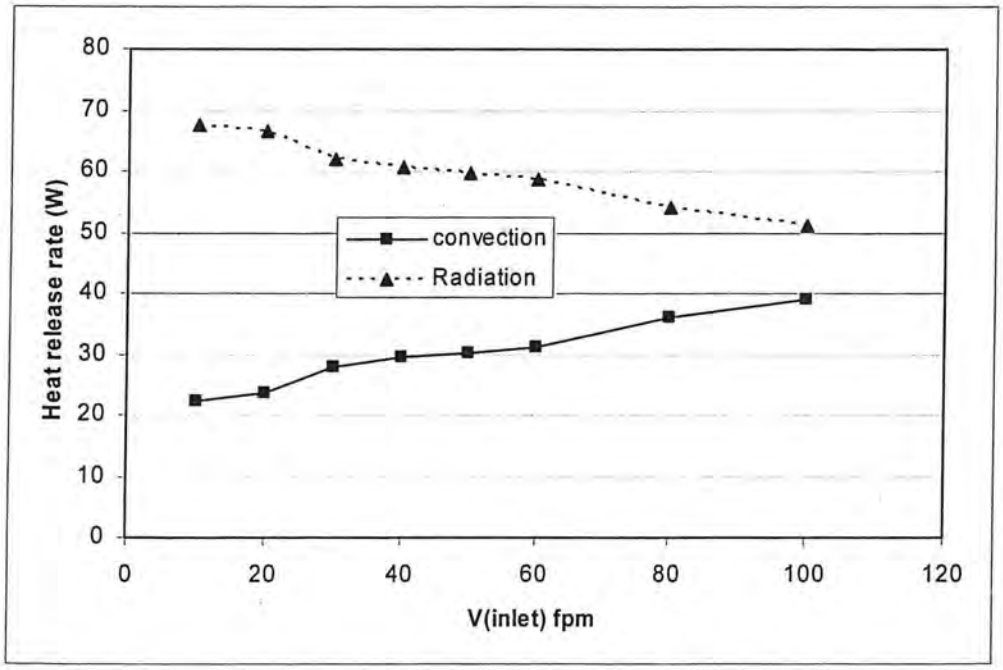

Figure 0-23 Heat flux via convection and radiation with RNG turbulence model and averaged temperature boundary condition (B2)

The concentrations at the chest level are shown in Figure 3.24 and Figure 3.25. The computations capture the same trend as the experiments. By contrast, there is a 70-80% difference between the simulation results and the experimental data for the heated body in the V(inlet) range of 10-50 fpm. It seems that the free stream turbulence intensity influences the concentration with the unheated body, but it remains to be clarified whether the turbulence intensity has the same effect for the cases with the heated body.

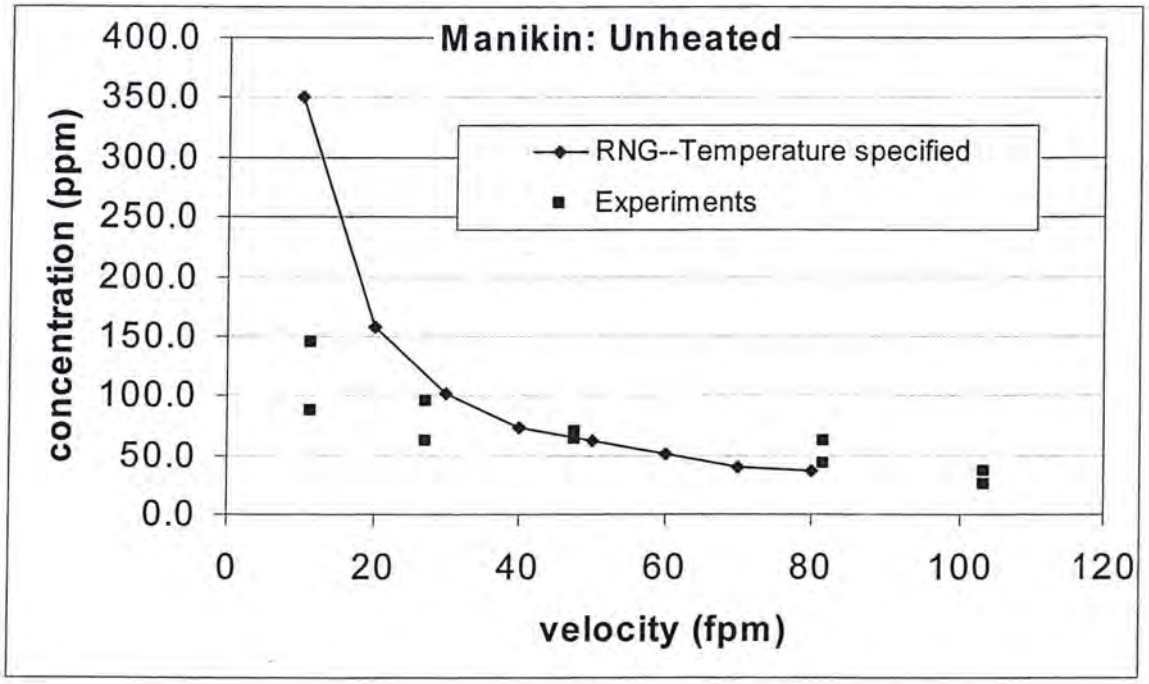

Figure 0-24 The effect of the ventilation intensity on the concentration at the chest

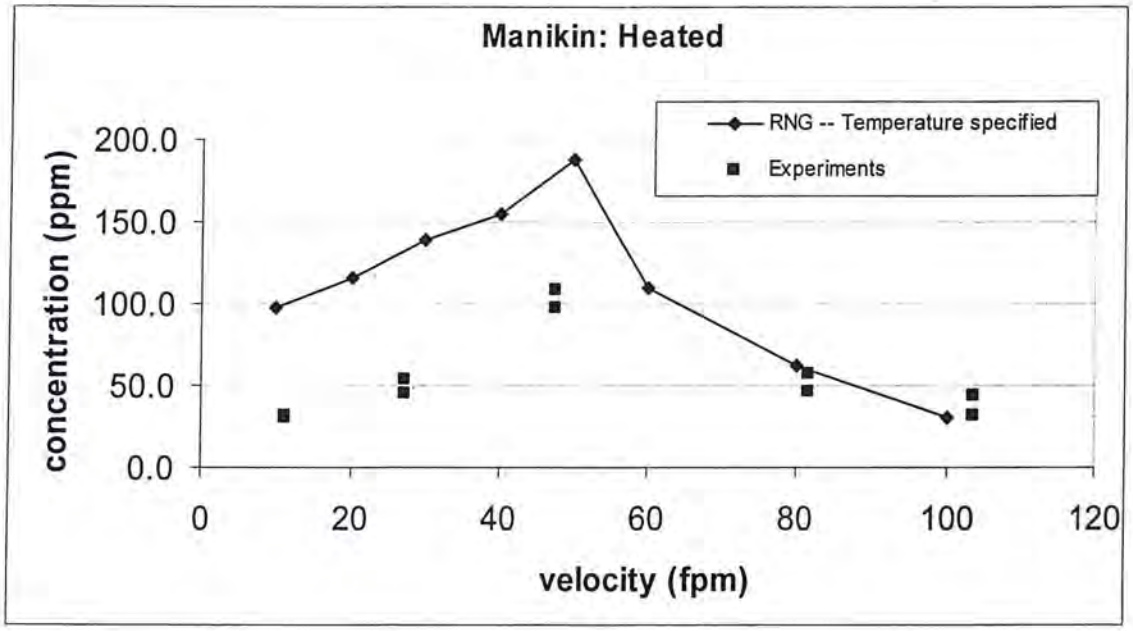

Figure 0-25 The effect of the ventilation intensity and the body heat on the concentration at the chest level

The turbulent kinetic energy contours and pathlines in the middle plane at different Reynolds number are presented in Figure 3.26. It is shown in Figure 3.26(a) that there are two recirculation zones in the immediate downstream of the unheated body at V(inlet) = 10 fpm, whereas, with the heated body, there is no recirculation region found in Figure 3.26(b). The heat flux from the body significantly affects the flow field and the turbulent kinetic energy in the downstream of the body. With the heated body, the characteristic buoyant velocity is around 0.2 m/s. At V(inlet) = 10 fpm (0.05 m/s), the upwards convection induced by the buoyancy is dominant so that there is no recirculation region formed at the breathing zone. The heat flux also increases the turbulence level around the body. All these effects consequently result in significantly different concentration distributions (as shown in Figure 3.27(a) and (b)). The exposure level in the breathing zone with heated body is much lower than the one with unheated body.

As the inlet velocity increases to 60 fpm (0.3 m/s) (Figure 3.26(c)), the flow structure predicted with the unheated body is similar as the pattern at V(inlet) = 10 fpm, whereas, the turbulent kinetic energy in the recirculation regions increases significantly, which leads to more diffusion, hence lower concentration in the breathing zone than at V(inlet) = 10 fpm (Figure 3.27(a)). The natural convection induced by the body heat at V(inlet) = 60 fpm (Figure 3.26(d)) brings the contaminant directly to the breathing zone, and at approximately the forehead height; then it is stopped by the ventilation airflow and changes its direction. This procedure retards the convection of the ethanol vapor out of the breathing zone, which results in a much higher exposure level than the one at V(inlet)=10 fpm (Figure 3.27(d) and 3.27(b)).

Note that the only difference between Figure 3.26(d) and (e) is the thermal boundary condition. With full convection (Figure 3.26(e)), the turbulent kinetic energy is larger than the one with partial convection (Figure 3.26(d)), which explains that the exposure level with full convection at V(inlet)=60 fpm is greater the one with partial convection at the same ventilation intensity (comparing Figure 3.27(d) and 3.27(e)).

As the ventilation intensifies further, i.e., V(inlet) = 100 fpm, the ventilation convection becomes dominant, and it induces a big recirculation region, which confines the ethanol vapor in the lower body region as shown in Figure 3.26(f).

It should be noted that the heat is released from the upper-body surface in this study to match the experimental condition. If the heat is released from the whole body, the Grashof number is expected to increase mainly due to the increasing of the length scale, hence, the peak in Figure 3.22 will move toward higher ventilation intensity. To the opposite side, if the heat is released from only the head (supposing that the rest of the body is covered by insulated work clothing), the Grashof number will decrease and the peak will move toward a lower ventilation intensity.

It should also be noted that the B2 boundary condition was imposed by the assumption of a uniform temperature distribution on the body. In the experiments with a heated manikin without clothing, the temperature measured on the head is 2°C different from the one on the abdomen. The temperature distribution on a real human body could be significantly non-uniform, due to clothing. This may contribute to the uncertainty of the predictions and may be considered in further study.

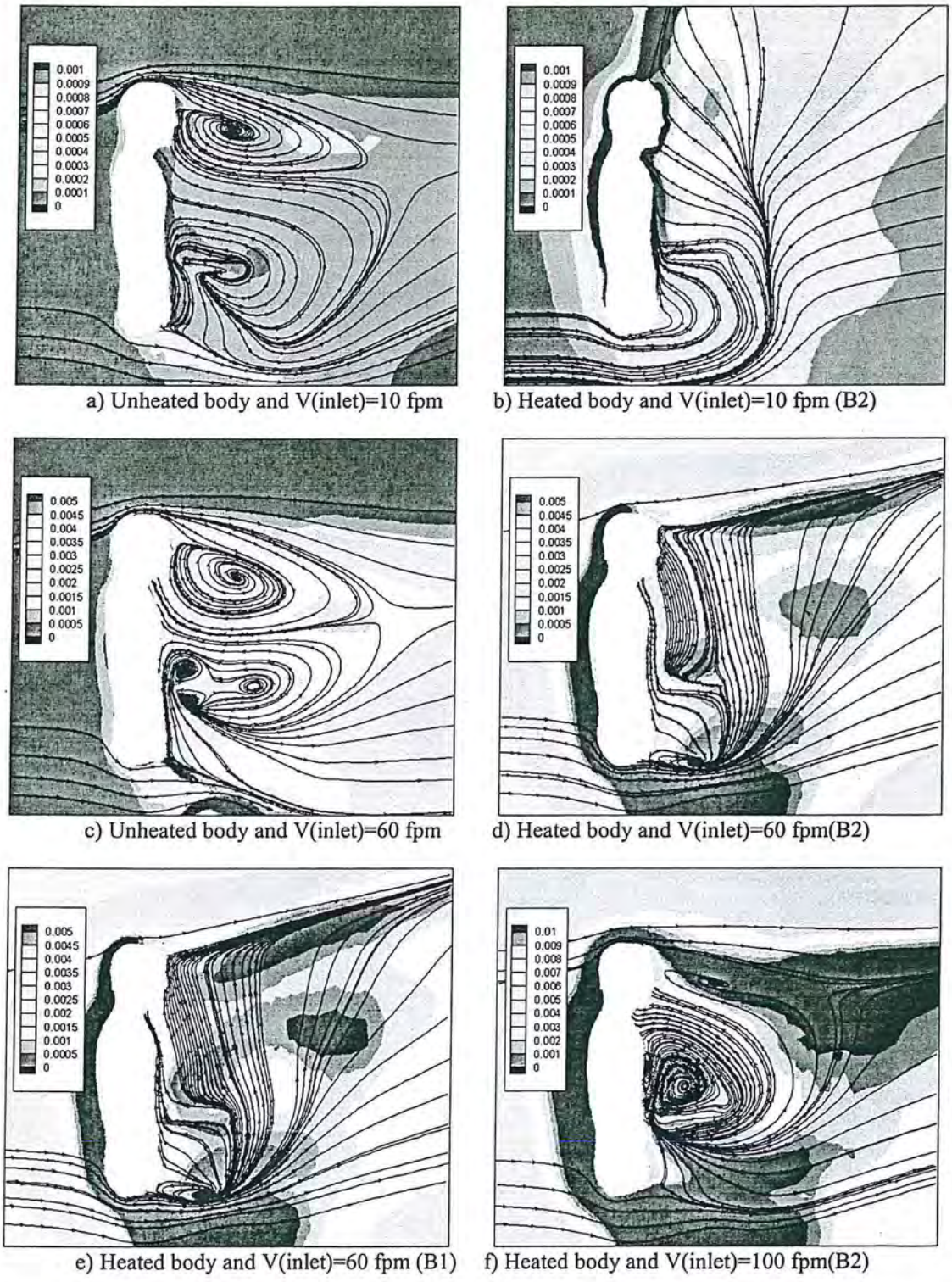

a) Unheated body and V(inlet)=10 fpm

b) Heated body and V(inlet)=10 fpm (B2)

c) Unheated body and V(inlet)=60 fpm

d) Heated body and V(inlet)=60 fpm(B2)

e) Heated body and V(inlet)=60 fpm (B1)

f) Heated body and V(inlet)=100 fpm(B2)

Figure 0-26 Turbulent kinetic energy contours and pathlines in the middle plane at different ventilation intensity with unheated and heated bodies

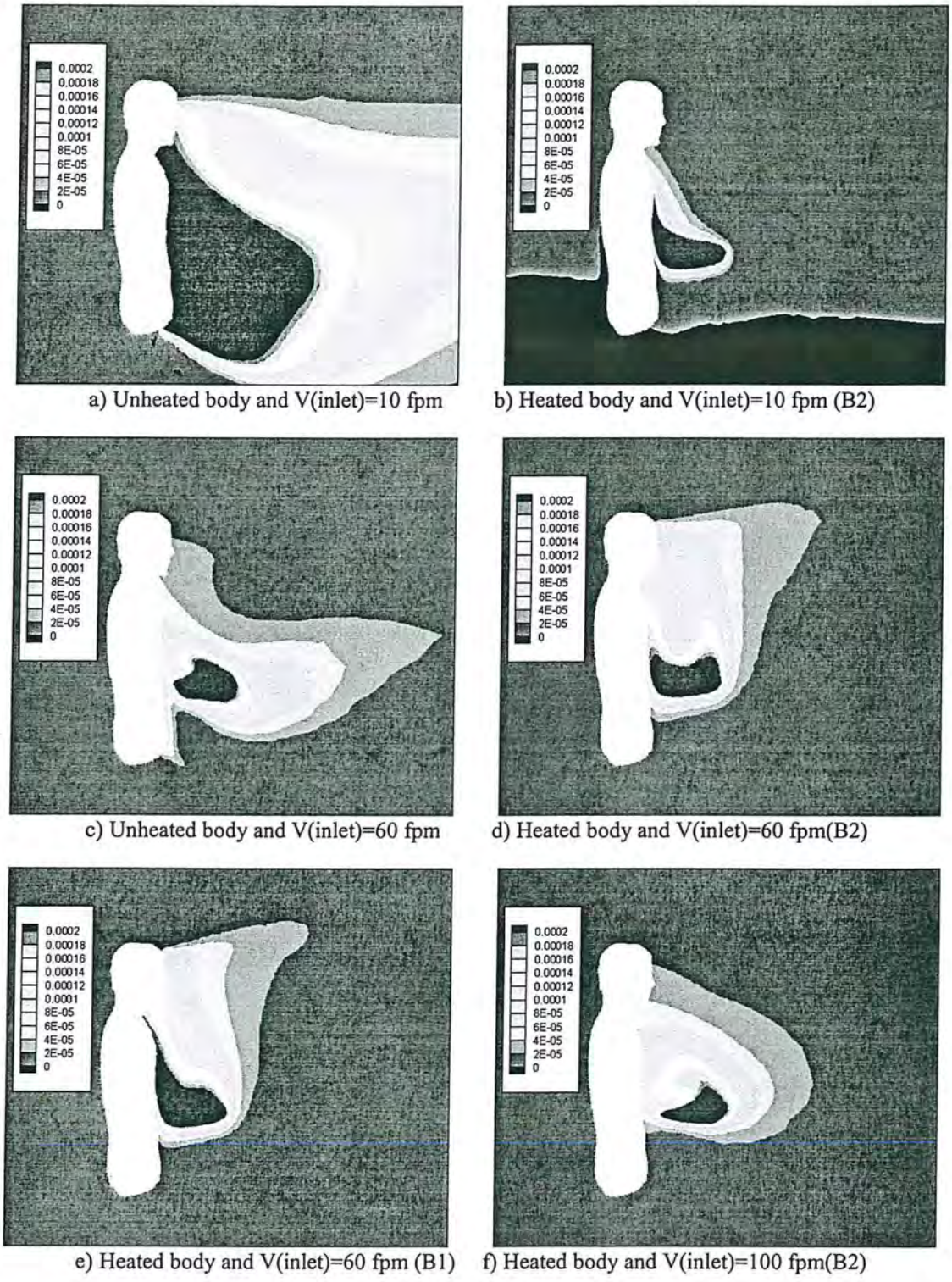

a) Unheated body and V(inlet)=10 fpm

b) Heated body and V(inlet)=10 fpm (B2)

c) Unheated body and V(inlet)=60 fpm

d) Heated body and V(inlet)=60 fpm(B2)

e) Heated body and V(inlet)=60 fpm (B1)

f) Heated body and V(inlet)=100 fpm(B2)

Figure 0-27 Concentration contours and pathlines in the middle plane at different ventilation intensity with unheated and heated bodies

Figure 3.28 shows the effect of the free stream turbulence on flow around the unheated body. A turbulent intensity of 60% is used at inlet for this study. Comparing Figure 3.28(a) with Figure 3.26(a), larger turbulent kinetic energy is observed in the recirculation regions with Tu = 60%, which results in a more smeared concentration field as shown in Figure 3.28(b) than the one with Tu = 10% (Figure 3.27(a)).

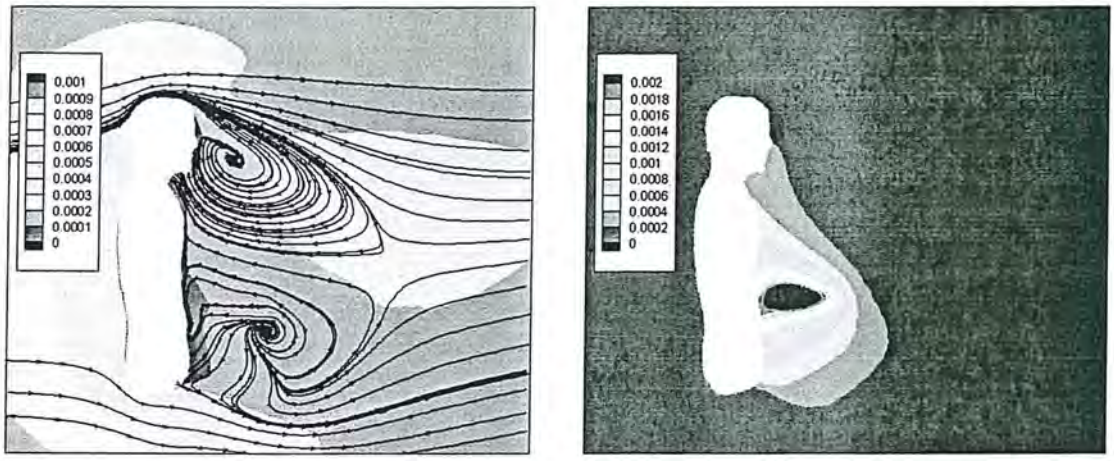

a) k contours and pathlines b) Concentration contours

Figure 0-28 The effect of the free stream turbulence with the unheated body at V(inlet) = 10 fpm and Tu = 60%

Flow unsteadiness

A closer examination of the flow unsteadiness study was aimed to understand the flow dynamics in the formation and the development of the wake flow in the downstream of human body as well as the relation to the contaminant transport. A LES run was conducted since the LES approach is conceptually more suitable in such situations as it resolves the large-scale unsteady motions and requires modeling of only the small-scale turbulent motion which is less influenced by the boundary conditions.

The same grid as shown in Figure 3.18 is utilized. The inlet velocity for this case is 20 fpm. A time step of 0.5 s was used, which is about 10 times larger than the Kolmogorov time scale and is sufficient for the LES simulation in this case according to Frisch (1995). The Smagorinsky subgrid scale model is used for the prediction of small scale turbulence. A zero initial velocity field is specified at t = 0 s. The inlet turbulence is assumed isotropic and with an intensity of 10%. Simulation results in the first two flow-through times are discarded to allow the flow formation and developing. The maximum y+ of the first cells on the body is around 4.

Instantaneous pathlines and the concentration contours in the middle plane at t = 600s are shown in Figure 3.29. It is seen that flow separates on the forehead and forms an eddy in

the downstream of the head, and another eddy is developed in the chest region. It seems that not much ethanol is transported from the lower eddy to the upper one. At the same moment, if observed from a horizontal plane (z = 1.51m) cutting through the breathing zone (Figure 3.30), the instantaneous flow seems to be asymmetric and highly three-dimensional. Figure 3.31 shows the flow on a horizontal plane across the waist (z = 1.16m). Again, the flow is asymmetric and three-dimensional. Eddies are not only formed at the shear layer along the arms, but triggered by the leaking jet flow between the arms and the body. Considering the interaction of the jet flow and the wake, the flow pattern in this case is certainly more complicated than simple flows such as the flow over a circular cylinder. The flow structure in the middle plane at t = 620 s (Figure 3.32) is totally different from the one at 20 s earlier (Figure 3.29).

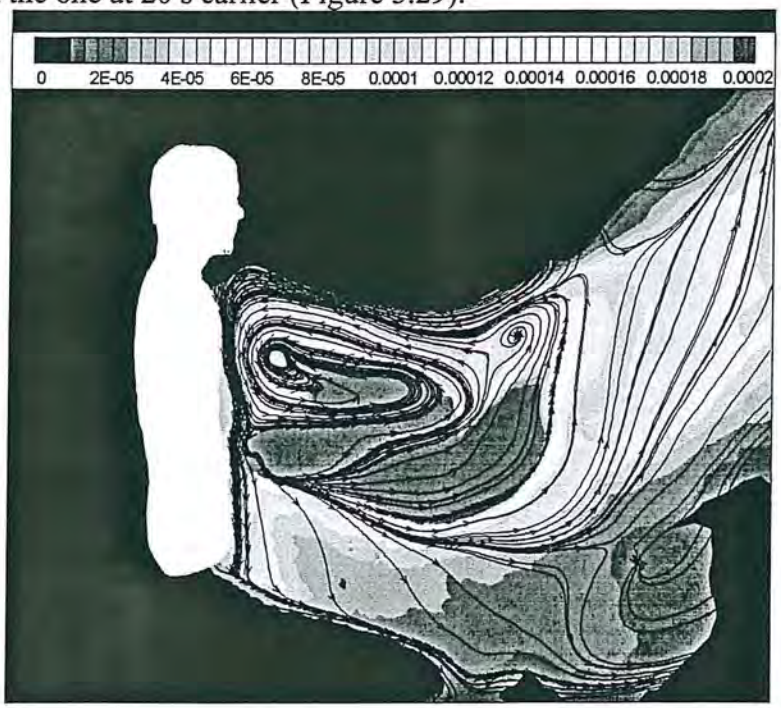

Figure 0-29 Instantaneous Pathlines and concentration contours in the middle plane at t = 600 s (concentration :kg/kgair)

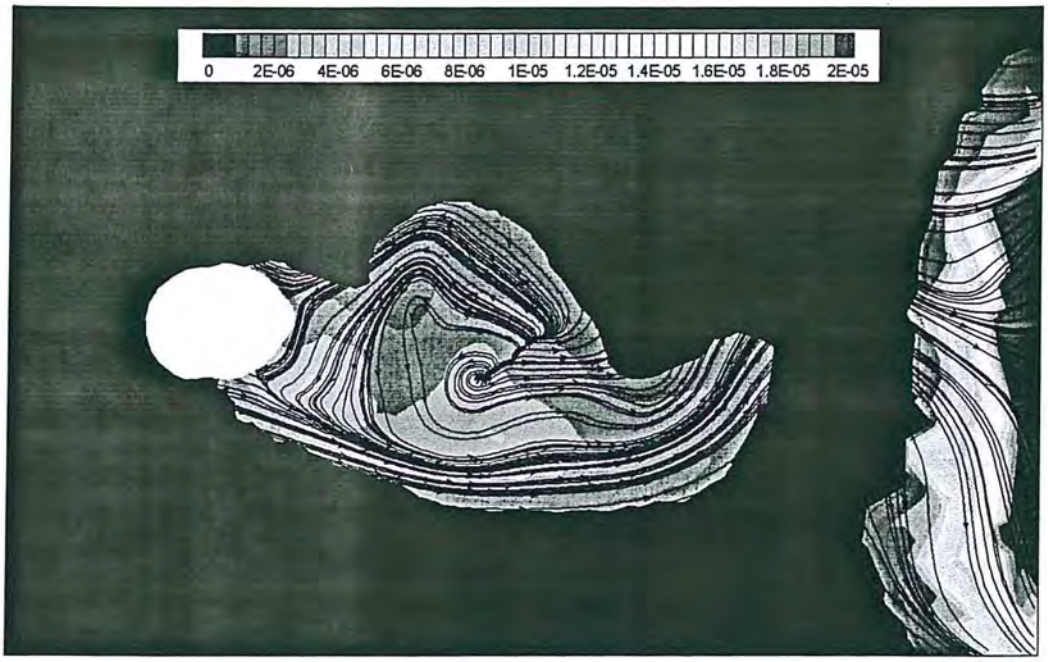

Figure 0-30 Instantaneous Pathlines and concentration contours in the horizontal plane z = 1.51 m at t=600 s (concentration :kg/kgair)

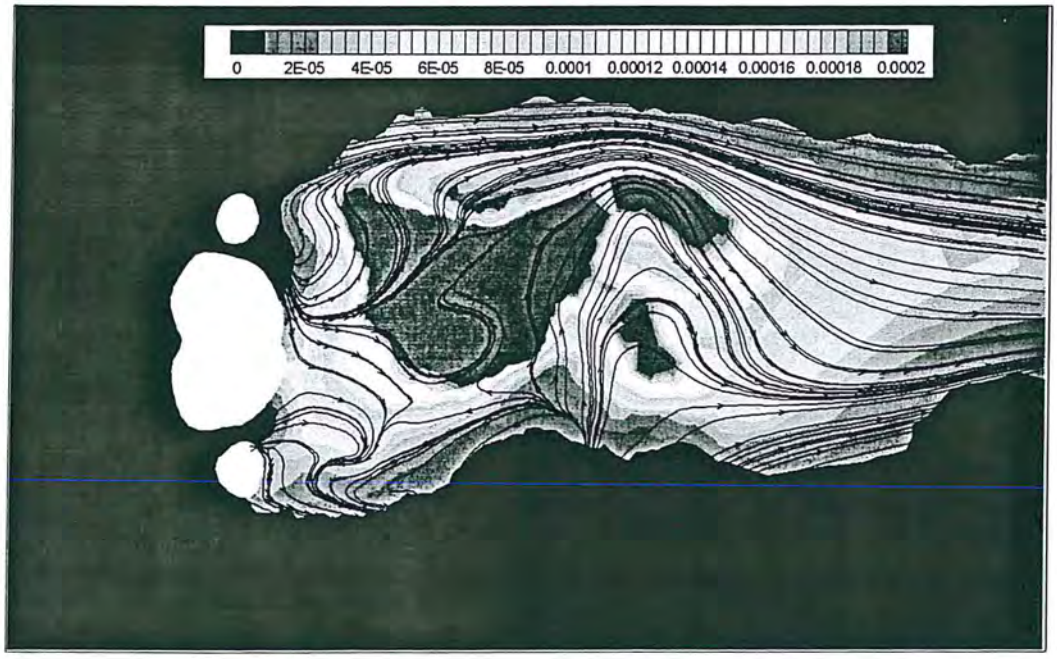

Figure 0-31 Instantaneous Pathlines and concentration contours in the horizontal plane z = 1.16 m at t=600 s (concentration :kg/kgair)

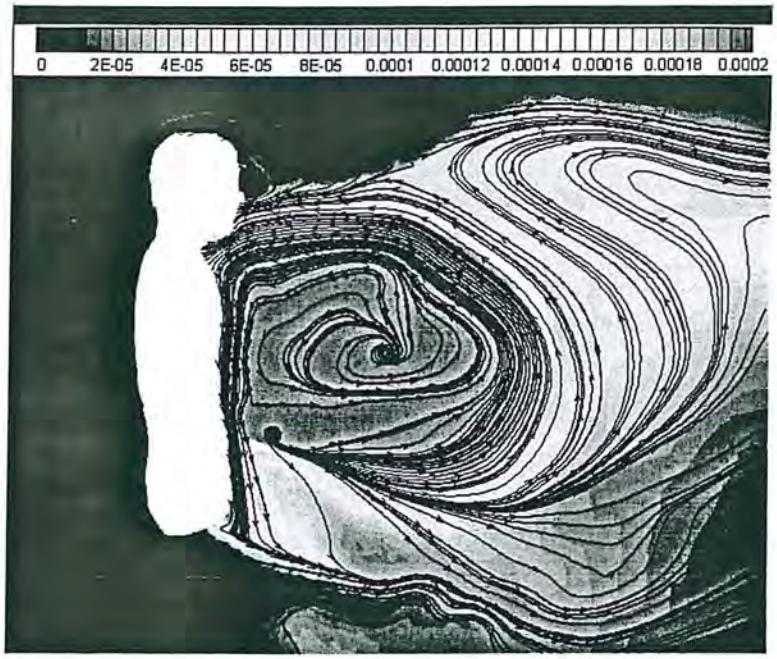

Figure 0-32 Instantaneous Pathlines and concentration contours in the middle plane at t = 620 s (concentration :kg/kgair)

The time evolution of the concentration at the breathing zone and the central chest are shown in Figure 3.33 and Figure 3.34, respectively. The mean and the standard deviation of the concentration at the breathing zone are 115 kg/kgair (72 ppm) and 101kg/kgair (64ppm), respectively. Comparing to the concentration predicted with the RNG and low-Reynolds-number RNG models, it is seen that the averaged concentration in the breathing zone calculated with LES lies in the mid range. More importantly, the LES results reveal that the concentration variation is so large that the instantaneous value cannot be used to estimate the averaged exposure level.

The power spectrum of the concentration in the breathing zone is calculated via Fourier transformation (Figure 3.35). The Strouhal number is defined by $St = fD/U$. The typical frequency corresponding to a Strouhal number of St = 0.047 is 0.0235 s^{-1}. The period is approximately 43 s, which means the experimental sampling time (15 minutes) is sufficient for this case.

It should be noted that it takes a couple of weeks to finish the LES simulation for just 15 minutes of real time. LES costs 20 times more than the steady RANS simulation with RNG model in this case.

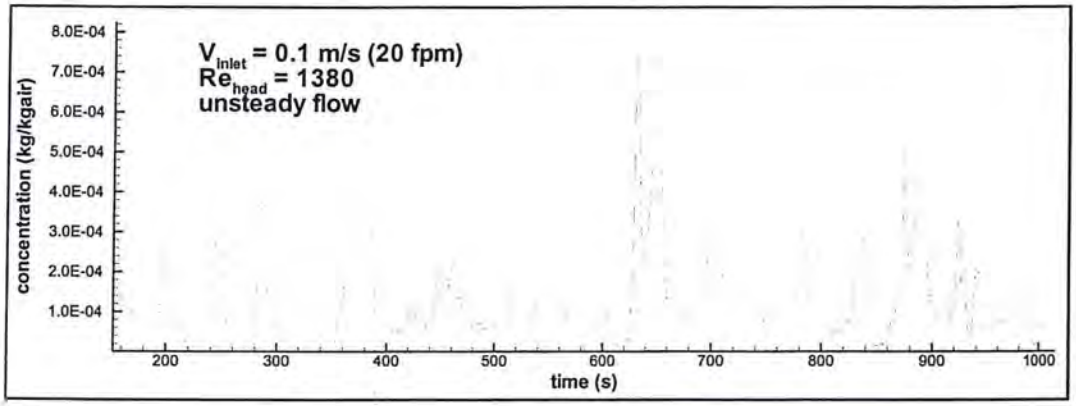

Figure 0-33 Concentration at the breathing zone changing with time (unheated body; LES)

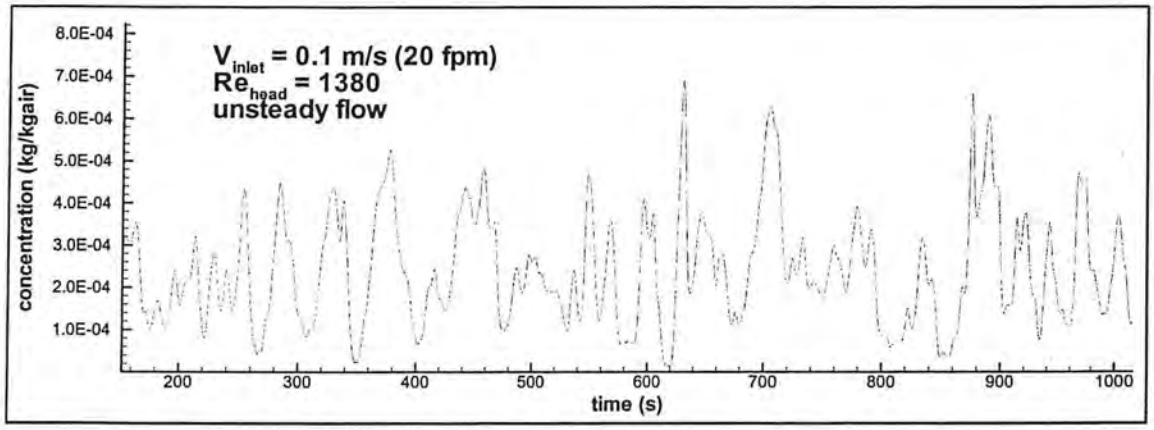

Figure 0-34 Concentration at the central chest changing with time (unheated body; LES)

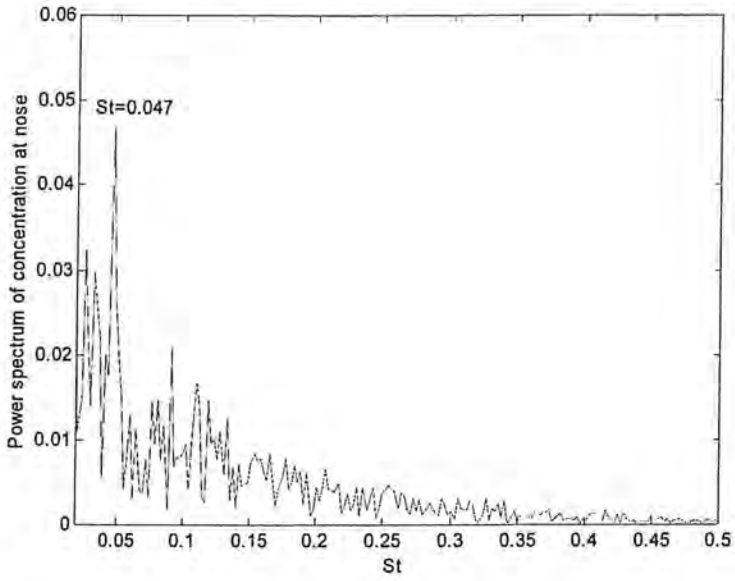

Figure 0-35 The power spectrum of concentration at the breathing zone

Summary

In this study, critical factors including body shape, ventilation intensity, free stream turbulence, body heat, and flow unsteadiness were scrutinized with respect to their effect on the air flow and gaseous pollutant transport in a wind tunnel when the body faces towards downstream of the flow and pollutant is released from a hand hold source pan. Part of the results were compared to experimental data (Guffey, 2005), which shows good agreement. An extensive grid convergence study was performed to determine the numerical uncertainty induced by finite numerical grid size. The overall discretization uncertainty is in the range of 5-10%.

The influence of the shape of the human body used on worker exposure to contaminants was studied. It was observed to have a major impact on the flow-field and, consequently, on the concentration field. In fact, this study showed that the predictions with a rounded body, which is one of the closest approximation of a human body used in simulations in the literature (to the best of the author's knowledge), resulted in much lower predicted concentration levels. This suggests during modeling, oversimplified body shapes should not be preferred for worker exposure assessment. Specific details of rounded body may have a significant influence on the exposure and should be considered in certain circumstances. This presents a great challenge to CFD modelers as every worker may exhibit a significant variation on body shape depending on what clothes are worn and factors related to many other body size and shape.

It has to be noted that the heat flux from the body has a significant impact on predicted flow-field and concentration levels, so that it can not be simply neglected especially

when the convection induced by the buoyancy dominates. The effect of the ventilation intensity on the exposure levels with an unheated body exhibits a simple expected pattern, i.e., as ventilation intensifies, exposure declines. However, for a heated body, the ventilation intensity region for maximum exposure levels moves to approximately 30-50 fpm (0.15 – 0.25 m/s) from 10 fpm (0.05 m/s) for an unheated body. As the free stream turbulence increases, the exposure levels decrease.

The Eulerian scalar transport model and the Lagrangian trajectory tracking method were compared in their ability to predict the concentrations around a human shaped body exposed to gaseous contaminants within the length of an arm's reach. It was seen that the Eulerian method exhibited a more diffusive nature than the Lagrangian method. However, the concentration predictions obtained with the Lagrangian method may converge with the Eulerian prediction if an adequate number of trajectories are tracked. Nevertheless, the results obtained from both predictions suggest that the concentrations measured at the lapel could be very different than the concentrations measured near the mouth (generally, significantly higher). The present study indicates that the latter will be significantly lower under the specific condition of the present simulations, particularly in the absence of heat flux from the body. However, this conclusion should not be generalized to the cases with uniform concentration distribution, which may resulte from by a non-local source or even from the motion of the worker.

On another note, it was demonstrated that the numerical mesh size and its distribution have significant effects on the quality of predictions. It is recommended that in exposure studies grid convergence of CFD simulations should be assessed in order to reduce and quantify the degree of discretization errors.

Conclusions and recommendations (CFD Simulation)

Conclusions

In this study, critical issues including body shape, ventilation intensity, free stream turbulence, body heat, and flow unsteadiness were scrutinized for their effect on the air flow and the gaseous pollutant transport in a wind tunnel when the body faces downstream of the flow and pollutant is released from a hand held source pan. Part of the results were compared to experimental data (Guffey, 2005), which has shown good agreement.

The body shape was observed to have a major impact on the flow-field and the concentration field. In fact, this study showed that the predictions with a rounded body, which is one of the closest approximation of a human body (to the best of our knowledge) used in simulations in the exposure assessment literature, results in much lower concentration levels. Simplified body shapes, such as a block and a sharp body, which either block the flow between legs or between the arm and the body, or change the separation profiles, could result in significantly higher exposure levels. This suggests that during modeling oversimplified body shapes should not be used in worker exposure assessment. Specific details, such as the hairstyle, the size and shape of the hat work, the angle of forehead, and the work clothing, may have a significant influence on the

exposure and should be considered in certain circumstance. This presents a great challenge to CFD modelers as every worker may exhibit a significant variation on body shape depending on what clothes are worn and factors related to body size and shape.

The effect of the ventilation intensity on the exposure levels with an unheated manikin exhibits a simple pattern, i.e., as ventilation intensifies, exposure declines. However, for a heated manikin, the exposure level reaches its maximum at ventilation intensity in the range of 30-60 fpm (0.15-0.30 m/s), where presumably the buoyant force balances the inertial force. At a low ventilation intensity, i.e. 10-20 fpm (0.05-0.1 m/s), the buoyancy is dominant. A plume forms and blocks the transport of contaminants from the source pan to the breathing zone, which, in turn, the exposure levels are relatively low. This suggests that the heat flux from the body has a significant impact on the concentration levels and should be considered especially when the convection induced by the buoyancy dominates.

The heat transfer by radiation from the body is an important way for heat release. Neglecting it may lead to underpredicted exposure levels. It should be noted that the heat flux by sweating/evaporative cooling is not considered in the current experiments and simulations. The evaporative cooling can not only affect the exposure by changing the heat transfer boundary condition, it is also directly related to the comfort level of the worker. Consideration of both the exposure and the comfort level index is desired for today's working environment.

In this study, it was assumed that the heat is released from the upper-body surface to match the experimental conditions. The Grashof number should be the key parameter to understand and estimate the effect of the heat release by the whole body surface or partial body (such as head). Another assumption was that the heat transfer was imposed by either a uniform temperature distribution or a uniform heat transfer distribution. The temperature distribution on a real human body could be significantly non-uniform due to the clothes worn. This also challenges CFD modelers as the clothes worn by the worker may vary significantly.

The effect of the free stream turbulence on the worker exposure was studied since turbulence intensity may vary to a great extent due to different work environment. The results showed that the concentration at the breathing zone reduces as the free stream turbulence intensifies. This could be used in the design of ventilation systems or local ventilation devices to further reduce the exposure levels.

The Eulerian scalar transport model and the Lagrangian trajectory tracking method were compared in their ability to predict the concentrations around a human shaped body exposed to gaseous contaminants within the length of an arm's reach. It was seen that the Eulerian method exhibited a more diffusive nature than the Lagrangian method. However, the concentration predictions obtained with the Lagrangian method may converge with the Eulerian prediction if an adequate number of trajectories are tracked. These models are not limited to predict the concentration of gaseous contaminants, they could also be applied to simulate the transport of aerosol particles.

Nevertheless, the results obtained from both Eulerian and Lagragian predictions suggest that the concentrations measured at the lapel could be very different than the concentrations measured near the mouth (generally, significantly higher). The present study indicates that the latter will be significantly lower under the specific conditions pertaining to the current simulations, particularly in the absence of heat flux from the body. However, this conclusion should not be generalized to the cases with uniform concentration distribution, which may be caused by a non-local source or even by the motion of the worker.

The results from this study show that significant differences in predicted concentration levels are observed when different turbulence models are utilized. The coefficient of variation for species concentrations predicted with four different turbulence models ranged between 30-40%. That is why one of the objectives of this study was to recommend a suitable turbulence model for worker exposure studies.

On another note, it was demonstrated that the numerical mesh size and its distribution have significant effects on the quality of predictions. It is recommended that in exposure studies grid convergence of CFD simulations should be assessed in order to reduce and quantify the degree of discretization errors.

Recommendations

Further numerical simulations can be done that include the breathing phenomena and the motion of the worker. An inlet boundary at mouth with a user defined velocity function can be used to present the breathing phenomena. The motion of the worker is more difficult to simulation since it will require the capability of handling the moving boundary for a complex geometry.

Radiation was not directly modeled and evaporative cooling was not considered in this study. Radiation and evaporation models may be incorporated to predict the temperature distribution in the wake of the human body. Introducing these models would enable us to calculate the comfort level which would be another desirable issue for the work places.

BIBLIOGRAPHY FOR ALL STUDIES

Experimental Studies

Baldwin, P.E.J., and Maynard, A.D. (1998). A Survey of WindSpeeds in Indoor Workplaces, Ann. Occup. Hyg. 42:303-313.

Bjørn, E. (2002). Dispersal of Exhaled Air in Stratified Surroundings-CFD Studies, proc. of the 8th conference on air distribution in rooms. ROOMVENT 2002, Copenhagen, Denemark, Vol. 1

Bjørn, E., and Nielsen, P.V. (2002). Dispersal of Exhaled Air in Displacement Ventilated Rooms, Indoor Air journal, Blackwell-Munksgaard 2002. (In Press)

Bjørn, E. and Nielsen, P.V. (2002). CFD Simulations of Contaminant Transport Between Two Breathing Persons, proc. of the 8th conference on air distribution in rooms, ROOMVENT 2002, Copenhagen, Denemark, Vol. 1

Bjørn, E., and Nielsen, P.V. (1996). Exposure due to Interacting Air Flows betweenPersons. Proc. ROOMVENT '96, 5th Int. Conf. on Air Distribution in Rooms, Yokohama, Japan. Vol.1, pp.107-114.

Brohus, H., and Nielsen, P.V. (1996). "CFD Models of Persons Evaluated by Full-ScaleWind Channel Experiments." Proc. ROOMVENT '96, 5th Int. Conf. on Air Distribution in Rooms, Yokohama, Japan. Vol.2. pp 137-144.

Brohus, H. and Nielsen, P. V. (1996). Personal exposure in displacement ventilated rooms. Indoor Air: 6, 157-167.

Bjørn, E., and Nielsen, P.V., (1996): Exposure Due To Interacting Air Flows Between Two Persons: Proceedings Of Proceedings Of Roomvent '96, 5th international Conference On Air Distribution In Rooms, Yokohama, Japan, Vol.1, Pp. 107 - 114, 1996.

Brohus, H., (1997). Measurement Of Personal Exposure Using A Breathing Thermal Manikin, Proceedings Of Ventilation '97, The 5th International Symposium On Ventilation For Contaminant Control, Global Developments In Industrial Ventilation, Ottawa, Canada, Vol. 2, P. 781-791

Cermak, R., Holsøe, J., Meyer, K.E., Melikov, A.K. (2002). PIV Measurements at the Breathing Zone with Personalized Ventilation, proc. of the 8th conference on air distribution in rooms, ROOMVENT 2002, Copenhagen, Denemark, Vol. 1

Colin, J., Houdas, Y. (1967). Experimental Determination of Coefficient of Heat Exchanges by Convection of Human Body, Journal of Applied Physiology 22:31

Clark, R. and Edholm, O.G. (1985): Man and His Thermal Environment. Edward Arnold Ltd, London.

Carlton, GN and Flynn, M.R (1997). A model to estimate worker exposure to spray paint mist: Appl. Occup. Environ. Hyg. 12(5):375382-39

Cohen, B.S., Harley, N.H., Lippman, M. (1984). Bias in Air Sampling Techniques Used to Measure Inhalation Exposure. Am Ind Hyg.Assoc.J.44: 187-192

Chatterjee, B.B., Williams, M.K., Walford, J., and King, E. (1969). The Location of Personal Samplers Filter Heads. Am.Ind Hyg.Assoc.J.30: 643-645

Cermak, R., Majer, M., Melikov, A.K. (2002), Improved quality of inhaled air with personalized ventilation. In: Proceedings of Indoor Air 2002, Monterey, pp. 1054-1059.

Donaldson, H.M. and Stringer, W.T (1980). Beryllium Sampling Methods. Am. Ind.Hyg.Assoc.J.41: 85-90

Flynn, M.R., Chen, M.M., Kim, T.H. and Muthedath, P. (1995). Computational Simulation of Worker Exposure using a Particle Trajectory Method: Ann. Occup. Hyg. Vol. 39, pp. 277-289.

Flynn, M.R., and George, D.K. (1991). Aerodynamics and Exposure Variability. Applied Occupational and Environmental Hygiene. 6:36-39

Flynn, M.R., and Ljungqvist, B. (1995). A Review of Wake Effects On a Workers Exposure. Ann.Occup.Hyg. 39: 211-221

Fletcher, B., and Johnson, A.E. (1989). Comparison of Personal and Area Concentration Measurements, and the Use of a Mannikin In Sampling. In Ventilation'88, edited by J.H.Vincent. New York: Pergamon Press, pp.161-167.

Guffey, S.E., Flanagan, M.E., Van Belle, G. (2001). Air Sampling at the Chest and Ear as Representative of the Breathing Zone. Am Ind Hyg.Assoc.J.62: 416-427

George, D. K., Flynn, M. R., Goodman, R. (1990). The Impact of Boundary Layer Separation on Local Exhaust Design and Worker Exposure. App. Occup. Environ. Hyg. 5(8):501-509

Heist, D.K., Eisner, A.D., Mitchell, W., and Wiener, R. (2003). Airflow around a Child-

Size Manikin in a Low-Speed Wind Environment, Aerosol Science and Technology 37: 303-314.

Holmer, I., Nilsson, H., Havenith, G., and Parsons, K. (1999). Clothing Convective Heat Exchange Proposal for Improved Prediction in Standards and Models Ann. occup. Hyg., Vol. 43, No. 5, pp. 329-337

Ichihara, M., Saitou, M., Nishimura, M. and Tanabe, S. (1997). Measurement of Convective and Radiative Heat Transfer Coefficients of Standing and Sitting Human Body Using Thermal Manikin, J. Archit. Plann. Environ. Eng., AIJ, No.501, 45-51

Johnson, A.E., Fletcher, B., Saunders, C.J. (1996).Air Movement Around a Worker in a Low-Speed Flow Field. Ann.Occup.Hyg. 40: 57-64

Kaczmarczyk J, Zeng Q., Melikov A., Fanger PO, (2002a). The effect of personalized ventilation system on air quality prediction, SBS symptoms, and occupant's performance. In: Proceedings of Indoor Air 2002, Monterey, pp. 1042-1047.

Kaczmarczyk J, Zeng Q., Melikov A., Fanger PO, (2002). Individual control and people's preferences in experiments with Personalized Ventilation System. In: Proceedings of Roomvent 2002, pp. 57-60.

Kim, T. and Flynn, M. R. (1991a). Modeling a Worker's Exposure from a Hand-Held Source in a Uniform Freestream. Am. Ind. Hyg. Assoc. J. 52(11) : 458-463

Kim, T. and Flynn, M.R. (1991b). Airflow Pattern Around a Worker in a Uniform Freestream. Am. Ind. Hyg. Assoc. J. 52 (7): 287-296

Kim, T. and Flynn, M.R. (1991): A Revised Model to Predict the Average Concentration in the Reverse Flow Region Downstream of a Worker in a uniform Freestream. Ventilation 1991, ASHRAE

Kim, T. and Flynn, M.R. (1992). The Effect of Contaminant Source Momentum on a Workers Breathing Zone Concentration in a Uniform Freestream. Am Ind Hyg.Assoc.J.53: 757-766

Kulmala, I., Saamanen, A., Enbom, S. (1996). The Effect of Contaminant Source Location on Worker Exposure in the Near-Wake Region. Ann.Occup.Hyg. 40: 511-523

Kroemer, K.H.E., and Grandjean, E. (1997). Fitting The Task To The Human. Fifth Edition. Taylor and Francis.

Ljungqvist, B. (1979). Some Observations on Interactions Between Air Movement and the Dispersion of Pollution (Swedish Council for Building Research Document D8:1979). Stockholm, Sweden: Swedish Council for Building Research

Li, J., Yavuz, I., Celik, I., and Guffey, S.E. (2005). A Numerical Study of Worker Exposure to a Gaseous Contaminant: Variations on Body Shape and Scalar Transport Model. Journal of Occupational and Environmental Hygiene, 2:323-334.

Lotens, W. A. (1993). Heat transfer from humans wearing clothing. Doctoral dissertation, Delft University of Technology, February 1993, Delft.

Lotens, W. A. and Havenith, G. (1991). Calculation of clothing insulation and vapour resistance. Ergonomics 34, 233-254.

Malek, R.F., Daisy, J.M., Cohen, B.S (1996). Breathing Zone Concentrations Variations in the Reinforced Plastic Industry; Field measurements in a Boat Manufacturing Plant. Appl.Occup.Environ.Hyg. 14(11): 777-784

Martinelli, C.A., Harley, N.H., Cohen, B.S. (1983). Monitoring Real-time Aerosol Distribution in the Breathing Zone. Am Ind Hyg.Assoc.J.44: 280-285

Montgomery, D.C. (1997). Design and Analysis of Experiments. New York: John Wiley and sons.

Melikov, A., and Zhou, G. (1996). Air Movement at the Neck of the Human Body. In Proceedings, 7th International Conference on Indoor Air Quality and Climate: Indoor Air '96, edited by S. Yoshizawa et al., International Society of Indoor Air Quality and Climate, Nagoya, Japan, 1:209-214.

Melikov, A.K., Pitchurov, G., Naydenov, K., Langkilde, G. (2002). Field study on occupant comfort and office thermal environment in rooms with displacement ventilation, in preparation for submission to HVAC&R Research Journal.

Melikov, A., (1999). Design of localised ventilation, Proceedings of the 20th International Congress of Refrigeration, IIR/IIF, Sydney, Paper 746.

Melikov, A., Cermak, R., Mayer, M., (2001). Personalized ventilation: evaluation of different air terminal devices, Proceedings of CLMA 2000, Napoli, Paper 524.

Melikov, A., Cermak, R., Mayer, M.: (2002). Personalized Ventilation - Part 1: Criteria for Design and Performance Assessment, in preparation for submission to HVAC Research.

Melikov, A., Cermak, R., Mayer, M. (2002). Personalized Ventilation - Part 2: Performance Evaluation and Comparison of Five Design Options, in preparation for submission to HVAC&R research journal.

Melikov A, Kaczmarczyk J, Cygan L. (2000a) Indoor Air Quality Assessment by A Breathing Thermal Manikin, Proceedings of ROOMVENT'2000, vol(1), Reading, UK.

Melikov A, Kaczmarczyk J, Cygan L. (2000) A "Breathing" Thermal Manikin for indoor air quality assessment, in preparation for submission to Indoor AirJournal.

Murakami, S., Kato, S., and Zeng, J. (1996). CFD Analysis of Thermal Environment around Human Body. In Proceedings, 7th International Conference on Indoor Air Quality and Climate: Indoor Air '96, edited by S. Yoshizawa et al., International Society of Indoor Air Quality and Climate, Nagoya, Japan, 2:479-484.

McCullough, E. A., Jones, B. W. and Huck, P. E. J. (1985) A comprehensive database for estimating cloth ing insulation. ASHRAE Trans. 91, 29-47.

McCullough, E. A., Jones, B. W. and Tamura, T. (1989). A database for determining the evaporative resistance of clothing. ASHRAE Trans. 95, 316-328.

Naydenov, K., Pitchurov, G., Melikov, A., Langkilde, G. (2002). Performance ofDisplacement Ventilation in practice. In: Proceedings of ROOMVENT02, pp. 483-486.

Neter, J., Kutner, M.H., Nachtsheim, C.J., and Wasserman, W. (1996). Applied Linear Regression Models. Richard D. Irwin, Inc.

National Institute of Occupational Safety and Health (NIOSH). The IndustrialEnvironment - Its Evaluation and Control. Washington, DC: US Government Printing Office, 1973.

OSHA Technical Manual: CPL2-2.20B, Chapter 1, Personal Sampling for Air Contaminants. OSHA, Cincinnati, OH, 1985.

Ojima, J. (2003). Evaluation of the Reverse Flow Around a Worker's Body Produced by a Local Exhaust Hood. Sangyo EiseigakuZasshi. Jul 45(4):125-32

Pitchurov, G., Naidenov, K., Melikov, A.K., Langkilde, G. (2002). Field survey of Occupants Thermal Comfort in Rooms with Displacement Ventilation. In: Proceedings of ROOMVENT02, pp. 479-482.

Parsons, K. C, Havenith, G., Holmer, I., Nilsson, H., and Malchaire, J. (1999). The Effects of Wind and Human Movement on the Heat and Vapour Transfer Properties of clothing Ann. occup. Hyg., Vol. 43, No. 5, pp. 347-352

Rodes, C.E., Kamens, R.M., and Wiener, R.W. (1995). Experimental Considerations for the Study of Contaminant Dispersion Near the Body, Am. Ind. Hyg. Assoc. 56:535-545.

Rodes, C.E., Kamens, R.M., Wiener, R.W. (1995). Experimental Consideration for the Study of Contaminant Dispersion near the Body Am Ind Hyg.Assoc.J.56: 535-545

Silva, M.C.G. and Coelho, J.A. (2002). Convection Coefficients For The Human Body Parts Determined With a Thermal Mannequin, proc. of the 8th conference on air distribution in rooms, ROOMVENT 2002, Copenhagen, Denemark, Vol. 2

Tanabe, S., Arens, E.A., Bauman, F.S., Zhang, H. and Madsen, T.L. (1994). Evaluating Thermal Environments by Using a Thermal Manikin with Controlled Skin Surface Temperature, ASHRAE Transactions, 3739, Vol.100, Part 1, pp.39-48.

Van Der Wal, J.F., Moerkerken, A. (1984). The Performance of Passive Diffusion Monitors for organic Vapours for Personal Sampling of Painters. Ann.Occup.Hyg. 28: 39-47

Welling I, Andersson IM, Rosen G, Raisanen J, Mielo T, Marttinen K, Niemela R. (2000). Contaminant dispersion in the vicinity of a worker in a uniform velocity field. Ann Occup Hyg. May: 44(3):219-25.

Welling I, Andersson IM, Rosen G, Raisanen J, Mielo T, Marttinen K, Niemela R. (2001). Extent of the Reverse Flow Wake Region Produced by a Body in a Uniform Flow Field: Appl. Occup. Environ. Hyg. Vol 16 (9):900-904

Yang, J.H., Kato, S., Hayashi, T., Murakami, S. (2002). Measurement of Local Convective Heat Transfer Coefficients of the Human Body in Outdoor and Indoor Environments, proceedings of the 8th conference on air distribution in rooms, ROOMVENT 2002, Copenhagen, Denemark, Vol. 1.

Zeng, Q., Kaczmarczyk, J., Melikov, A., Fanger, P.O. (2002): Design ranges for acceptable air temperature and flow rate for Personalized Ventilation System, in preparation for submission to HVAC&R Research.

Simulation Study

Abe, K. and Kondoh, T., and Nagano, Y., 1995, "A new turbulence model for predicting fluid flow and heat transfer in separating and reattaching flows – II. Thermal field calculations," *Int. J. Heat Mass Transfer*, **38**, 1467-1481.

Achenbach, E., 1968, "Distribution of local pressure and skin friction around a circular cylinder in cross-flow up to Re = 5x106," *J. Fluid Mech.*, **34**, 625-639.

Achenbach, E., 1974, "Vortex shedding from spheres," *J. Fluid Mech.*, **62**, 209-221.

Baldwin, P. E. J. and Maynard A. D., 1998, "A Survey of Wind Speeds in Indoor Workplaces" *Ann. Occup. Hyg.*, **42**(5), 303-313.

Bjørn, E. and Nielsen, P.V., 1996, "CFD Models of Persons Evaluated by Full-scale Wind Channel Experiments" *Roomvent '96*, **2**, 137-144.

Bjørn, E. and Nielsen, P. V., 1998, "CFD Simulations of Contaminant Transport Between Two Breathing Persons," *Roomvent '98*, **2**, 133-140.

Bredberg, J., and Davidson, L., 2004, "Low-Reynolds Number Turbulence Models: An Approach for Reducing Mesh Sensitivity Transactions" *ASME Journal of Fluids Engineering*, **126**, 14-21.

Brohus, H., and Nielsen, P.V., 1996, "CFD Models of Persons Evaluated by Full-Scale Wind Channel Experiments," *Proceedings of Roomvent 96*, 5th International Conference on Air Distribution in Rooms, Yokohama, Japan, July 17-19, **2**, 137-144.

Bräuer, A., English, M. J. M., Sander, H., Timmermann, A., Braun, U. & Weyland, W., 2002, "Construction and evaluation of a manikin for perioperative heat exchange," *Acta Anaesthesiologica Scandinavica,* **46** (1), 43-50.

Carlton, G., and Flynn, M.R., 1997, "Field Evaluation of an Empirical-Conceptual Exposure Model," *Appl. Occup.Env. Hyg.*, **12**(8), 555-561.

Celik, I. and Karatekin, O., 1997, "Numerical Experiments on Application of Richardson Extrapolation with Non-uniform Grids," *Journal of Fluids Engineering*, **119**, 584-590.

Celik, I.B. and Li, J., 2005, "Assessment of Numerical Uncertainty for the Calculations of Turbulent Flow over a Backward Facing Step" Accepted for publication in *International Journal of Numerical Methods in Fluids*, May 2005

Chen, H. C. & Patel, V. C., 1988, "Near-wall turbulence models for complex flows including separation," *AIAA J.*, **26**, 641-648.

Craft, T.J., Launder, B.E., and Suga, K., 1996, "Development and application of a cubic eddy-viscosity model of turbulence," *Int. J. Heat and Fluid Flow*, **17**, 108-115.

Craft, T.J., Iacovides, H., Yoon, J.H., 1999, "Progress in the use of non-linear two-equation models in the computation of convective heat-transfer in impinging and separated flows," *Flow, Turbulence & Combustion*, 63, 59-80.

Flynn, M.R. and Ljungqvist B., 1995, "A Review of Wake Effects on Worker Exposure," *Ann. Occup. Hyg.*, **39**(2), 211-221.

Flynn, M.R., and Sills, E., 2000, "On the use of Computation Fluid Dynamics in the Prediction and Control of Exposureto Airborne Contaminants - an illustration using Spray Painting," *Ann. occup. Hyg.*, **44**(3), 191-202.

Flynn, M.R. and Sills, E.D., 2001, "Numerical Simulation of Human Exposure to Aerosols Generated during Compressed Air Spray-Painting in Cross-Flow Ventilated Booths," *Journal of Fluids Engineering*, **123**, 64-70.

Frisch, U., 1995, *Turbulence*, Cambridge University Press.

George, D., Flynn, M.R., and Goodman, R., 1990, "The Impact of Boundary Layer Separation on Local Exhaust Design and Worker Exposure," *Appl. Occup.Env. Hyg.*, **5**(8), 501-509.

Gibson, M.M., and Launder., B.E., 1978, "Ground Effects on Pressure Fluctuations in the Atmospheric Boundary Layer," *J. Fluid Mech.*, **86**, 491-511.

Guffey, S.E., Flanagan, M.E., and van Belle, G., 2001, "Air Sampling at the Chest and Ear as Representative of the Breathing Zone," *AIHA J.*, **62**, 416–427.

Guffey, S.E., 2004-2005, private communication

Hancock, P.E., and Bradshaw, P., 1983, "The effect of free-stream turbulence on turbulent boundary layers," *Journal of Fluids Engineering*, **105**, 284–289.

Hancock, P.E., and Bradshaw, P., 1989, "Turbulence structure of a boundary layer beneath a turbulent free stream," *Journal of Fluids Engineering*, **205**, 45–76.

Hanjalic, K. 2002 "One-Point Closure Models for Bouyancy-Driven Turbulent Flows", *Annu. Rev. Fluid Mech.* **34**, 321-347.

Hjelmfelt Jr., A. T., and Mockros, L. F., 1966, "Motion of discrete particles in a turbulent fluid," *Appl. Sci. Res.*, **16**, 149-161.

Hyun, S. and Kleinstreuer, S., 2001, "Numerical Simulation of Mixed Convection Heat and Mass Transfer in a Human Inhalation Test Chamber," *International Journal of Heat and Mass Transfer,* **44**, 2247-2260.

Hwang, R.R and Peng, Y.F., 1995, "Computation of Backward-facing Step Flows by a Second-order Reynolds Stress closure model," *International Journal for Numerical Methods in Fluids*, **21**, 223-235.

Kim, T. and Flynn, M.R., 1991, "Air Flow Patterns Around a Worker in a Uniform Freestream," *Am. Ind. Hyg. Assoc. J.,* **52**(7), 287-296.

Kondjoyan, A., Péneau, F., and Boisson, H.C., 2002, "Effect of high free-stream turbulence on heat transfer between plates and air flows : A review of existing experimental results," *Int. J. Therm. Sci.*, **41**, 1—16.

Kulmala, I, Säämänen, A. and Enbom, S., 1996, "The Effect of Contaminant Source Location on Worker Exposure in the near-wake region," *Ann.Occup.Hyg.,* **40**, 511-523.

Lan, N.S., and Viswanathan, S., 2001, "Numerical simulation of airflow around a variable volume/constant face velocity fume cupboard," *AIHAJ.* **62**(3), 303-312.

Launder, B.E. and Spalding, D.B., 1974, "The Numerical Computation of Turbulent Flows," *Computer Methods in Applied Mechanics and Engineering*, **3**, 269-289.

Launder, B.E., 1989, "Second-moment Closure and its Use in Modeling Turbulent Industrial Flows," *International Journal for Numerical Methods in Fluids*, **9**, 963-985.

Leonard, B. P., 1979, "A stable and accurate convective modelling procedure based on quadratic upstream interpolation," *Computer Methods in Applied Mechanics and Engineering*, **19**, 59-98.

Li, J., Yavuz, I., Celik, I.B., and Guffey, S.E., 2005, "A Numerical Study of Worker Exposure to a Gaseous Contaminant: Variations on Body Shape and Scalar Transport Model," *Journal of Occupational and Environmental Hygiene,* **2**,323 - 334

Li, J., Yavuz, I., Celik, I.B., Guffey, S.E. and Bird, A., 2003, "The Effect of Turbulence and Scalar Transport Models on Prediction of Worker Exposure to Aerosols," *Proceedings of FEDSM'03*, 4TH ASME_JSME Joint Fluids Engineering Conference, Honolulu, Hawaii, USA, July 6–11

Lien, F.S. and Leschziner, M.A., 1994, "Modeling the flow in a transition duct with a non-orthogonal FV procedure and low-Re turbulence-transport models," Proc. ASME FED Summer Meeting, Symposium on *Advances in Computational Methods in Fluid Dynamics*, 93-106.

Lien, F.S. and Leschziner, M.A., 1994, "Assessment of turbulence –transport models including non-linear RNG eddy-viscosity formulation and second-moment closure for flow over a backward facing step" *Computers Fluids*, **23**, 8, 983-1004.

Lilly, D.K., 1966, "In the Application of the Eddy Viscosity Concept in the Inertial Subrange of Turbulence," NCAR Manuscript 123.

Longest, P.W., Kleinstreuer, C. and Kinsey, J.S., 2000, "Turbulent Three-dimensional Air Flow and Trace Gas Distribution in an Inhalation Test Chamber," *Journal of Fluids Engineering*, **122,** 403-411.

Mathieu, J. and Scott, J., 2000, *An Introduction to Turbulent Flow*, Cambridge University Press.

Mills, A.F., 1999, *Basic Heat and Mass Transfer*, Prentice-Hall.

Patel, V. C., Rodi, W. & Scheuerer, G., 1985, "Turbulence Models for Near-Wall and Low Reynolds Number Flows: A Review," *AIAA J.*, **23**, 1308-1319.

Péneau, F., Boisson, H.C., and Djilali, N., 2000, "Large eddy simulation of the influence of high free-stream turbulence on spatially evolving boundary layer," *Int. J. of Heat and Fluid Flow*, **21**, 640-647.

Raisee, M., Noursadeghi, A., and Iacovides, H., 2004, "Application of a non-linear k-ε model in prediction of convective heat transfer through ribbed passages," *Int. J. of Numerical Methods for Heat & Fluid Flow*, **14,** 285-304.

Roache, P.J., 1994, "Perspective: A Method for Uniform Reporting of Grid Refinement Studies," *Journal of Fluids Engineering*, **116**, 405-413.

Rodi, W., Mansour, N.N., and Michelassi, V., 1993, "One-Equation Near-Wall Turbulence Modeling With the Aid of Direct Simulation Data," *ASME J. Fluids Eng.*, **115**, 196-205.

Saamanen, A., Kulmala, I., Welling, I., Rosen, G., and Anderson I.M., 2000, "Person in a Uniform Airflow – Effects of Freestream Air Velocity and Body Convection," *Proceedings of the Ventilation 2000*, 6th International Symposium on Ventilation for Contaminant Control, 4-7 June, Helsinki, Finland.

Saga, T., Hu, H., Kobayashi, T., Murata, S. 0, Okamoto, K.and Nishio, S., 2000, "A Comparative Study of the PIV and LDV Measurements on a Self-induced Sloshing Flow," *Journal of Visualization*, **3**, 145-156.

Smagorinsky, J., 1963, "General Circulation Experiments with the Primitive Equations. I. The Basic Experiment," *Month. Wea. Rev.*, **91**, 99-164.

Spiegel, E. A., and Veronis, G., 1960, "On the Boussinesq approximation for a compressible fluid," *The Astrophysical Journal*, **131**, 442-447.

Taneda, S., 1956, "Experimental investigation of the wake behind a sphere at low Reynolds number," *J. Phys. Soc. Japan*, **11**, 1104-1108.

Taneda, S., 1978, "Visual observations of the flow past a circular cylinder performing a rotary oscillation," *J. Phys. Soc. Japan,* **45**, 1038-1043.

Tritton, D. J., 1959, "Experiments on the flow past a circular cylinder at low Reynolds numbers," Journal *of Fluid Mechanics*, **6**(4), 547

van Driest, E.R., 1956, "On Turbulent Flow Near a Wall," *Journal of the Aeronautical Sciences*, **23**, 1007-1011.

Welling, I., Andersson, I.M., Rosen, G., Raisanen, J., Mielo, T., Marttinen K., and Niemela, K., 2000, "Contaminant Dispersion in the Vicinity of a Worker in a Uniform Velocity Field," *Ann. Occup. Hyg.* **44**(3), 219-225.

Yakhot, V. and Orszag, S.A., 1986, "Renormalization Group Analysis of Turbulence. I. Basic Theory," *J. of Sci. Comp.*, **1**, 3-51

PUBLICATIONS FROM ALL STUDIES.

Any published or "in press" articles that have resulted from the grant support (such support from NIOSH should be acknowledged in the articles), should be listed and annotations should be provided that describe how the articles relate to the specific aims. Please do not submit manuscripts or other restricted information.

Three copies of all reprints are needed. In addition, investigators are encouraged to inform NIOSH of other publications resulting from this project as they are published after the final report is submitted.

Dissertation/Thesis

El-Nahaas W: [2005] Effects of Heating, Breathing, Hair Style, Posture, and Air Velocity on Breathing Zone Concentrations for an Anthropometrically-Correct Manikin in a Wind Tunnel, PhD Dissertation, West Virginia University

Comment: Describes all manikin exposure studies done for this project.

Li J: [2005] Critical Issues for Predicting Worker Exposure to Gaseous Contaminants in a Wind Tunnel, Ph.D. Dissertation, West Virginia University

Comment: Describes development of CFD approach for work done for this project and the results, including comparison to manikin experimental results.

Kulkarni SR [2003] Comparison of Concentrations in the Breathing Zone, MS Thesis, West Virginia University

Comment: Describes first set of human experiments for this project.

Journal Papers

Li J, Yavuz I, Celik IB, Guffey SE: [2005] A Numerical Study of Worker Exposure to a Gaseous Contaminant: Variations on Body Shape and Scalar Transport Model. Journal of Occupational and Environment Hygiene, 2(6):323-334

Comment: Describes development of CFD approach for work done for this project and the results.

Conference Papers

Yavuz I, Li J, Celik I, Guffey SE: [2002] Numerical Simulation of Airflow around a Human Body in Wind Tunnel. Presented at the ASME Fluids Engineering Division Summer Meeting, Montreal, Quebec, Canada. July 14 – 18.

Yavuz I, Li J, Celik IB, and Guffey SE: [2003] CFD Simulation of Human Aerosol Exposure in a Wind Tunnel. British Occupational Hygiene Society 2003 Annual Conference, London, England, April 8-10. Only Abstract published

Li J, Celik IB, Yavuz I, Guffey SE: [2003] The Effect of Turbulence and Scalar Transport Models on Prediction of Worker Exposure to Aerosols. Proceedings of the ASME Fluids Engineering Division Summer Meeting, Honolulu, Hawaii.

Li J, Yavuz I, Celik IB, Guffey SE: [2004] The Effect of Reynolds Number on the Ventilation Efficiency in a Wind Tunnel. Proceedings of HT-FED2004, ASME Heat Transfer/Fluids Engineering Summer Conference, July 11-15, 2004, Charlotte, North Carolina, USA, HT-FED2004-56035

Comments:

This study will be productive in terms of peer-reviewed journal articles, conference procedings Masters theses, and doctoral theses.

In addition to the items listed above, we are scheduled to do 3 technical presentations at the AIHCE in Chicago this summer. In addition, we have first drafts of three papers to be submitted to peer-reviewed research publications and at least two others planned. Another doctoral dissertation will be completed and defended by May '06. It focuses on the human studies results. The latter (and this Final Report) were held up by personal problems of the doctoral student. In addition, we are using other funds to extend the human studies results beyond that originally proposed for this study.

INCLUSION OF GENDER AND MINORITY STUDY SUBJECTS.

The gender and minority inclusion table provided in the PHS-2590 is attached.

INCLUSION OF CHILDREN.

None included

MATERIALS AVAILABLE FOR OTHER INVESTIGATORS.

We are still developing publications from our data, so we would prefer not to release it until 1 July 2008. After that, we will share all data.

The procedure to do CFD simulation is described in great detail in this report, so there is nothing additional to provide for it. We did obtain a laser map of the manikin used in the study. That could be available to other researchers with the permission of the person who provided it to us.

To obtain from us, email the PI at Steve. Guffey@mail.wvu.edu

B. FINAL FINANCIAL STATUS REPORT

All of these were provided by the WVU Office of Supported Research.

C. FINAL INVENTION STATEMENT AND CERTIFICATION FORM.

None. Form provided by the WVU Office of Supported Research

CONTACTS FOR FINAL REPORTS

Send hard copies of Final Reports to: Final Report Office Attn MaryAnn P. Monroe Acquisition and Assistance Field Branch, PGO Centers for Disease Control and Prevention 626 Cochrans Mill Road Pittsburgh, Pennsylvania 15236-0070 Phone: 412-386-5075 Send electronic copies of Final Reports to: MPMonroe@cdc.gov and lfranklin1@cdc.gov) For questions, contact: CDC/PGO – Larry Guess, e-mail lguess@cdc.gov, phone 412-386-6826 NIOSH – Ms. Linda Franklin, e-mail: lfranklin1@cdc.gov, phone 404-498-2523

APPENDIX: PEER-REVIEWED PUBLICATION ATTACHED.

Steven E. Guffey, Ph.D., C.I.H.
West Virginia University
College of Engineering and Mineral Resources
Dept of Industrial Management and Systems Engineering
PO Box 6070
353C Mineral Resources Engineering
Morgantown, WV 26506-6070

Journal of Occupational and Environmental Hygiene, 2: 323–334
ISSN: 1545-9624 print / 1545-9632 online

DOI: 10.1080/15459620590961684

A Numerical Study of Worker Exposure to a Gaseous Contaminant: Variations on Body Shape and Scalar Transport Model

Jun Li,[1] Ibrahim Yavuz,[1] Ismail B. Celik,[1] and Steven E. Guffey[2]

[1]Mechanical and Aerospace Engineering Department, West Virginia University, Morgantown, West Virginia
[2]Industrial and Management Systems Engineering Department, West Virginia University, Morgantown, West Virginia

Three-dimensional computational fluid dynamics simulations are used to investigate the distribution and level of contaminant concentrations in the true breathing zone (at the nose and mouth) when toxic airborne contaminants are released within an arm's length in front of the worker who has his back to the airflow. The effects of different body shapes on fluid flow and concentration patterns around the body in a wind tunnel were evaluated and clarified that a sharp body or a block may not be a good surrogate for the human form in consideration of occupational and environmental health studies. The comparison of the concentration field calculated with the Eulerian and Lagrangian methods revealed that the Eulerian method has a more diffusive nature than the Lagrangian method. The concentrations at different locations were also compared to determine the optimum sampling location. It was found that the concentration at the breathing zone may be significantly different from the one at the chest area. The influence of the heat flux from the body was studied at two different Reynolds numbers. Predictions indicate that the heat flux may have a significant impact on exposure especially when the convection induced by buoyancy dominates the flow.

Keywords body shape, numerical simulation, scalar transport, worker exposure

Address correspondence to: Ibrahim Yavuz, Mechanical and Aerospace Engineering Department, West Virginia University, P.O. Box 6106, Morgantown, WV 26506-6106; e-mail: Ibrahim.Yavuz@mail.wvu.edu.

INTRODUCTION

Predicting human exposure to toxic airborne contaminants in the workplace is important. Occupational hygiene engineers, confronted with the design of ventilation systems to minimize human exposures to contaminants, need experimental data and modeling tools to assist in optimizing such controls. Computational fluid dynamics (CFD) has become a powerful tool that enables a detailed investigation of a particular factor isolated from other factors and a reliable estimation of various trends,[1] although knowledge in fluid mechanics is necessary in applying CFD.

Wind tunnels are widely used to study human exposures to airborne contaminants because they allow investigators to control airflow conditions. The factors that could affect the worker exposure in the wind tunnel include: the contaminant generation rate and its position and momentum, the orientation of the worker, the locations and size of facilities in the room, the inlet velocity, the turbulence intensity, the body temperature, and the body shape and breathing and motion of the worker. Understanding the effects of these factors on the flow field and the personal exposure will be extremely important to exposure control.

A subject that has not yet been studied thoroughly is the body shape that determines the local flow field and the resulting contaminant distribution. Simple body shapes such as rectangular body, cylinder body, and the combination of simple geometries have been widely used, despite lack of positive proof that they are capable of representing the real human body well. Bjørn and Nielsen[2] investigated the effects of body shapes using three different models, all of which were made of rectangular geometries and are insufficient to simulate a real human body accurately. In this study, a rounded body was generated to represent a real human body as closely as possible so that we could get more accurate information about the flow field behind the human body, especially the separation of the flow around the head, which is significant in evaluating the worker exposure.[3]

When predicting the concentration of contaminants, both Eulerian and Lagrangian methods have been used in the literature. Flynn and Sills[4] used the Lagrangian particle tracking method to predict human exposure to aerosols generated during compressed air spray painting in cross-flow ventilated booths. They found that the predicted dimensionless breathing-zone

NOMENCLATURE

C	mean concentration
c_1, c_2, c_μ	empirical constants in the standard k-ε turbulence model
C_D	particle drag coefficient
C_p	specific heat coefficient for constant pressure process
D_P	diameter of the particle
F_d	drag function
F_x	diffusive force
G_k	production rate of turbulent kinetic energy
G_b	generation rate of turbulent kinetic energy due to buoyancy
g_i	component of the gravitational vector in the ith direction.
h	enthalpy
k	turbulent kinetic energy
P	dynamic pressure
Pr_L	laminar Prandtl number
Pr_T	turbulent Prandtl number
Re	Reynolds number
t	time
u_i	mean velocity component in direction x_i
u_P	velocity of the particle
x_i	Cartesian coordinate in tensor notation
Sc_L	laminar Schmidt number
Sc_T	turbulent Schmidt number
S_T	heat generation source term
S_ϕ	scalar generation source term
T	temperature
T_{ref}	reference temperature
$\alpha_1 - \alpha_3$	empirical constants for calculating the drag coefficient
β	thermal expansion ratio
ρ	density
ρ_0	density at reference temperature
ρ_P	density of the particle
κ	thermal conductivity
σ_k, σ_ε	empirical constants in the standard k-ε turbulence model
μ	dynamic viscosity
ν	kinematic viscosity
ν_t	turbulent eddy viscosity
ε	turbulent dissipation energy

concentrations were in agreement with the measured values. Longest et al.[5] applied Reynolds Averaged Navier-Stokes (RANS) simulation in conjunction with the Eulerian scalar transport equation to investigate the distribution of carbon monoxide in a human inhalation test chamber. For the Eulerian method, empirical Schmidt numbers are used to calculate the diffusion of the contaminants in the bulk flow, whereas the Lagrangian method does not need as many empirical constants and would constitute a better alternative to predict turbulent diffusion, in fact, if the particles are small enough and follow the flow closely, the need for empirical constants vanishes. However, for the Lagrangian method, the computational cost and the storage requirement increase when a large number of parcel trajectories are tracked. In the current study, the predictions from the Lagrangian and Eulerian methods are compared in order to provide some guide as to which one is better when determining human exposure to gaseous contaminants.

The buoyancy effect due to the heat flux from the body has been considered recently in numerical studies. For instance, Hyun and Kleinstreuer[1] showed that the flow field in a test chamber could be changed significantly when using a heated body instead of an unheated one at a relatively low inlet velocity. In this article, the heat effect at different Reynolds numbers is preliminarily assessed.

Experimental studies with manikins strongly support the supposition that lapel sampling does not well represent inhaled concentrations.[6] In this study, the concentrations at different locations are compared to determine the optimum sampling location and to determine errors from using samples taken at the lapel as the surrogates for inhaled concentrations.

METHODS

Computational Details

In this study, a three-dimensional wind-tunnel simulation was performed with the FLUENT CFD software package (FLUENT, Inc., Lebanon, N.H.). The geometrical configuration of the flow domain is shown in Figure 1, consisting of the wind tunnel (4.6 m width × 2.6 m height × 11 m length), and a nonbreathing human body (1.8 m height). The human body faces downstream of the flow. Constant velocity inlet and pressure outlet boundary conditions were used. The inlet velocity was taken as 0.3 m/sec with a turbulence intensity of 0.3% to study the effect of the body shapes and the transport methods, values representative of typical working environments.[7] To investigate the thermal impact of the body, an inlet velocity of 0.1 m/sec was also used. The characteristic

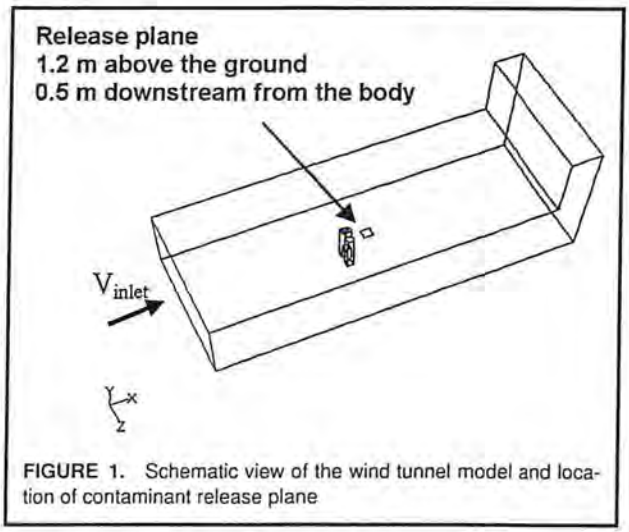

FIGURE 1. Schematic view of the wind tunnel model and location of contaminant release plane

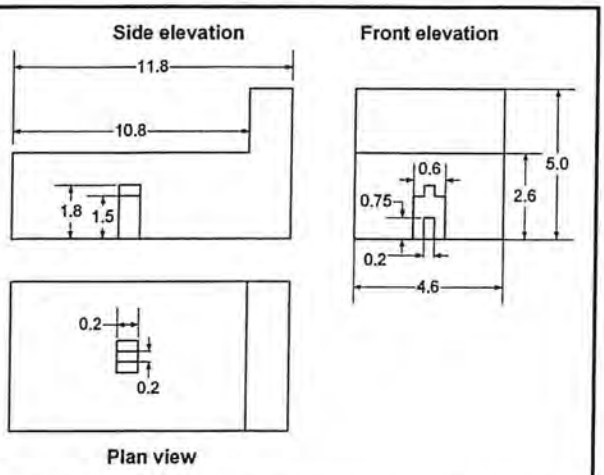

FIGURE 2. The geometry of the wind tunnel and the human body (all dimensions in m)

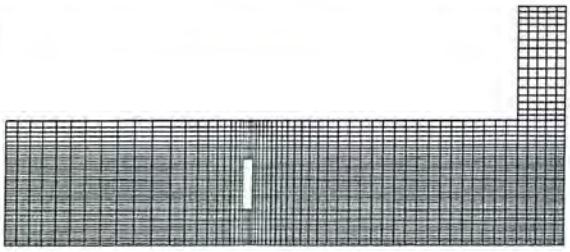

FIGURE 4. An example of a computational mesh used in the simulations (mesh #2 for the sharp body, 115,824 hexahedral cells; the empty area represents the center of the sharp body)

turbulent length scale was chosen to be 0.01 m, which represented the turbulence generating grid size at the inlet of the tunnel. The dimensions of the wind tunnel and the sharp body configuration are illustrated in Figure 2. The source box is 0.3 m (length) × 0.3 m (width) × 0.05 m (height) in size, and the box center is 1.2 m from the ground and 0.5 m from the body. In addition, block and rounded body models were created as shown in Figure 3 to investigate the effect of the shape of the human body on concentration levels near the breathing zone. It should be noted here that the breathing zone mentioned in the paper is represented by one point that is 1.65 m from the ground and 0.01 m from the body (i.e., a point directly in front of the nose at a horizontal distance of 0.01 m).

Different grid distributions, also known as meshes, were constructed as listed in Table I in order to quantify the discretization error using Richardson Extrapolation with grid convergence index (GCI).[8,9] Richardson Extrapolation uses calculations on multiple sets of grids to calculate the extrapolated value of a dependent variable to zero grid size. GCI uses the extrapolated value to determine the numerical uncertainty caused by limited grid size, also known in the literature as the discretization error. For each body, the whole domain was divided into several subdomains each with different grid sizes so that the mesh in the region around the body could be much finer than that in other regions (Figure 4). It should be emphasized that the grids are refined proportionally for each subdomain to maintain similar grids as suggested by Celik and Karatekin.[10] The only exception was mesh #3 (the sharp body), for which we refined only the region around the body based on mesh #2. We did this to illustrate whether we could achieve better convergence with fewer cells using nonuniform grids.

The heat transfer boundary condition for the human body surface was taken as a convective heat flux of 25 W/m^2,[9] which was based on a 2000-calorie diet and corresponded to a moderate activity level of a standing person. The fluid medium was air and the contaminant was acetone vapor. The turbulence model of choice was the two-equation standard k-ε model,[11] which is one of the most commonly used turbulence models in practical engineering flow calculations. The k-ε model is based on the eddy-viscosity approximation, which expresses the Reynolds stress in terms of the mean velocity.

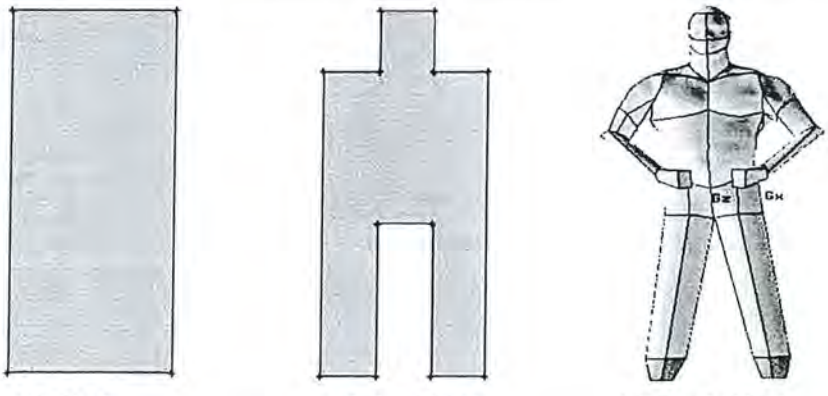

FIGURE 3. Different body shapes used in the present study

TABLE I. Different Meshes Used for the Grid Convergence Study

Mesh #	Block Body	Sharp Body	Rounded Body
1	125,103 node 116,712 hexahedral cells	30,621 nodes 27,396 hexahedral cells	92,166 nodes 339,350 mixed cells[A]
2	229,874 nodes 217,212 hexahedral cells	124,326 nodes 115,824 hexahedral cells	136,302 nodes 470,234 mixed cells
3		188,583 nodes 169,430 hexahedral cells	208,600 nodes 659,110 mixed cells
4		347,595 nodes 330,598 hexahedral cells	
5		1,077,176 nodes 1,041,318 hexahedral cells	

[A] Some cells are hexahedral cells and the other are tetrahedral cells.

The shortcomings of the eddy-viscosity approximation have been documented in the literature,[12] and numerous more sophisticated models such as the Reynolds stress model have been developed to overcome the defects of eddy-viscosity approximation. The choice of model for a specific application should be made carefully, depending on considerations such as the physics encompassed in the flow, the established practice for a specific class of problem, the level of accuracy required, the available computational resources, and the amount of time available for the simulation. In the present study with complex geometry, the standard k-ε model is used because of its robustness, economy, and reasonable accuracy for a wide range of turbulent flows.

Governing Equations

The mathematical formulation of the governing equations and the turbulence models used are the time-averaged Navier-Stokes equations with the standard two-equation k-ε turbulence model.

$$\frac{\partial}{\partial x_i}(u_i) = 0 \tag{1}$$

$$u_j\frac{\partial u_i}{\partial x_j} = -\frac{1}{\rho}\frac{\partial P}{\partial x_i} + \frac{\partial}{\partial x_j}\left[(\nu + \nu_t)\left(\frac{\partial u_i}{\partial x_j} + \frac{\partial u_j}{\partial x_i}\right)\right] - \beta(T - T_{ref})g_j \tag{2}$$

The Bousssinesq model[13] is employed for the calculation of the buoyancy force. This model treats density as a constant value in all solved equations, except for the buoyancy term in the momentum equation.

The eddy viscosity, ν_t, is given by

$$\nu_t = c_\mu\frac{k^2}{\varepsilon} \tag{3}$$

The turbulent kinetic energy, k, and its rate of dissipation, ε, are obtained from the following transport equations:

$$u_i\frac{\partial k}{\partial x_i} = \frac{\partial}{\partial x_i}\left[\left(\nu + \frac{\nu_t}{\sigma_k}\right)\frac{\partial k}{\partial x_i}\right] + G_k + G_b - \varepsilon \tag{4}$$

$$u_i\frac{\partial \varepsilon}{\partial x_i} = \frac{\partial}{\partial x_i}\left[\left(\nu + \frac{\nu_t}{\sigma_\varepsilon}\right)\frac{\partial \varepsilon}{\partial x_i}\right] + c_1\frac{\varepsilon}{k}G_k - c_2\frac{\varepsilon^2}{k} \tag{5}$$

G_k is the production rate of turbulent kinetic energy and G_b is the generation rate of k due to buoyancy

$$G_k = \nu_t\left(\frac{\partial u_i}{\partial x_j} + \frac{\partial u_j}{\partial x_i}\right)\frac{\partial u_j}{\partial x_i} \tag{6}$$

$$G_b = \beta g_i\frac{\nu_t}{Pr_T}\frac{\partial T}{\partial x_i} \tag{7}$$

where Pr_T is the turbulent Prandtl number for energy and is 0.85. It should be noted here that the buoyancy effects on ε is neglected. The constants used in the standard k-ε model are:

$c_1 = 1.44$, $c_2 = 1.92$, $c_\mu = 0.09$, $\sigma_k = 1.0$, and $\sigma_\varepsilon = 1.3$

For the temperature distribution calculations, the energy equation can be written as:

$$u_j\frac{\partial T}{\partial x_j} = \frac{\partial}{\partial x_j}\left[\left(\frac{\nu}{Pr_L} + \frac{\nu_t}{Pr_T}\right)\frac{\partial T}{\partial x_j}\right] + S_T \tag{8}$$

where Pr_L is the laminar Prandtl number which is defined by $Pr_L = C_p\mu/\kappa$ and S_T is the source term.

These three-dimensional equations are solved using a segregated grid approach with pressure projection. The well-known QUICK scheme[14] is used for all the convective terms, and a central differencing scheme is used for the diffusion terms. Two types of boundary conditions are applied to the system under study, namely, the wall boundary conditions and the entry-exit conditions. All of the solid walls in this investigation are at rest; therefore, both the mean and fluctuating velocities of the fluid at these boundaries are identically zero for the turbulent flow, as there is no slip and no mass transport at the walls. In addition, wall functions are used to model the near wall region with an empirical logarithmic velocity profile in terms of the distance from the wall. The inlet boundary condition is set as a specified velocity inlet, whereas the exit (outlet) boundary condition is set as a specified pressure outlet.

Eulerian Scalar Transport

If a species (acetone vapor in the present study) is added to the system, the mean concentration can be calculated by

making use of the following transport equation:

$$\frac{\partial C}{\partial t} + \frac{\partial}{\partial x_i}\left[u_i C - \left(\frac{\nu}{Sc_L} + \frac{\nu_i}{Sc_T}\right)\frac{\partial C}{\partial x_i}\right] = S_\phi \qquad (9)$$

Here, Sc_L is the laminar Schmidt number and Sc_T is the turbulent Schmidt number. The mass flow rate of the scalar is $\dot{m}$ = 1.0e–4 kg/s. The volume $\forall$ of the source region is ~0.005 m^3. The source term S_ϕ is set to $\dot{m}/\forall$ kg/($m^3 \cdot s$). The source region is 1.2 m above the ground and 0.5 m downstream of the human body. The values of Sc_L = 1.42 (Mills[15]) and Sc_T = 1.30 are selected for the purpose of this study.

Lagrangian Trajectory Tracking

Each of the parcels represents a certain amount of acetone vapor and closely follows the airflow. These fictitious particles are released from the plane shown in Figure 1. In order to conform to the Eulerian scalar transport method, the flow rate, and the diameter of the representative particles are set equal to 0.1 g/s, and 1 μm, respectively.

Modeling gases with 1-μm particles presents negligible errors because the particles follow airflows so faithfully, as is demonstrated mathematically elsewhere.[16] Indeed, one of the most important laboratory measurement devices for velocity and turbulence, particle image velocimetry, uses much larger aerosols (up to 50 μm)[17] to track the fluid motions.

Also, note that the concentration levels for the Eulerian method are calculated at the cell center for that particular cell, and the concentration levels using the Lagrangian method are calculated by dividing the cumulative trajectory mass by the volume of that particular cell they are residing in. In both methods one would get a single value for that particular cell.

All simulations were three-dimensional and only steady-state solutions were sought.

RESULTS AND DISCUSSION

The results are presented and discussed in three parts. First, the grid dependency is investigated, which is followed by the predictions of the impact of the heated body on the flow field at different Reynolds numbers. Then, comparisons of the flow field and contaminant concentrations using three different body shapes and two transport methods are presented as the main focus of this study.

Grid Convergence and Iterative Convergence

Five different numerical grid distributions, as listed in Table I, were used to assess the grid dependency of the results for the sharp body simulations. The streamwise velocity component (velocity component in x direction as shown in Figure 1), turbulent kinetic energy (k), and concentration distributions (with Eulerian method) along four different vertical lines on the center plane for all grid distributions are shown in Figure 5, where d represents the downstream distance of the vertical line measured from the body. It can be seen that mesh #1 and mesh #2 are so coarse that the turbulent kinetic energy predicted with them in the downstream of the leg are much higher than the one with other meshes. With meshes #3, #4, and #5, the results are very close in the downstream of the upper body, which is believed to be the most important region for the worker exposure. We have mentioned that mesh #3 is refined just in the region around the body based on mesh #2 and it has fewer cells than mesh #4; however, the turbulent kinetic energy with mesh #3 is even closer to the result with mesh #5 (the finest grid) at some regions. Since running a case with mesh #3 takes less time than with mesh #4, it has been used to study the effect of body shapes and transport methods.

TABLE II. k and Concentration at the Breathing Zone for the Sharp Body

	Grid #5	Grid #4	Grid #2
h/h5	1.0	1.465	2.08
k (m^2/sec^2)	0.001799	0.001939	0.001814
Concentration (kg/m^3)	0.00482	0.00472	0.00448

The value of turbulent kinetic energy and concentration for the sharp body with mesh #2, #4 and #5 are listed in Table II, where h is the averaged grid size calculated as

$$h = \sqrt[3]{\frac{\text{volume}}{\text{number of cells}}} \qquad (10)$$

and h5 is the finest average grid size. Convective transport due to recirculation regions formed in the wake of the body and the diffusive nature of the gaseous contaminants causes a nonzero concentration field upstream of the source. Using Richardson extrapolation on the concentration data that shows monotonic convergence, we can get the observed order of the numerical schemes that is consistent with the initial arrangement (QUICK for convection terms and central differencing for diffusion terms). The extrapolated "exact" concentration is 0.00489 kg/m^3. The GCI of concentration at the breathing zone for mesh #2 is approximately 11%. For the turbulent kinetic energy data at the breathing zone, nonmonotonic convergence is shown since k(#5) < k(#2) < k(#4), while h5 < h4 < h2. The relative error of k for mesh #2 is 8% based on mesh #5.

The concentrations at the breathing zone (mouth) using the Eulerian method are compared in Figure 6, where h1 is the coarsest average grid size. Figure 6 shows that the lowest exposure is predicted for the simulations with the rounded body. The concentrations did not approach an asymptotic value as we expected. Instead, the cells composing the source region changed with the mesh itself, which affected the grid convergence in terms of concentration as a function of the source position and source size.[18] Additional setup effort is needed to keep the source region exactly the same for each mesh. On the other hand, for the purpose of this study, it has been shown clearly that the body shape has significant influence on the worker exposure.

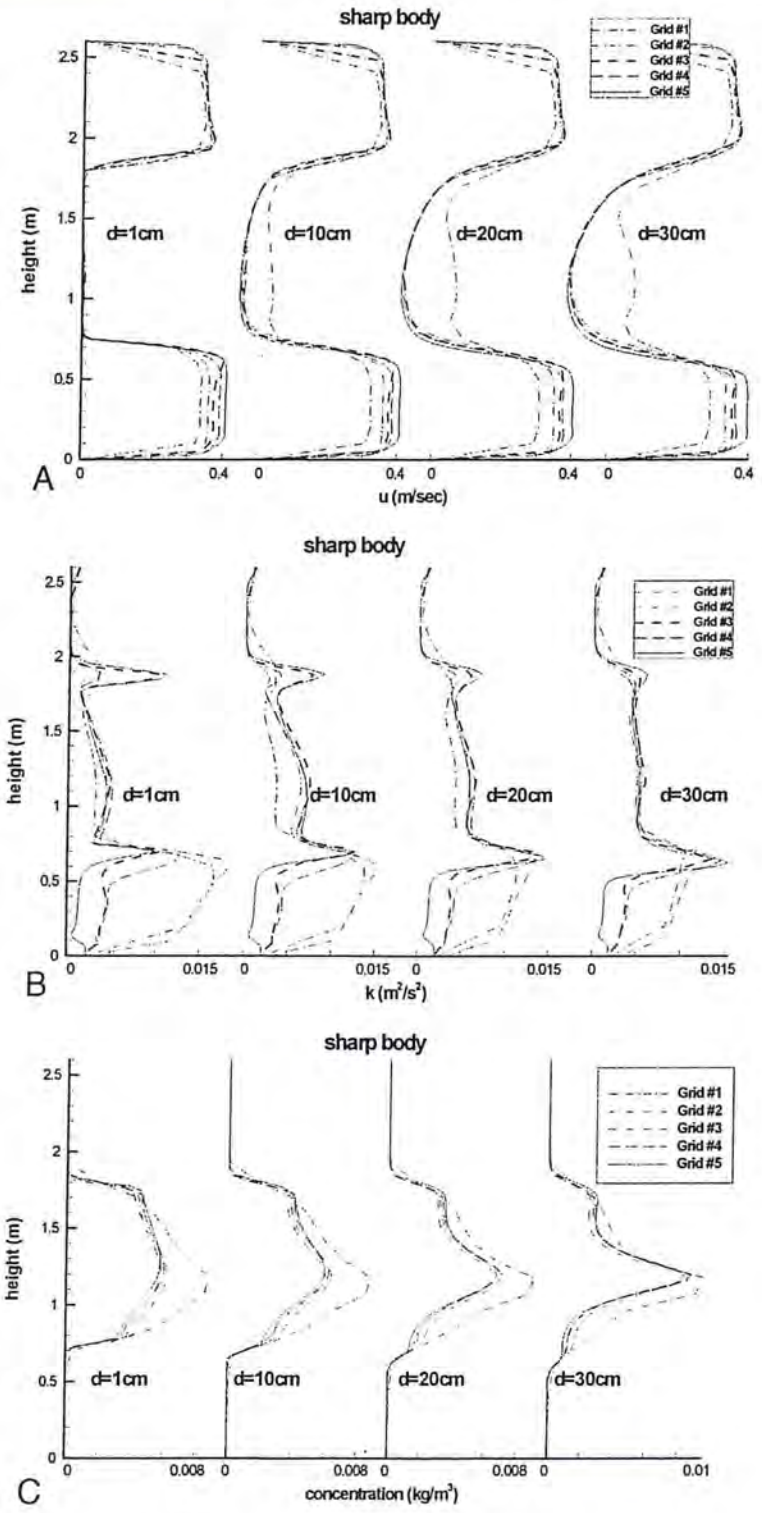

FIGURE 5. Streamwise velocities, turbulent kinetic energy and concentrations at several distances (d) downstream of the body on the central plane with different grid distributions for the sharp body model

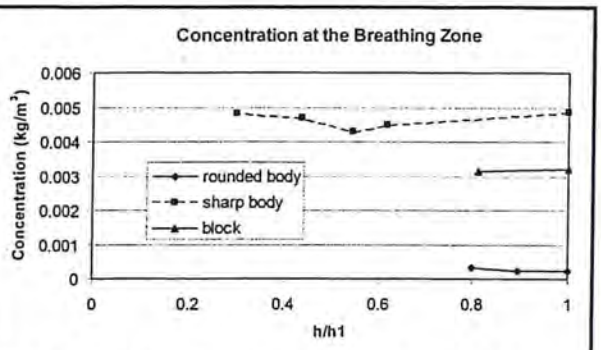

FIGURE 6. Concentrations at the breathing zone with different grid distributions and different body shapes

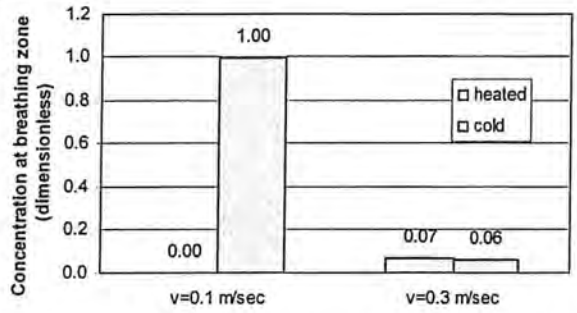

FIGURE 8. Nondimensional concentration levels at the breathing zone at different inlet velocities and thermal conditions with the rounded body model and Eulerian method

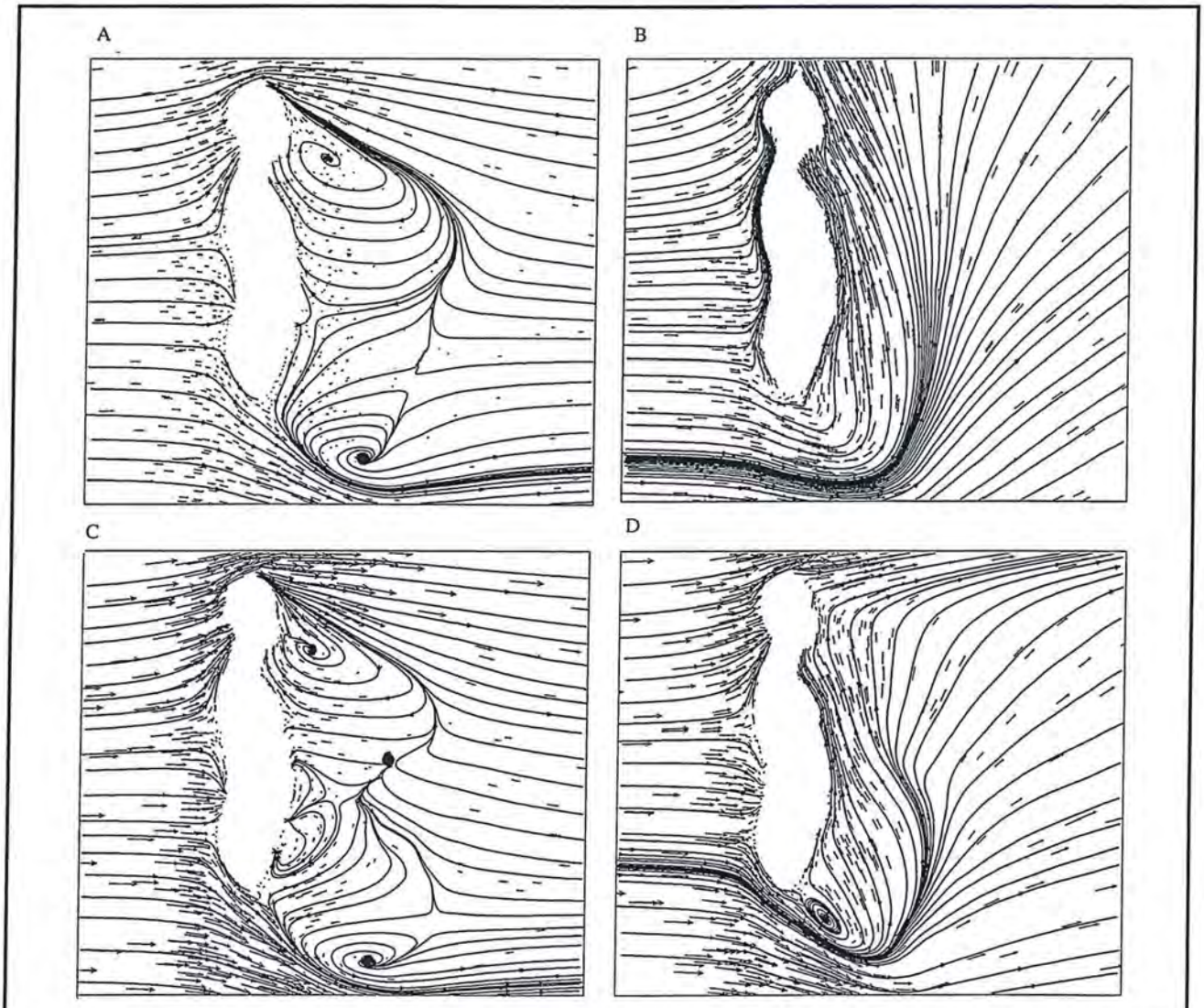

FIGURE 7. Velocity vectors and streamlines on the center plane for different inlet velocities and thermal conditions with the rounded body model

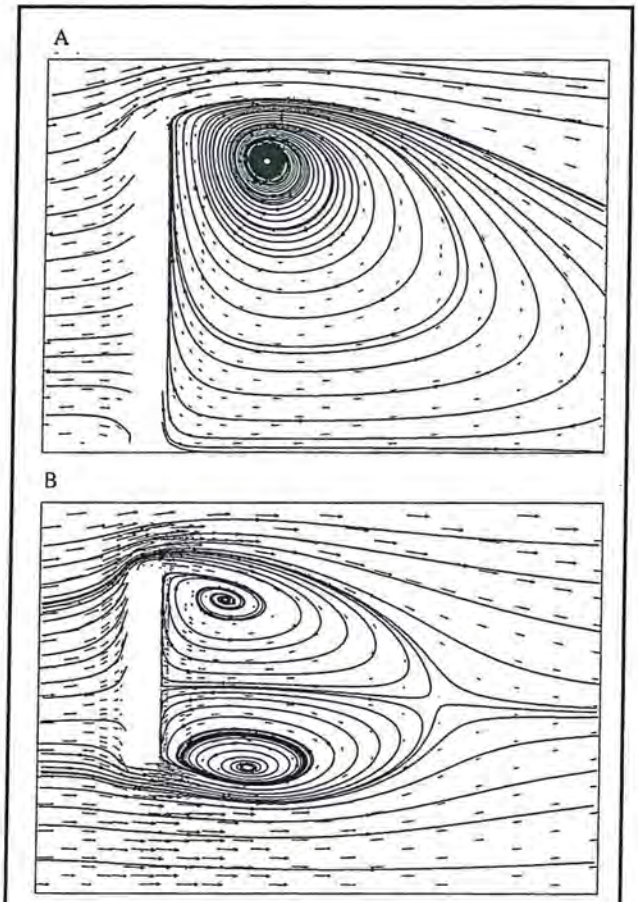

FIGURE 9. Comparison of the flow field with a block and a sharp body; velocity vectors and streamlines on the center plane (side elevation)

There is no distinguishable difference between the results at a residual criterion of 1.0e–3 and of 1.0e–4, so a residual of 1.0e–4 used in this study should achieve a good convergence in terms of iteration. The streamwise velocity component at the mouth was also monitored in the calculation to check if it approached an asymptotic value when the assigned residual is reached. In this way we tried to avoid false convergence by using a fixed value of residual.

Effect of Thermal Conditions

Comparison of the velocity fields with the body, heated and "cold" (body temperature is the same as that of the surroundings), shows that the heat flux from the body affects the exposure dramatically at relatively low Reynolds numbers (Figure 7). For the heated body at $Re_b = 4100$ ($v_{inlet} = 0.1$ m/sec, where Re_b is calculated based on the width of the body), the upwards convection is dominant due to the buoyancy and there is no recirculation region formed at the breathing zone. Figure 8 shows that there is almost no contaminant in the breathing zone for the heated body at $v_{inlet} = 0.1$ m/sec since the contaminant is 0.5 m from the body and the thermal plume is stronger than the concentration diffusion. If the pollution source were placed closer to the body, the difference in exposure levels with a heated body and a cold body may be smaller.

At $Re_b = 12300$ ($v_{inlet} = 0.3$ m/sec), a recirculation region is still formed in the heated body simulations, as the air flows through the gap between the legs. The buoyant flow will bring the contaminant to the breathing zone and merge with the convected flow. Figure 8 shows that the concentration has an 11% variation with and without heat flux from the body. However, to isolate the thermal effect from other factors, the cold body is used in analyzing the influence of the body shapes and the contaminant transport models.

Effect of the Body Shape

Comparison of the flow-field predictions with the block, the sharp, and the rounded body indicates that the predicted flow-field with the block has one large recirculation region, whereas the sharp and rounded bodies each induce two smaller recirculation regions (Figure 7c and Figure 9). The recirculation zone around the head could suggest that contaminants trapped in that

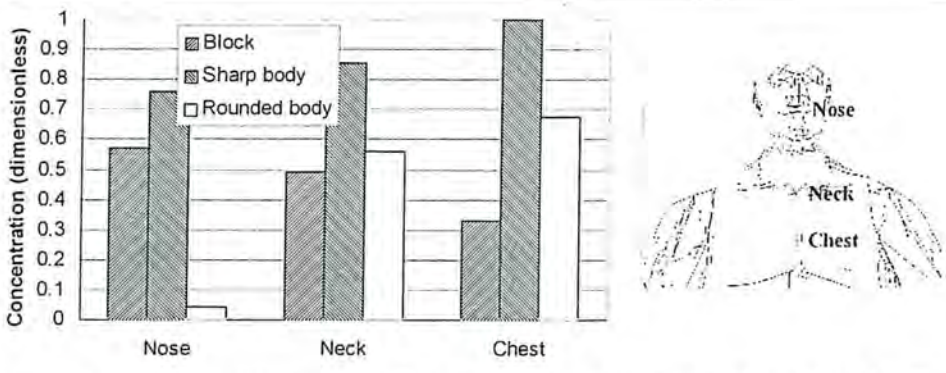

FIGURE 10. Comparison of normalized concentration at different points 1.0 cm downstream of human body for different body shapes (normalized with the highest concentration value)

region are more likely to be inhaled. Moreover, the contaminants accumulated in the waist region could be transferred to the breathing zone from the lower recirculation zone. However, the flow around the sharp and rounded bodies shows different separation profiles, which is an important issue. For the sharp body, the flow separates at the corner of the head, whereas with the rounded body, the air flows along the forehead and separates from the body near the eye level. This means that such small issues as hairstyle, the size and shape of headgear worn, and the angle of the forehead could affect the exposure levels.

Using the Eulerian method for each body shape, the predicted nondimensionalized concentration levels of the contaminant gas at various locations were compared for trend analysis (see Figure 10). It is clear that the block body cannot be used to represent a worker accurately. With the sharp and rounded body, the concentration level at the chest region is higher than that at the breathing zone (C_{chest}/C_{nose} is 13.6 for the rounded body). This observation qualitatively agrees with experimental results[6] that concluded the concentrations at the chest averaged about 2.9 times the concentrations at the nose and the ratio decreased significantly with increasing velocities ($C_{chest}/C_{nose} = 2.4$ at $V_{inlet} = 0.24$ m/s). It should be noted that the experimental conditions are different from the current study in some aspects. For instance, SF_6 was used in the experiments and the geometric average of the concentrations at three points (left chest, middle chest, and right chest) was taken to represent the concentration in the chest area. In addition, the manikin shape and the source size in the experiments are also different. These differences may contribute to the different ratios of C_{chest} to C_{nose} found in the calculations and the experiments. However, the same trend observed by both the calculations and the experiments suggests that it may not be a good practice to measure the concentrations around the chest area as surrogates for the inhaled concentrations, as is current practice. With the block figure the concentration ratio of chest to nose is reversed, which illustrates that the trend could be inaccurately predicted with crude representatives of the human body.

Figure 11 presents the predicted concentration distributions 1 cm downstream of the body obtained from the simulations using the Eulerian scalar transport method. It is seen that the contaminants are accumulated at the top of the block, whereas the contaminants for the sharp and rounded body are diffused over a much wider region of the body accumulating mostly in the chest region. This again shows that using less accurate shapes for the human body may lead to inaccurate results.

Effect of the Contaminants Transport Method

Using the Lagrangian method, the concentration at a plane 1.0 cm downstream of the body is shown in Figure 12d. Compared with the results of the Eulerian method in Figure 11b, it can be argued that both methods predict the concentration levels on the same order, although the Lagrangian method shows much more randomness, which is directly associated with the

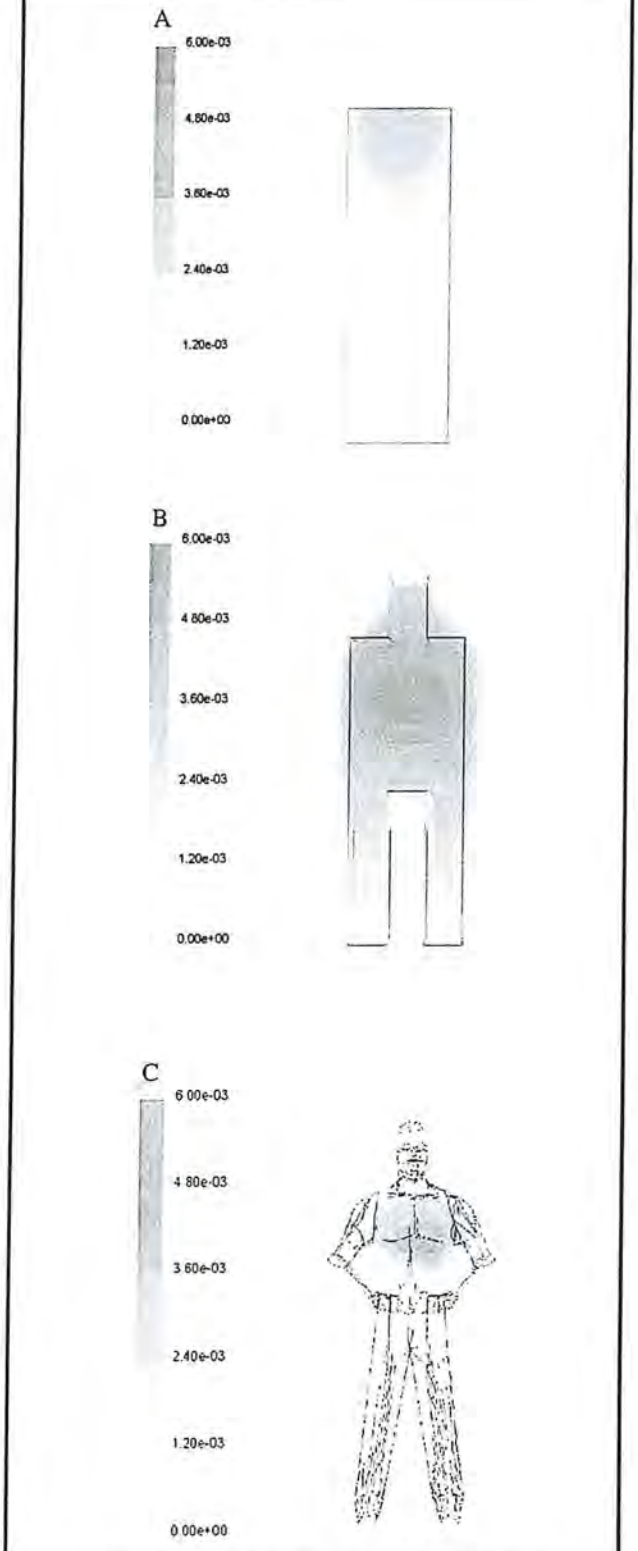

FIGURE 11. Concentration distribution; Eulerian method, on a cross section 1.0 cm downstream of the body

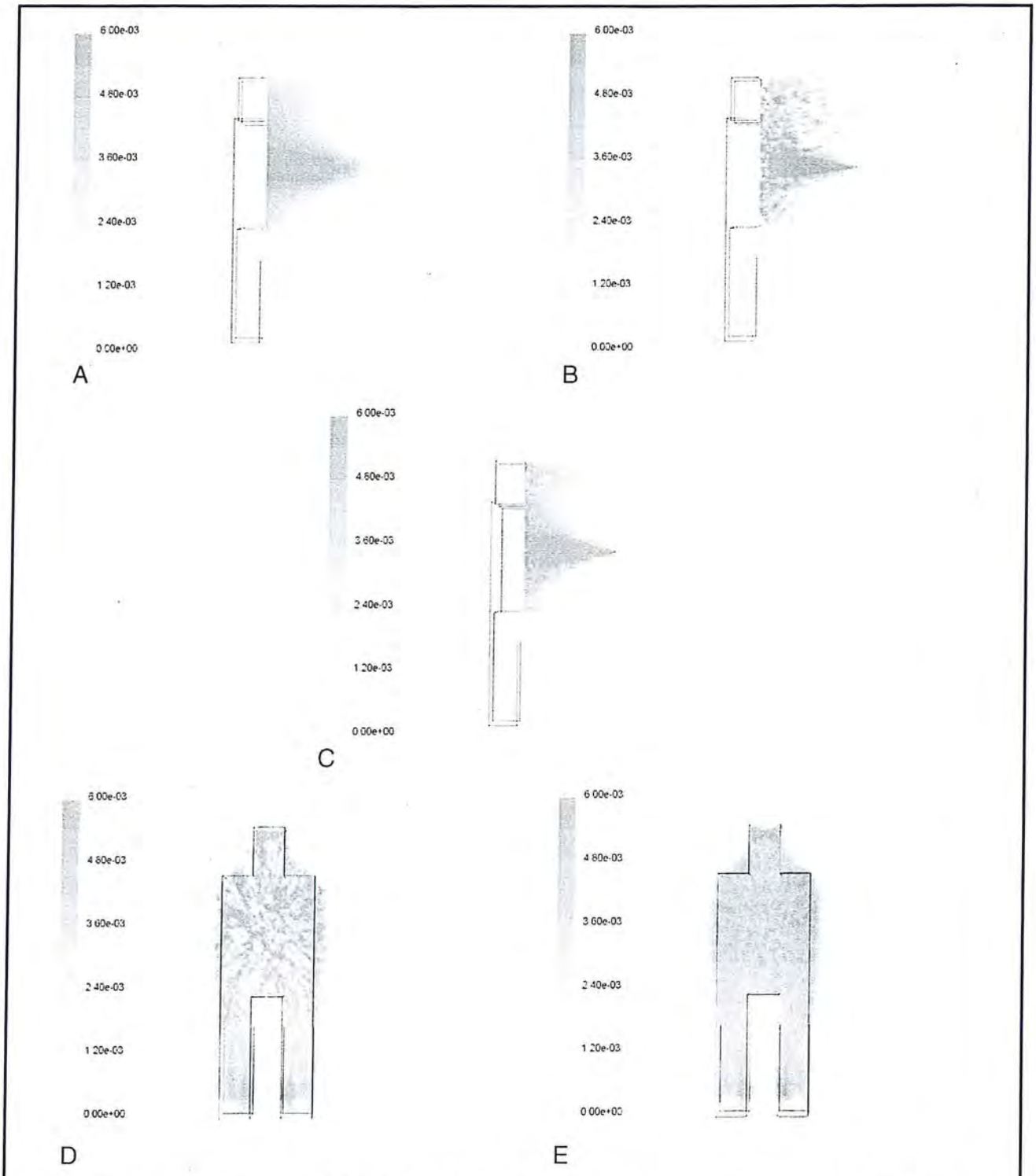

FIGURE 12. Concentration contours (a, b, c) on the center plane (d, e) on a cross section 1.0 cm downstream of the sharp body model

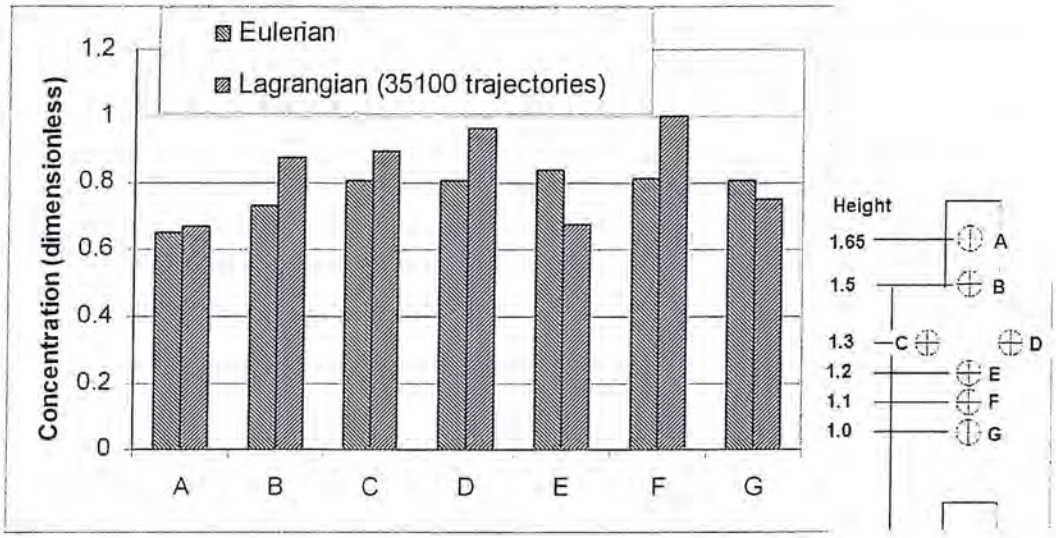

FIGURE 13. Normalized concentrations at different locations at a cross section 1 cm downstream of the sharp body model

method itself since a random velocity component is added to the mean fluid velocity to simulate trajectory dispersion due to turbulence. It has been seen during the simulations that the number of trajectories tracked in the Lagrangian simulations is also an important factor affecting the predicted concentration levels. The more trajectories tracked, the smoother the concentration contours become (see Figures 12c and 12e), since a better averaging over a volume can be applied to calculate the concentration levels.

The symmetry plane concentration contours are shown in Figures 12a, 12b, and 12c for both the Eulerian method and the Lagrangian method. The latter was repeated for different numbers of representative particle trajectories. Here again, the Eulerian method exhibits a more diffusive concentration field than the Lagrangian method. The latter shows a higher degree of irregularity because of the applied discrete random walk tracking model used in the FLUENT code. Nevertheless, the predictions of the two methods are in fairly good agreement with each other (Figure 13).

The local concentrations at different locations 1.0 cm downstream of the sharp body are compared for both the Eulerian and Lagrangian predictions in Figure 13. The values are normalized by dividing by the highest concentration value (C_{max} = 0.00484 kg/m^3) that was predicted for both simulations. This was done since the trend of the concentrations is the main concern of this study, not the absolute values of the concentrations. The Eulerian method predicts a more uniform concentration when compared with the predictions obtained via the Lagrangian method. Although it is true that tracking more trajectories creates a more uniform concentration field for the Lagrangian method, it should be noted that it is computationally expensive to use a large number of trajectories. It is noteworthy to mention that both methods tend to predict higher concentrations near the lapel compared with the mouth/nose level.

CONCLUSIONS

In this study, the Eulerian scalar transport model and the Lagrangian trajectory tracking method were compared in their ability to predict the concentrations around a human shaped body exposed to gaseous contaminants within the length of an arm's reach. It was seen that the Eulerian method exhibited a more diffusive nature than the Lagrangian method. However, the concentration predictions obtained with the Lagrangian method may converge with the Eulerian prediction if an adequate number of trajectories are tracked. Nevertheless, the results obtained from both predictions suggest that the concentrations measured at the lapel could be very different from the concentrations measured near the mouth. The present study indicates that the latter will be significantly lower under the specific condition of the simulation, particularly in the absence of heat flux from the body. However, this conclusion should not be generalized in the cases of uniform concentration distributions; results may be affected by a nonlocal source or even the motion of the worker.

The influence of the shape of the human body used in the simulations was also studied. It was observed to have a major impact on the flow-field and, consequently, on the concentration field. In fact, this study showed that the predictions with a rounded body, which (to our knowledge) is one of the closest approximation of a human body used in simulations in the literature, resulted in much lower concentration levels. This suggests that during modeling, oversimplified body shapes should not be preferred for accurate predictions in worker exposure assessment. Specific details of rounded body may have

large influence on the exposure and should be considered in certain circumstances. This presents a great challenge to CFD modelers, as every worker may exhibit a significant variation on body shape depending on what clothes are worn and factors related to body size and shape.

On another note, it was demonstrated that the numerical grid size and its distribution have significant effects on the quality of predictions. It is recommended that in exposure studies, grid convergence of CFD simulations should be assessed in order to reduce and quantify the degree of discretization errors.

Finally, it should be noted that these analyses were performed for a cold body. We found that the heat flux from the body may have a significant impact on predicted flow-field and concentration levels, so it cannot be ignored, especially when the convection induced by the buoyancy dominates. Further numerical simulations should be done that include the heat-flux from the body and, if applicable the breathing phenomena and the motion of the worker.

ACKNOWLEDGEMENTS

We particularly acknowledge Dr. Aaron J. Bird from NIOSH for his comments and help in providing the grid of the human torso. We'd like to express our appreciation to the editor whose valuable comments and suggestions make this paper much better than the original version.

This work was performed under a National Institute of Occupational Safety and Health project sponsored by the Centers for Disease Control and Prevention through grant R01 OH07587-01.

REFERENCES

1. **Hyun, S., and Kleinstreuer, S.:** Numerical simulation of mixed convection heat and mass transfer in a human inhalation test chamber. *Int. J. Heat Mass Trans. 44*:2247–2260 (2001).
2. **Bjørn, E., and Nielsen, P.V.:** CFD models of persons evaluated by dull-scale wind channel experiments. In *Proceedings of Roomvent '96, Fifth International Conference on Air Distribution in Rooms*, Yokohama, Japan, Vol. 2, 1996. pp. 137–144.
3. **Li, J., I. Yavuz, I.B. Celik, S.E. Guffey, and A. Bird:** The effect of turbulence and scalar transport models on prediction of worker exposure to aerosols. In *Proceedings of FEDSM'03*, 4th ASME/JSME Joint Fluids Engineering Conference, Honolulu, July 6–11, 2003.
4. **Flynn, M.R., and E.D. Sills:** Numerical simulation of human exposure to aerosols generated during compressed air spray-painting in cross-flow ventilated booths. *Trans. ASME. J. Fluids Eng. 123*:64–70 (2001).
5. **Longest, P.W., C. Kleinstreuer, and J.S. Kinsey:** Turbulent three-dimensional air flow and trace gas distribution in an inhalation test chamber. *Trans. ASME. J. Fluids Eng. 122*:403–411 (2000).
6. **Guffey, S.E., M.E. Flanagan, and G. van Belle:** (2001) Air sampling at the chest and ear as representative of the breathing zone. *Am. Ind. Hyg. Assoc. J. 62*: 416–427 (2001).
7. **Baldwin, P.E.J., and A.D. Maynard:** A survey of wind speeds in indoor workplaces. *Ann. Occup. Hyg. 42*:303–313 (1998).
8. **Roache, P.J.:** Perspective: A method for uniform reporting of grid refinement studies. *J. Fluids Eng. 116*:405–413 (1994).
9. **Celik, I., and O. Karatekin:** Numerical experiments on application of Richardson extrapolation with nonuniform grids. *J. Fluids Eng. 119*:584–590 (1997).
10. **Bjørn, E., and P.V. Nielsen:** CFD simulations of contaminant transport between two breathing persons. In *Proceedings of Roomvent '98*, Vol. 2, pp. 133–140. 6th International Conference on Air Distribution in Rooms, Stockholm, June 14–17, 1998.
11. **Launder, B.E., and D.B. Spalding:** *Lectures in Mathematical Models of Turbulence*. London: Academic Press, 1972.
12. **Mathieu, J., and J. Scott:** *An Introduction to Turbulent Flow*. Cambridge University Press, 2000.
13. **Spiegel, E.A., and G. Veronis:** On the Boussinesq approximation for a compressible fluid. *Astrophysical J. 131*:442–447 (1960).
14. **Leonard, B.P.:** A stable and accurate convective modelling procedure based on quadratic upstream interpolation. *Comput. Meth. Appl. Mech. Eng. 19*:59–98 (1979).
15. **Mills, A.F.:** *Basic Heat and Mass Transfer*, Second Ed. Upper Saddle River, N.J.: Prentice-Hall, 1999.
16. **Hjelmfelt, A.T. Jr., and L.F. Mockros:** Motion of discrete particles in a turbulent fluid. *Appl. Sci. Res. 16*:149–161 (1996).
17. **Saga, T., H. Hu, T. Kobayashi, S.O. Murata, K. Okamoto, and S. Nishio:** A comparative study of the PIV and LDV measurements on a self-induced sloshing flow. *J. Visual. 3*:145–156 (2000).
18. **Kulmala, I, A. Säämänen, and S. Enboni:** The effect of contaminant source location on worker exposure in the near-wake region. *Ann. Occup. Hyg. 40*:511–523 (1996).

Principal Investigator/Program Director (Last, First, Middle): Guffey, Steven E.

Inclusion Enrollment Report

This report format should NOT be used for data collection from study participants.

Study Title: Comparison of Concentrations at Personal Exposure Sampling Locations

Total Enrollment: 13 **Protocol Number:** 15035

Grant Number: 1 RO1 OH07587

PART A. TOTAL ENROLLMENT REPORT: Number of Subjects Enrolled to Date (Cumulative) by Ethnicity and Race

Ethnic Category	Sex/Gender			
	Females	Males	Unknown or Not Reported	Total
Hispanic or Latino	2	1	0	3 **
Not Hispanic or Latino	0	10	0	10
Unknown (individuals not reporting ethnicity)	0	0	0	0
Ethnic Category: Total of All Subjects*	2	11	0	13 *
Racial Categories				
American Indian/Alaska Native	0	0	0	0
Asian (mostly Indian)	0	10	0	10
Native Hawaiian or Other Pacific Islander	0	0	0	0
Black or African American	0	0	0	0
White	0	0	0	0
More Than One Race	2	1	0	3
Unknown or Not Reported	0	0	0	0
Racial Categories: Total of All Subjects*	0	10	0	13 *

PART B. HISPANIC ENROLLMENT REPORT: Number of Hispanics or Latinos Enrolled to Date (Cumulative)

Racial Categories	Females	Males	Unknown or Not Reported	Total
American Indian or Alaska Native	2	1	0	3
Asian	0	10	0	10
Native Hawaiian or Other Pacific Islander	0	0	0	0
Black or African American	0	0	0	0
White	0	0	0	0
More Than One Race	0	0	0	0
Unknown or Not Reported	0	0	0	0
Racial Categories: Total of Hispanics or Latinos**	2	11	0	13 **

* These totals must agree.
** These totals must agree.